Réponse contractile des systèmes actomyosines biomimétique

Hajer Ennomani

UNIVERSITÉ GRENOBLE ALPES

THÈSE

Pour obtenir le grade de

DOCTEUR DE L'UNIVERSITÉ GRENOBLE ALPES

Spécialité : **Doctorat Physique/ Physique pour les sciences du vivant**

Arrêté ministériel : 7 août 2006

Présentée par

« Hajer ENNOMANI »

Thèse dirigée par **« Laurent BLANCHOIN»**

préparée au sein du **Laboratoire de Physiologie Cellulaire et Végétale, équipe "Physique du Cytosquelette et de la Morphogénèse"**
dans **l'École Doctorale de Physique de Grenoble.**

Contractile response of biomimetic actomyosin systems.

Thèse soutenue publiquement le **« 6 Novembre 2015 »**,
devant le jury composé de :

Mr. Bertrand FOURCADE
Professeur - Unversité Joseph Fourier, Grenoble, Président.
Mr. Pascal MARTIN
Directeur de recherche- Institut Curie, Rapporteur.
Mr. Yohanns BELLAICHE
Directeur de recherche - Institut Curie, Rapporteur.
Mr. Pierre NASSOY
Directeur de Recherche - Université de Bordeaux, Membre.
Mr. Benoit LADOUX
Professeur Institut Jacques Monod, Université Paris Diderot, Membre.
Mr. Laurent BLANCHOIN
Directeur de recherche - CEA, Grenoble, Directeur de thèse

Table of contents

Second part

Third part

Fourth part

Introduction

Foreword: Why studying contractility?

I remember once Laurent telling me at the end of one of our discussions ”People are asking me quite often why I am doing some research. I reply them that every day, we are doing something pretty heroic. We try to bring ourselves to the boundary between what we know and what we do not know. We are always at the limit between what we plan to do and what we are able to do. Our goal is simply to discover something truly new, so we are in a way THE LAST ADVENTURERS”. I liked this image and when I look back in time at what I was doing during my Ph.D., I believe it was true.

Cell structural integrity, mechanical properties and morphological changes are principally governed by the properties of their cytoskeleton, a complex system made of highly dynamic polymers extending throughout the cytoplasm. At the basis of cell movement, it is also an essential factor in the propagation of cancers by migration of metastatic cells to other organs.

Therefore substantial efforts are devoted to understand how the cellular cytoskeleton exerts its physiological functions. Distinct and complementary approaches converge towards the same purpose, either at the tissue or cell level or through reconstituted systems *in vitro*.

Remarkably, scientists had a very precise and accurate view of cytoskeletal organization before they could even observe it. Indeed, as early as in the mid-ninteenth century, the French Felix Dujardin had already suspected the existence of cytoskeletal structures through his observations of the mechanical properties of what he called “sarcodes” in the amoeba. He went deeper than most of the other scientists of his time and defined the cell material by its mechanical properties, describing it as "elastic and contractile". He even mentioned "cellular tissue with invisible stitches," which is nothing else than the first description of the cytoskeletal structure. Later, the development of microscopy and biochemical techniques made observations of the cellular cytoskeleton possible, and the characterization of its interactions with other proteins. Protein assemblies were no longer

deducted only from the macroscopic properties of the cells, but directly observed by microscopy. Direct observations and mechanical characterizations are still being explored in a complementary manner. Since Dujardin's discoveries about this “elastic and contractile” material in 1842, I am always surprised that we never stop improving our understanding around this field. But I can feel that we are still very far to fully understand the mechanical properties of a cell mediated by the cytoskeleton. The Ph.D. for me was a good opportunity, to participate in this long-term effort.

Using biophysical approaches, developed in our laboratory, I was interested in a key role of the cytoskeleton: the forces generated by its contraction. To achieve this goal, the strategy adopted by our team is to build a system that mimics cytoskeletal architectures. This biomimetic approach allows us to study in a controlled way the cytoskeleton contractile response. The use of simplified systems and the ability to modify individual components without the active contribution and complexity of the cell has proven beneficial in understanding emerging properties of a variety of biological systems.
Therefore the main goal of my thesis was to understand how the cytoskeleton architecture influences the actomyosin contractile response. I was particularly interested in the main actomyosin structures found in cells: the disorganised and branched contractile networks, the sarcomeric antiparallel fibers and mixed polarity fibers. My work has allowed us to determine some general rules of actomyosin contractile systems, relative to the architecture of the cytoskeleton.

I. The actomyosin system

I will dedicate the first part of this introduction to a biochemical and biophysical description of the key molecular players involved in myosin-dependent contractile systems. This description will begin by the actin molecule itself, and some of its most important regulators. More than 60 families of proteins are known to interact with the actin cytoskeleton, and many of them are involved in the regulation of contractile processes. In the last part of this introduction, I will focus on myosin motors, which are key players in most actin-dependent contractile behaviours in eukaryotic cells.

I.1. Actin and related protein

Actin was isolated for the first time by Straub and collaborators in 1942. It was extracted by an acetone dehydration of skeletal muscle, followed by a re-suspension in a low salt buffer. The resulting solution presented an original property: its viscosity would increase after salt addition, indicating that the system transitions to a gel-like behaviour. This observation provided one of the first evidences that the actin molecule is able to assemble into a polymer. Later, while motile and contractile behaviours were also characterized in non muscle cell types, other isoforms of actin were identified (Ishikawa, Bischoff, & Holtzer, 1969). This discovery revealed a more complex role of the actin cytoskeleton than previously imagined. Nowadays, we know that actin is involved in a wide diversity of cellular functions, and is one of the most expressed proteins in eukaryotic cells (Pollard and Earnshaw 2002)

The actin molecule is extremely conserved during evolution. For example, mammalian actins and *Acanthamoeba* actin are more than 90% identical, and the sequences of skeletal muscle actins are strictly identical in all warm-blooded vertebrates. Such a high degree of conservation is unusual and indicates a high selection pressure. It is believed that the high number of essential proteins interacting with actin is responsible for this slow evolution. Indeed, while point mutations on actin could have positive effects on one of these interactions, it usually also triggers negative effects on others. Therefore, evolution brought changes mostly on actin-associated proteins rather than on the actin molecule itself.

I.1.1. Actin assembly *in vitro*: from monomers to filaments

The actin molecule is a 43 kDa-protein constituted of four subdomains. It binds a divalent cation ($Mg2^+$ in physiological conditions) and one nucleotide, which can be ATP or ADP, between its subdomains 2 and 4. The binding affinity of actin monomers to ATP is higher than to ADP, and the spontaneous hydrolysis of the nucleotide is very slow. This explains why actin monomers are mostly found in an ATP-state in the cytoplasm of cells.

Actin is constantly transitioning from its monomeric form to its filamentous form. Actin filaments are semi-flexible polymers; with a persistence length of about 15 μm. Actin filaments are polarized. One end of the filaments, called the barbed end, is very dynamic. Elongation at this end is fast in the presence of actin monomers. The other end is called the pointed end, and is on the contrary non dynamic (Pollard, 1986). This naming " barbed, pointed" was based on the appearance of actin filaments when they were first decorated with myosin heads and observed by electron microscopy (Figure 1). Indeed, in these images, myosin arrowheads were pointing toward the slow growing end of the filaments (Milligan et al 1990).

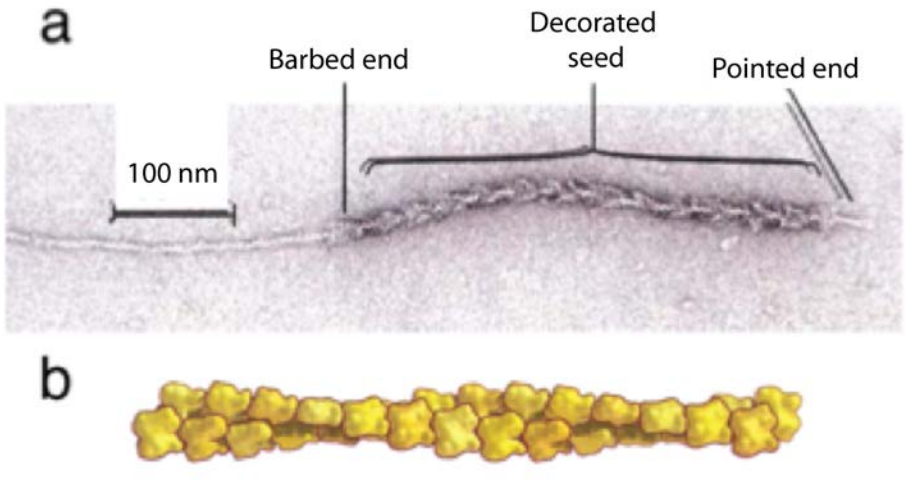

Figure 1 Actin filaments structure. (a) An actin filament decorated by myosin II heads reveals the structural polarity. Images were taken using electron microscopy (b) Schematic drawing of an actin filament, showing its double helix structure. Figure modified from Pollard and Earnshaw, 2002.

The barbed end of actin filaments has a rate constant of association (k_+), which is 10 times higher than the pointed end in the presence of free monomers (Figure 2) (Pollard,

1986). Quickly after their incorporation in the filament, the ATP nucleotide of the actin subunits hydrolyses into ADP, and the phosphate produced from this reaction is slowly released from the filament (Murakami et al., 2010). As a consequence, every actin subunit in an actin filament has a specific conformation and identity depending on whether it is bound to ATP, ADP-Pi or ADP.

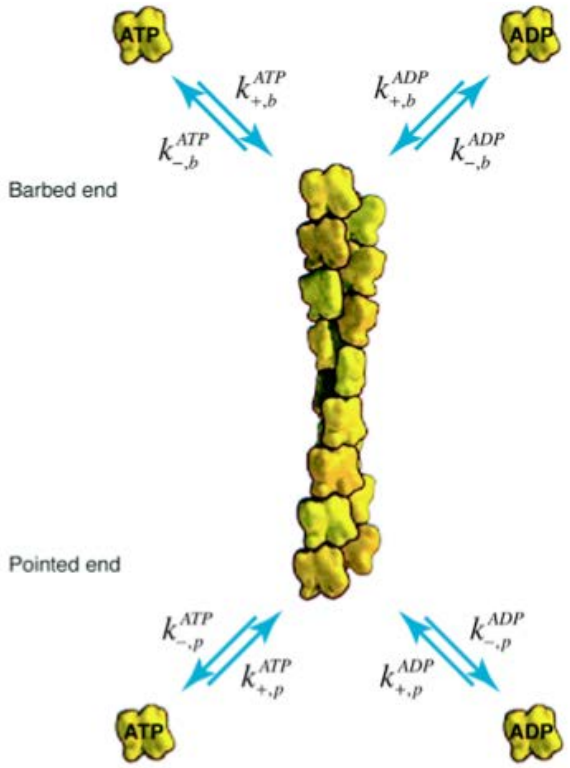

$k_{+,b}^{ATP}$	11.6 μM^{-1} s^{-1}
$k_{-,b}^{ATP}$	1.4 s^{-1}
$k_{+,b}^{ADP}$	3.8 μM^{-1} s^{-1}
$k_{-,b}^{ADP}$	7.2 s^{-1}

$k_{+,p}^{ATP}$	1.3 μM^{-1} s^{-1}
$k_{-,p}^{ATP}$	0.8 s^{-1}
$k_{+,p}^{ADP}$	0.16 μM^{-1} s^{-1}
$k_{-,p}^{ADP}$	0.26 s^{-1}

Figure 2 Association and dissociation rates constants of actin ADP and ATP at both ends of the actin filament (Pollard, 1986). Only the addition of ATP-actin subunits to the barbed end is fast and limited by diffusion (adapted from Pollard & Borisy 2003).

Figure 2 indicates the measured values of association and dissociation rate constants at both ends of the filament. For each end, their association and dissociation rate constants define their respective critical concentrations ($Cc=k_{-}/k_{+}$). Therefore, for barbed ends, Cc=, and for pointed ends, Cc=. When the concentration of actin monomers in solution exceeds the value of a critical concentration, actin monomers add at the corresponding end of the filament. On the contrary, when the concentration of actin monomers in solution stands below the value of a critical concentration, actin subunits dissociate from this end of the filament.

Overall, because critical concentrations are different at the two ends of the filament, actin filaments at steady state continuously polymerise actin subunits at their barbed ends, and

disassemble from their pointed ends. This *in vitro* artificial situation is called treadmilling (addition of subunits in an extremity and loss of subunits at the other extremity) (Wanger et al 1985) (Wegner, 1976).

Therefore, above the barbed end critical concentration, an *in vitro* polymerization of actin monomers follows a three step-kinetic reaction (Figure 3):

- In the first phase, called the nucleation step, actin monomers self assemble into thermodynamically unstable dimers and trimers. However, as soon as the actin oligomers exceed the size of a trimer, they adopt a thermodynamically stable helical conformation, and the polymerization reaction can occur at both ends of the actin filament. This first phase is the rate-limiting step of the polymerization reaction due to the low probability of assembling stable oligomers in solution.

- In the second phase, called the elongation step, the number of filaments formed in solution becomes high enough, so that the polymerization reaction of actin reaches progressively a maximal rate.

- In the third phase, called the equilibrium phase, the reaction reaches a stationary state, corresponding to the treadmilling reaction described above. Actin is in equilibrium between its two forms: monomeric and filamentous. Actin exists under its monomeric form in a concentration equal to the barbed ends critical concentration; the rest of the actin is under filamentous form.

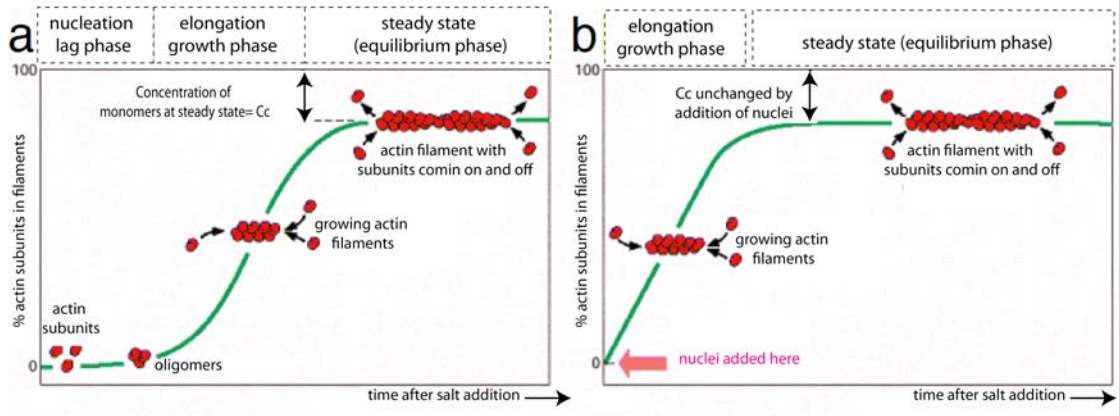

Figure 3: Schematic actin polymerization kinetics. (a) Polymerization is typically triggered by increasing the concentration of salt in the presence of actin subunits. (b) An alternative elongation assay, where actin seeds are introduced to act as nuclei for filament growth. (Adapted from Albert et al. 2002)).

I.1.2. Actin dynamics *in vivo*: a structure in motion

The situation *in vivo* is very different from what I have just described in the previous paragraph. *In vivo*, the ratio between the filamentous form and the monomeric form of actin has been estimated to vary between species, from 0.1 in plants (Staiger & Blanchoin, 2006), 0.3 in Xenopus eggs, to 200 and in yeast or amoebas (Pollard et al. 2000). However, we should be careful with these numbers which only represent estimations, and which may vary depending on where and how this ratio is measured.

Also, it is important to remind that actin does not have a fixed form (monomeric or filamentous), but is constantly in a dynamic equilibrium between these two forms. While the corresponding turnover rate is slow for the *in vitro* treadmilling reaction, it is much faster *in vivo*. This allows cells to quickly reorganize their cytoskeleton in response to a need or an extracellular signal. Living cells constantly disassemble aging parts of their actin cytoskeleton to re-polymerize it elsewhere where and when it is needed. This renewal is very fast, usually between a few seconds and minutes (Theriot & Mitchison, 1991; Wang, 1985).

To illustrate the cellular actin dynamics, I will take as an example the lamellipodium. The lamellipodium is a system that has been extensively studied because of its size, its fast dynamics, and for its importance in a large number of motile processes. In 1985, Wang injected labelled actin rhodamine into fibroblasts (Wang, 1985). The photobleaching of a small area in the lamellipodium (3-4 μm) allowed him to show that the actin cytoskeleton assembles quickly at proximity of the plasma membrane and then moves toward the centre of the cell at a rate of 0.79 microns/min (Wang, 1985). This was also the first study to propose that actin dynamics in the lamellipodia is, directly or via other molecular interactions, involved in the force required for the protrusion of the plasma membrane during motility (Wang, 1985). This model proposed that microfilaments elongation at the cell edge would push forward the plasma membrane, to extend directly the lamellipodia and subsequently induce cell movement.

To promote a fast turnover *in vivo*, fast actin assembly needs to be counterbalanced by a fast disassembly. In a following study, Theriot and Mitchison photoactivated newly assembled actin filaments within the lamellipodium of keratocytes (Figure 4). They observed that actin filaments were progressively relocated towards the cell body as the cell moved forward. Eventually, these filaments would disassemble in order to be recycled for a new polymerization cycle.

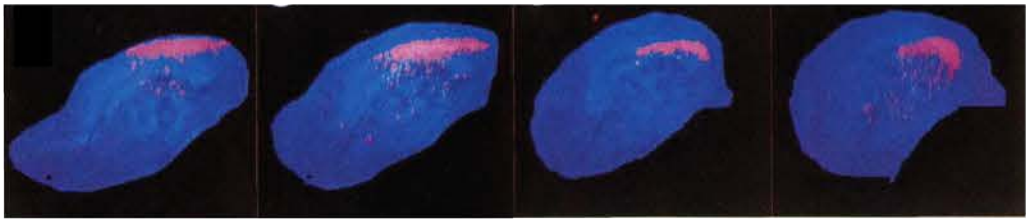

Figure 4: Actin filament retrograde flow in moving keratocytes. Activated area of Caged Resorufin-labelled actin (CR-actin: CRIA; in pink) in a moving keratocytes (in blue), at 40 seconds time intervals. (Adapted from Theriot and Mitchison, 1991).

Together, these observations indicated that in protrusive structures, most of the actin filaments were likely to be oriented with their barbed end towards the cell membrane, while their pointed ends were mainly directed towards the inner part of the cell (Symons et al., 1990). This result would be confirmed later in numerous studies by electron microscopy.

The situation *in vivo* is completely different from what happens *in vitro* in the presence of actin alone. The assumption of treadmilling at the scale of single actin filaments is far from being sufficient to explain the fast turnover of actin networks within the lamellipodium (Wang et al., 1985). *In vitro* the rate-limiting step of the treadmilling cycle comes from the rate of disassembly of actin subunits at the pointed end of filaments. A rapid calculation indicates that a $k_- = 0.26\ s^{-1}$ for ADP-actin subunit dissociation at pointed ends corresponds to an approximate 0.05 μm.min^{-1} possible turnover rate, which is 1 to 2 orders of magnitude lower than in cells.

In conclusion, one of the major challenges for the cell is to generate actin networks next to the membrane (or where a force needs to be applied), assemble them at a fast rate, while disassembling older networks at a fast rate to retain a sufficient pool of actin monomers.

I.1.3. Actin binding proteins

To overcome all the limitations described above, cells have a repertoire of accessory proteins involved in the modification of the actin cycle. Actin binding proteins (ABPs) can be classified according to their role in controlling the dynamics and organization of actin filaments (some ABPs can simultaneously control several aspects of this dynamic). ABPs can:

1) Bind to monomeric actin to control its level of assembly. This is essential to sustain a large pool of actin monomers.
2) Nucleate (or initiate) actin filaments. This is essential to overcome the nucleation-limiting step when the assembly of new filaments is required
3) Control the elongation rate of actin monomers at the barbed end of filaments
4) Disassemble actin filaments. This is essential for the recycling of aging actin structures
5) Organize and crosslink actin filaments in elaborate structures. This is essential to generate actin networks of appropriate geometry and mechanical properties.

Among the more than 60 families of proteins interacting with actin, we will focus on a subset of them, mostly the ones that are essential to understand the results and conclusions of my work. These proteins include profilin, capping protein, the Arp2/3 complex, ADF/cofilin and crosslinkers (α-Actinin, Fascin, Fimbrin, spectrin, filamin).

I.1.3.1. Description of the properties of ABPs of interest.

1. Profilin: How do cells maintain a pool of unpolymerized actin?

Profilin is abundant in most cell types, and interacts with the large pool of actin monomers (Pollard et al., 2000). Profilin is a small 14 kDa-protein, present in the cytoplasm at concentrations up to 100 μM. *In vivo,* actin monomers are principally bound to profilin. Profilin binds to the "barbed end" of the actin monomer (Schutt et al., 1993) (Schutt et al., 1993). It interacts more strongly with ATP-actin (Kd = 0.1-0.5 μM) than ADP-actin (Kd = 0.5-2 μM) (Vinson et al. 1998), and speeds up the exchange of the ADP nucleotide to an ATP nucleotide (Perelroizen et al., 1996, Blanchoin & Pollard, 1998, Vinson et al., 1998).
When actin monomers are binding to profilin, they can add onto free-barbed ends of actin filaments at the same rate than free actin monomers, but profilin does not remain bound to the actin subunit once it has incorporated the filament. The dissociation mechanism of profilin bound to actin subunits at the barbed end of actin filaments is controversial. One group showed that the dissociation of profilin is coupled with the hydrolysis of the actin nucleotide and the dissociation of the phosphate(Gutsche-Perelroizen et al., 1999; Perelroizen et al., 1996). This model implies that any filamentous actin polymerized in the presence of profilin, as is the case in the cell, has only ADP-actin. Conversely, another study with the physiological form of actin (MgATP-actin) showed that the

dissociation of the profilin is not coupled with the hydrolysis of the nucleotide (Blanchoin et al. 2000), and must be based on a change of conformation of actin subunits after their association into the filament.

Profilin-actin monomers can no longer add to the pointed ends of actin filaments (Thomas D Pollard & Cooper, 1984). In addition, the presence of profilin totally inhibits the formation of thermodynamically stable oligomers. Therefore, profilin totally prevents spontaneous nucleation of actin filaments in cells. Another fundamental property of profilin is to interact with proteins containing poly-proline rich domains, such as WASP or formins. *In vitro*, profilin interacts optimally with sequences of ten successive prolines (Kd ≈10-50 μM) (Perelroizen, Marchand, Blanchoin, Didry, & Carlier, 1994; Petrella, Machesky, Kaiser, & Pollard, 1996).

2. Capping protein: How do cells control actin networks elongation?

As we have just seen, the presence of profilin does not allow eukaryotic cells to maintain a high concentration of monomeric actin, since it allows the addition of actin monomers to any free barbed end of actin filament present in cells. To limit the fast depletion of the monomeric actin pool bound to profilin, several families of proteins are present in cells to limit the elongation of actin filament barbed ends (Rogers et al., 2003; Schafer & Cooper, 1995). *In vivo*, most of the growing barbed ends are rapidly blocked to prevent any unproductive elongation away from the target. This mechanism limits the length of actin filaments and the amount of actin monomers used to build a specific actin organization (Rogers et al., 2003).

There are several families of proteins interacting to the barbed ends with a strong affinity. First, capping proteins are α/β heterodimers with an α subunit of 32-36 kDa and a β subunit of 28-32 kDa. Capping proteins interact with barbed ends with a high affinity in the nM range. *In vivo*, high concentrations of capping proteins (in the μM range in vertebrates (Cooper and Schafer, 2000)) are present in cells. Their activity is regulated directly or indirectly by numerous factors. For example, at the membrane, the presence of phosphatidylinositol (4,5)-biphosphate (PtIns [4,5] P2) is reported as an inhibitor of capping proteins, in order to allow actin polymerization near the membrane (Iwasa & Mullins, 2007; Schafer et al., 1996).

Several other families of proteins can cap actin filament barbed ends, including gelsolin and villin. The sequence of these two proteins revealed the presence of six homologous domains of 100 to 120 amino acids, called gelsolin-like domains (Burtnick et al., 1997).

In addition to these six domains, villin has an extra domain in its C-terminal region called the villin headpiece, responsible for a Ca^{2+}-dependent actin filament crosslinking into parallel bundles (Kinosian et al., 1998; Kumar et al., 2004). These two protein families have the additional ability to bind to the side of actin filaments with a high affinity and to fragment them (Way et al., 1989).

3.Actin nucleation factors: How do cells generate new filaments?

To enable the controlled polymerization of actin filaments, eukaryotic cells must spatially and temporally control the use of the pool of monomeric actin. The spontaneous formation of new filaments is limited in the cell, since most of actin monomers are in complex with profilin. Therefore, the initiation of new actin filaments can only be done by 3 alternative ways: 1/ by the severing of a pre-existing filament 2/ by the uncapping of a capped filament, or 3 / by the nucleation of a new actin filament by specific factors called nucleation factors.

During my PhD, I used one highly conserved family of nucleation factors: the Arp2/3 complex.

The Arp2/3 complex is involved in numerous cellular processes including cell motility or endocytosis. It allows for the nucleation of actin filaments from the side of pre-existing filaments at a 70°-angle from the mother filament (Figure 6). This property leads to the progressive formation of branched actin networks, also called dendritic networks. Newly formed filaments elongate spontaneously from their free barbed ends (Blanchoin et al, 2000; Machesky & Gould 1999; Marchand et al. 2001). All subunits in the complex bind to the side of the mother filament (Rouiller et al., 2008). The binding affinity is higher for ATP subunits in the mother filament, making the initiation of new branch more likely to occur near the growing barbed ends (Ichetovkin et al., 2002). Overall, branched networks can become dense arrays of actin filaments able to resist to mechanical constraints, or to produce high levels of forces against loads.

The complex is constituted of the assembly of 7 polypeptides. It contains two main subunits, Arp2 and Arp3, which have three-dimensional structures very close to actin monomers (Robinson et al., 2001). Their role is to mimic an actin dimer from which new subunits will be able to add onto. The 5 other subunits are called ARPC1 to ARPC5. The complex can have an active or an inactive conformation in which it has a low nucleation

activity. The activation of the complex is triggered by other families of proteins called nucleation-promoting factors (NPF). The protein ActA, localized at the surface of the motile bacterium Listeria monocytogenes, was the first identified activator of the Arp2/3 complex (Welch et al., 1998). Listeria monocytogenes uses the Arp2/3 to infect cells of the intestinal endothelium by hijacking the actin polymerization cellular machinery to promote their propulsion in the host cell cytoplasm. In eukaryotes, the two first NPFs to be identified were the Wiskott-Aldrich syndrome protein (WASp) and the suppressor of cAMP receptor (Scar). Nucleation promoting factors have three common domains (Figure 5). The domain "WASP-homology-2" (WH2), which corresponds to a α-helix, recruits actin monomers (Chereau et al., 2005). The connector (C) domain and the acidic region (A) recruit and activate the Arp2/3 complex (Machesky & Gould, 1999; Marchand et al., 2001). NPFs are multi-modular proteins, which are constitutively inactive *in vivo*. Indeed, their folding engages the C-terminal region with the N-terminal region in a relatively stable interaction. Signalling proteins such as Rac interact and activate NPFs, by inducing a conformational change, which exposes their C-terminal regions (Rohatgi et al., 1999). In my projects, I have simply used short constructs of these proteins, which contain the activating domains of the Arp2/3 complex.

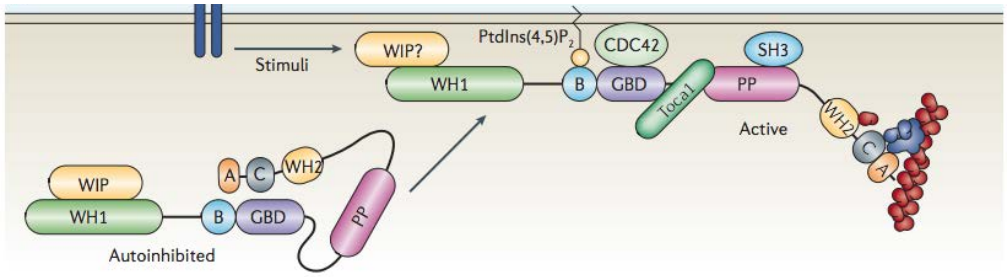

Figure 5 Regulation of WASP signals for Arp2/3 activation. WASP and N-WASP exist in an autoinhibited conformation in which intramolecular interactions between the GTPase-binding domain (GBD) and the central (C) region hide the regions WASP-interacting protein (WIP) with WASP and N-WASP through the WASP-homology-1 (WH1) domains and modulate activation. Some interaction are involved in the regulation of this autoinhibition (binding of the lipid second messenger to the basic (B) region; the binding of GTP-loaded CDC42 to the GBD region, and the binding of Src-homology-3 (SH3) -domain to the poly-proline (PP) region). Those are the main steps to promote ARP2/3 complex activation (adapted from Goley and Welch, 2006)

While the nucleation of branched actin filament networks by the Arp2/3 complex requires the presence of NPFs and actin monomers, it also requires the presence of a precursor microfilament called a “primer”. The function of the primer is to provide the first mother filament, acting as a substrate for the creation of branches and the progressive development of the network.

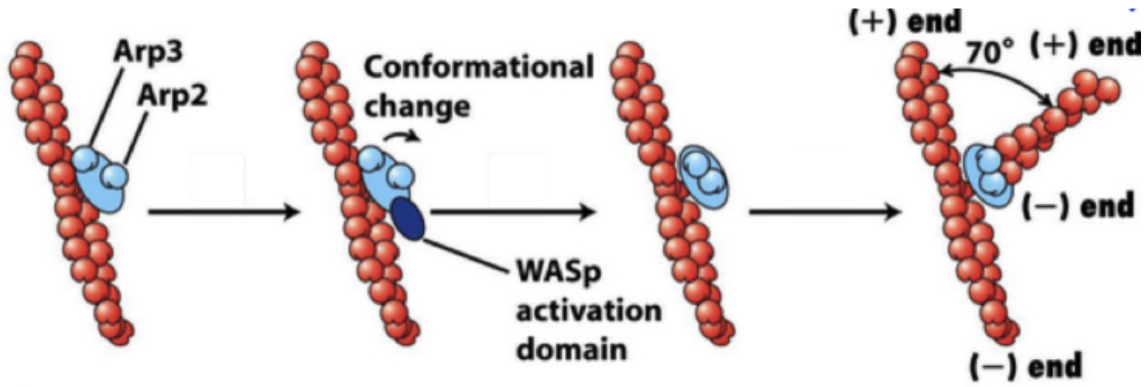

Figure 6 Branch nucleation by Arp2/3 complex. NPFs change the conformation of Arp2/3 complex and gather it and actin monomers to nucleate new branches (of 70°) from the side of pre-existing filaments. Arp2/3 complex remains at the minus end of the filament (adapted from Lodish et al. 2000)

Hence, the nucleation reaction triggered by the Arp2/3 complex is a multi-molecular reaction, which requires the simultaneous presence of 4 components: the Arp2/3 complex, actin monomers, a nucleation promoting factor and a "primer filament". In the presence of a nucleation factor, actin monomers and Arp2/3 only, this reaction is auto-catalytic, because the progressive generation of new filaments is fuelling the reaction.

4. Disassembly factors: How do cells recycle actin subunits?

The main protein involved in disassembling actin filaments *in vivo* is ADF/cofilin. ADF/cofilin is extremely well conserved among eukaryotes and is essential. ADF/cofilin was discovered from brain extracts in 1980 (Bamburg et al., 1980) and its function was progressively unveiled through biochemical and genetic studies.

ADF/cofilin binds to both actin monomers and actin filaments with affinities in the 100 nM to μM range. The binding of ADF/cofilin along actin filaments is highly cooperative, meaning that the binding of one ADF/cofilin to an actin subunit will strongly influence the binding of the subsequent ones to the neighbouring actin subunits. The mechanism of action of ADF/cofilin has remained controversial for a long time, but today, a general

consensus seems to be accepted in the community to describe ADF/cofilin as a severing protein. ADF/cofilin binds with a stronger affinity to ADP subunits than ADP-Pi or ATP subunits inside the filaments (Blanchoin and Pollard 1999; Mabuchi 1983). Thus, it severs preferentially older parts of the filament. This is a key regulation aspect for actin disassembly, as cells need to recycle specifically aging parts of its cytoskeleton. In addition, the binding of ADF/cofilin increases the rate of phosphate dissociation from actin subunits, making actin filament aging from ATP to ADP faster (Blanchoin & Pollard 1999). ADF/cofilin always excludes the actin filaments "ATP" growing barbed end from decoration.

The efficiency of ADF/cofilin's fragmentation is highly dependent on its level of saturation along the actin filament (Andrianantoandro and Pollard 2006; Elam et al. 2013; De La Cruz 2009). Indeed, when ADF/cofilin's binding density to the filament is low, its fragmentation efficiency will increase with increasing ADF/cofilin binding, until reaching a saturation level (Figure 7A). Single molecule observations have determined that fragmentation indeed occurs at an optimal of 23 molecules along an actin filament, which corresponds roughly to one pitch of the helix. Above this threshold density, the filament is highly decorated by ADF/cofilin and the severing is reduced.

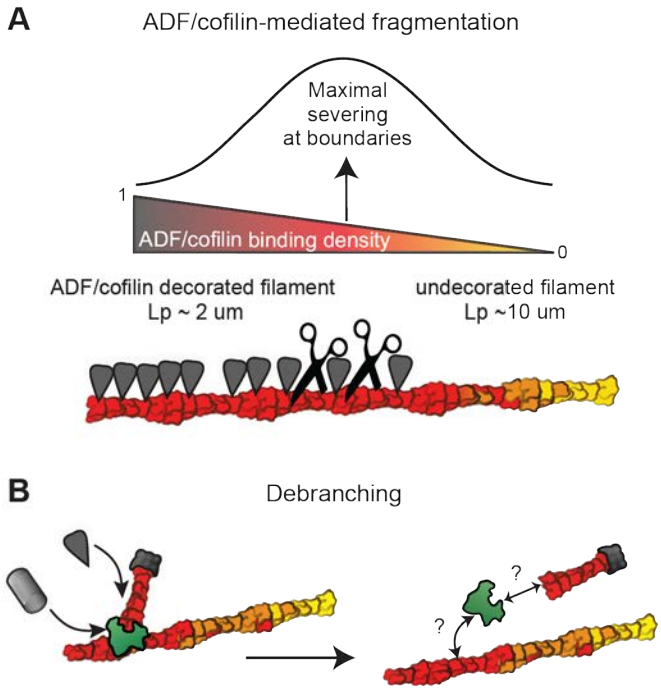

Figure 7 ADF cofilin functions. A: Actin filament persistence length decreases when ADF-cofilin binds to it. The fragmentation of the actin filaments happens at the boundary of ADF-decorated and non-decorated portions of the filament, (due to the difference in the persistence length). B: disassembly by ADF/cofilin can also occur by of the Arp2/3 complex debranching network (adapted from Blanchoin et al. 2014).

How can these observations be reconciled? In fact, it was shown that ADF/cofilin binding to actin filaments has important consequences on the structure of actin filaments, which adopt a different conformation. In particular, ADF/cofilin decreases the persistence length of actin filaments fivefold, down to a persistence length of 2 μm (Figure 7A, McCullough et al. 2008). This suggests a tight relationship between biochemistry and mechanics. From these observations, a model has emerged to explain fragmentation by ADF/cofilin based on local stress accumulation at mechanical discontinuities, i.e., at boundaries of bare and ADF/cofilin-decorated filament segments (Figure 7A) (De La Cruz 2009; McCullough et al. 2011). Direct observation with evanescent wave microscopy confirmed this interaction model of ADF/cofilin with actin filaments, which demonstrates that fragmentation occurs at the boundary (Breitsprecher et al., 2011; Gressin et al., 2015; Suarez et al., 2015).

In vitro, generated fragments are able to polymerize, justifying the necessity of other factors such as capping protein to cooperate and limit the elongation of the newly formed fragments. However, even in the presence of capping protein, ADF/cofilin by itself is still not able to promote the disassembly of actin filaments from their pointed ends, and does not modify importantly the critical concentration of actin assembly. To understand why ADF/cofilin is so important in disassembling actin networks *in vivo*, our community has been putting a lot of efforts to identify additional collaborative factors such as Aip1. It is still unclear by which mechanism ADF/cofilin and Aip1 are able to disassemble actin, but they can together disassemble actin filaments *in vitro* at rates comparable to *in vivo*.
Additionally to its severing effect, ADF/cofilin has a debranching effect on branched actin networks. In fact, ADF/cofilin will not only severs actin filament daughter generated by the Arp2/3 complex, but will also dissociate the branch (Figure 7B). The mechanism of branch dissociation is not fully understood, but a combination of dissociation of the Arp2/3 complex from the mother filament and/or from the pointed end of the daughter filaments has been proposed (Blanchoin et al. 2000; Chan et al. 2009; Mahaffy and Pollard 2006). This mechanism is important for branched networks, as dense networks can be dismantled and disappear, even without the disassembly of the individual small filaments.

Here, I presented the ADF/cofilin as a protein that disassembles actin filament, but as you will see later, I also used it during my PhD as a modulator of connectivity.

5. Crosslinkers: How do cells create cohesion between actin filaments?

In cells, actin filaments are not found as disorganized meshwork, but are organized collectively in specific architectures. In addition to the Arp2/3 complex, various additional families of proteins provide possibilities for the cells to organize actin networks spatially and temporally. Among these proteins are families of crosslinking proteins, which are capable of binding simultaneously to the side of two actin filaments. The binding of crosslinkers creates a bridge between filaments, and multiple bridges allows for the organization of multiple actin filaments into connected networks. A consequence of this organization process is that the rheological properties of these networks are very different from those of pure actin filaments (Gardel et al., 2004; Shin et al., 2004; Tseng et al., 2001). Actin bundles are usually thicker and stiffer than individual actin filaments.

Actin crosslinkers are classified in two families. Some crosslinkers can form actin filaments bundles, where actin filaments have the same orientation. If bundled actin filaments have a similar orientation, they are called parallel bundles. If their orientation is random, they are called antiparallel bundles. Other crosslinkers can simply form connected meshworks, where actin filaments have different orientations. The geometrical organization of actin filaments within actin networks depends on the respective position of the actin binding domains of the crosslinkers (Figure 8; Revenu et al. 2004), but also depends highly of the binding density of the crosslinkers. For example, some crosslinkers like α-actinin can assemble actin filaments into connected networks at low binding densities, and into bundles at higher binding densities (Wachsstock et al. 1993).

The principal crosslinking proteins known to form bundles of actin filaments are α-actinin, fascin, fimbrin, and villin. Fascin and fimbrin are monomers, which form compact actin cables (Bretscher & Weber, 1980; Yamashiro-Matsumura & Matsumura, 1986). For example, fascin is present in the filopodia, where tightly crosslinked parallel bundles provide the rigidity, which is needed to overcome the resistive force of the plasma membrane. On the contrary, the protein α-actinin is dimeric, and the two actin binding domains stand further away from each other because they are separated by a helical spacer region of 40 nm-long (Revenu et al 2004). The bundles are less dense, and are anti-parallel in the case of α-actinin.

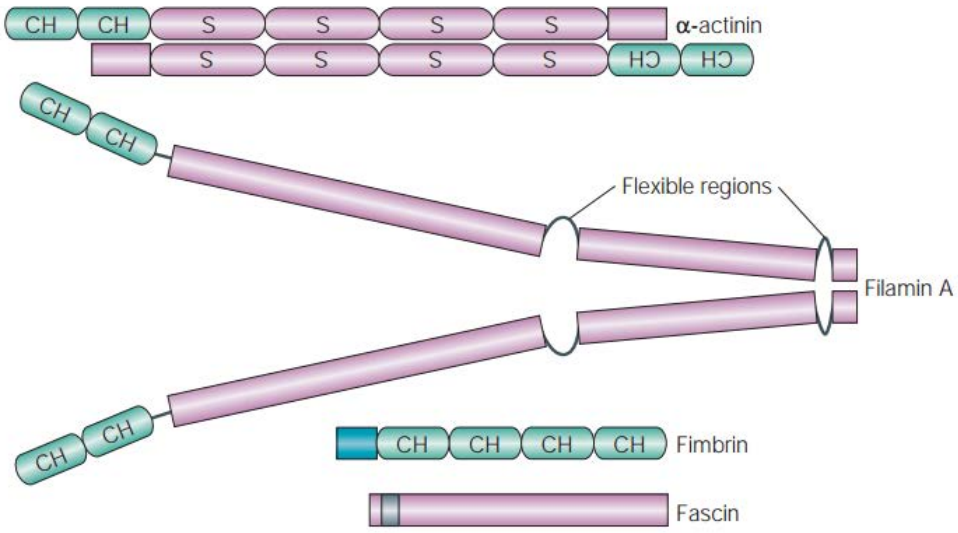

Figure 8 Four crosslinkers structures (α-actinin, filamin A, fimbrin and Fascin). Actin Binding Domains (ABD) of the first three crosslinkers are calponin-homology domains (CH). The fascin contains only one ABD. (Revenu et al. 2004)

Crosslinkers give the cytoskeleton its ability to combine 1/structural integrity, 2/ mechanical stability, and 3/ the possibility of fast network rearrangement and restructuring. The molecular properties of each crosslinkers define the structure of the network, its viscoelastic properties and its dynamical properties (Table 1).

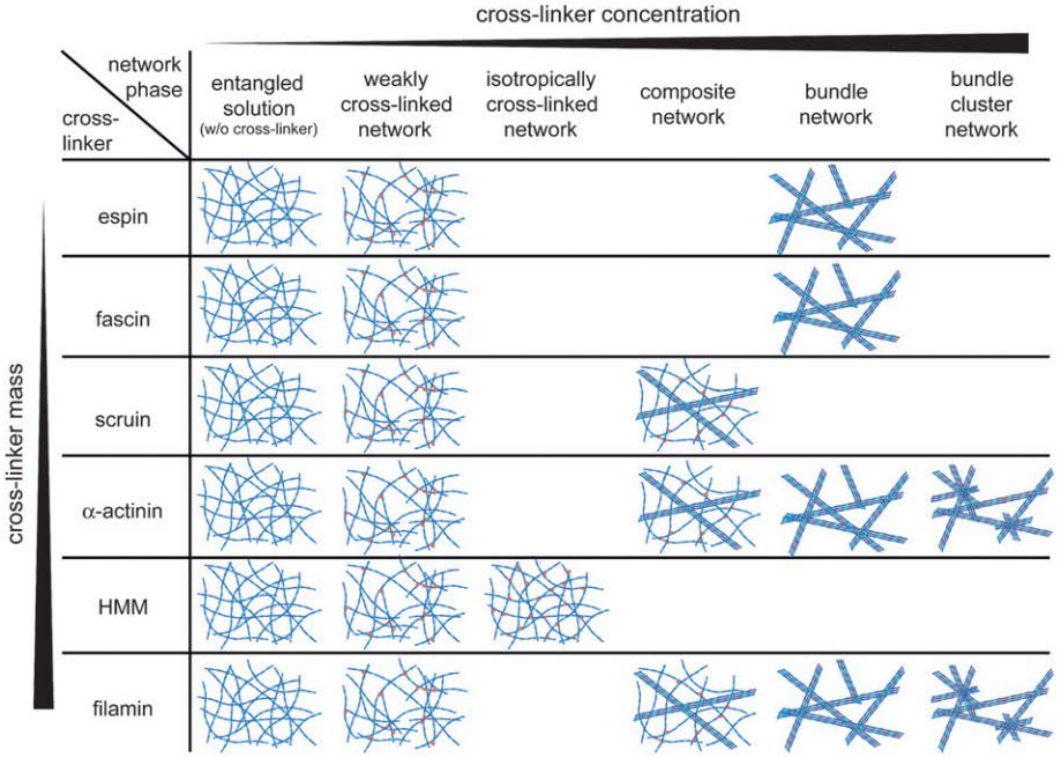

Tableau 1 Summary of actin networks structure/ phase difference. Crosslinked actin network architecture is detailed according the type and the concentration of crosslinkers (Lieleg et al. 2010)

Applying a force to actin networks can give crosslinkers an opportunity to redistribute. In this case, the global shape of the network changes irreversibly and keeps its new conformation even when the force is released (Xu et al., 1998). This behaviour is usually highly dependent of the time scale of the force application. The force has to be applied for a long enough time to allow crosslinker reorganization. If the force is applied for a too short time, crosslinkers resist against the load. The network finally returns to its original shape once the force disappear, which is characteristic of an elastic material (Xu et al., 1998).

In general cases, the structure of crosslinked networks is a mixture of bundles and entangled networks. Their response to external forces is not a linear viscoelastic response, since the different actin architectures respond differently (Nakamura et al., 2002). Therefore, a better comprehension of the actin architecture is crucial to understand the relationship between actin organization, level of crosslinking and mechanical response. All this will be more developed in my second project presented in this manuscript.

I.2. Myosin

I.2.1. Myosin family

Among the proteins that bind to actin filaments, myosins are considered as motors because they consume energy. Motors possess the ability to convert chemical into mechanical energy, by hydrolysing the ATP bound to their active site. In this part of the thesis, I will detail the most important parameters related to myosins.

The wide variety of myosin genes found throughout the eukaryotic phyla was named as they were discovered.

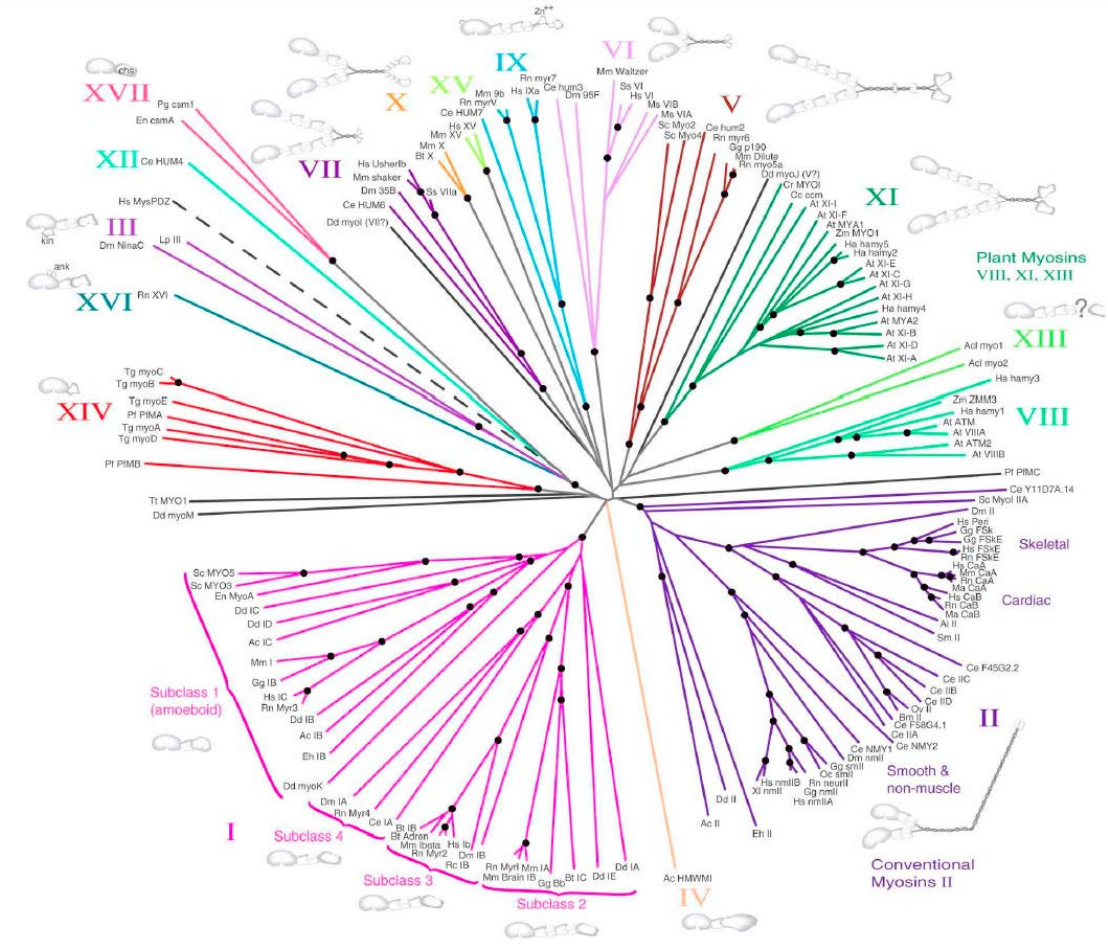

Figure 9 The Myosin Tree. (Hodge & Cope, 2000)

Different analyses were done to obtain the phylogenetic tree of myosins, which is eventually based on a comparison of their motor domain sequences. This tree divides myosins into seventeen classes (Figure 9). As for the tail domains, analysis of the amino

acid sequences of different myosins demonstrates a huge variability. This is presumably due to the myosin tail interaction with a variety and large number of cargoes, while the interaction with the actin filaments remains the same and therefore requires the same machinery in the motor.

I.2.2.Structures and domains

All myosins are composed of three different domains: head, neck and tail domains.

The head domain is the motor domain. It binds to actin filaments and uses chemical energy to walk along the filaments and generate forces.

Crystallographic studies have shown that the neck domain undergoes a rotational movement during the transition from low to strong binding to the filament, thus the neck domain acts as a lever arm for transducing the force generated by the catalytic motor domain. The neck gives also to the molecular motor some flexibility.

The tail domain insures the myosin interaction with cargoes and/or other myosin subunits. In some cases, the tail domain may play a role in regulating the motor activity.

In strong denaturing solutions, myosin dissociates into six polypeptide chains: two heavy chains and four (two identical pairs) light chains. The two heavy chains are wrapped around each other to form 150 nm long coiled-coil rods of α-helices i.e. for the myosin II to form a double helical structure. At one end both chains are folded into separate globular structures to form the two heads. Each head is associated with a pair of light chains (Figure 10). Each pair consists of an “essential light chain” and a “regulatory light chain” that is the substrate for several kinases, which regulate myosin's activity (Toyoshima et al., 1987).

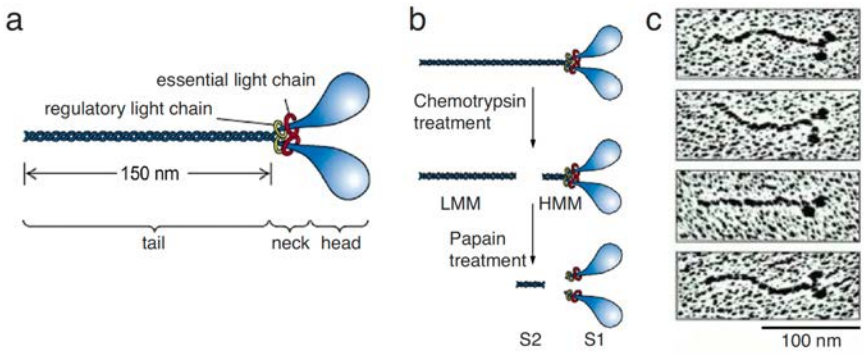

Figure 10 Myosin II molecule. (a) Schematic representation of a myosin. (b) A myosin molecule can be split up into Heavy Meromyosin (HMM) that is still an active ATPase and Light Meromyosin (LMM). HMM can be also divided into subfragments S1 and S2, (only S1 is an ATPase) (c) Electron micrographs of myosin II. Figures adapted from Alberts et al. (2002).

I.2.3. Mechanism of molecular motor

Myosins are biological molecular motors. They bind to actin filaments and use the energy derived from repeated cycles of ATP hydrolysis to produce a sufficient mechanical energy to their displacement along this molecular rail (actin filaments). Within a cell, three main functions are based on the action of myosins. Myosins can act (1) as an engine of contraction (2) as a particle carrier or molecular cargo (3) as a mechano-sensitive link between the cytoskeleton and another structure (such as a membrane or focal adhesion points).

We can distinguish two types of myosins: conventional myosins forming spontaneously bipolar assemblies via their homo-oligomerisation (for example myosin II) and unconventional myosins. Unconventional myosins are not capable of large oligomerisation, but some can dimerize (for example myosins V and VI) to form double-headed myosins. Double-headed myosins can walk processively along actin filaments.

When a myosin is bound to ATP, the head remains unbound from the actin filament. The interaction between the myosin head and the actin filament is correlated with the hydrolysis of the ATP (Figure11). Therefore, within the myosin ATP cycle, the myosin affinity to the actin filament depends on the nucleotide (in a simplified manner, ATP = weak bond, ADP = strong bond). The force generation or the power stroke (called also "lever arm swing") is related to the phosphate dissociation.

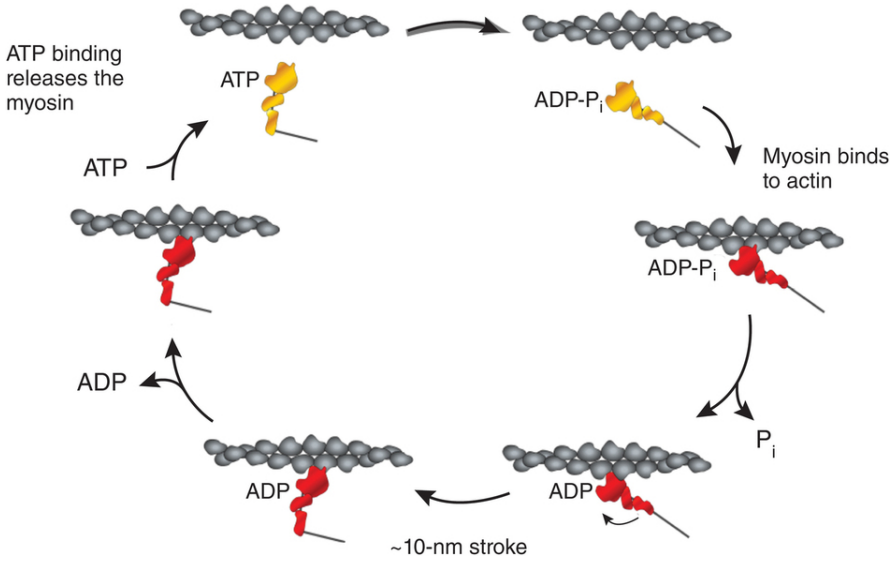

Figure 11 The myosin chemomechanical cycle adapted from Lymn 1971. A mechanical stroke only occurs when the myosin is strongly bound to actin. ADP-Pi. ADP and inorganic phosphate, remain bound to the active site until actin binds to the myosin (Spudich, 2012).

If all myosins generally follow a similar kinetic cycle, transition rates between different states are highly variable. The time that myosins remain in a strongly bound state to the filament, called the rigor state, is also variable. The relative time occupancy between the rigor state and the dissociation of the filament is called the duty ratio. A high duty ratio reflects a long residence time on the actin filament, which gives double-headed myosins the property of being processive: having the ability to perform multiple cycles by advancing a step ahead of the other on the same filament. So for a high duty ratio, the probability that the two heads unbind the filament simultaneously is very low.

In general, the rate at which myosin moves along an actin filament depends on three parameters: the displacement per ATP cycle (d), the duty ratio (f) and the total time of the ATPase cycle (enabled by binding with actin). V = d*kATPase/f. An independent measurement of these three parameters leads mostly to a good estimate of the speed of movement. However, for some myosins, the measurement of their rates reveals a wide range depending on experimental conditions. This indicates that some myosins have their rates regulated to perform various cellular functions. For example, myosins Myosin VI and Myosin V accomplish both transport and anchoring functions according to the environment in which they are located. In addition to a biochemical control, the activity of various myosins can also be regulated by the architecture of the interacting actin network (Brawley & Rock, 2009; Nagy et al., 2008). However, it is largely unkown how parameters such as actin organization, density, polarity, and the presence of crosslinking proteins within a cell could serve as a regulator of the activity of molecular motors.

The processivity of a myosin may also be increased through effective long-range communication between the two heads of the same myosin, a process called gating (De La Cruz et al. 2001; Robblee et al. 2004; Veigel et al. 2002). The structural basis for the gating mechanism is not fully understood, but could be based on an intramolecular stress (estimated at around 2 pN) that develops between the two heads. This stress could block the first myosin head in a bound state (either by inhibition of ADP dissociation or by inhibition of the ATP association) until the next head rebinds to the filament. The steps involving the movement of myosin are also sensitive to the load carried by the myosin, which gives these molecular motors the property to be mechanically sensitive (Purcell et al. 2005; Watanabe et al. 2010). Indeed, the presence of increasing loads inhibits ADP dissociation since it is coupled to the movement of the lever arm, thereby increasing the "duty ratio" of myosins.

Our understanding of myosins properties has greatly improved as imaging techniques were developed. Originally, evanescent wave microscopy offered the first possibilities to measure myosins run length properties along individual actin filaments. This fluorescence imaging technique was later coupled with additional tools such as super-resolution imaging or optical tweezers to the study the processivity mechanism and the force-velocity relationship (Dunn, Chuan, Bryant, & Spudich, 2010; Oguchi et al., 2010). Other imaging techniques that led to improved observations include $(TR)^2$FRET ("transient time-resolved FRET"). This technique relies on an adequate fluorescence labelling of the two-myosin heads. With the addition of ATP, the inter-probe distance is quickly measured using FRET (Figure 12). $(TR)^2$FRET offers a best resolution in space and time, and has allowed direct visualization of the transitional states of myosin II, with the kinetics of biochemical transitions (Nesmelov et al., 2011).

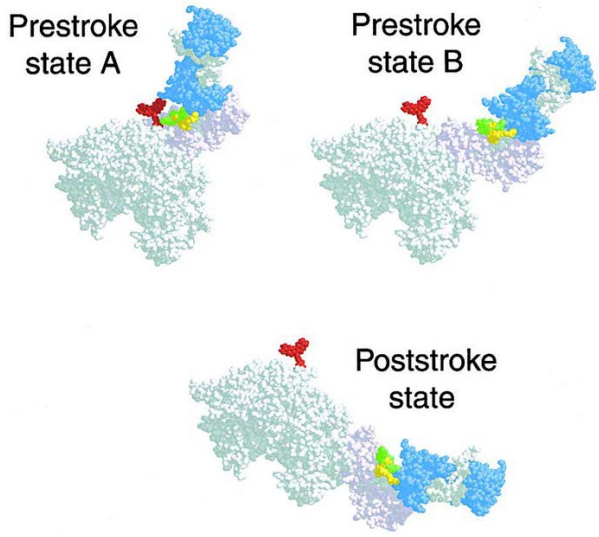

Figure 12 View of myosin-II S1 with three proposed lever arm angles. Parts of the myosin were labelled, and the distance between the donor and acceptor dyes was controlled. Images were taking using the technic FRET (Shih W et al., 2000).

Recently, the use of high-speed atomic force microscopy (AFM) allowed for the real time visualization of a myosin race on an actin filament (Figure 13). To this day, this way of imaging confirmed various properties related to myosin V, including a processive walking with a step of 36 nm (Kodera et al., 2010). The advantage of AFM is that we can now expect in the future to correlate the structural properties of myosins with their binding state to actin filaments.

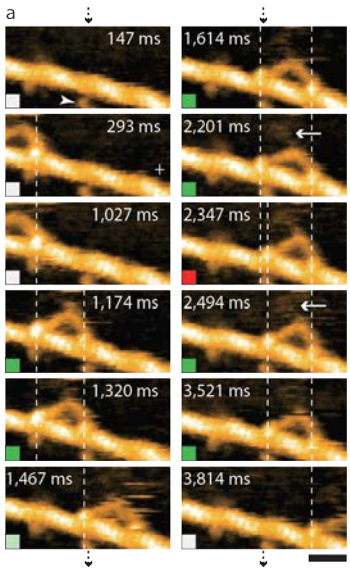

Figure 13 Kinetics of myosin V walking on a actin filaments observed by AFM (Atomic Force Microscopy). (a) The dotted lines reflect the attachment between myosin head and actin filaments. The arrowhead indicates a streptavidin molecule stabilizing actin filament interaction with the surface (picture 147 ms). Scale bar = 30 nm (Kodera et al., 2010)

The enormous advances in recent years of our imaging technologies gradually changed our comprehension of myosin motors.

1.2.4. A comparison between myosin VI and other myosins

In this paragraph, I will describe more precisely the peculiarities of myosin VI, which I mainly used during my thesis.

Myosin VI is involved in a wide range of cellular processes, including cell migration (in particular of certain cancer cell lines), maintenance of cell-cell contacts (Maddugoda et al., 2007), Golgi maintenance or contraction of stereocilia of the inner ear (Sahlender et al., 2005; Warner et al., 2003). Furthermore, it was shown that two pathologies, deafness and cardiomyopathy, are linked to mutations of myosin VI (Avraham et al., 1995; Hertzano et al., 2008).

For many cellular functions, in particular during cargo transport, the processive ability of myosins to move along actin filaments for a long distance without dissociation from their track is essential. Indeed, a long-term interaction with the same actin filament increases the efficiency of directed force production. In addition, the number of binding cycles of myosin with actin filaments without dissociation increases the efficiency of the anchor or the phenomenon of contraction with a minimal number of myosins. Two types of

processive myosins have been extensively studied, myosin V and myosin VI. Their mode of interaction with the actin filament is similar, even if the directionality of these two myosins along the filament is opposite. Indeed, myosin VI is the only myosin walking towards the minus end of actin filaments (Figure 14).

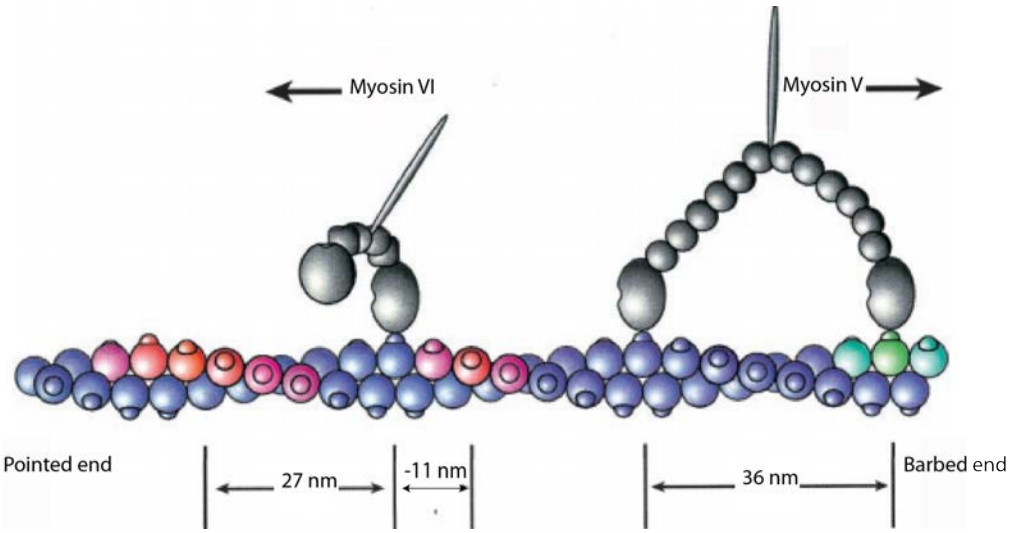

Figure 14 Model of Myosin VI and Myosin V stepping. Myosin V and VI molecules are shown in gray, and the actin filament is shown in blue. Colors corresponds to the monomers that will be bind by myosin heads (Rock et al., 2001)

When, we compare the non-conventional Myosin VI properties with conventional myosin II ("skeletal and smooth muscle myosin"), it appears that Myosin II has a duty ratio of approximately 0.05. As a consequence each myosin head remains attached to the actin filament for 10 to 20% of its cycle. Clearly, it is optimum for the contraction of the muscular tissue in which the myosin myofilaments are organized and where many myosin heads interact simultaneously with the same actin filament to produce a fast contraction. The heads must quickly interact and dissociate from actin filaments to avoid the disruption the displacement of actin by the other myosin heads. In contrast, myosin VI uses its high duty ratio of 0.8, to maintain a continuous interaction with the same actin filament (myosin stays attached to actin filaments during 90% of the cycle). This is why myosin VI is particularly adapted to long-distance transport. Indeed, a dimer of myosin VI can move *in vitro* over distances up to 200 nm without detaching. Furthermore, it was suggested that a dimer of myosin VI had the ability to maintain the catalytic cycles of its two heads in opposite phases, which facilitates processivity (Dunn et al., 2010; Elting et al. 2011). The processivity of myosin VI may be finely regulated by the load exerted on it, making it a robust mechano-sensitive motor (Altman et al. 2004; Chuan et al.).

According to those studies, myosin VI could be an effective carrier for loads up to 2 pN but could also act as an anchor on cytoskeletal elements for higher loads.

For the purpose of my thesis, I did use myosin VI as a myosin that can exert forces on actin organization without the need of self-assembly in higher organization. Indeed, to obtain a similar duty ratio of 0.8, we need two heads of myosin VI, 15 heads of myosin 2A or 150 heads of muscle myosin. Myosin VI therefore represents a very simple model system to study actin-based contractile mechanisms.

1.2.5. Myosin engineering

It is more and more common to use engineering to built motors with specific properties. This approach represents a very interesting way to generate biomimetic systems, and really challenges our understanding of the mechanism of these molecular engines.

The possibility to engineer molecular motors with well-controlled properties brings a new dimension to this field. For example, in 2012, Chen and collaborators (Chen et al., 2012) engineered myosin VI motors with artificial lever arm structures derived from α-actinin. These artificial myosin motors can have their direction of motion reversibly switched in response to a calcium signal. Another very interesting molecule, designed by a group from the Stanford University (Bryant Lab), relies on the idea of developing engineered motors specifically amenable for long-range transport on actin filaments. Controlling in real time the property of motors could be a key step in understanding cell mechanics at the molecular level. There is also the possibility of using tunable motors outside of biology, for example in diagnostic devices.

To obtain a precise and simple control over molecular motion, Nakamura and colleagues in 2014 (Nakamura et al. 2014) sought to create autonomous genetically encoded motors that can be specifically and reversibly switched between functional states using a spatially restricted light signal (Figure 15). When exposed to light, the new protein motors change direction or change speed. With the appropriate spatial and temporal control of the light, it is possible to obtain a perfect control over the motor.

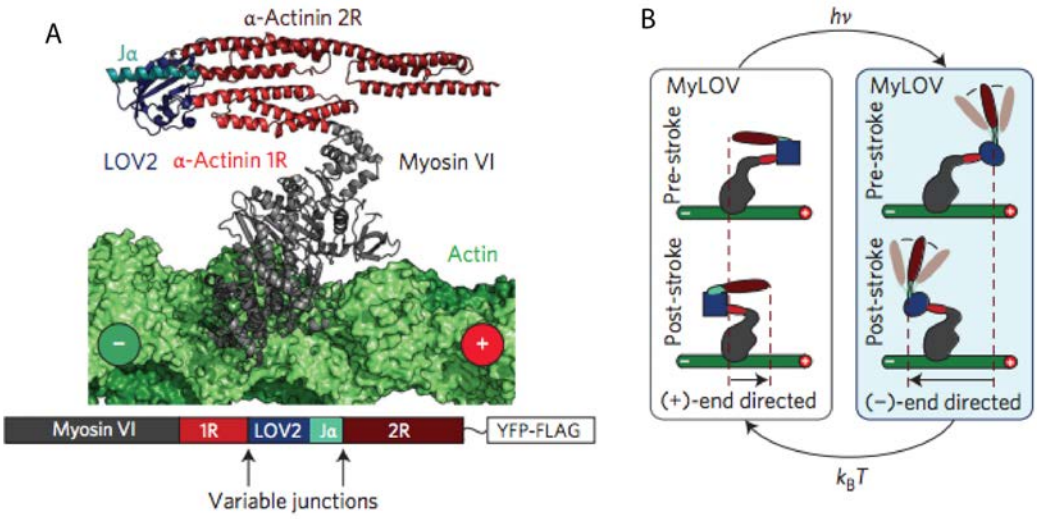

Figure 15. Myosin VI motors with artificial lever arm structures (A) The MyLOV design shown in the post-stroke state, with labels indicating the structures and the modelled actin filament. A block diagram (below) indicates which junction regions were varied in different MyLOV constructs. (B) Schematic draw of the MyLOV switching mechanism. When the molecule is in the dark (left), the lever arm is rigid and the tip of the lever arm moves toward the plus end of the actin filament during the power stroke. When the molecule is exposed to blue light (right), the LOV2 domain change its conformation and the C-terminal portion of the lever arm don't contribute to the mechanical stroke, resulting in minus end-directed motion (Nakamura et al. 2014).

In another study, Schindler and al 2013 improved the processivity of engineered motors by designing a serie of constructs based on myosin VI. They generated dimeric, trimeric and tetrameric motors with flexible elements between heads. They used single-fluorophore tracking to quantify the processivity of the engineered constructs (Figure 16). These highly processive motors can reach a speed of 10 μm.s^{-1}, making possible to correlate processivity with speed. With this basic system, they could establish very simple rules on how processivity could be enhanced.

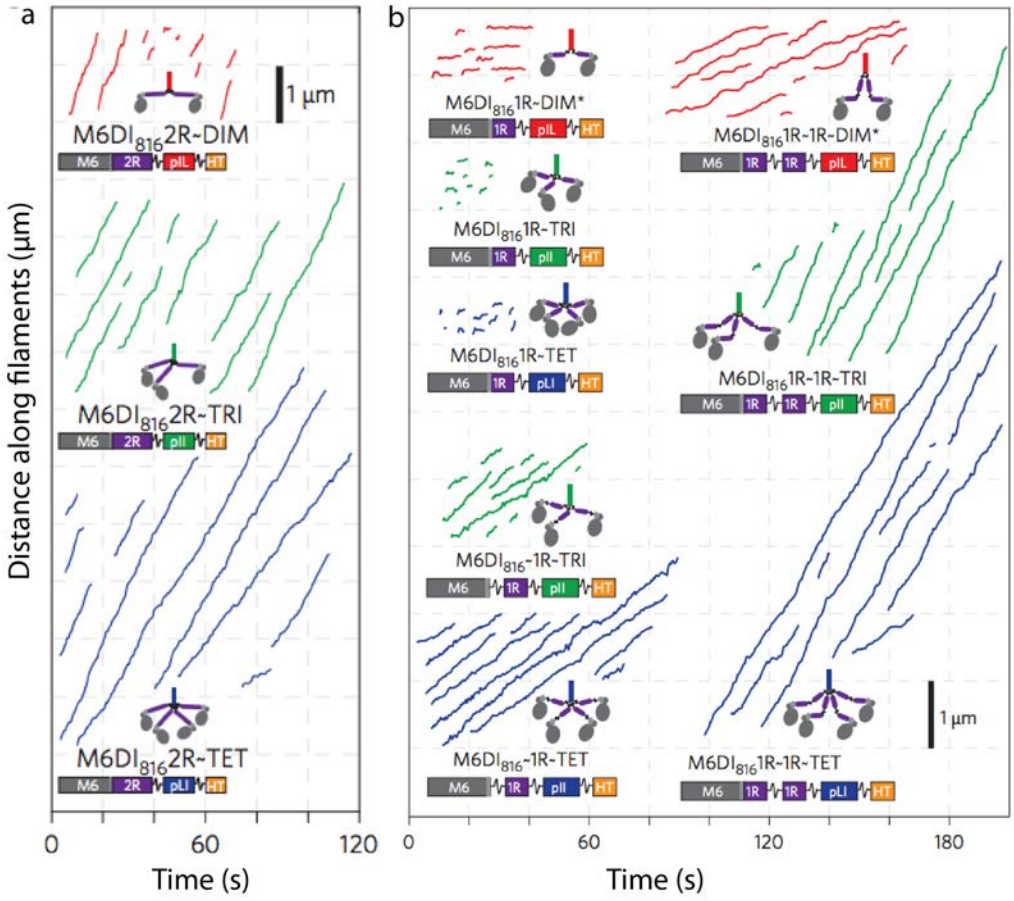

Figure 16 Myosin VI constructs. (a) Dimeric, trimeric or tetrameric constructs effects on myosin VI processivity and stepping behaviour; (b)Effects of increased flexibility on myosin VI constructs with short lever arms. Wandered distance of the constructs on actin filaments is presented with different colours lines (adapted from Schindler et al. 2014)

All the studies that I present in this section, showed myosin displacement along actin filament, but they never check their contractile effect on actin network. In fact, I had the chance to be accepted as a postdoc fellow in the Bryant lab, and one of the perspectives that I have, is to characterize the interaction of these molecules with random and then organized actin network.

In conclusion, these bio-engineered motors may represent the missing tools to really understand contraction. With these tools, we will move forward in our understanding of the molecular mechanisms that dictate the contractile properties of actin systems.

II. *In vivo* actomyosin cytoskeletal structure

Cells use contractile force to ensure different functions such as shape changes, organelle movements, intracellular transport or the formation and maintenance of a multicellular tissue during development (Gardel et al., 2010; Munjal & Lecuit, 2014; Salbreux, Charras, & Paluch, 2012; Vicente-Manzanares, Ma, Adelstein, & Horwitz, 2009)

Murrell et al. 2015 classified the cellular contractile deformation into four classes (Figure 17):

- Isotropic contraction: cells reduce their overall size homogeneously.
- Anisotropic contraction: cells establish a front–back polarity and generate anisotropic stresses.
- Cytokinesis: contractile stresses are localized at the cell equator to drive furrow ingression and locally contract the cell.
- Cell migration: a spatio-temporal regulation of contractility is used both for breaking the cell symmetry and during cell retractions.

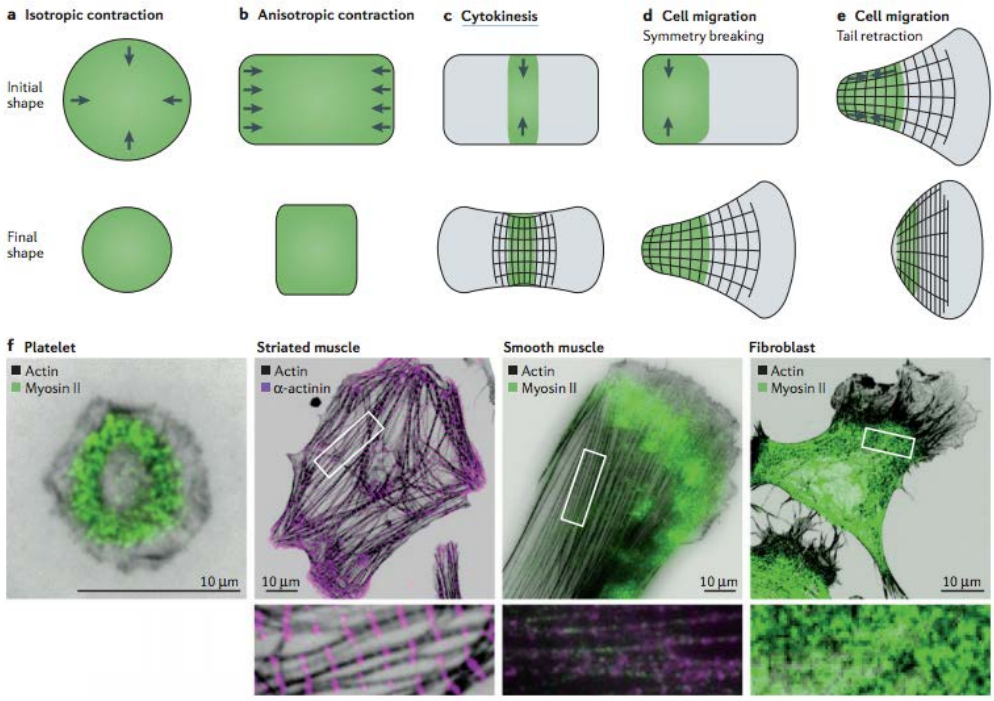

Figure 17: Cellular and tissue contractile deformations. (a) Isotropic contraction. (b) Anisotropic contraction. (c) Deformations in cytokinesis, (d) Symmetry breaking in migrating cells. (e) Tail retraction in migrating cells. (f) Different adherent cell lines labelled for proteins involved in cellular actomyosin organization. Boxed regions in (f) are magnified below to highlight the different types of actomyosin organization found in the different cell types. (Murrell 2015)

In this part, I will describe these different contractile events while giving some examples of the main cellular contractile structures and their specific organizations.

II.1. Muscle cells

III.1.1. Muscle cell architecture

Historically, contractility has been discovered and studied extensively in the context of striated muscle tissue (Figure 18). Muscle cell is an elongated multinucleated cell, containing a large number of cylinders: the myofibrils, which are packed in a complex network of membranes. Myofibrils are constituted by the succession of identical elements: the sarcomeres. Each sarcomere consists in an entanglement between thin actin and thick myosin filaments. This gives rise to the alternation of bright bands (named bands I for isotropic) and dark bands (named bands A for anisotropic) observed by electron microscopy (Figure 18 A). The repetition of these elements gives to the skeletal muscle its striated appearance.

Figure 18 Representation of the sarcomere structure. (A) A sarcomere imaged by electron microscopy. (B) Schematic representation of actin and myosin filaments within the sarcomere. (Adapted from Cooper 2000).

III.1.2. Sarcomeric contractility

In the sarcomere, myosin II heads are localized close to the pointed end of the actin filaments. These filaments have opposite polarity on the two sides of the Line M delimiting the middle of the myosin filament (Figure 18 B). As the myosin heads are moving toward the barbed ends of the filaments, their movements will slide the filaments toward the Line M. Thus the myosin heads will pull together the anti-parallel actin filaments. The actin and myosin overlap increases in consequence, leading to a length reduction of the sarcomere (Huxley 1957) .

The “force-velocity” curve is an important representation to describe the contraction of the sarcomeres. It corresponds to the relationship between the force applied by a Myosin and the rate at which it moves on Actin filaments. This “force-velocity” curve depends on the mechanochemistry of the Myosin II. Because there is almost no variation in sarcomeric spacing and myosin II rate of contraction, the contractile response of striated muscle is largely constant (Gordon et al. 2000). The number of parallel motor heads within each sarcomere defines the stall force of the structural unit of a muscle fiber

(myofibril). Since all the myofilaments have the same size, the myofibril stall force is also almost constant. The highest level of contraction in sarcomeres is thus controlled by the maximal overlapping surface of actin and myosin. Finally, the organization of sarcomeres favours a fast contractile response, and the contractility mechanism does not seem to rely on actin filaments polymerization. Nonetheless, it should be noted that one study showed that actin filaments in a sarcomeric system are surprisingly dynamic (Littlefield et al. 2001).

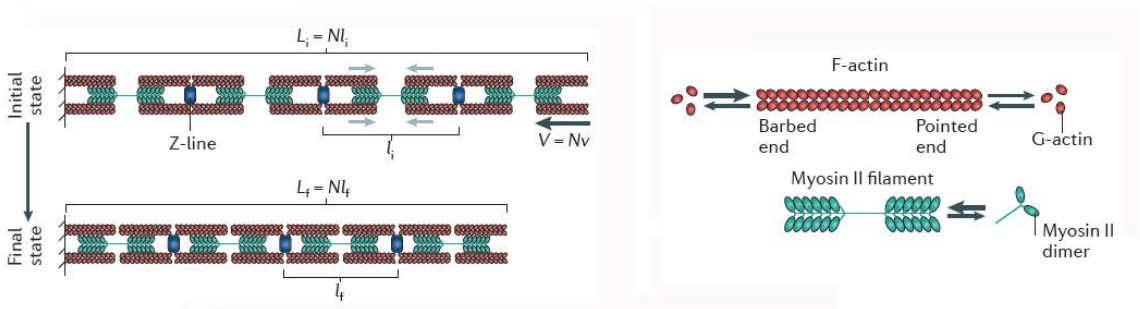

Figure 19 Schematic representation of the actomyosin contraction within a sarcomere. Black arrows in the initial state indicate the direction of actin filament translocation. The initial and final contractile units lengths are respectively indicated as l_i and l_f. The sarcomeric reduction in length arises from increased overlap between actin filaments and myosin. The bundle shortening velocity is expressed as: V = Nv where N is the number of contractile units and v is the myosin gliding velocity. (Adapted from Murell et al., 2015)

II.2. Non-muscle cells

II.2.1. Contractile ring

During cell division, the formation of a ring around the equator of the cell can be observed. The contraction of this ring allows the separation of the cell in two daughter cells.

Electron microscopy suggested that this ring consists of many filaments (Schroeder, 1970). These filaments can be arranged in several distinct, closely packed, filament bundles, close to each other near the cell membrane (Maupin & Pollard, 1986). These bundles were found to contain actin (Schroeder 1970) and myosin (Fujiwara & Pollard, 1976; Otto & Schroeder, 1990).

Due to its critical role in cell division, the contraction of this ring has been the subject of many studies. Marsland first formulated the concept as well as the terminology of the “contractile ring” in his contractile gel theory of cell furrowing (Marsland and Landau 1954). Then Wolpert et al., in 1960 further developed it. Inspired by the

mechanics of muscle cells, similar sarcomere-like mechanism based on the sliding hypothesis of actin filaments, was proposed for the case of the contractile ring (Schroeder, 1990). This "standard model" of cell division has been investigated using more rigorous physical descriptions and considering also chemical reactions as well as the different properties of the network made of actin filaments (He & Dembo, 1997). Then Zhang and Robinson (Zhang & Robinson, 2005) proposed a physical theory to explain the characteristic cell shapes observed in cytokinesis, based on active stresses and passive elements, such as the Laplace pressure.

To understand the contraction of the ring, it is important to study its structural organisation and proteins composition. During metaphase the actin filaments involved in the ring have a slight preferential orientation along the spindle axis, while during anaphase the filaments in the furrow are oriented along the equator (Fishkind & Wang, 1993; Kamasaki, Osumi, & Mabuchi, 2007). The orientation seems to be more constrained in regions where the cell adheres to a substrate or other cells. Besides actin and myosin, the ring contains many other proteins (Feierbach & Chang, 2001; D. N. Robinson & Spudich, 2000). Prior to ring formation, actin and a large number of associated proteins are temporally recruited to an equatorial domain of the cell cortex (Glotzer, 2005; Wu et al., 2003). These associated proteins could play different roles for the generation of the contractile forces. The concerted action of these proteins leads to the formation of actin bundles in the mature contractile ring. At the end of mitosis, the mature ring begins to contract, in response to a cellular signal.

Mishra et al., in 2013, established an experimental system composed of a minimal contractile cytokinetic ring to study its full contraction in vitro. They demonstrate that, in the absence of other cytoplasmic constituents and in an ATP- and myosin-II-dependent manner, the contractile ring of permeabilized fission yeast cells, sustain a rapid contraction (Figure 20). Strikingly, polymerization of actin bundles and their further disassembly are not required for the whole ring contraction, although they notice that the extra addition of an exogenous crosslinking protein (α -actinin) inhibits the ring contraction. Using this method of contractile rings isolation, they conclude that the proteins that are important for the ring assembly are not essential for its contraction in vitro.

Figure 20 Extracted cytokinetic ring from permeabilized fission yeast and its time-lapse contraction in presence of exogenous Myosin II and ATP (adapted from Mishra et al. 2013)

II.2.2. Contractile fibers

The stress fibers were originally described as wide bridged fibers of actin filaments. They are now, known to be made of short bipolar filaments on which myosin II and α-actinin form alternating patterns (Langanger et al., 1986). Contrary to the repeated cycles of contraction-relaxation in muscle fibers, the stress fibers are constantly contracted, spaced by occasional relaxation and elongation phases only. Mammalian cells have three categories of stress fibers: ventral stress fibers attached at both ends to focal adhesion, dorsal stress fibers attached on one side to a focal adhesion, and non-connected transverse arcs (Figure 19, (Hotulainen & Lappalainen, 2006)). Within a cell, these three types of fibers have a well-defined spatial organization. The ventral fibers are in the back of the cell. They are responsible for the rear cell retraction on the substrate and associated with cellular shape variations during the motility. The dorsal fibers are located near the front edge of the cell in a perpendicular way. Studies have shown that they are not real stress fibers since no contraction was detected and because of their lack of typical patterns of α -actinin and myosin II. Some model predictions proposed that they could be the precursor of the ventral fibers (see Letort, Ennomani et al., 2015, Figure 2-C). Furthermore, it seems that they play a role of physical link between the substrate and the transverse arcs, which are parallel to the cell membrane (Hotulainen and Lappalainen 2006; Naumanen, Lappalainen, and Hotulainen 2008).

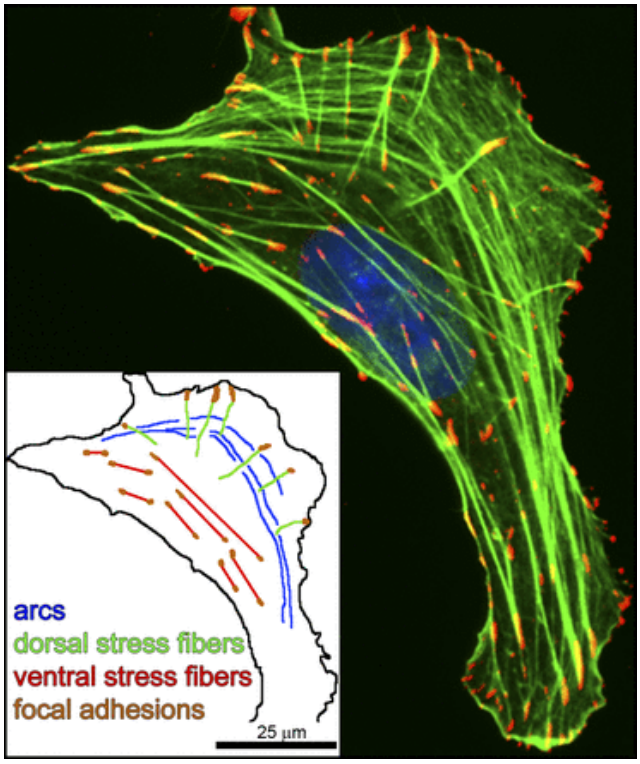

Figure 21 Representation of cellular actin contractile structures. Immnofluorescence of U2OS cell exhibit the three main types of actin stress fibers: transverse arcs, dorsal, and ventral stress fibers and are they are represented schematically in the inset. Focal adhesions (red), actin filament and SFs (green), and the nucleus (blue) (Burridge & Wittchen, 2013).

The main components of the stress fibers are actin and myosin II. The depletion of myosin results in loss of stress fibers, which makes this protein a crucial element for the integrity of these structures. Other proteins are also presents and maintain the integrity of the architecture. For example α- actinin, in addition to its crosslinking function between the filaments, ensures the recruitment of other proteins like palladine, ALP, or CLP-36.

II.2.3. Non-sarcomeric actomyosin mechanism

Smooth muscle cells are made of actomyosin structures that lacks a precise organization compare to the sarcomere structure, and thus have been described as 'smooth' (Gunst & Zhang, 2008; Lavoie et al., 2009). Although some of the smooth muscle actomyosin structures exhibit sarcomeric like banding structures of α-actinin and myosin (Aratyn-Schaus, Oakes, & Gardel, 2011; Hotulainen & Lappalainen, 2006), they do not reproduce the remarkable regulation of length and polarity of actin filaments presents in myofibrils

(Svitkina & Borisy, 1999). Unlike muscle cells, the rate of contraction and the force production of these cells follow a big variation over time (it could vary from few seconds to hours). But, in this case, the dynamic of actin polymerization must match the stress generated by the molecular motors to maintain a coherent actomyosin system (Luo et al., 2013). Thus, in comparison to sarcomeric contraction systems, non-sarcomeric actomyosin systems are extremely dynamic and not at all organized.

Despite this lack of organization, smooth muscle cells can produce local contraction, necessary for the cellular processes. Here, I will present three models of contractility that were discussed and studied in the case of non-muscle cell.

Quasi-sarcomere organizations

We can find this organization in some specific cytoskeleton structures like the contractile ring of the Schizosaccharomyces pombe, in which myosin and formins are forming nodes inside the bundles (Figure 22). The filaments are thus overlapping in an anti-parallel fashion in between those nodes.

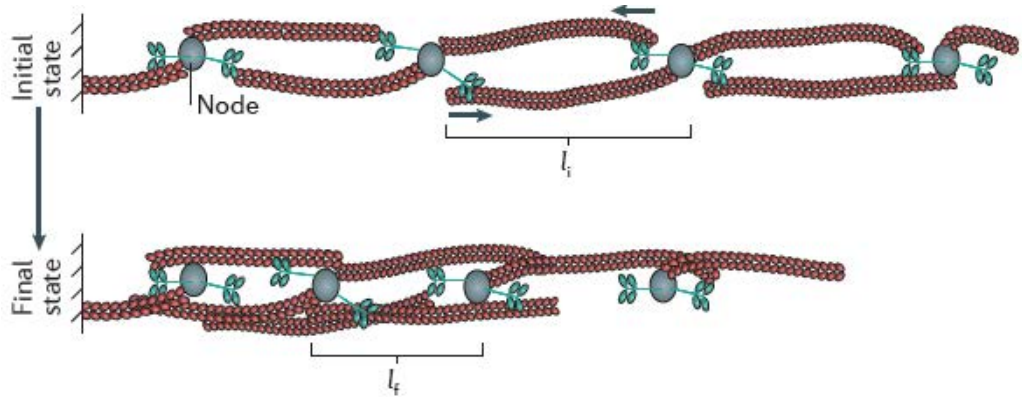

Figure 22 Contractility in quasi-sarcomere organization. This mechanism of contraction is similar to the sarcomere one and results in the reduction of contractile unit length over time. Myosins (green) and formins (grey circles) form nodes inside the actin filaments (red) bundle. Actin filaments overlap in antiparallel way between the nodes. (Murrell et al., 2015)

Disordered network without connectivity

In an actomyosin network of aligned filaments of random polarity, molecular motor activity results in the internal separation and polarity sorting of actin filaments but does not reduce the overall size/length of this network (the initial length will be equal to the final length (Figure 23) (Lenz et al. 2012 ; Ennomani, Letort et al., in revision).

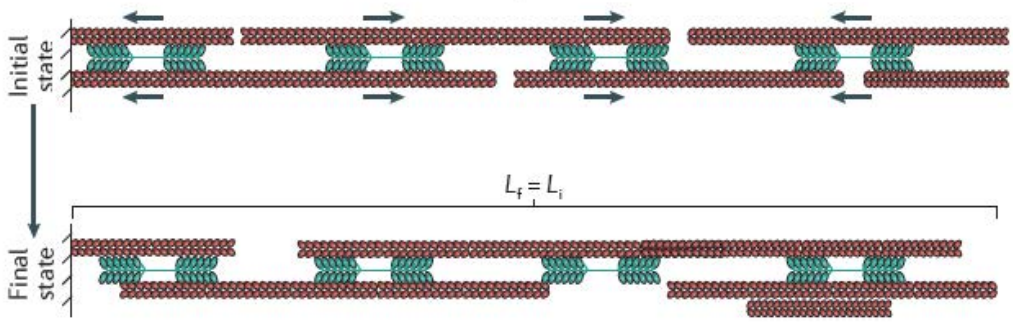

Figure 23 Contractility in disordered actomyosin without connectivity. Myosin II (green) activity results in actin filaments (red) polarity sorting but does not generate a reduction in the bundle length (Lf = Li). (Murrell et al 2015)

Disordered actomyosin bundle

This case is similar to the previous network, but the bundle contains crosslinkers. The molecular motors generate internal stresses, which could induce compression or an extension of the short actin filaments pairs (Figure 24). This depends on the position of myosin and crosslinkers relatively to the barbed end of the actin filament. The segment of filament in between the myosin and the crosslinker is under internal stress due to the difference of velocity of the two proteins. If this segment is long enough, it will buckle, which generates a compressive stress (Lenz et al. 2012, Murrell and Gardel 2012)

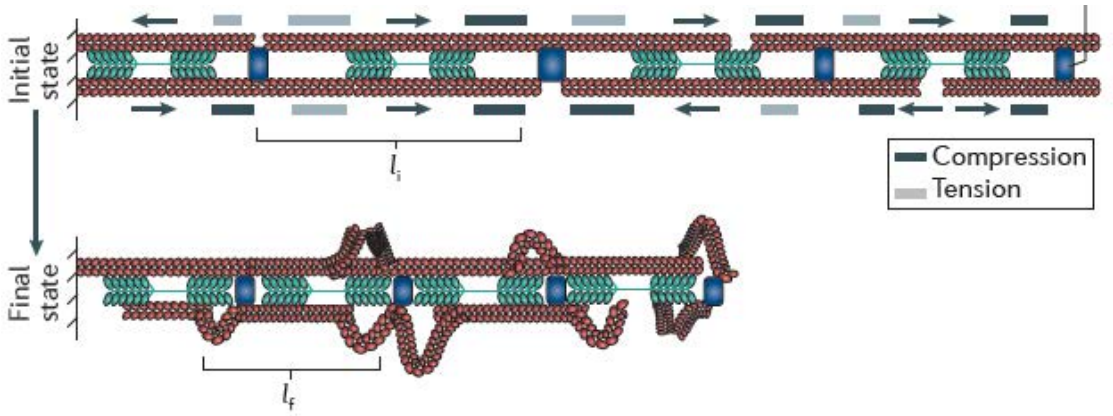

Figure 24 Contractility in disordered actomyosin system with connectivity. Myosin II activity causes the compression or the extension of actin filaments, depending on the relative position of motors (green) and crosslinkers (blue) with respect to the barbed ends of actin filaments (red). The applied stress then results in actin filaments deformation and buckling. The contractile unit length is defined as the distance between actin filaments buckles (Murell et al, 2015).

II.2.3. Cortex

II.2.3.1. Structure

The cell cortex is a complex network of actin filaments attached to the inner face of the plasma membrane (Figure 25). Besides actin, this network includes many regulatory proteins besides actin and myosin II (Pollard, 1986). Its thickness can vary

from 50 nm to 2 μm and its viscoelastic properties allow it to oppose an isotropic strength to deformation (Clark, Dierkes, & Paluch, 2013; Morone et al., 2006). This cortex has a high dynamic of polymerization that makes it a generator of cortical tension and its contractile behaviour is essential in cytokinesis. It is also a central player in motile cell and tissue morphogenesis (Bray & White, 1988). Despite the involvement of the cortex in many cellular events, dynamics at the molecular level remains largely unknown. Even though its microscopic structure has been resolved by electron microscopy observations, understanding its formation still remains an area of study.

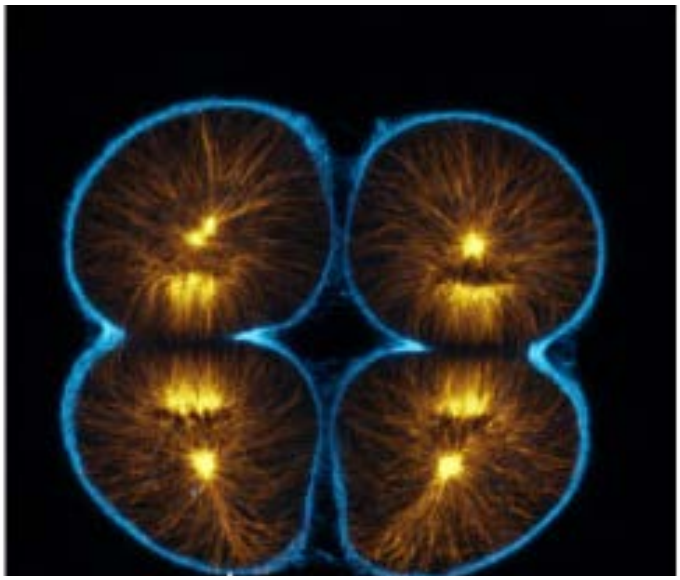

Figure 25 Cortex during cytokinesis. Confocal section of an embryo cell showing internal microtubules (orange) and the actin (blue) organization at the cortex. Figure taken from the University of Washington Center for Cell Dynamics (website: http://celldynamics.org/celldynamics/research/cytokinesis/index.html).

Electron microscopy reveals that the actin filaments are oriented parallels to the membrane in a random array. The mesh of these networks varies from 41 nm (in a keratocyte) to 230 nm (for fibroblasts) (Morone et al., 2006). The thickness varies also according to the cell type. For example it is 100 nm in Dictyostelium (Hanakam et al., 1996) and 1 μm for fibroblasts(Bar-Ziv et al., 1999). From a biochemical standpoint, the cortex is mainly composed of, beside cortical actin, myosin II and crosslinkers proteins. Thus the cortex is a contractile structure. In addition of myosins II, myosins I (Charras et al., 2006) and myosins V (Nelson et al., 2009) are also presents. The cell cortex plays an important role in cell division; but its regulation but is still little known.

A recent study (Bovellan et al., 2014) tried to identify the cortical actin nucleators with two differents ways: cortex-rich isolation blebs and shRNA. They showed that it is mainly generated by two proteins (formin mDia1 and the Arp2/3 complex). Each

nucleator can be accounted for a similar amount of actin filament to the cortex but will trigger very different polymerization kinetic of the filaments.

II.2.3.2. Acto-myosin cortex mechanics

The tension applied by myosin on the cortex was characterized previously and directly measured by micropipette aspiration on a localized region of the cell (Hochmuth, 2000). This applied tension is linearly correlated to the molecular motor activity since decreasing their activity induces a low strain value (Bergert et al., 2012) . The membrane and cortical tension do not have the same definition, actually one could affect the other, but we cannot use the same experimental tool or technique to measure them. Indeed, the membrane tension can be measured by pulling a tube of membrane since the energy to pull this tube will depend on membrane tension, at least in the case of simple artificial membrane. In the cellular context, the measure of cortex tension is more difficult because of its complex composition and its connections to the cytoplasm and other cytoskeleton networks. The measured energy or force by pulling tubes, dependents in some cases only on the required force to fully detach the membrane from the cytoskeleton network, while with other cell types, the force to pull a tube reflects directly the membrane tension (Batchelder et al., 2011). In addition, the cellular membrane contains complex composition, like the transmembrane proteins and this could create an additional force of friction that affects the equilibrium of the membrane (Campillo et al., 2013). The main message related to the membrane versus cortical tension is that, even if micropipette aspiration can immediately measure cortical tension, it is difficult to quantify how much of this tension is related to the membrane and how much is related to the cortex, unless it is possible to detach the membrane from its underlying cytoskeleton, to help the separate analysis of both structures (Campillo et al. 2013).

III. Dynamic reorganization of the actin cytoskeleton

We can notice from what I just present above, that the cell contain a variety of actin-based structures, which are insuring different cellular role. Even though these structures emerge from the same origin, their biochemical composition and filaments organization are completely different. This could be explained by the highly dynamic of actin structures, in fact they are nucleated, polymerised, and disassembled in a time scale of a second. Therefore the reorganization of a given actin structure can promote the formation of another. This was discussed in the review bellow. This review allowed us to highlight the process that is involved in the dynamic transitions between different types of cell architectures. One of the main questions that could be asked and that we wanted to address through this review is how these structures coordinate temporally and spatially at the cellular level to enable a suitable macroscopic physiological response.

Version acceptée dans F1000 Reports

Dynamic reorganization of the actin cytoskeleton

Gaëlle Letort[1*], Hajer Ennomani[1*], Laurène Gressin[1], Manuel Théry[1,2], and Laurent Blanchoin[1#]

[1]Laboratoire de Physiologie Cellulaire et Végétale, Institut de Recherches en Technologies et Sciences pour le Vivant, iRTSV, CNRS/CEA/UGA, Grenoble, France
[2]Unité de Thérapie Cellulaire, Hôpital Saint Louis, Institut Universitaire d'Hematologie, UMRS1160, INSERM/AP-HP/Université Paris Diderot, Paris, France.

[*] These authors contributed equally to this work

[#] Correspondence: laurent.blanchoin@cea.fr

Abstract

Cellular processes including morphogenesis, polarization, and motility rely on a variety of actin-based structures. Although the biochemical composition and filament organization of these structures are different, they often emerge from a common origin. This is possible because the actin structures are highly dynamic. Indeed, they assemble, grow and disassemble in a time scale of a second to a minute. Therefore the reorganization of a given actin structure can promote the formation of another. Here, we discuss such transitions and illustrate them with computer simulations.

Cellular-actin assembly can generate a variety of architectures. These highly dynamic actin-based structures lie at the heart of a diverse array of cellular processes (1, 2). Actin filaments are found inside cells in three basic patterns: branched-filament networks, parallel- or mixed-polarity filament bundle arrays. These different types of organization can contribute to more complex structures and determine their functions (3). Although most of the time many actin structures are localized to different parts of the cell, they are rarely independent and their dynamics often influence each other. In this review, we will discuss the dynamic reorganization of actin inside the cell and explore the crosstalk between different architectures.

Actin structures in the cell: formation, architecture and functions

The cell cytoplasm provides a large reservoir of actin monomers, and this reservoir is necessary for the assembly of complex actin-based structures (4). The initial step in building such a large structural array containing different types of actin-filament arrangements (Figure 1) requires controlled actin assembly and the inhibition of spontaneous polymerization (4). Two actin-binding proteins play a major role in regulating this process: thymosin and profilin (5). Thymosins sequester actin monomers to which they bind and thus fully block filament assembly (6). Profilins also bind to actin monomers but only inhibit spontaneous nucleation (7). Indeed the profilin/actin complex can add on to any preexisting free filament barbed end and therefore participate to actin elongation (8).

Several types of proteins, classified as actin nucleators, can counteract the inhibitory effects on actin assembly by thymosin, profilin or other monomer binding proteins (9,10). These actin nucleators include the Arp2/3 complex, formins, and proteins containing WASP homology 2 (WH2) domains. However, the Arp2/3 complex (11,12) is the only definitive actin nucleator in the sense that it can overcome the limiting step in the formation of an efficient actin nucleus during assembly. Indeed, this complex contains two actin-related proteins (Arps), Arp2 and Arp3 that mimic an actin dimer (11). Other actin nucleators including formins (13,14) or WH2-domain containing proteins (15) appear to stabilize preexisting dimers rather than generating or mimicking new ones (16,17). Interestingly profilin in yeast and mammalian cells can inhibit Arp2/3 complex nucleation activity thus favoring the actin filament elongation activity of formin or Ena/VASP (18, 19).

The lamellipodium is a dense branched array of filaments that occurs at the leading edge of a motile cell and its formation is dictated by the activity of Arp2/3 complex (Figure 1 and 19). This specific type of actin organization pushes forward the plasma membrane during motility (1,21,22). This property relates to the lamellipodium's optimal composition of arrays of growing actin-filaments which are oriented at ±35° with respect to the membrane. Once growing, actin filaments extend beyond ~1 μm, they form parallel-filament bundles and emerge as finger-like protrusions called filopodia (23,24).

Filopodia direct how the cell probes the extra-cellular matrix (Figure 1, and 25), and control the orientation of lamellipodium (26). The parallel-filament bundles within the filopodium also serve as tracks for protein transport (27). Filopodia are ~1-10 μm long (28,29), with 10-30 actin filaments (~1-10 μm long) crosslinked in parallel arrays by fascin (30). Structural models predict that the densely-packed nature of these actin arrays is important for the filaments to resist the loads coming from the membrane such that filament elongation (by insertion of monomeric actin at the growing tip) remains uninhibited (29,31). Moreover, the filaments within the filopodium have a turnover rate of ~20 min (32) and hence are far more stable than those filaments within the lamellipodium, which have a turnover rate of ~1 min (33), or even only few seconds at the very front of the lamellipodium (34).

The cell can also contain actin structures assembled from short filaments that are sites for action of molecular motors of the myosin family. Depending on their orientation, the short filaments can act as tracks for myosin or as contractile fibers such as the transverse arcs or ventral stress fibers (35), and the perinuclear actin cap (Figure 1 and 36). Radial and ventral stress fibers, oriented parallel to the migration axis (37), are anchored at focal adhesions at one (radial) or both (ventral) ends (35). Transverse arcs are formed just behind the lamellipodium (35, 38). Ventral stress fibers are made of filaments of >2 μm in length, whereas transverse fibers are made of shorter filaments of ~1 μm in length. These fibers contain on average 10-30 filaments by width section (39). Filament polarities inside stress fibers can be random (i.e. mixed polarity), graded or sarcomeric (i.e. anti-parallel) (39,40). Contractility is triggered by myosins that mediate sliding of anti-parallel filaments along each other (41). The equilibrium between contractile stress and adhesion strength can act as a modulator of cellular tension (42), and of the conversion of mechanical signals (tension) into biochemical signals (focal adhesion maturation), thus regulating the communication between the cell and the ECM (36,43). Indeed, the assembly of stress fibers may only occur once the cell is under mechanical stress (36). Ventral fibers allow the retraction of the motile cell's trailing edge (39), and may also initiate cell motility (44). By connecting the lamellipodium and the lamella, the transverse arcs, in the flattened perinuclear region (45), participate in the persistence of cell motility (35,46). The perinuclear cap, a structure consisting of acto-myosin fibers positioned around the nucleus, regulates the shape and position of the nucleus (47).

The actin structures described above are highly dynamic in terms of formation, elongation/contraction, and disassembly; and these processes can be interdependent (Figure 2). Therefore, to have a more complete understanding of the cellular actin organization, it is essential to take into account the cytoskeleton dynamics inside the cell.

From one actin structure to another: dynamical transitions

From lamellipodium to filopodia

The potential for filopodia to emerge from the lamellipodium near the plasma membrane (Figure 2A) raised the question of how a structure made of parallel actin bundles can arise from a densely branched actin network. Two overlapping theoretical models have attempted to explain this transition: the convergent-elongation model and the nucleation model (23,48,49).

According to the convergent-elongation model, filopodia are initiated by reorganization of the branched actin network due to a fine-tuning of actin-filament elongation at their growing ends (25). The branched actin filaments of the lamellipodium are short due to the regulation of their growth by capping proteins (50,51). An attractive hypothesis to explain the transition between short filaments in the lamellipodium and the longer filaments driving filopodium formation is that some of the barbed actin filament ends in the lamellipodium are protected from capping proteins by cellular elongation factors such as Ena/VASP proteins (52,53) or formins, (54), and will therefore grow longer. In support of this hypothesis, Ena/VASP and formin proteins have been observed at filopodia tips (30,55) and can induce filopodia formation (56,57).

Moreover, depletion of capping protein promotes filopodia formation at the expense of lamellipodia extension, and Ena/VASP proteins have been shown to play an important role in filopodia formation (58). Indeed, Ena/VASP proteins promote the convergence of filament barbed ends and have an enhanced activity when bound to trailing barbed ends in a fascin bundle, thus allowing the trailing ends to catch up with the leading barbed ends (59). Longer actin filaments can, after positional fluctuations and bending, be captured and aligned into bundles by fascin (Figure 2), depending on

the angle of their association (60,61). These initial thin bundles can be further reinforced by other actin filaments to form a rigid body that is necessary for filopodium growth (29). Convergence of actin network filaments into filopodia-like bundles can be recapitulated by both *in-vitro* reconstitution (23,58) and Monte-Carlo simulation (58,63).

The nucleation model is supported by the observation that filopodia can form even when the lamellipodium is absent as a consequence of lack of Arp2/3 complex or its activation (64,65,66,67). In this model, formin and/or Ena/VASP promoting *de-novo* tip nucleation form actin filaments in filopodium. Further support for this model comes from the recent observation that fibroblasts lacking Arp2/3 complex produce more prominent filopodia than wild-type cells (68). However, it is not yet clear how precisely filaments are initiated in absence of Arp2/3 complex. In a very elegant study using fission yeast, inhibition of the Arp2/3 complex disturbed the balance of different actin structures that were, in effect, competing for actin monomers from the same reservoir, and resulted in the enhanced formation of formin-dependent structures (69). The abundance of filopodia when Arp2/3 complex is knocked down might also be explained by the disruption of actin homeostasis causing an increased incidence of spontaneous assembly of actin filaments in the cytoplasm (68). A proportion of these spontaneously-formed actin filaments may be capped by Ena/VASP and/or formins, whose activities are enhanced by the absence of Arp2/3 complex, to promote filopodia formation (49). Together, the two models are not necessarily mutually exclusive and might be reconciled by a capture-elongation model mediated by Ena/VASP or formins.

To interrogate and illustrate the dynamic transition from lamellipodia to filopodia, we performed mathematical simulations, using the cytoskeleton simulation software Cytosim (70). In the simulation, a lamellipodium-like branched network was grown by distributing Arp2/3 complex-like nucleators within a broad, two-dimensional area (Figure 3A, top and 61). To create the variation of lengths among those actin filaments, formin-like (could also be Ena/VASP-like) entities were added, to capture the barbed ends of growing actin filaments and accelerate filament elongation. The growing actin filaments then extended out of the lamellipodium network, and merged into bundled filaments by fascin-like crosslinkers. In the simulation, a synergy between the modulation of actin-filament elongation at growing barbed ends by Ena/VASP and/or formin and actin-filament crosslinking into tight bundles is sufficient (Figure 3A, top) and necessary to induce filopodium formation (Figure 3A, bottom panel).

Although the principle of the transition from lamellipodium to filopodium may be simple, it is quite difficult to exactly identify which proteins or pathways are involved in the formation of a filopodium. There exists potential competition or redundancy between different cellular actors, illustrated by formins that constitute a large family of different isoforms (71). Moreover, the interactions between filaments and the membrane could also regulate this transition. The tension produced by the membrane can determine filopodia dimensions (29) and can induce filament alignment in protrusions even in the absence of crosslinkers (72).

From lamellipodium to contractile structures

A considerable amount of information about the assembly mechanisms of contractile structures has been obtained from numerous studies using live-cell imaging (36,38,46,73,74). The current model for the assembly of radial fibers is based on a simple mechanism of initiation, whereby the fibers are generated by formin-mediated nucleation at focal adhesions (75). Following this initiation step, the growing actin filaments are brushed into parallel bundles by the retrograde flow toward the cell center (38). Radial fibers further recruit crosslinked filaments from the lamella, giving rise to an organization of filaments with graded polarity (36).

4

The model for the formation of transverse arcs is clearly different to that of radial fibers (38). Transverse arcs are assembled by end-to-end annealing of myosin filaments and actin bundles that have come from the reorganization of the Arp2/3 complex-branched network at the back of the lamellipodium (Figure 2, 46). The reorganization of a branched network into actin bundles of mixed polarity includes several steps. First, disassembly factors such as ADF/cofilin and GMF disconnect the network by debranching Arp2/3 complex links (76–78). Second, the released short filaments are captured by myosin and actin-filament crosslinkers such as α-actinin, which are present in the lamella to trigger the formation of small bundles (Figure 2B). Third, the alignment of the filaments is enforced by the high mechanical stress produced by the interaction between focal adhesions and the extracellular matrix, and by centripetal flow at the lamellipodium/lamella interface (79). Fourth, the nascent bundles are pushed away from the cell edge by the actin centripetal flow (74), while condensing and forming transverse arcs, until they encounter focal adhesions and pre-formed radial fibers (38,80). The radial fibers and transverse arcs will then associate, with crosslinked actin bundles incorporating into the ends of radial fibers through the activity of myosin filaments.

We have also performed simulations of the transition from a branched-actin network to a contractile fiber using Cytosim and the same simulation starting point using Arp2/3 complex-like nucleators as described above (Figure 3A). To mimic focal adhesions nucleating the radial fibers, two small zones of adherence (friction points) with a few parallel filaments growing toward the cell center were placed at the bottom of a growing branched network. Arp2/3 complex connections were removed to simulate the lamellipodium debranching effect mediated by ADF/cofilin or GMF, and then motors (to simulate myosins) and crosslinkers (to simulate α-actinin) were added. A slow, directed flow was added to simulate the effect of centripetal actin flow. With only these few ingredients, the transition from a branched, non-contractile network to a mixed polarity, contractile fiber emerged from numerical simulations (Figure 3B, top panel). These ingredients all seem essential, since removal of the motors, crosslinkers or friction points all prevented the efficient formation of the contractile-cable (Figure 3B, bottom panel).

Other transitions:

Fusion of contractile and non-contractile structures

Radial fibers can associate with transverse arcs by the incorporation of myosin II filaments and subsequently develop into ventral fibers (37,38). During this process, first, two independent radial fibers connect with a pre-existing transverse arc that is pushed to the trailing edge of the motile cell by the flow. As a consequence, arc contractile forces get transmitted to radial fibers. Second, the distal parts of the transverse arc dissociate because of local stress relaxation (Figure 2C). Finally, the radial fibers fuse with what remains of the contracting transverse arc to form a ventral stress fiber that is attached to focal adhesions at both ends (38).

In addition, a ventral stress fiber could be formed by fusion of two dorsal stress fibers (without transverse-arc incorporation (80)). This latter case has been observed in Arp2/3 complex knockdown cells (38).

Filopodia disassembly and their fate.

The mechanisms by which filopodia disassemble remains to be determined. However, stationary

5

filopodia can be disassembled into small bundles by ADF/cofilin (81). Filopodia may also develop kinks after a decrease and/or change of direction of the actin flow between the lamellipodium and lamella leading to their integration into the lamella (73,74,82). In both scenarios, short actin bundles generated by filopodia disassembly would then participate in the formation of contractile structures, by feeding preexisting contractile fibers with actin filaments.

Conclusion

Cellular functions depend on complex actin choreography. To orchestrate such a diversity of actin organizations, the dynamic integration of different mechanistic pathways is necessary. Some pathways are quite specific to the formation and maintenance of a particular basic actin organization; but because these actin structures may reorganize and transform, they may also indirectly participate in the emergence of other structures. The prevalence of these different basic actin organizations also varies in different cell types (e.g. lamellipodia predominate over filopodia in keratocytes and neutrophils, whereas filopodia predominate over lamellipodia in dendritic cells or neuronal growth cones). Within a given cell type, the predominance and/or existence of the different actin structures can be regulated to achieve specific functions for example during collective migration (83). Thus, focusing on the behavior of a single type of actin structure may only provide an incomplete view of its formation and maintenance *in vivo*. Hence the development of more appropriate experimental systems that can reconstitute more than one actin structure at a time should improve understanding the complexity of cellular actin dynamics. Mathematical simulations demonstrate that only few components and simple boundary conditions are sufficient to mediate transitions between or during the emergence of complex actin structures. These mathematical approaches may also help in elaborating more appropriate experimental systems to unveil the general law behind dynamic cytoskeletal reorganization.

Acknowledgments

We thank F. Nedelec for providing an unpublished code used to run the simulations with Cytosim. LB is supported Agence Nationale de la Recherche (ANR) grant N° ANR-12-BSV5-0014 (Contract). HE and LG are supported by IRTELIS grant from CEA.

References

1. Pollard TD, Borisy GG. **Cellular motility driven by assembly and disassembly of actin filaments.** Cell. 2003; **112**: 453–65.

2. Blanchoin L, Boujemaa-Paterski R, Sykes C, Plastino J. **Actin dynamics, architecture, and mechanics in cell motility.** Physiological Reviews. 2014; **94**: 235–63.

3. Fletcher DA, Mullins RD. **Cell mechanics and the cytoskeleton.** Nature. 2010; **463**: 485–92.

4. Pollard TD, Blanchoin L, Mullins RD. **Molecular mechanisms controlling actin filament dynamics in nonmuscle cells.** Annual Review of Biophysics and Biomolecular Structure. 2000; **29**: 545–76.

6

5. Carlier MF, Pantaloni D. **Actin assembly in response to extracellular signals: role of capping proteins, thymosin β4 and profilin**. Seminars in Cell Biology. 1994; **5**: 183–91.

6. Pantaloni D, Carlier MF. **How profilin promotes actin filament assembly in the presence of thymosin β4**. Cell. 1993; **75**: 1007–14.

7. Goldschmidt-Clermont PJ, Machesky LM, Doberstein SK, Pollard TD. **Mechanism of the interaction of human platelet profilin with actin.** The Journal of Cell Biology. 1991; **113**:1081–9.

8. Pollard TD, Cooper JA. **Quantitative analysis of the effect of Acanthamoeba profilin on actin filament nucleation and elongation.** Biochemistry. 1984; **23**: 6631-41.

9. Chesarone MA, Goode BL. **Actin nucleation and elongation factors: mechanisms and interplay.** Current Opinion in Cell Biology. 2009; **21**: 28–37.

10. Campellone KG, Welch MD. **A nucleator arms race: cellular control of actin assembly.** Nature Reviews Molecular Cell Biology. 2010; **11**: 237–51.

11. Machesky LM, Atkinson SJ, Ampe C, Vandekercldaove J. **Purification of a cortical complex containing two unconventional actins from Acanthamoeba by affinity chromatography on profilin-agarose.** The Journal of Cell Biology. 1994; **127**:107–15.

12. Mullins RD, Heuser JA, Pollard TD. **The interaction of Arp2/3 complex with actin: Nucleation, high affinity pointed end capping, and formation of branching networks of filaments.** Proceedings of the National Academy of Sciences. 1998; **95**: 6181–6.

13. Pruyne D, Evangelista M, Yang C, Bi E, Zigmond S, Bretscher A, et al. **Role of formins in actin assembly: nucleation and barbed-end association.** Science. 2002; **297**: 612-5.

14. Sagot I, Rodal AA, Moseley J, Goode BL, Pellman D. **An actin nucleation mechanism mediated by Bni1 and profilin.** Nature Cell Biology. 2002; **4**: 626–31.

15. Paunola E, Mattila PK, Lappalainen P. **WH2 domain : a small , versatile adapter for actin monomers.** FEBS Letters. 2002; **513**: 92–7.

16. Xu Y, Moseley JB, Sagot I, Poy F, Pellman D, Goode BL, et al. **Crystal structures of a Formin Homology-2 domain reveal a tethered dimer architecture.** Cell. 2004; **116**: 711–23.

17. Renault L, Deville C, van Heijenoort C. **Structural features and interfacial properties of WH2, β-thymosin domains and other intrinsically disordered domains in the regulation of actin cytoskeleton dynamics.** Cytoskeleton. 2013; **70**: 686–705.

18. Rotty JD, Wu C, Haynes EM, Suarez C, Winkelman JD, Johnson HE, et al. **Profilin-1 serves as a gatekeeper for actin assembly by Arp2 /3-dependent and -independent pathways.** Developmental Cell. 2015; **32**: 54–67.

7

19. Suarez C, Carroll RT, Burke TA, Christensen JR, Bestul AJ, Sees JA, et al. **Profilin Regulates F-actin network homeostasis by favoring formin over Arp2/3 complex**. Developmental Cell. 2015; **32**: 43–53.

20. Svitkina TM, Borisy GG. **Organization and treadmilling of actin filament array in lamellipodia.** The Journal of Cell Biology. 1999;**145**:1009–26.

21. Keren K, Pincus Z, Allen GM, Barnhart EL, Marriott G, Mogilner A, et al. **Mechanism of shape determination in motile cells.** Nature. 2008; **453**: 475–80.

22. Mogilner A. **Mathematics of cell motility: Have we got its number?** Journal of Mathematical Biology. 2009; **58**: 105–34.

23. Vignjevic D, Yarar D, Welch MD, Peloquin J, Svitkina T, Borisy GG. **Formation of filopodia-like bundles in vitro from a dendritic network.** The Journal of Cell Biology. 2003; **160**: 951–62.

24. Le-Clainche C, Carlier M. **Regulation of actin assembly associated with protrusion and adhesion in cell migration.** Physiological Reviews. 2008; **88**: 489–513.

25. Mattila PK, Lappalainen P. **Filopodia : molecular architecture and cellular functions.** Nature Reviews Molecular Cell Biology. 2008; **9**: 446-54.

26. Johnson HE, King SJ, Asokan SB, Rotty JD, Bear JE, Haugh JM. **F-actin bundles direct the initiation and orientation of lamellipodia through adhesion-based signaling.** The Journal of Cell Biology. 2015; **208**: 443-55.

27. Zhuravlev PI, Lan Y, Minakova MS, Papoian GA. **Theory of active transport in filopodia and stereocilia.** Proceedings of the National Academy of Sciences USA. 2012; **109**:10849–54.

28. Welch MD, Mullins RD. **Cellular control of actin nucleation.** Annual Review of Cell and Developmental Biology. 2002; **18**: 247–88.

29. Mogilner A, Rubinstein B. **The physics of filopodial protrusion.** Biophysical Journal. 2005; **89**: 782–95.

30. Svitkina TM, Bulanova EA, Chaga OY, Vignjevic DM, Kojima S, Vasiliev JM, et al. **Mechanism of filopodia initiation by reorganization of a dendritic network.** The Journal of Cell Biology. 2003; **160**: 409–21.

31. Lan Y, Papoian GA. **The Stochastic Dynamics of Filopodial Growth.** Biophysical Journal. 2008; **94**: 3839-52.

32. Mallavarapu A, Mitchison T. **Regulated actin cytoskeleton assembly at filopodium tips controls their extension and retraction.** The Journal of Cell Biology. 1999; **146**:1097–106.

8

33. Theriot JA, Mitchison TJ. **Actin microfilament dynamics in locomoting cells.** Nature. 1991; **352**: 126–31.

34. Lai FPL, Szczodrak M, Block J, Faix J, Breitsprecher D, Mannherz HG, et al. **Arp2/3 complex interactions and actin network turnover in lamellipodia**. The EMBO Journal. 2008; **27**, 982–92.

35. Pellegrin S, Mellor H. **Actin stress fibres.** Journal of Cell Science. 2007; **120**: 3491–9.

36. Tojkander S, Gateva G, Lappalainen P. **Actin stress fibers assembly, dynamics and biological roles.** Journal of Cell Science. 2012; **125**:1855–64.

37. Small JV, Rottner K, Kaverina I, Anderson KI. **Assembling an actin cytoskeleton for cell attachment and movement.** Biochimica et Biophysica Acta (BBA) - Molecular Cell Research. 1998; **1404**: 271–81.

38. Hotulainen P, Lappalainen P. **Stress fibers are generated by two distinct actin assembly mechanisms in motile cells.** The Journal of Cell Biology. 2006; **173**: 383–94.

39. Cramer LP, Siebert M, Mitchison TJ. **Identification of novel graded polarity actin filament bundles in locomoting heart fibroblasts: Implications for the generation of motile force.** Journal of Cell Biology. 1997; **136**:1287–305.

40. Naumanen P, Lappalainen P, Hotulainen P. **Mechanisms of actin stress fiber assembly.** Journal of Microscopy. 2008; **231**: 446–54.

41. Warrick HM, Spudich JA. **Myosin structure and function in cell motility.** Annual Review of Cell Biology. 1987; **3**: 379–421.

42. Goffin JM, Pittet P, Csucs G, Lussi JW, Meister J-J, Hinz B. **Focal adhesion size controls tension-dependent recruitment of alpha-smooth muscle actin to stress fibers.** The Journal of Cell Biology. 2006; **172**: 259–68.

43. Shemesh T, Bershadsky AD, Kozlov MM. **Physical model for self-organization of actin cytoskeleton and adhesion complexes at the cell front.** Biophysical Journal. 2012; **102**:1746–56.

44. Cramer LP. **Forming the cell rear first: breaking cell symmetry to trigger directed cell migration.** Nature Cell Biology. 2010; **12**: 628–32.

45. Ingram VM. **A side view of moving fibroblasts.** Nature. 1969; **222**: 641–4.

46. Burnette DT, Manley S, Sengupta P, Sougrat R, Davidson MW, Kachar B et al. **A role for actin arcs in the leading-edge advance of migrating cells.** Nature Cell Biology. 2011; **13**: 371–81.

9

47. Nagayama K, Yahiro Y, Matsumoto T. **Stress fibers stabilize the position of intranuclear DNA through mechanical connection with the nucleus in vascular smooth muscle cells.** FEBS Letters. 2011; **585**: 3992–7.

48. Faix J, Rottner K. **The making of filopodia.** Current Opinion in Cell Biology. 2006; **18**: 18–25.

49. Yang C, Svitkina T. **Focus on the Arp2/3 complex and formins Filopodia initiation.** Cell Adhesion & Migration. 2011; **5**: 402–8.

50. Edwards M, Zwolak A, Schafer DA, Sept D, Dominguez R, Cooper JA. **Capping protein regulators fine-tune actin assembly dynamics.** Nature Reviews Molecular Cell Biology. 2014; **15**: 677-89.

51. Wear MA, Cooper JA. **Capping protein: new insights into mechanism and regulation.** Trends in Biochemical Sciences. 2004; **29**: 418–28.

52. Krause M, Bear JE. **The Ena/VASP enigma.** Journal of Cell Science. 2002;**115**: 4721-6.

53. Breitsprecher D, Kiesewetter AK, Linkner J, Vinzenz M, Stradal TEB, Small JV, et al. **Molecular mechanism of Ena/VASP-mediated actin-filament elongation.** The EMBO Journal. 2011; **30**: 456–67.

54. Zigmond SH, Evangelista M, Boone C, Yang C, Dar AC, Sicheri F, et al. **Formin leaky cap allows elongation in the presence of tight capping proteins.** Current Biology. 2003; **13**: 1820–3.

55. Schirenbeck A, Bretschneider T, Arasada R, Schleicher M, Faix J. **The Diaphanous-related formin dDia2 is required for the formation and maintenance of filopodia.** Nature Cell Biology. 2005; **7**: 619–26.

56. Pellegrin S, Mellor H. **The Rho family GTPase Rif induces filopodia through mDia2.** Current Biology. 2005; **15**: 129–33.

57. Block J, Stradal TE, Hänisch J, Geffers R, Köstler SA, Urban E, et al. **Filopodia formation induced by active mDia2/Drf3**. Journal of Microscopy. 2008; **231**:506-17.

58. Mejillano MR, Kojima SI, Applewhite DA, Gertler FB, Svitkina TM, Borisy GG. **Lamellipodial versus filopodial mode of the actin nanomachinery: Pivotal role of the filament barbed end.** Cell. 2004; **118**: 363–73.

59. Winkelman JD, Bilancia CG, Peifer M, Kovar DR. **Ena/VASP Enabled is a highly processive actin polymerase tailored to self-assemble parallel-bundled F-actin networks with Fascin**. Proceedings of the National Academy of Sciences USA. 2014; **111**: 4121–6.

60. Reymann A-C, Martiel J-L, Cambier T, Blanchoin L, Boujemaa-Paterski R, Théry M. **Nucleation geometry governs ordered actin networks structures.** Nature Materials. 2010; 9: 827–32.

10

61. Letort G, Politi A, Ennomani H, Thery M, Nedelec F, Blanchoin L. **Geometrical and mechanical properties control actin filament organization.** PLOS Computational Biology. 2015; 11(5): e1004245.

.62. Haviv L, Brill-karniely Y, Mahaffy R, Backouche F, Ben-shaul A, Pollard TD, et al. **Reconstitution of the transition from lamellipodium to filopodium in a membrane-free system.** Proceedings of the National Academy of Sciences USA. 2006;**103**: 4906-11.

63. Brill-Karniely Y, Ideses Y, Bernheim-Groswasser A, Ben-Shaul A. **From branched networks of actin filaments to bundles.** Chemphyschem: a European journal of chemical physics and physical chemistry. 2009; **10**: 2818–27.

64. Steffen A, Faix J, Resch GP, Linkner J, Wehland J, Small JV, et al. **Filopodia formation in the absence of functional WAVE- and Arp2/3-complexes.** Molecular Biology of the Cell. 2006; **17**: 2581–91.

65. Suraneni P, Rubinstein B, Unruh JR, Durnin M, Hanein D, Li R. **The Arp2/3 complex is required for lamellipodia extension and directional fibroblast cell migration.** Journal of Cell Biology. 2012; **197**: 239–51.

66. Wu C, Asokan SB, Berginski ME, Haynes EM, Sharpless NE, Griffith JD, et al. **Arp2/3 is critical for lamellipodia and response to extracellular matrix cues but is dispensable for chemotaxis**. Cell. 2012; **148:** 973–987.

67. Steffen A, Ladwein M, Dimchev GA, Hein A, Schwenkmezger L, Arens S, et al. **Rac function is crucial for cell migration but is not required for spreading and focal adhesion formation**. Journal of Cell Science. 2013; **126:** 4572–88.

68. Suraneni P, Fogelson B, Rubinstein B, Noguera P, Volkmann N, Hanein D, et al. A **Mechanism of leading edge protrusion in the absence of Arp2/3 complex.** Molecular Biology of the Cell. 2015; **26**: 901-912.

69. Burke TA, Christensen JR, Barone E, Suarez C, Sirotkin V, Kovar DR. **Homeostatic actin cytoskeleton networks are regulated by assembly factor competition for monomers.** Current Biology. 2014; **24**:579–85.

70. Nedelec F, Foethke D. **Collective Langevin dynamics of flexible cytoskeletal fibers.** New Journal of Physics. 2007; 9:

71. Faix J, Grosse R. **Staying in Shape with Formins.** Developmental Cell. 2006; **10**: 693–706.

72. Liu AP, Richmond DL, Maibaum L, Pronk S, Geissler PL, Fletcher DA. **Membrane-induced bundling of actin filaments.** Nature Physics. 2008; **4**: 789–93.

73. Nemethova M, Auinger S, Small JV. **Building the actin cytoskeleton: filopodia contribute to the construction of contractile bundles in the lamella.** The Journal of Cell Biology. 2008; **180**:1233–44.

11

74. Anderson TW, Vaughan AN, Cramer LP. **Retrograde flow and myosin II activity within the leading cell edge deliver F-Actin to the lamella to seed the formation of graded polarity actomyosin II filament bundles in migrating fibroblasts.** Molecular Biology of the Cell. 2008;**19**: 5006–18.

75. Skau CT, Plotnikov SV, Doyle AD, Waterman CM. **Inverted formin 2 in focal adhesions promotes dorsal stress fiber and fibrillar adhesion formation to drive extracellular matrix assembly**. Proceedings of the National Academy of Sciences USA, 2015; E2447–E2456

76. Chan C, Beltzner CC, Pollard TD. **Cofilin dissociates Arp2/3 complex and branches from actin filaments**. Current Biology. 2009; **19**: 537–45.

77. Gandhi M, Smith BA, Bovellan M, Paavilainen V, Gelles J, Lappalainen P. **GMF is a cofilin homologue that binds Arp2/3 complex to stimulate filament debranching and inhibit actin nucleation.** Current Biology. 2010; **20**: 861–7.

78. Ydenberg CA, Padrick SB, Sweeney MO, Gandhi M, Goode BL. **GMF severs actin-Arp2/3 complex branch junctions by a cofilin- like mechanism.** Current Biology. 2013; **23**:1037–45.

79. Shemesh T, Verkhovsky AB, Svitkina TM, Bershadsky AD, Kozlov MM. **Role of focal adhesions and mechanical stresses in the formation and progression of the lamellipodium-lamellum interface**. Biophysical Journal. 2009; **97**:1254–64.

80. Zimerman B, Volberg T, Geiger B. **Early molecular events in the assembly of the focal adhesion-stress fiber complex during fibroblast spreading.** Cell Motility and the Cytoskeleton. 2004; **58**:143–59.

81. Breitsprecher D, Koestler SA, Chizhov I, Nemethova M, Mueller J, Goode BL. **Cofilin cooperates with fascin to disassemble filopodial actin filaments.** Journal of Cell Science. 2011; **124**: 3305–18.

82. Koestler SA, Auinger S, Vinzenz M, Rottner K, Small, JV. **Differentially oriented populations of actin filaments generated in lamellipodia collaborate in pushing and pausing at the cell front.** Nature Cell Biology. 2008; **10**: 306-13.

83. Lim JI, Sabouri-Ghomi M, Machacek M, Waterman CM, Danuser G. **Protrusion and actin assembly are coupled to the organization of lamellar contractile structures.** Experimental Cell Research. 2010; **316**: 2027–41.

12

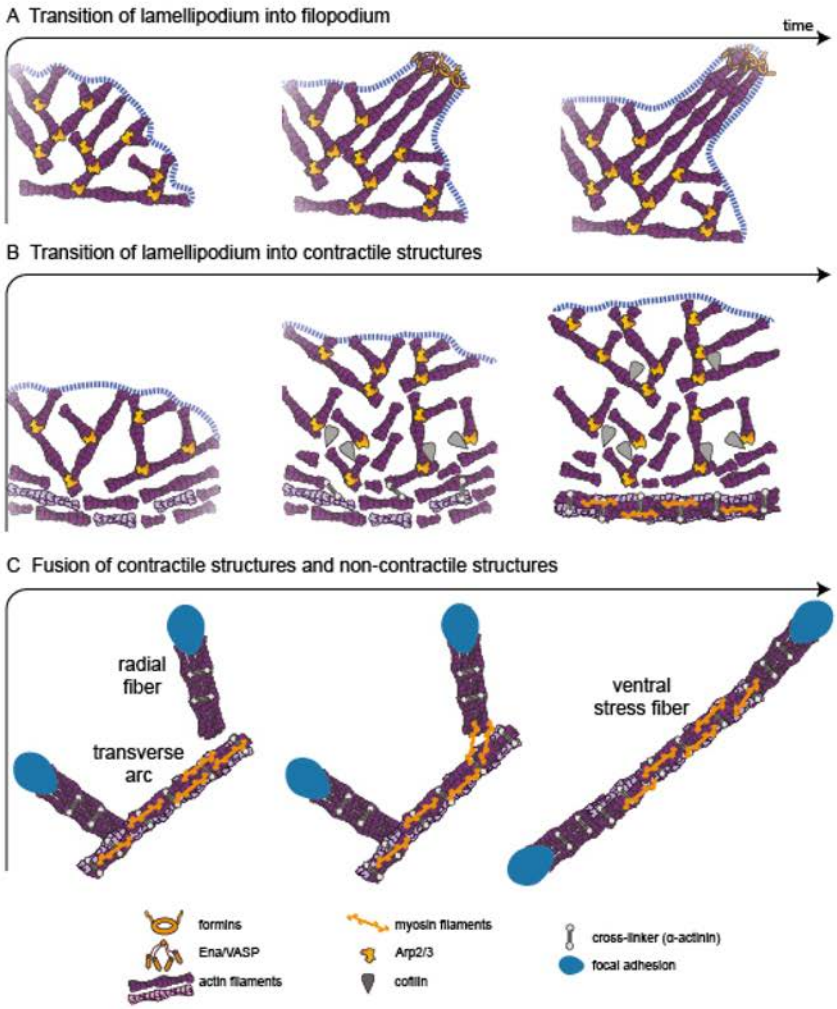

Figure 2: Actin architecture transitions.

(**A**) In the convergent-elongation model, the transition from lamellipodium to filopodium involves the formation of parallel actin filaments from a branched network created by Arp2/3 complex.Elongation factors like Ena/VASP or formin protect barbed ends from capping protein and induce the rapid polymerization of parallel bundles. (**B**) The transition from lamellipodium to contractile structures is triggered by the disassembly of the branched network at the rear of the lamellipodium by ADF/cofilin and myosin. Myosin induces actin-filament alignment and the formation of fibers stabilized by crosslinkers such as α-actinin. (**C**) The fusion of contractile structures, the transverse arcs, and non-contractile structures, the radial fibers, can lead to the formation of ventral stress fibers. In this scheme, myosins connect a transverse arc and two radial fibers and after contraction align the radial fibers with the transverse arc, creating a ventral stress fiber. This contractile antiparallel fiber is anchored at its two ends to focal adhesions.

14

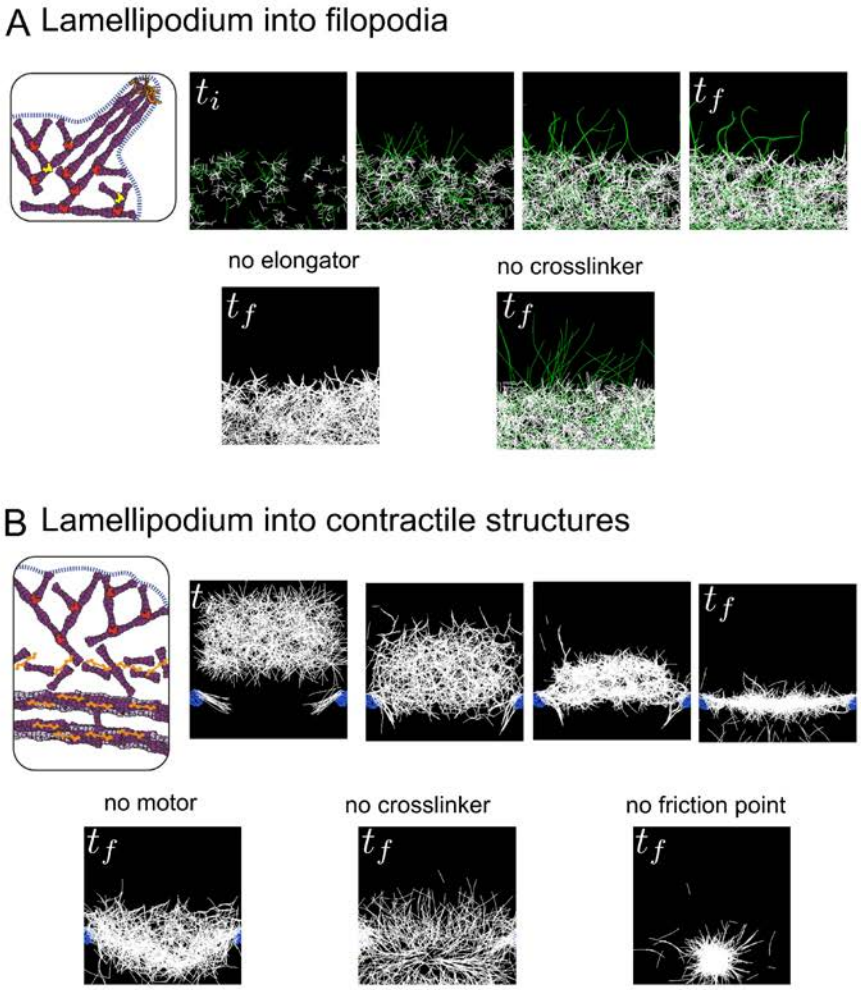

Figure 3: Simulation of transitions between actin structures.

(**A**) Emergence of filopodia-like protusions from a lamellipodium-like network. Simulations were performed using the Cytosim software. Top panel, the actin network grows by branched nucleation via the Arp2/3 complex, and a proportion of actin filaments grow longer due to capture of their growing barbed ends by an elongation factor (formin/VASP, green filaments). Actin filaments contact each other by chance due to thermal fluctuations and are stabilized in bundles by crosslinkers (fascin). Bottom panel, the presence of elongation factors in the simulation is essential for the emergence of protrusions (left), while the crosslinkers are necessary to group the protrusions into one rigid bundle (right). (**B**) Transition between lamellipodium-like and stress-fiber like networks. Simulations were performed using the Cytosim software. Top panel, a branched network is formed and moved towards friction points (mimicking focal adhesions nucleating dorsal fibers)

15

associated with parallel filaments. In the contact zone, the action of crosslinkers and myosins induces the disassembly of the branched network leading to the formation of a contractile structure of anti-parallel filaments. This structure is further compacted by a slow vertical flow (~centripetal actin flow) until it co-aligns with the friction points to form one contractile fiber. Bottom panel, in the absence of motors, the network has no tension and is thus highly curved and spread (left). The crosslinkers are essential to maintain the connectivity between the filaments and in their absence, a hole structure is formed (middle). The friction points are essential to keep the network elongated at a given length, otherwise the network collapses to one point in the middle due to the tension (right). and indicate initial time and final time of simulations (empirical).

Supplemental movie legends:

Movie S1 (related to Figure 3A)

Transition of lamellipodium into filopodium: assembly of parallel bundles (Filopodia) triggered by the dense branched network (lamellipodium)

https://www.dropbox.com/s/77xg5zoezp7mlow/BlanchoinVideo1.10.04.15.mov?dl=0

Movie S2 (related to Figure 3B)

Transition of lamellipodium into contractile structures: Formation of a contractile structure generated by the combined action of 3 parameters: actin flow, molecular motors and crosslinkers.

https://www.dropbox.com/s/xu6mcwufd7y9xag/BlanchoinVideo2.10.04.15.mov? dl=016

VI. In vitro actomyosin systems

As we discussed previously, the different architectures of actin network lead to a variety of cellular events. But a single mechanism to explain such events based on cytoskeleton organization cannot be proposed because the cellular actin cytoskeleton is highly complex and often different organizations overlap in space and time. However, knowledge on how actin architecture modulates physiological functions is essential to understand a large variety of cellular processes. Our field has largely benefited of reconstituted systems in vitro that mimic in a simplified way a given physiological function. This is called "biomimetic" approach. Likewise the famous gliding assay dedicated to study the movement of actin filaments on molecular motors (Kron & Spudich, 1986). In the following paragraph, I will highlight some of the key findings based on biomimetic system that contributed on our understanding of cytoskeleton organization in general and in particular on the understanding of the actomyosin contractile response.

VI.1. Biochemical and spatiotemporal regulations of contractility

Non-muscle cells have the capacity to adjust spatially their contractility with a scale ranging from a subcellular to a full tissue, in order to realize multiple processes such as the polarity establishment, cell migration and tissue morphogenesis (Green, Paluch, & Oegema, 2012; Lecuit, Lenne, & Munro, 2011; Levayer & Lecuit, 2012).

This control relies on the ability to generate and transmit a contractile response to the entire network and the capacity of the actin filament to respond to the stresses induced by the myosin.

VI.1.1. Biochemical regulations of contractility

VI.1.1.1 Connectivity

Actin and myosin are the key constituents of a contractile system. I*n-vitro* studies have tried to understand and model the minimal contractile actin network by considering it as an active gel. The addition of myosin (with ATP) makes this gel looses its equilibrium, contracts and deforms. Using active gel technique, studies tried to understand the conditions at which the contractility is transmitted in actomyosin gels. For this, they varied the density of myosin and the density of crosslinker, locally or globally.

In a very interesting study, (Bendix et al., 2008), authors used this method to characterize specifically the effect of α-actinin on the actomyosin gel contractility. They imaged the dynamic of an actin gel in which they added different concentration of myosin II and α-actinin. They observed the macroscopic behaviour of the active network for different crosslinkers to actin ratio ($R_{a:A}$) and motors to actin ratio ($R_{M:A}$). They were able to show that the gel contraction happens only for a window of crosslinker densities and above a myosin density threshold (Figure 26). Finally, they suggested that tuning either the local activity of motors or the crosslinker density could sensitively tune the actomyosin network contractility.

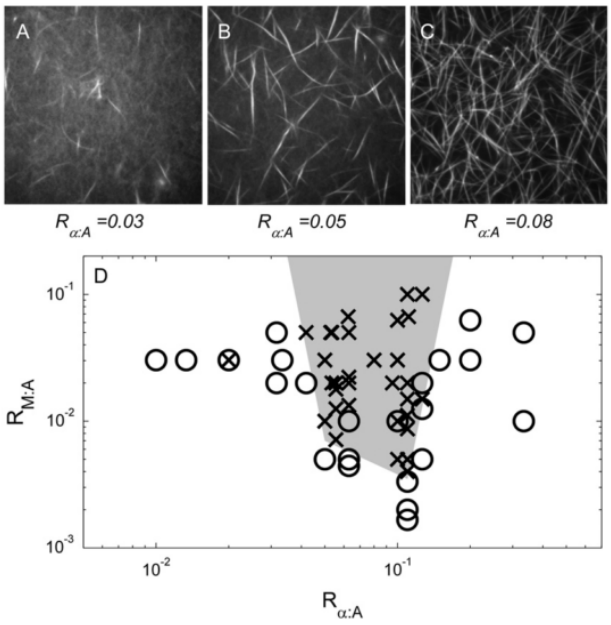

Figure 26 Actin network contractility is controlled by crosslinkers concentration. (A–C) Z projections of crosslinked actin networks with three increasing α-actinin concentrations. (D) Diagram of the myosin to actin ratio (y axis) as a function of the crosslinker to actin ratio (x axis) showing the dependency of contractility on the molar ratios of a-actinin and myosin II to actin, at a fixed actin concentration. Crosses and circles represent respectively contractile and non-contractile networks. At low myosin and α-actinin concentrations and at high α-actinin concentrations, macroscopic contraction was not observed. (Bendix et al., 2008)

More recently, different studies on contractile system have also been focusing on the role of the crosslinkers density in active gel and specifically on the role of network connectivity. They highlighted how in weakly connected network, motors slide on actin filaments, contract them and form clusters (Köhler et al. 2011) and in a well-connected network undergoes contractile stresses generated by motors, which stiffen the network by pulling against crosslinkers (Koenderink et al., 2009), or cause full contraction (Köhler et al., 2012). Theoretical models were developed to study the dependence of the macroscopic contraction on the degree of connectivity and in particular how the level of crosslinking of the network determine the contraction of the gel in one or more clusters (Alvarado et al. 2013; Wang and Wolynes 2012).

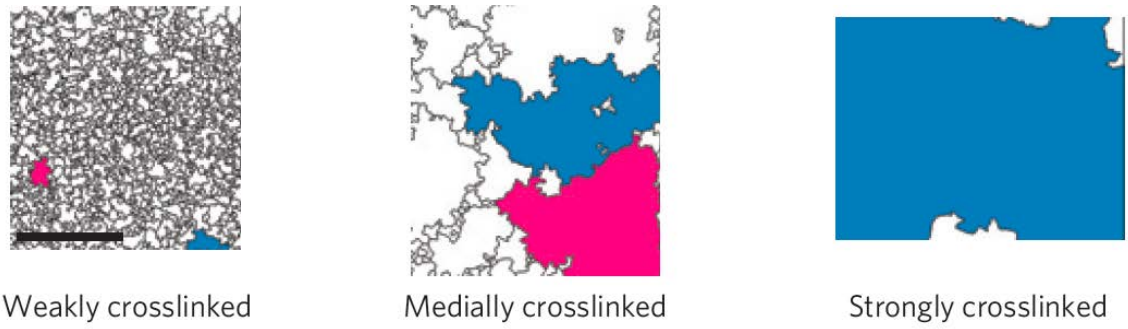

Figure 27 Dependency of macroscopic actin network contraction on the degree of connectivity. The network is segmented into clusters delimited by black lines, blue and pink representing respectively the largest and the second largest cluster. When the network is highly crosslinked, it does not have the second largest cluster (Alvarado et al. 2013).

In fact, these models showed that motors actively contract the networks into disordered clusters that exhibit a large range of sizes. This behaviour is defined by the classical conductivity percolation (Stauffer & Aharony, 1994).

Alvarado et al. 2013 simulated the macroscopic behaviour of networks with variable the connectivity. The results of the simulations allowed them to present a schematic phase diagram of active gel contraction behaviour in function of the network connectivity and the motor activity (Figure 27). This phase diagram revealed that global contraction is happening for low motor activity and high network connectivity. In this regime, the network deformed slightly because of its high rigidity induced by stiff actin bundles. On the other hand, at low connectivity, the contraction will only be local (indeed, the filaments are connected into a lot of independent small clusters). For intermediate to high connectivity coupled with high motor activity (yellow area in Figure 28), the contraction will be global but the network will aggregate into few smaller clusters.

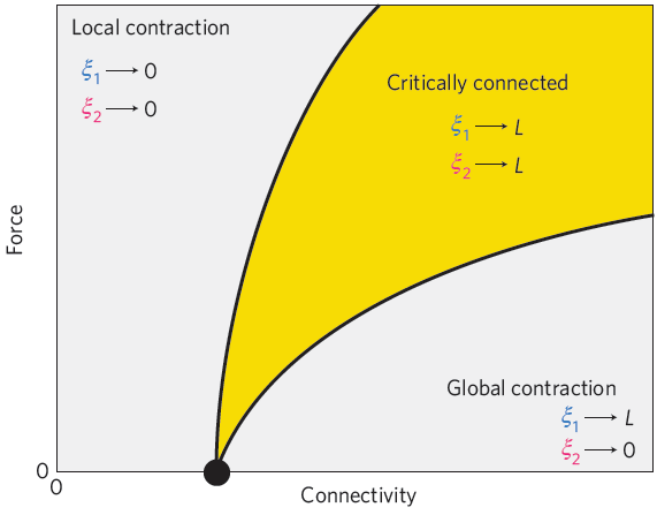

Figure 28: Phase diagram of the contraction regime as a function of connectivity and motor force. 3 types of contractile regime are described: local contraction regime which corresponds to local deformation not transmitted to the global network; critically connected regime in which global contraction occurs and disrupts the network; global contraction regime in which the whole network contracts. (Koenderink et al., 2009)

VI.1.1.2 Mechanical response

The mechanical response of actin filament that governs network contractility was studied recently using a minimal actomyosin system.

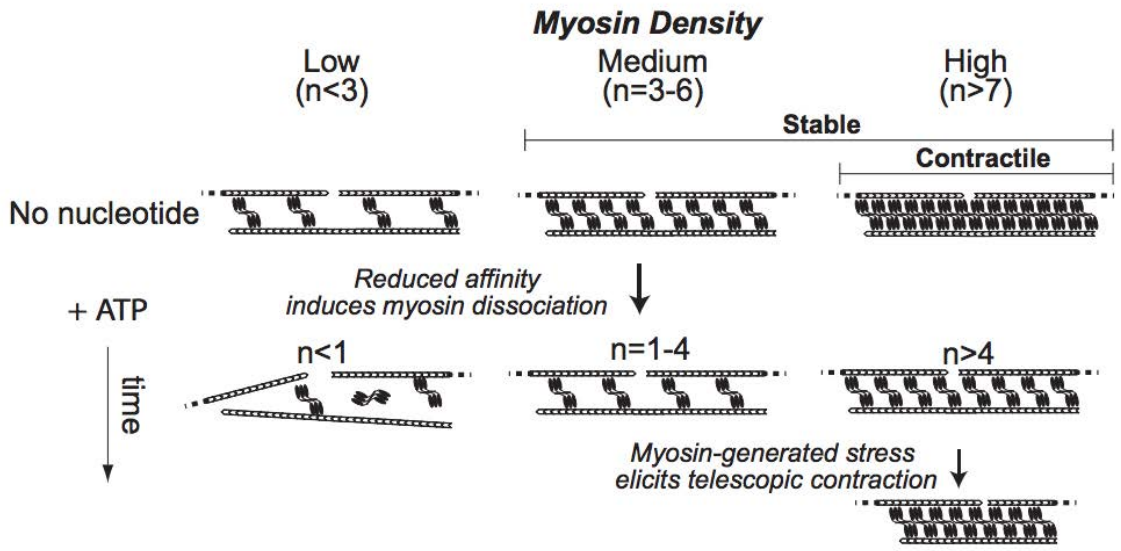

Figure 29 Myosin density effect on actin filaments bundles stability and contraction. In absence of ATP, actin filaments are stable for different myosin densities (top row). Upon ATP addition, different configurations are encountered over time. For low myosin density (n < 1), myosin dissociates and the bundle structure is lost. For intermediate myosin density, the crosslinking is maintained but does not produce contraction. For high myosin density (n > 4), contraction occurs resulting in bundles length reduction (bottom row) (Thoresen et al. 2013).

To measure the force generated by the myosin, Thoressen and collaborators, (2011) used a soft gel (polyacrylamide gel) with small beads imbedded and large beads on top of the gel that initiated the formation of contractile bundles. To sense the effect of myosin on

the actin filaments they followed small beads displacement. This displacement could be later translated as force and mechanical energy (Vignaud et al. 2014). They observed that this minimum system is able to generate force above a minimum concentration of myosin. They proposed that this minimum corresponds at the concentration of myosin necessary to obtain an efficient connection between the actin filaments.

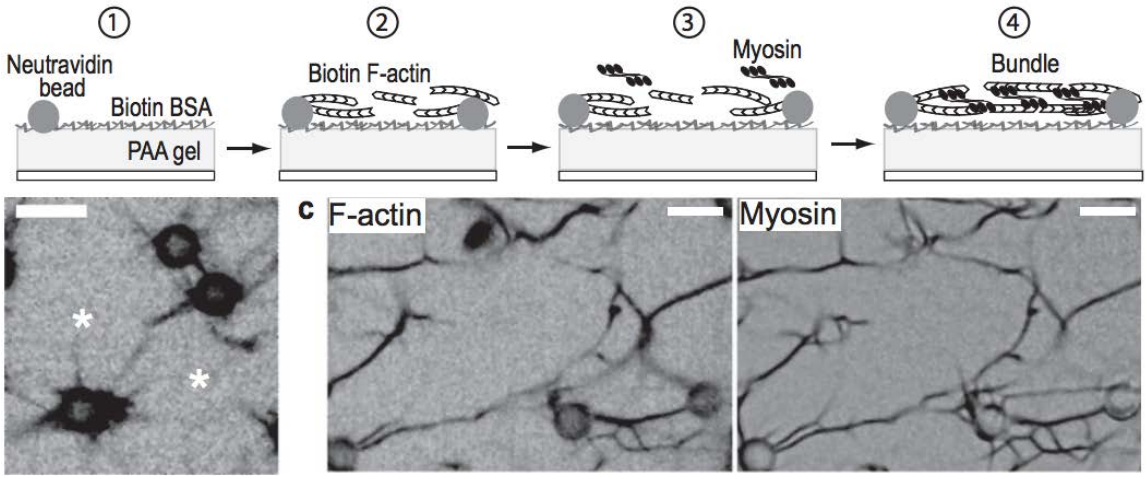

Figure 30 Actomyosin network assembly on soft gel. The first row illustrates the experimental set up used for actin bundles assembly. The contrast images in the bottom row left show actin bundles and myosin before myosin perfusion. Asterisks indicate free F-actin ends. Bottom row right images show illustrating network of bundles formed after 30 min incubation of actin filaments asters with myosin thick filaments. Scale bar is 5 μ m. (Thoressen 2011)

We saw previously, that the molecular motor density defines the amplitude of the mechanical response. In addition, the nature of the actin crosslinkers and their density inside the network also participate in the modulation of this response. When the density of the crosslinkers is increased in the network above a certain limit, the amplitude of the contractile response decreases. Indeed, a high density of crosslinkers stiffens the actin network that now resists to the myosin-induced deformation (Ennomani, Letort et al. 2015; Gardel et al., 2004; Bendix et al., 2009). Different crosslinkers will act differently regarding their impact on the contractile response. We can find diversity in crosslinkers' parameters like their size, affinity and compliance that will impact their actin during contraction. Some studies have shown that crosslinkers like fascin that bind only parallel actin filaments do not sustain deformation and will strongly impaired the contractile response (Köhler et al., 2011). In polar active networks, actin filament bundles are initially formed, and then reorganized. The cluster dimensions in this dynamic network results from a complex equilibrium between the stabilization, which is induced by crosslinkers, and the destabilization induced by myosins. In contrast, apolar crosslinkers

form bundle right away after actin filament reorganization by myosin-II motor filaments. This will lead to a formation of significantly smaller clusters than in the polar active gels (Figure 31).

Therefore, the nature of crosslinking molecules (polar or apolar) will determine the self-organization of actin filaments and impact on the network deformation.

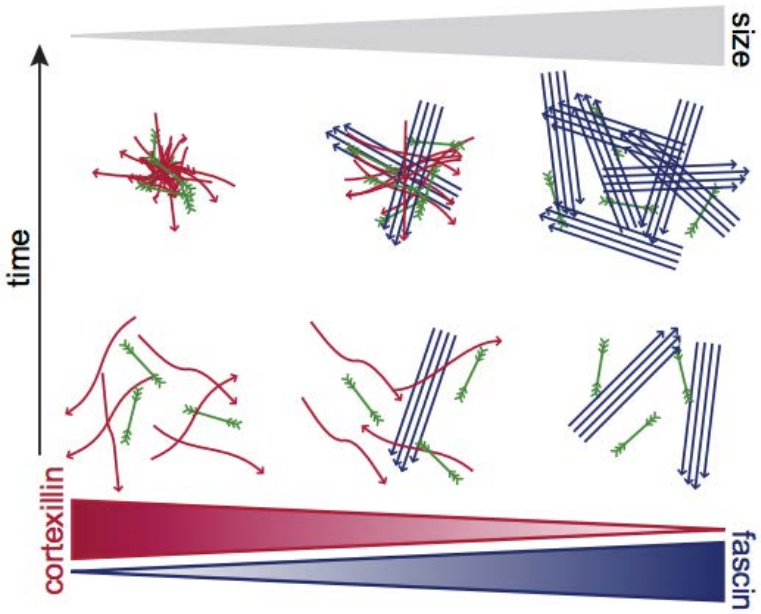

Figure 31: Contraction mechanism in active networks with different types of crosslinkers. Schematic representation of the contraction mechanisms in polar (fascin), apolar (cortexilin) and composite active actin networks. Actin filaments are presented in blue (same polarity) or red (randm polarity) and myosin filaments are present in green(Köhler et al., 2012)

V. Limitations: Why using new biomimetic system?

We have seen in the previous paragraphs that a variety of in vitro reconstituted system are developed to study the actomyosin system. However, none of them are able to study precisely how/if the organization of the actin network impacts the contractile response. In our laboratory was developed new biomimetic systems to try to tackle this question.

V. 1. Hard patterning

Until recently, the geometrical parameter controlling actin network assembly in biomimetic systems could not be easily adjustable. The experiments were most of the time done using simple geometry of nucleation. Therefore answering the question of possible architecture control and properties of actin network via the nucleating geometry was not experimentally possible. Our laboratory pioneered a method allowing the geometrical control of actin assembly (Reymann et al., 2010). This method was very important to define the parameters responsible for the formation of different actin organization (Letort et al., 2015). We have also used this method to investigate how the activity of myosin motors depends on network architecture (Figure 32 and Reymann et al. 2012)

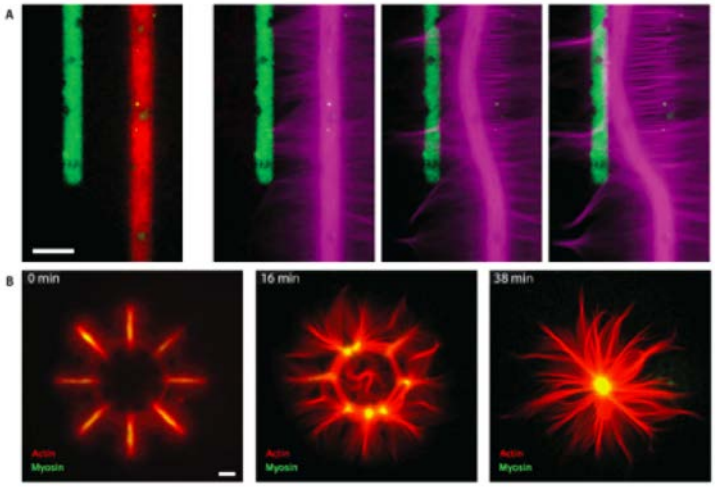

Figure 32 Myosin-inducted actin deformation on micropatterns. (A) Actin filaments (purple) grow out of the nucleating coated bars (red), reach the myosin coated bar (green) where they are put under tension. This induces the global deformation of the dense meshwork (B) Actin network (red) generated by a star-shape pattern is deformed by myosin in solution (green).

We demonstrated that myosins selectively contracted and disassembled specifics actin structures, while parallel others remained unaffected. This “orientation selection”

mechanism for selective contraction and disassembly suggests how the dynamics of the cellular actin cytoskeleton can be spatially controlled by actomyosin contractility. However, this method was developed on hard substrate and it was not possible to correlate deformation of the actin architecture by the molecular motors and the force generated during contraction. To improve this technique and to be able to access to the force generated by the actomyosin system I developed a soft patterning technique compatible with biomimetic system in vitro. In the method below, Timothée Vignaud used soft patterning to constrain cell shape and I optimized this technique for in vitro studies.

V. 2. Soft patterning on polyacrylamide gel

CHAPTER

Polyacrylamide Hydrogel Micropatterning

6

Timothée Vignaud[*,†,‡,§], **Hajer Ennomani**[*,†,‡,§], **and Manuel Théry**[*,†,‡,§]

[*]*Laboratoire de Physiologie Cellulaire & Végétale, CNRS, UMR 5168, Grenoble, France*
[†]*LPCV, University of Grenoble Alpes, Grenoble, France*
[‡]*LPCV, DSV, CEA, iRTSV, Grenoble, France*
[§]*LPCV, INRA, USC1359, Grenoble, France*

CHAPTER OUTLINE

Methods in Cell Biology, Volume 120

ISSN 0091-679X
http://dx.doi.org/10.1016/B978-0-12-417136-7.00006-9

Abstract

This chapter describes the production of micropatterns of extracellular matrix proteins on a 2D flat polyacrylamide (PAA) gel. The technique is divided into two parts. First, micropatterns are produced on glass or directly on a photomask using deep UV. Then the micropatterns are transferred on acrylamide gel by polymerization of the gel directly on the template coverslip.

This procedure is easy to perform and does not require any expensive equipment. It can be performed in no more than 2 h once you get your hands on it. It combines the advantages of other existing techniques: good spatial resolution, suitable for very soft gel, no need for the use of chemical crosslinkers for attachment of the proteins to the acrylamide, no modification of the mechanical properties of the gel by the process, and suitable for multiple protein patterning.

We also discuss the storage issues of such substrates and provide a brief review of other existing techniques for micropatterning on PAA.

INTRODUCTION AND RATIONALE

Since the introduction of cell culture experiments in Petri dishes, several technical improvements have been developed to better reproduce *in vitro* the actual physiological metazoan cell microenvironment. Microenvironment geometry and architecture can be mimicked and modulated using surface micropatterning. It consists of the creation of extracellular matrix (ECM) protein islands of controlled size and shape, called micropatterns, surrounded by antifouling polymers preventing nonspecific protein and cell adhesion. Surface micropatterning has already revealed the implication of cell adhesive microenvironment geometry in the regulation of many critical physiological processes (cell shape, cell architecture, internal cell organization, cell migration, cell division, cell differentiation, tissue architecture, etc.) (Théry, 2010; Vignaud, Blanchoin, & Théry, 2012).

Microenvironment rigidity has also been shown to be a key parameter in the regulation of several key physiological processes, including pathological ones (cell polarity, cell growth, cell differentiation, tumoral transformation, etc.) (de Rooij, Kerstens, Danuser, Schwartz, & Waterman-Storer, 2005; Engler, Sen, Sweeney, & Discher, 2006; Klein et al., 2009; Pitaval, Tseng, Bornens, & Thery, 2010; Prager-Khoutorsky et al., 2011).

As both the spatial organization of the ECM protein and the substrate stiffness have implications for cell physiology it is relevant to combine both in order to faithfully reproduce and control cell microenvironment. Polyacrylamide (PAA) hydrogels have several interesting physico-chemical properties that are useful for protein and cell micropatterning. They are optically transparent, low cost, and chemically simple compounds that can be used in almost any lab. They have been used for decades in molecular biology, notably for the manufacturing of western blots, due to the possibility to modulate their mesh size by changing the ratio of monomers to crosslinkers before polymerization. Interestingly, this mesh size is also related to the stiffness of the gel and this technique has been successfully adapted for the production of cell culture substrates of defined mechanical properties (Pelham & Wang, 1997). Importantly for mechanical measurements, the stiffness of the gel does not depend on the applied strain (Storm, Pastore, MacKintosh, Lubensky, & Janmey, 2005). In addition, PAA has constitutive antifouling properties preventing nonspecific protein and cell adsorption. Alternatively, acrylamide groups can be used as a substrate to make covalent link with proteins of interest. Therefore, many recent efforts have been devoted to the development of experimental methods to micropattern proteins on PAA hydrogels (Damljanovic, Christoffer Lagerholm, & Jacobson, 2005; Grevesse, Versaevel, Circelli, Desprez, & Gabriele, 2013; Polio, Rothenberg, Stamenović, & Smith, 2012; Rape, Guo, & Wang, 2011; Tang, Yakut Ali, & Saif, 2012; Tseng et al., 2011; Versaevel, Grevesse, & Gabriele, 2012; Wang, Ostuni, Whitesides, & Ingber, 2002; Yu, Xiong, Tay, Leong, & Tan, 2012; Zhang, Guo, Rape, & Wang, 2013). However, these methods still have intrinsic limitations. Most of them involve a microcontact printing (μCP) step to physically pattern the proteins onto the PAA. This step is time consuming, poorly reproducible in terms of amount of transferred proteins, and has a limited spatial resolution (typically few micrometers). We circumvent these limitations by using a direct (one step) activation of the PAA with deep UV through a photomask in contact with the gel (Tseng et al., 2011) and improve the spatial resolution of the micropatterns. In addition, most methods require chemical crosslinkers such as sulfosuccinimidyl 6-[4′-azido-2′-nitro-phenylamino]hexanoate (sulfo-SANPAH) or *N*-Hydroxysuccinimide (NHS)–ethyl(dimethylaminopropyl) carbodiimide (EDC) to bind the proteins of interest to the PAA. However, these reagents are poorly stable in the presence of water and the efficiency of the crosslinking is variable. Recently, Wang and colleagues used PAA polymerization itself to directly bind the protein of interest and transfer prepatterned proteins onto the PAA (Rape et al., 2011). Here we propose two rapid, accurate, reliable, and easy-to-use methods that combine all these improvements. They are based on production of micropatterns on hard substrate using deep UV photopatterning followed by protein transfer on PAA hydrogel. Thereby, we associated the advantages of deep UV patterning (micrometer to submicrometer resolution, production of highly reproducible

micropatterns) to the efficacy and reproducibility of protein covalent linking with acrylamide polymerization. The "glass method" is based on the transfer from a micropatterned glass coverslip while the "mask method" produces micropatterns directly on the quartz photomask before transfer on PAA, thus bringing the resolution of the technique to submicrometer level (Fig. 6.1I and II).

6.1 SAFETY RECOMMENDATIONS

Many of the reagents used during the processes described below are potentially dangerous. Acrylamide, acetone, isopropanol, silane, and *N*,*N*,*N*′,*N*′-tetramethylethylenediamine (TEMED) are very volatile compounds that should be handled under a chemical hood with adapted personal security protection (lab coat, gloves, protective glasses) and should be discarded specifically as they usually have particular destruction circuits.

The UV lamp will produce some ozone gas by the reaction of UV with the dioxygen from the air. As a consequence, the UV lamp should also be placed in a chemical hood.

6.2 PREPARATION OF REAGENTS COMMON TO BOTH TECHNIQUES

6.2.1 Materials

- Glass coverslip no. 1 (Knittek glass, Germany)
- Ethanol
- Silane solution (3-(Trimethoxysilyl)propyl methacrylate, M6514, Sigma, USA)
- pLL–PEG as powder (PLL20K-G35-PEG2K, JenKem Technology, USA)
- 4-(2-hydroxyethyl)-1-piperazineethanesulfonic acid (HEPES) (HN 77.5, Carl Roth, Germany)
- Parafilm
- Ice
- Acrylamide solution (01697, Fluka Analytical, USA)
- *N*,*N*′-Methylenebisacrylamide solution (66675, Fluka Analytical, USA)
- TEMED (T9281, Sigma, USA)
- Ammonium persulfate (APS) (A3678, Sigma, USA)
- Water milliQ
- Filter 0.222 μm pore size (SLGP033RS, Millex, IRL)
- Acetic acid

6.2.2 Equipment

- pH meter
- Plasma cleaner
- Beaker
- Oven
- Your favorite metallic tweezers to handle glass coverslip
- Upright fluorescence microscope

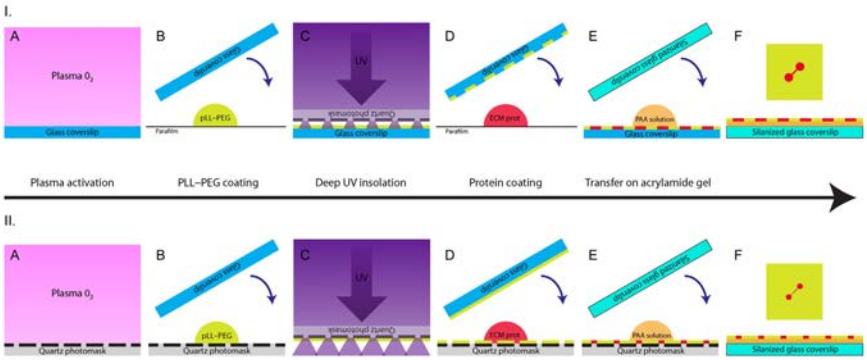

FIGURE 6.1

Description of the procedure. Two variants of the same technique are described. One is using the transfer from micropatterns produced on glass while the other from micropatterns directly produced on the quartz photomask. This latter procedure allows for production of micropattern with submicrometer spatial resolution. I. Transfer from a micropatterned glass coverslip (referred to as the "glass method"). This process consists in glass activation by plasma (a), coating with the repellent compound poly-L-lysine–PEG (pLL–PEG) (b), surface activation of the surface through a chrome photomask using deep UV (c), extracellular matrix (ECM) protein adsorption on the UV-activated sites (d) leading to the production of a glass micropatterned coverslip as previously described (Azioune et al., 2010). Then, a drop of PAA solution mix is sandwiched between the patterned coverslip and a silanized glass coverslip (e). After 30 min polymerization, the patterned coverslip is detached from the acrylamide gel while ECM protein remains on the gel (f). Note that due to the diffraction of the UV light at step (c), the shape of the final micropatterns is larger than the original on the photomask. II. Transfer from micropatterns produced directly on the quartz photomask (referred to as the "mask method"). This process is the same as previously except that the initial micropatterns are now produced directly on the quartz photomask. First, the mask and a glass coverslip are activated together with plasma (a), then a pLL–PEG drop is sandwiched between the chrome side of the mask and the glass coverslip (b). After 30 min incubation, the glass coverslip is removed and saved for step (d) as it is now a passivated surface. The photomask is exposed to deep UV from the quartz side (c), activating the pLL–PEG at defined loci with minimum loss of resolution due to diffraction. Then again, a drop of ECM protein is sandwiched between the mask and the passivated glass coverslip and incubated for 30 min (d). Transfer on acrylamide is then performed as in I (e and f).

6.2.3 Methods

6.2.3.1 Coverslip silanization

- This glass treatment is necessary to ensure a good attachment between the PAA gel and the underlying coverslip.
- As silane solutions are very toxic, as many steps as possible of this process should be performed under a chemical hood with appropriate user protection, at least the silane solution should not leave the hood outside of a hermetically closed container.
- Start the oven at 120 °C and let it warm up.
- Warm up the pump of the plasma cleaner for few minutes (according to manufacturer's instruction).
- In a 500 mL beaker, prepare a solution of ethanol containing 2% (v/v) 3-(trimethoxysilyl)propyl methacrylate and 1% (v/v) acetic acid (silanization solution).
- Put the glass coverslips in your plasma cleaner either horizontally or in a specific holder that will allow both sides of coverslips to be in contact with the ionized gas during the plasma treatment.
- Start pumping out the air in the reactor and wait for the pressure to stabilize (2 min).
- Open the oxygen inlet, set the gas flow to 5 mL/min (sscm) and wait 2 min for the pressure to stabilize (if you can control the pressure on your device, set it to 1 Torr = 133 Pa).
- Run the plasma for 3 min at 100 W.
- Close the gas inlet, stop pumping, and ventilate the reactor (a filter should be placed on the air inlet to avoid dust intake into the reactor).
- If the coverslips were horizontal in the reactor, flip them and repeat the plasma process (vacuum–oxygen–plasma).
- Soak the coverslips in the silanization solution one by one for 10 min altogether in the solution, shake occasionally.
- Discard solution.
- Rinse once with ethanol in the same beaker and then remove them from the ethanol one by one with tweezers (while others staying in the ethanol) and rinse once again in another beaker of ethanol (keep holding the coverslip with the tweezers) and finally blow off the ethanol carefully using pistol airflow and place them on the oven plate.
- Cure for 1 h at 120 °C.
- Blow off dust with pistol airflow and store at room temperature. This treatment is quite stable over few weeks so you can do many coverslips at the same time to avoid always repeating this fastidious time-consuming process.

6.2.3.2 pLL–PEG solution preparation

- This solution will be used for the passivation of coverslips before UV insolation and protein coating to avoid unspecific adsorption of protein outside of the insolated area.

- pLL–PEG is usually received as powder and should be stored under protective atmosphere (Argon) if possible, at −20 °C. The final concentration we want to achieve is 0.1 mg/mL. Since the powder is usually made of grains that weigh a few mg each, we first produce 1 mg/mL solution that is aliquoted and stored at −20 °C. The final solution will be diluted from stock.
- Prepare HEPES 10 mM from powder and milliQ water.
- Equilibrate the pH of the HEPES solution to 7.4 using NaOH.
- Weigh the pLL–PEG and add corresponding HEPES volume to reach a final concentration of 1 mg/mL. Then filter the solution using a syringe and a filter of 0.22 µm mesh size. Aliquot the solution and store at −20 °C.
- When needed, thaw an aliquot and dilute it 10 times in HEPES solution to achieve at 0.1 mg/mL pLL–PEG concentration. The pLL–PEG solution should be then stored at 4 °C and used within few days.

6.2.3.3 Preparation of acrylamide solution and polymerization reagent

- Again, as acrylamide is carcinogenic, handle it with care under chemical hood and using proper user protection.
- Gel stiffness from a given acrylamide/bis-acrylamide ratio was reproducible in our hands but the stiffness measured using atomic force microscopy (AFM) for a given acry/bis-acrylamide ratio was very different from those reported by others, so we highly recommend to verify the actual stiffness of the gel in your own experimental conditions. As a starting point, one can use the table from Tse and Engler (2001) which covers a wide range of stiffnesses.
- Mix acrylamide and bis-acrylamide solution in water to obtain the desired concentration.
- This solution can be stored for few weeks at 4 °C.
- TEMED solution was used as received without further preparation.
- APS solution was prepared from powder in water milliQ at a concentration of 10% w/w and immediately frozen in small 10 µL aliquots and stored at −20 °C.
- Since APS is not very stable, one aliquot was used for each experiment and the remaining solution was systematically discarded.

6.3 ACRYLAMIDE PATTERNING FROM UV GLASS PATTERNING ("GLASS METHOD")

6.3.1 Materials

- ECM protein solution (i.e., Fibronectin solution (FF1141, Sigma, USA) and fibrinogen (FNG) Alexa Fluor 647 conjugate solution (F35200, Invitrogen, USA)
- Photomask (Toppan, France). Be careful to use a photomask compatible with deep UV exposure (see Azioune, Carpi, Tseng, Théry, & Piel, 2010 for more information)
- Silanized glass coverslip (see Section 6.2.3.1)

- Glass coverslips
- pLL–PEG solution (0.1 mg/mL in HEPES 10 mM, see Section 6.2.3.2)
- Sodium bicarbonate solution 100 mM pH 8.3 (0865 AMRESCO, USA)
- Trypsin/Ethylenediaminetetraacetic acid (EDTA)
- Cell culture medium
- Dulbecco's phosphate buffered saline (DPBS) (14190, Gibco, France)
- Cell culture dish

6.3.2 Equipment

- Deep UV lamp (UVO Cleaner Model NO.342A-220, Jelight Company, USA)
- Oxygen plasma oven
- Vacuum mask holder (custom, SMGOP, France) (see supplementary information for a picture of the mask holder) http://dx.doi.org/10.1016/B978-0-12-417136-7.00006-9
- Vacuum bell

6.3.3 Methods

6.3.3.1 pLL–PEG glass coating

- Remove dust from the glass coverslips.
- Warm up the pump of the plasma cleaner for few minutes (according to manufacturer's instruction).
- Put the glass coverslips in your plasma cleaner either horizontally or in a specific holder that will allow both sides of coverslips to be in contact with the ionized gas during the plasma treatment.
- Start pumping out the air in the reactor and wait for the pressure to stabilize (2 min).
- Open the oxygen inlet, set the gas flow to 5 mL/min (sscm), and wait for the pressure to stabilize (2 min).
- Run the plasma for 15 s at 30 W.
- Close the gas inlet, stop pumping, and ventilate the reactor (a filter should be placed on the air inlet to avoid dust intake into the reactor).
- Meanwhile put a drop of pLL–PEG solution (25 $\mu L/cm^2$) on parafilm.
- Take the coverslip with tweezers and flip it on the droplet in order to have the plasma-activated side of the coverslip facing the pLL–PEG solution and let incubate for 30 min.
- Afterwards, gently lift up the coverslip from the side using tweezers and put it vertically. Let the pLL–PEG run off by gravity. If needed, pipette the solution and put it back on the coverslip to help it run off the coverslip. Usually, one drop remains at the corner of the coverslip. You can remove it by gentle airflow from the other side of the coverslip in the direction of the corner.
- Store the coverslips at 4 °C with nothing in contact with the treated side of the coverslip and use within 2 days.

6.3.3.2 Deep UV insolation

- At this step, we will burn the passivized surface at specific positions by shining UV light through the chrome photomask. This will then allow us to adsorb protein at these specific positions.
- Heat up the UV lamp. This is very important. Power measurements of the lamp have shown that the steady state power is reached after 2–5 min (see supplementary information figure 1 for curve of the power in function of time) http://dx.doi.org/10.1016/B978-0-12-417136-7.00006-9 depending on the age of the lamp. We usually let it run for 5 min and then immediately put the sample inside the lamp and start the insolation process. The power measured at steady state was 6 mW/cm^2 at a distance of 1 cm from the lamp and a wavelength of 190 nm (you should take care to control the power frequently).
- Clean the photomask. First rinse it with milliQ water, then remove the liquid carefully using nitrogen gas flow, repeat the procedure with acetone and then isopropanol.
- Remove dust from the pLL–PEG coated glass coverslips, then put them on the vacuum mask holder, treated sides facing up. You should put at least three coverslips to have the mask horizontal. Then put carefully the mask on top, with the chrome side facing the coverslips. Plug the mask holder to house vacuum. The mask holder has a grid etched on it that corresponds to the grid we design on the photomask to easily find the shapes we want to produce. Then, put metallic pillars on two sides of the grip. Put the border of the mask in contact with these pillars in order to have a proper positioning of the coverslips in front of the desired matrix of shape on the mask.
- Put the entire setup in the warmed up UV lamp with the mask a few millimeters from the UV source. Expose for 5 min.
- Unplug the mask holder from the vacuum. Then carefully flip the photomask. If the contact between the mask and the coverslip was sufficient (no dust, no leaking of air from the side of the mask holder), the coverslips should stay stuck to the photomask.
- Detach the coverslips from the mask using a flexible tube connected to vacuum. Then store them activated side facing up at 4 °C and use within few days.

6.3.3.3 Protein coating and transfer on acrylamide gel

- The protein coating and the transfer on acrylamide gel should be performed in succession because otherwise the transfer is not as efficient. Here we will attach the ECM protein at the UV-activated sites on the glass coverslips and then transfer this protein on acrylamide gel by polymerization in contact.
- Prepare protein coating solution: we use a solution of 20 μg/mL of fibronectin diluted in sodium bicarbonate 100 mM. A small amount of fluorescently labeled protein could be added in order to see the micropatterns by fluorescence microscopy (typically 2 μg/mL of fibrinogen (FNG)—Alexa 647). Store the solution on ice.

- Rinse once the insolated side of the pLL–PEG coated coverslip with sodium bicarbonate and let the solution run of by putting the coverslip vertically. If some solution remains on the other side, it is not a problem.
- Put a droplet of protein solution on parafilm (25 μL/cm^2) and then put the pLL–PEG–UV-insolated side of the coverslip on the droplet. Protect from light and let it incubate for 30 min.
- In the meantime, aliquot the desired amount of acrylamide solution and allow it to degas in a vacuum bell.
- At the end of the incubation, put the glass vertically and let it dry. Then rinse three times with PBS.
- If you have used fluorescently labeled protein, check the quality of the procedure with fluorescence microscopy.

6.3.3.4 Transfer on acrylamide gel

- Here we will polymerize the acrylamide gel sandwiched between the patterned coverslip and the silanized coverslip. During detachment, the gel will stay attached to the silanized coverslip and the protein from the patterned coverslip will be transferred to the free surface of the acrylamide gel, resulting in a micropatterned acrylamide surface.
- If possible, one should use a silanized coverslip and patterned coverslips of two different sizes because it will then be much easier to detach them from each other.
- Put the larger of the two coverslips on a parafilm with the side of interest facing up. If both are of the same size, put a small drop of water on the parafilm and cover it with the patterned coverslip with the side of interest facing up. The small drop of water will prevent the acrylamide solution from sliding under the patterned coverslip.
- Collect the acrylamide solution from the vacuum bell and keep the container closed.
- *Optional*: If you want to add some fluorescent beads to your gel for force measurements, they should be added at this stage of the process in the acrylamide solution and the solution should be sonicated for 5 min to destroy any bead aggregates that could have formed during storage.
- Prepare TEMED, APS, and other coverslips. You will add TEMED and APS solution to the acrylamide with the following proportions: 1 μL of TEMED and 1 μL of APS 10% for 165 μL of acrylamide solution. You should proceed as fast as possible in the next steps.
- Add TEMED to the acrylamide solution, mix briefly but vigorously.
- Add APS solution to the acrylamide solution, mix briefly but vigorously.
- Put a drop of 7 μL/cm^2 of the acrylamide polymerization mix on each glass coverslip previously placed on parafilm.
- Slowly place the other coverslip of interest on top while taking care to avoid bubbles.

- Put a cap (to prevent evaporation) and let the gel polymerize for 30 min. Keep the rest of the acrylamide in a closed container as a control of gel polymerization.
- Once the polymerization is finished (you should check it by detaching the remaining acrylamide from the tube, it should have the shape of the container and be elastic if you try to pinch it with a pipette tip), immerse the sandwiched coverslips in PBS and let the gel hydrate for 5 min.
- Detach the patterned glass coverslip from the acrylamide gel using a scalpel, make sure that the gel is fully immersed during the entire detachment process, otherwise you will end up with collapsed micropatterns.
- Rinse the acrylamide gel attached to silanized coverslip (acrylamide coverslips) in PBS several times.
- Control quality with fluorescence microscopy if possible.
- Store at 4 °C and use as soon as possible.

6.3.3.5 Cell seeding

- Warm up your cell culture reagents as usual.
- Using ethanol sterilized tweezers, transfer the acrylamide coverslip in sterile tissue culture petri dish filled with sterile PBS (gel facing up).
- Rinse once with PBS and cover with warmed medium.
- In the meantime resuspend your cell in warmed medium.
- Remove the medium from the petri dish and center the coverslip in the middle of the dish. This way, if convection movements of fluid tend to aggregate cell in the middle of the dish, it will be over the acrylamide gel.
- Gently cover the gel with the cell suspension (a deposition of 100,000 cells/cm^2 has shown optimal cell attachment for RPE1, this should be adapted to your favorite cell line).
- Put the petri dish in the incubator.
- Check the cell attachment regularly (every 30 min). When a substantial number of cells have started spreading on micropatterns, renew the medium to remove unattached cells and replace in the incubator for further spreading.
- Have a nice experiment!

6.4 ACRYLAMIDE PATTERNING FROM PATTERNING ON QUARTZ PHOTOMASK ("MASK METHOD")

Here the procedure relies on the same principles except that the first patterned surface is produced directly on the chrome photomask. This allows higher resolution and thus will produce much more defined structures due to the absence of diffraction issues during insolation. We will activate the chromium side of the mask, coat it with pLL–PEG to prevent unspecific protein adsorption, burn the coating by shining UV through the shapes of the photomask, coat the insolated zones with ECM protein, and finally transfer these motifs by acrylamide polymerization in contact.

6.4.1 Materials

- ECM protein solution (i.e., Fibronectin solution (FF1141, Sigma, USA) and FNG (Alexa Fluor 647 conjugate solution (F35200, Invitrogen, USA))
- Photomask (Toppan, France). Be careful to use a photomask compatible with deep UV exposure (see Azioune et al., 2010 for more information)
- Silanized glass coverslip (see Section 6.2.3.1)
- Glass coverslips
- pLL–PEG solution (0.1 mg/mL in HEPES 10 mM, see Section 6.2.3.2)
- Sodium bicarbonate solution 100 mM pH 8.3 (0865 AMRESCO, USA)
- Trypsin/EDTA
- Cell culture medium
- DPBS (14190, Gibco, France)
- Cell culture dish

6.4.2 Equipment

- Deep UV lamp (UVO Cleaner Model NO. 342A-220, Jelight Company, USA).
- Oxygen plasma oven big enough for the photomask to fit in, you can also consider cutting the mask into pieces that you can handle separately, since you do not need to use the vacuum mask holder in this case.
- Vacuum bell.

6.4.3 Method

6.4.3.1 pLL–PEG quartz mask coating

- Remove dust from the glass coverslips and clean the photomask. First wash it with soap, then rinse it with water milliQ, then remove the liquid carefully using nitrogen gas flow.
- Put the mask (chromium side facing the air) and the coverslips in the plasma.
- Start pumping out the air in the reactor and wait for the pressure to stabilize (2 min).
- Open the oxygen inlet, set the gas flow to 5 mL/min (sscm), and wait 2 min for the pressure to stabilize (if you can control the pressure on your device, set it to 1 Torr = 133 Pa).
- Run the plasma at 100 W for 3 min. This time is higher than for glass because the photomask is reused several times while glass coverslips are usually already quite clean. Exposition to successive coatings of protein makes it necessary to use a long plasma treatment to clean the mask properly.
- Close the gas inlet, stop pumping, and ventilate the reactor (a filter should be placed on the air inlet to avoid dust intake into the reactor).
- Put one drop of pLL–PEG solution (25 $\mu L/cm^2$) on the region of interest on the mask.
- Cover the drop by flipping the activated glass coverslip on it and let it incubate for 30 min.
- At the end of the incubation, lift the coverslips carefully without scratching the coating on the photomask. Put the photomask vertically and let it dry. The solution should run off by itself. If it is not the case, you can collect again the solution that has

fallen down and put it back on the region of interest. This should help the drying process. As the coverslips have been coated at the same time, we will keep them for the incubation with the ECM protein; they will provide a fully passivized surface that will be used to sandwich the ECM droplet on the activated mask after UV insolation. You should rinse them once with water and let them dry. Be careful to remember which size has been coated with pLL–PEG to prevent any damage on this side.

6.4.3.2 Deep UV insolation and protein coating

- At this step, we will burn the passivized surface at specific positions by shining UV light through the chrome photomask from the unpassivized side. The UV light will burn the passivized treatment directly on the mask and this will then allow us to adsorb protein at these specific positions.
- Heat up the UV lamp. This is very important. Power measurements of the lamp have shown that the steady state power is reached after 2–5 min depending on the age of the lamp. We usually let it run for 5 min and then immediately put the sample inside the lamp and start the insolation process. The power measured at steady state was 6 mW/cm^2 at a distance of 1 cm from the lamp and a wavelength of 190 nm (you should take care to control the power frequently).
- Flip the mask to have the coated side away from the UV source. You can use small holders on the squares of the mask to prevent scratching of the coating. Expose to UV for 5 min.
- Prepare protein coating solution: we use a solution of 20 µg/mL of fibronectin diluted in sodium bicarbonate 100 mM. A small amount of fluorescently labeled protein could be added in order to see the micropatterns by fluorescence microscopy. Store the solution on ice.
- Remove the mask from the UV lamp and set it on a horizontal surface, passivized side now facing up.
- Put a droplet of protein solution (25 $\mu L/cm^2$) on the region of interest and then put the pLL–PEG coated coverslips (saved at Section 6.4.3.1) on the top, passivized side facing the droplet. Protect from light and let it incubate for 30 min.
- In the meantime, aliquot the desired amount of acrylamide solution and put it to degas in a vacuum bell.
- At the end of the incubation, remove the glass coverslips and discard them. Put the mask vertically and pour some bicarbonate solution on it to rinse. Let the solution dry by itself.

6.4.3.3 Transfer on acrylamide gel

- Here we will polymerize the acrylamide gel sandwiched between the patterned photomask and the silanized coverslips. During detachment, the gel will stay attached to the silanized coverslip and the protein from the patterned mask will be transferred of the free surface of the acrylamide gel, resulting in a micropatterned acrylamide surface.
- Set the photomask horizontally with the pattern side facing up. Make sure that you have waited long enough for the solution to dry.

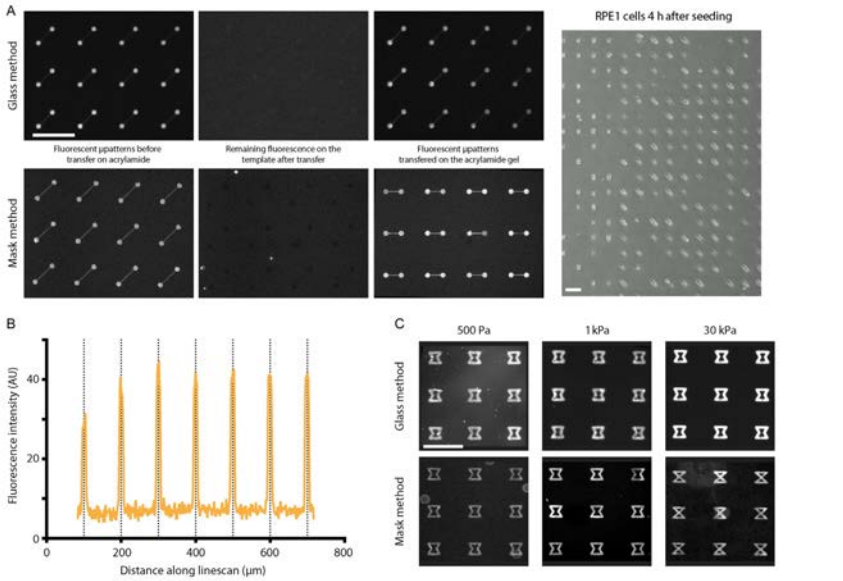

FIGURE 6.2

Both techniques provide robust protein transfer over a wide range of PAA stiffnesses. (A) Both techniques are presented in parallel. (Left) Micropatterns labeled with FN-Cy3 before transfer on acrylamide, (middle—left) remaining fluorescence on the initial micropatterned surface after transfer on acrylamide, (middle—right) micropatterns on acrylamide gel after detachment from the initially patterned surface. (Right) Phase contrast images of RPE1 cells 4 h after cell seeding. (B) Linescan of ECM protein fluorescence taken along several micropatterns, showing reproducible spacing between micropatterns and robust fluorescence intensity. (C) Fluorescence pictures of micropatterns labeled with FN-Cy3 produced using both techniques on PAA gel of 0.5 (left), 1 (middle), and 30 kPa (right). All scale bars correspond to 100 µm.

- Collect the acrylamide solution from the vacuum bell and keep the container closed.
- *Optional*: If you want to add some fluorescent beads in your gel for force measurements, they should be added at this stage of the process in the acrylamide solution and the solution should be sonicated for 5 min to destroy any bead aggregates that could have formed during the storage.
- Prepare TEMED and APS and silanized coverslips. You will add TEMED and APS solution to the acrylamide with the following proportions: 1 µL of TEMED and 1 µL of APS 10% for 165 µL of acrylamide solution. You should proceed as fast as possible in the next steps.
- Add TEMED to the acrylamide solution, briefly but vigorously mix.
- Add APS solution to the acrylamide solution, briefly but vigorously mix.
- Put a drop of 7 µL/cm^2 of the acrylamide polymerization mix on the mask in each patterned area of interest.
- Slowly place the silanized coverslip on top while taking care to avoid bubbles.
- Put a cap (to prevent evaporation) and let the gel polymerize for 30 min. Keep the rest of acrylamide in a closed container as a control of gel polymerization.
- Once the polymerization is finished (you should check it by detaching the remaining acrylamide from the tube, it should have the shape of the container and be elastic if you try to pinch it with the a pipette tip), cover the coverslips with PBS and let the gel hydrate for 5 min.
- Detach the acrylamide gel by carefully lifting the silanized coverslip using a razor blade. Due to the silanization process, the gel will stay attached to the coverslip. Make sure that the gel is fully immersed during the entire detachment process otherwise you will end up with collapsed micropatterns.
- Rinse the acrylamide gel attached to silanized coverslip (acrylamide coverslips) in PBS several times.
- Control quality with fluorescence microscope if possible.
- Store at 4 °C and use as soon as possible.

6.4.3.4 Cell seeding

- For the cell seeding, proceed as described in Section 6.3.3.5.

6.5 DISCUSSION

6.5.1 Storage

The best results were obtained when the gels were used immediately after production. If one wants to use a lot of gels on the same day, the "glass method" can be interrupted at the step of protein coating on the template. You can then produce many templates and store them in buffer for few days before transfer. The template should not be stored dry because it impairs the efficiency of the transfer process (Fig. 6.3A). If the storage of the gel is really necessary, one should store it wet in buffer as dry storage irreversibly deforms the micropatterns and detaches part of the protein coating (Fig. 6.3B).

6.5.2 Chemical modifications of protein for stronger protein adhesion to the PAA gel

Here we have described a protocol of protein transfer on acrylamide gel that does not require any specific chemistry for the crosslinking of the ECM protein to the gel. Observations of the fluorescence on the template micropatterned substrate (Fig. 6.2A and B) clearly show that the proteins were efficiently transferred on the acrylamide gel and cells were stably confined for a few days but not weeks. The technique was efficiently used on PAA gels of stiffnesses from 0.5 to 30 kPa (Fig. 6.2C) and used to perform traction forces experiments (Schiller et al., 2013).

Interestingly, if a polystyrene-coated coverslip was used for the template production, the transfer was then inefficient. The polystyrene coating has been shown to increase micropatterns stability for cell lines producing strong forces. In that case, the strength of the bond between acrylamide and the ECM protein is likely to be stronger than between ECM and glass, but weaker than between ECM and polystyrene (see Tang et al. (2012) for a detailed description of the detachment process and critical parameters). This strength is sufficient for the cell lines we have been using (RPE1, MCF10A, mouse fibroblasts) but it could be insufficient for other cell lines or for very long cell confinement. The passivation of the PAA could be improved by bovine serum albumin (BSA) incubation after micropattern production, and the stability of the micropatterns can be increased via chemical crosslinking strategies. Some groups have already put effort in this direction. Damljanovic et al. (2005) used a reducing agent, hydrazine hydrate, to modify nonreactive amide groups in PAA to highly reactive hydrazide groups that can form covalent bonds with aldehyde or ketone groups in oxidized proteins. ECM proteins were oxidized using sodium periodate (Polio et al., 2012) dissolved NHS ester in neutralized acrylamide solution before polymerization. NHS groups then react with amino groups on the proteins to form covalent bonds. The rest of the gel was then passivized by BSA incubation. Grevesse et al. (2013) replaced NHS esters by *N*-hydroxyethylacrylamide monomers resulting in the presence of hydroxyl groups in the acrylamide gel that could form hydrogen bonds with proteins. One should play around with these solutions if an improvement of the stability of the protein attachment to the acrylamide gel is required.

6.5.3 Resolution considerations

Even though both methods seem very similar, the maximal resolution that each can achieve is not the same. The "mask method" allows for a very faithful reproduction of the shape on the mask because the UV light is burning the surface directly in front of the shapes on the photomask (Figs. 6.1II and 6.3C) whereas there is a small distance between the passivized coverslip and the photomask at the step of UV insolation in the "glass method." Due to diffraction of the UV light, the burned area on the coverslip will be larger and smoother than the original shape on the mask. The linescans on fluorescently labeled micropatterns suggest that submicrometer resolution is achieved using patterning on the photomask.

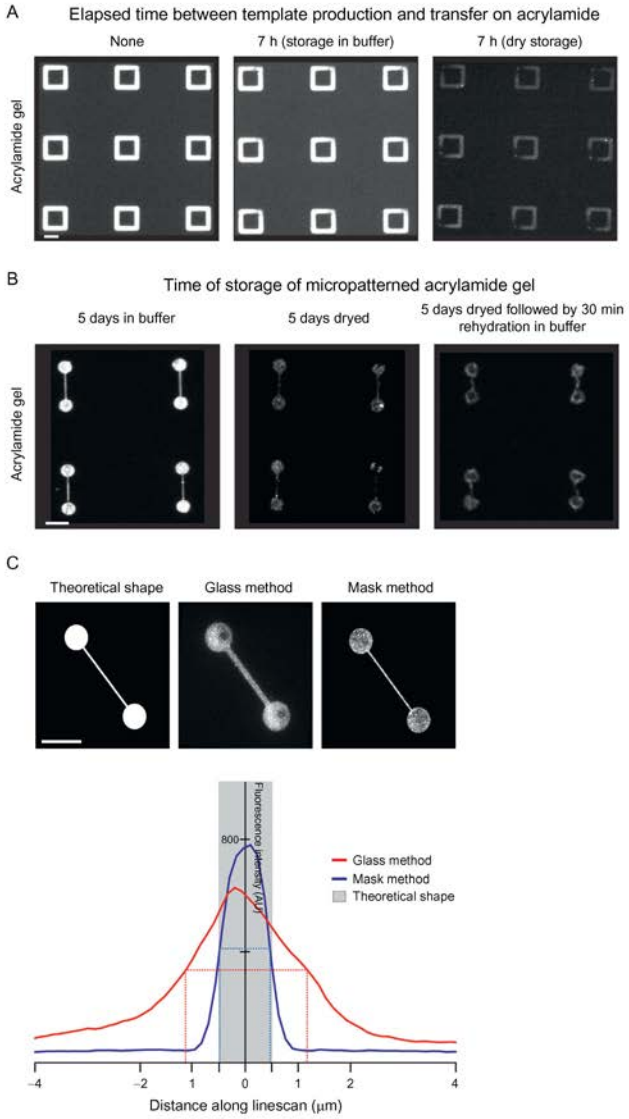

FIGURE 6.3

Conservation advice and micropattern resolution. (A) Fluorescent images of FN-Cy3 micropatterns on acrylamide gel. The template micropatterned glass coverslip was stored for 0 min (left), 7 h in PBS (middle), or 7 h dry (right) before acrylamide transfer. (B) Fluorescent

(*Continued*)

On the other hand, if your micropatterns can suffer a little enlargement then patterning on glass will allow you to produce many coverslips much more quickly. You can treat many coverslips with pLL–PEG at the same time, then insolate them sequentially and proceed through the other steps in parallel, while the full process has to be repeated sequentially when using the mask as the template surface.

The "glass method" might also be more suitable for sending coverslips to collaborators. Since the patterns on acrylamide should be used as soon as possible, one should consider sending UV-activated glass coverslips (produced at Section 6.3.3.2) that are more stable over time. The rest of the process (protein coating and transfer on acrylamide) does not require any expensive equipment and can be performed in any lab. You could even consider buying commercially available activated glass coverslips from micropatterning companies and just proceed through the protein coating and the transfer on acrylamide, with minimal equipment requirements.

6.5.4 Comparison to other techniques

The idea of producing micropatterns on acrylamide is not new. Several solutions have already been proposed to do this (Fig. 6.4 and Table 6.1), most of them are adaptations of existing techniques for micropatterning on hard substrates.

PDMS stencils (Fig. 6.4A) allow treatment at specific regions of the gel while keeping other regions unexposed. Once the gel is protected, the usual techniques of protein PAA functionalization can be used (Wang et al., 2002). Due to the elastic nature of the stencil, micropatterns may vary in their shapes due to deformation. Very small features are difficult to produce using this technique. If sulfo-SANPAH and UV insolation are performed through the stencil, a local modification of the stiffness of the acrylamide is likely to be created at the sites of micropatterns.

μCP (Fig. 6.4B) can also be performed on activated PAA (Damljanovic et al., 2005; Versaevel et al., 2012). A stamp covered with ECM protein is brought in contact with the activated PAA. This technique is difficult to perform on very soft gel and suffers from variability in protein transfer. Also deformation in the array of the micropatterns can occur if the PDMS is deformed at the step of stamping.

FIGURE 6.3—Cont'd images of FN-Cy3 micropatterns on PAA after storage of the gel for 5 days in PBS (left), 5 days dried (middle), 5 days dried, and after 30 min rehydration in PBS (right). (C) Assessment of the spatial resolution of both techniques. Theoretical shape of the micropatterns (up left), FN-Cy3 picture of a typical micropattern produced with the "glass method" (up middle) or the "mask method" (up right). Average of 20 linescans across the central line joining the head of the dumbbell shape of the micropatterns (down, red curve for the "glass method," blue curve for the "mask method," gray area for theoretical shape of the micropattern). The widths at half fluorescence maximum (doted lines) show that the "mask method" is very precise in reproducing the theoretical shape while the "glass method" suffers from enlargement of the micropatterns shape due to UV diffraction. All scale bars correspond to 20 μm.

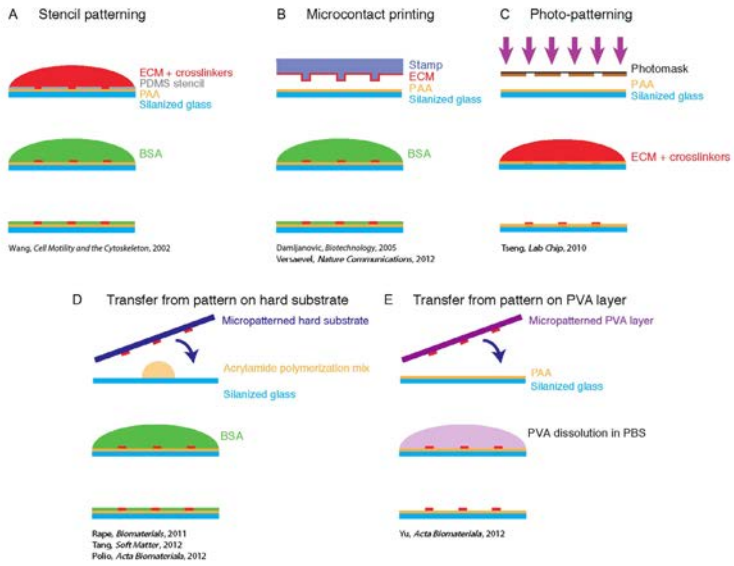

FIGURE 6.4

Existing techniques of micropatterning of polyacrylamide, see Section 6.5.4 for the description of each of them.

Table 6.1 Pros and cons of existing techniques for acrylamide patterning

	Spatial resolution (μm)	Robust pattern shape (no elastic deformation)	Suitable for soft (<1 kPa) substrate	Crosslinker-free procedure	Unchanged micropattern stiffness	Sequential patterning
Stencil patterning	1–10	–	+	–	+/–	+
Microcontact printing	1–10	–	–	–	+	+
Photo-patterning	>1	+	+	–	–	–
Transfer from pattern on hard substrate	1–10	–	+	+/–	+	+/–
Transfer from pattern on PVA layer	1–10	–	+	–	+	+
Mask method	>1	+	+	+	+	–
Glass method	1–2	+	+	+	+	+

Deep UV patterning (Fig. 6.4C) was successfully adapted to PAA patterning (Tseng et al., 2011). The gel is polymerized in contact with the photomask and then activated at specific loci using deep UV exposure. Incubation with chemical crosslinkers and ECM proteins leads to the production of micropatterned PAA gel. This technique creates patterns of very defined shape and organization due to the direct polymerization of the gel on the mask. This allows the development of force measurement techniques based only on the deformation of the micropattern with no need for traction force microscopy (TFM) expertise and cell detachment (Tseng et al., 2011). However, the use of sensitive chemical crosslinkers such as EDC introduces some variability in the protein attachment and deep UV exposure of the gel locally modifies the stiffness of the gel.

Transfer from micropatterned hard substrate (Fig. 6.4D) relies on polymerization of the acrylamide gel in contact with a previously patterned substrate (Polio et al., 2012; Rape et al., 2011; Tang et al., 2012). Crosslinkers in the solution allow for the transfer of ECM protein from the initial substrate to the surface of the acrylamide gel. This procedure is very attractive for laboratories that are already using micropatterns on hard substrate because only the transfer step has to be added to their standard protocol. However, the attachment between the initial hard substrate and the ECM protein has to be weak enough to allow for the transfer of the protein to the acrylamide gel. The resolution of the micropatterns is quite good in this case. However, it is less accurate than deep UV patterning due to the limitations of the technique used for the production of the template micropatterned substrate (μCP, stencil, etc.).

Transfer from patterned polyvinyl alcohol (PVA) film (Fig. 6.4E) (Yu et al., 2012) has been developed to solve the issues of μCP such as gel deformation due to mechanical contact and pattern deformation due to sticky interaction between the stamp and the PAA gel. Again, patterns are first produced on PVA film, then the PVA is put into contact with the activated soft substrate and dissolved in PBS. Thus, no deformation of the gel is induced by stamp detachment and the patterning is more accurate. However, the elastic properties of the layer could introduce some deformations in the micropatterns as for the stencil method. This technique is very promising for the patterning of curved surface such as implants or surgical tools since the initial PVA layer is flexible.

The method described here is combining many advantages that are found isolated in the other methods: no need for a chemical crosslinker, easy stamp production, no modification of acrylamide substrate due to crosslinkers or UV insolation, compatible with very soft gel (>1 kPa). Then one will have to choose between higher spatial resolution ("mask method") and higher throughput or multiple protein patterning ("glass method").

6.5.5 Future challenges and development

The process described here allows the robust and precise production of micropatterns on acrylamide gel of various stiffnesses. Multiple patterning can also be performed easily by the "glass method" technique with sequential insolation and protein coating on the glass template.

Submicrometer multiple patterning could be achieved using sequential laser patterning (Doyle, Wang, Matsumoto, & Yamada, 2009; Kim et al., 2010; Nakanishi et al., 2007) on glass or PVA and then transfer on acrylamide gel but the "mask method" is not suitable for this purpose. This will then provide heterogeneous cell environment for cell culture experiments that is more likely to reproduce complex *in vivo* cellular environment. It allows for the study of complex processes such as asymmetric stem cell division or tissue self-organization.

Traction force measurement based on dots micropatterns has been proposed as an alternative to fluorescent beads embedded in the acrylamide gel (Polio et al., 2012). This creates a platform for force measurement that is then quite similar to micropatterned PDMS microposts (Han, Bielawski, Ting, Rodriguez, & Sniadecki, 2014, Chapter 5 of Vol. 121) including the aspects of force computation from displacements. The technique described here is perfectly suited for this purpose.

Transfer on acrylamide from heterogeneous patterns produced on 3D substrate represents the next step in the improvement of these techniques, that is, for tissue engineering. It could provide the control of both topography and spatial localization of ECM protein. As the transfer is done using polymerization in contact with the template, the reproduction of topographical features is completely feasible (Charest, Califano, Carey, & Reinhart-King, 2011). If one is able to produce micropatterns on topographical features, using laser patterning on PDMS or polystyrene microstructures for instance, the transfer in acrylamide is then just one step ahead.

Real-time modification of the micropattern is something very challenging. This is already possible on hard substrates (Mandal, Balland, & Bureau, 2012; Nakanishi et al., 2007; Vignaud, Galland, et al., 2012) but as not yet been done on acrylamide. It could be another very useful tool for cell behavior studies and tissue engineering.

Finally, micropatterning has recently also been used for *in vitro* experiments (Reymann et al., 2014, Chapter 2 of Vol. 121). Patterning the nucleation of cytoskeleton proteins makes it possible to precisely study the role of boundary conditions in cytoskeleton organization with a minimal reconstituted system. Using patterning on PAA in the same way could allow for the study of the forces produced by these minimal mechanical architectures.

Acknowledgments

We would like to thank Mithila Burute for useful discussions on the micropatterning process and manuscript editing, Ben Fogelson and Aldo Leal-Egana for careful reading of the manuscript.

References

Azioune, A., Carpi, N., Tseng, Q., Théry, M., & Piel, M. (2010). Protein micropatterns: A direct printing protocol using deep UVs. *Methods in Cell Biology*, *97*, 133–146. http://dx.doi.org/10.1016/S0091-679X(10)97008-8.

Charest, J. M., Califano, J. P., Carey, S. P., & Reinhart-King, C. A. (2011). Fabrication of substrates with defined mechanical properties and topographical features for the study

of cell migration. *Macromolecular Bioscience*, *12*, 12–20. http://dx.doi.org/10.1002/mabi.201100264.

Damljanovic, V., Christoffer Lagerholm, B., & Jacobson, K. (2005). Bulk and micropatterned conjugation of extracellular matrix proteins to characterized polyacrylamide substrates for cell mechanotransduction assays. *Biotechnology*, *39*, 847–851. http://dx.doi.org/10.2144/000112026.

de Rooij, J., Kerstens, A., Danuser, G., Schwartz, M. A., & Waterman-Storer, C. M. (2005). Integrin-dependent actomyosin contraction regulates epithelial cell scattering. *Journal of Cell Biology*, *171*, 153–164. http://dx.doi.org/10.1083/jcb.200506152.

Doyle, A. D., Wang, F. W., Matsumoto, K., & Yamada, K. M. (2009). One-dimensional topography underlies three-dimensional fibrillar cell migration. *Journal of Cell Biology*, *184*, 481–490. http://dx.doi.org/10.1073/pnas.0604460103.

Engler, A. J., Sen, S., Sweeney, H. L., & Discher, D. E. (2006). Matrix elasticity directs stem cell lineage specification. *Cell*, *126*, 677–689. http://dx.doi.org/10.1016/j.cell.2006.06.044.

Grevesse, T., Versaevel, M., Circelli, G., Desprez, S., & Gabriele, S. (2013). A simple route to functionalize polyacrylamide hydrogels for the independent tuning of mechanotransduction cues. *Lab on a Chip*, *13*, 777–780. http://dx.doi.org/10.1039/c2lc41168g.

Han, S. J., Bielawski, K. S., Ting, L. H., Rodriguez, M. L., & Sniadecki, N. J. (2014). Decoupling substrate stiffness, spread area, and micropost density: A close spatial relationship between traction forces and focal adhesions. *Biophysical Journal*, *103*, 640–648. http://dx.doi.org/10.1016/j.bpj.2012.07.023.

Kim, M., Choi, J.-C., Jung, H.-R., Katz, J. S., Kim, M.-G., & Doh, J. (2010). Addressable micropatterning of multiple proteins and cells by microscope projection photolithography based on a protein friendly photoresist. *Langmuir*, *26*, 12112–12118. http://dx.doi.org/10.1021/la1014253.

Klein, E. A., Yin, L., Kothapalli, D., Castagnino, P., Byfield, F. J., Xu, T., et al. (2009). Cell-cycle control by physiological matrix elasticity and in vivo tissue stiffening. *Current Biology*, *19*, 1511–1518. http://dx.doi.org/10.1016/j.cub.2009.07.069.

Mandal, K., Balland, M., & Bureau, L. (2012). Thermoresponsive micropatterned substrates for single cell studies. *PLoS One*, *7*, e37548. http://dx.doi.org/10.1371/journal.pone.0037548.g001.

Nakanishi, J., Kikuchi, Y., Inoue, S., Yamaguchi, K., Takarada, T., & Maeda, M. (2007). Spatiotemporal control of migration of single cells on a photoactivatable cell microarray. *Journal of the American Chemical Society*, *129*, 6694–6695. http://dx.doi.org/10.1021/ja070294p.

Pelham, R. J., & Wang, Y. L. (1997). Cell locomotion and focal adhesions are regulated by substrate flexibility. *Proceedings of the National Academy of Sciences of the United States of America*, *94*, 13661–13665.

Pitaval, A., Tseng, Q., Bornens, M., & Thery, M. (2010). Cell shape and contractility regulate ciliogenesis in cell cycle-arrested cells. *Journal of Cell Biology*, *191*, 303–312. http://dx.doi.org/10.1083/jcb.201004003.dv.

Polio, S. R., Rothenberg, K. E., Stamenović, D., & Smith, M. L. (2012). A micropatterning and image processing approach to simplify measurement of cellular traction forces. *Acta Biomaterialia*, *8*, 82–88. http://dx.doi.org/10.1016/j.actbio.2011.08.013.

Prager-Khoutorsky, M., Lichtenstein, A., Krishnan, R., Rajendran, K., Mayo, A., Kam, Z., et al. (2011). Fibroblast polarization is a matrix-rigidity-dependent process controlled by focal adhesion mechanosensing. *Nature Cell Biology*, *13*, 1–10. http://dx.doi.org/10.1038/ncb2370.

Rape, A. D., Guo, W.-H., & Wang, Y.-L. (2011). The regulation of traction force in relation to cell shape and focal adhesions. *Biomaterials*, *32*, 2043–2051. http://dx.doi.org/10.1016/j.biomaterials.2010.11.044.

Reymann, A.-C., Martiel, J.-L., Cambier, T., Blanchoin, L., Boujemaa-Paterski, R., & Théry, M. (2014). Nucleation geometry governs ordered actin networks structures. *Nature Materials*, *9*, 827–832. http://dx.doi.org/10.1038/nmat2855.

Schiller, H. B., Hermann, M.-R., Polleux, J., Vignaud, T., Zanivan, S., Friedel, C. C., et al. (2013). β1- and αv-class integrins cooperate to regulate myosin II during rigidity sensing of fibronectin-based microenvironments. *Nature Cell Biology*, *15*, 625–636. http://dx.doi.org/10.1038/ncb2747.

Storm, C., Pastore, J. J., MacKintosh, F. C., Lubensky, T. C., & Janmey, P. A. (2005). Nonlinear elasticity in biological gels. *Nature*, *435*, 191–194. http://dx.doi.org/10.1038/nature03521.

Tang, X., Yakut Ali, M., & Saif, M. T. A. (2012). A novel technique for micro-patterning proteins and cells on polyacrylamide gels. *Soft Matter*, *8*, 7197. http://dx.doi.org/10.1039/c2sm25533b.

Théry, M. (2010). Micropatterning as a tool to decipher cell morphogenesis and functions. *Journal of Cell Science*, *123*, 4201–4213. http://dx.doi.org/10.1242/jcs.075150.

Tse, J. R., & Engler, A. J. (2001). *Preparation of hydrogel substrates with tunable mechanical properties*. Hoboken, NJ: John Wiley & Sons, Inc.

Tseng, Q., Wang, I., Duchemin-Pelletier, E., Azioune, A., Carpi, N., Gao, J., et al. (2011). A new micropatterning method of soft substrates reveals that different tumorigenic signals can promote or reduce cell contraction levels. *Lab on a Chip*, *11*, 2231–2240. http://dx.doi.org/10.1039/c0lc00641f.

Versaevel, M., Grevesse, T., & Gabriele, S. (2012). Spatial coordination between cell and nuclear shape within micropatterned endothelial cells. *Nature Communications*, *3*, 671. http://dx.doi.org/10.1038/ncomms1668.

Vignaud, T., Blanchoin, L., & Théry, M. (2012). Directed cytoskeleton self-organization. *Trends in Cell Biology*, *22*, 671–682. http://dx.doi.org/10.1016/j.tcb.2012.08.012.

Vignaud, T., Galland, R., Tseng, Q., Blanchoin, L., Colombelli, J., & Théry, M. (2012). Reprogramming cell shape with laser nano-patterning. *Journal of Cell Science*, *125*, 2134–2140. http://dx.doi.org/10.1242/jcs.104901.

Wang, N., Ostuni, E., Whitesides, G. M., & Ingber, D. E. (2002). Micropatterning tractional forces in living cells. *Cell Motility and the Cytoskeleton*, *52*, 97–106. http://dx.doi.org/10.1002/cm.10037.

Yu, H., Xiong, S., Tay, C. Y., Leong, W. S., & Tan, L. P. (2012). A novel and simple microcontact printing technique for tacky, soft substrates and/or complex surfaces in soft tissue engineering. *Acta Biomaterialia*, *8*, 1267–1272. http://dx.doi.org/10.1016/j.actbio.2011.09.006.

Zhang, J., Guo, W.-H., Rape, A., & Wang, Y.-L. (2013). Micropatterning cell adhesion on polyacrylamide hydrogels. *Methods in Molecular Biology*, *1066*, 147–156. http://dx.doi.org/10.1007/978-1-62703-604-7_13.

IV. Modelling the cytoskeleton

IV.1 What is a model?

A model is an abstract representation of reality that can be physical, graphical or more generally mathematical. It formalizes the relations between the different components of a system or a process in order to facilitate its comprehension predicts its evolution or validates some hypothesis.

By reducing the complexity of reality, the model can indeed offer valuable contribution to understand the phenomenon under study. It is built around assumptions about the modelled system and its behaviour, which are made from the experimental observations, and thus must be tested by confrontation with experimental data.

This confrontation can bring important information about the validity of the hypothesis done and their impact on the behaviour of the system. In particular, a negative result can be highly interesting as it shows that the hypothesis made are not valid or not enough to explain the experimental data (Mogilner et al. 2006). In this case, the model can then be progressively updated until it can explain the observations.

To make this confrontation step, a model is generally implemented by simulation. This method allows us notably to obtain “calculated” values, which can be confronted to ”observed values”. Once a model has been validated, it can generally be used as a predictive tool, to explore a wider range of conditions, but it is important to do so cautiously as it relies on the assumptions made to build it ("if it works like ... so if I do this, I should get that").

A model is a very interesting tool for its ability to provide enlightenment and/or “satisfactory” response to questions asked about the modelled object. By providing new insights about the studied object or by its predicative power, a model can also suggest the construction of new experiments to explore a specific system.

IV. 2. Contributions of modelling

IV.2.1. Quantify what is not measurable

One of the important contributions of scientific models to experimental science is their quantitative power. They can indeed give a measure of certain quantities that are not measurable because of the limits of instruments. In particular, in the case of actin, imaging techniques allow evanescent waves to observe individual filaments with a really low resolution (≈ 300 nm). Under this resolution, a pixel contains already a hundred monomers, which in consequence cannot be measured, whereas a mathematical model can accurately represent the state of each of the subunits in the polymer. Modelling can provides access to a wide variety of parameters like forces (generated by filament elongation (Kovar & Pollard, 2004), chemical constants (elongation rate, Vavylonis et al. 2006) or physical properties (persistence length measures, Bending-torsion coupling).

IV.2.2. Illuminating the role of different actors

Moreover, modelling allows to gain a better understanding of the role of each proteins involved in a particular process. In the context of in-vitro biology and reconstituted systems, we often have to handle several different proteins in parallel. Evaluate, by experience, the individual impact of each of these proteins on the final result is pretty difficult. Each protein is a "degree of freedom", for which one can vary the concentration or other parameters such as the affinity. The mathematical models help, via simulations or analytical considerations, to evaluate in a simple way the impact of each modelled parameter on the complete system. The sensitivity analysis of the parameters of a model can thus be an important point, not only to check the impact of the chosen parameters, but also to characterize the contribution of the different objects in the process.

IV.2.3. Guiding experience

Finally, after validation, the model is capable of guiding the experiment. In that case, it is the predictive modelling capabilities that are interesting. For example, in the first study of my thesis, we used simulations to predict the organisation of actin filaments from any given nucleation geometries. In the first project, I performed the in-vitro experiments on the simulated geometries and validated the predictive capacity of these simulations. Moreover, in the second study of my thesis, I presented an application of a model for

contractile actomyosin system used as guide tool of data explanation and prediction. Our model drove us to introduce the percolation term in the description of the experimental data, and allowed us to calculate the connectivity that regulates the contractile network. This analysis suggested to us to change dynamically the connectivity characteristic of the network to control its behaviour.

There are a huge variety of ways to build and use a model. The contribution of the model will thus rely on how and why it has been constructed. Generally, a model as simple as possible is preferable, but it has to be still complex enough to explain/explore the system. Therefore the main question in the development of a model is the biological question that motivates it and its possible contribution to it.

IV.3. The development of actin cytoskeleton modelling

A mathematical model always relies primarily on biological data. In the cytoskeleton field, it is quite often based on the characterization of individual action of many actin-binding proteins. By integrating the action of these proteins in the same model, we could model quantitatively certain functions of the actin cytoskeleton (filament polymerization protrusions, cytokinesis...). The exploitation of these models obviously involves a validation step, which consists in comparing the predictions with the biological datas.
Among the models on actin cytoskeleton we can find the model on the monomer interaction (Zheng et al. 2007), on actin filament creation (Vavylonis et al. 2005) (Vavylonis et al., 2005), model for connected networks (Carlsson, 2001) or for motility (Schaus et al. 2007).

As I have stated in part V.2.3, we have used this powerful tool of modelling in our study to complement our experimental approach. I will thus present the software that we have used, Cytosim. It has been developed by François Nédélec for simulating polymers dynamics and Gaelle Letort used it to model patterned actin cytoskeleton.

IV.4.Cytosim

IV.4.1. Presentation:

François Nédélec's team (EMBL, Heidelberg) has developed a software dedicated to the simulation of cytoskeleton polymers Nedelec and Foethke 2007 “Collective Langevin Dynamics of Flexible Cytoskeletal Fibers” 2009). He proposes a free version of this software on his website (www.cytosim.org) that can be used by the scientific community to study cytoskeleton dynamics. Moreover, François Nédélec shares the source code of this software upon request, so that it can be adapted to specific purposes by the user.

Cytoskeletal simulations involve multiple sides: (a) cellular chemical reactions, (b) cytoskeletal fibers assembly and disassembly (c) molecular motor transportation along fibers and (d) fibers deformation. The actual public or commercial codes are not adapted to simulate the entire cytoskeleton phenomenon. Fortunately, some algorithms related to what we just present are available like the diffusion reaction (Dobrzyński et al. 2007; Lemerle et al. 2005). Motor transportation can be modelled with their motion details (Kolomeisky, 2007). Fibers deformation is a classical problem related to mechanical equations (Landau & Lifshitz, 1986). However, the scale of living cells is associated with many specific features. The fibers are dynamic: they can lengthen or shorten by self-assembly. As a consequence, the physics of biological fibers is fundamentally distinct from other mechanical systems. Cytosim offers the possibility to study such systems.

IV.4.2. Principe:

Cytosim is a software dedicated to calculate the mechanics of an ensemble of fibers and objects. A biological polymer is represented as a fiber, which is discretized in a set of equidistant points (Figure 33). For each model points (mi in Figure 33), the motion equations are calculated at each discretized time points. It takes into account thermal fluctuations (with Brownian motion), bending elasticity, external forces (flow, physical constraints..) and steric interactions between fibers.

New objects in addition to fibers can be introduced like for example solid (non-deformable objects), which can be used to simulate the presence of other objects around the filaments (for example the nucleus in a cell). All objects (biological polymers or additional objects) are described by a set of points on which mechanical equations are

calculated (Figure 33). Finally, objects that can bind (and unbind) the fibers can be added and interact with them (exert forces, influence the growth dynamics of the fibers, nucleate new filaments...). These objects allow us to simulate the behaviour of different actin-binding or microtrubule-binding proteins, like in particular molecular motors.

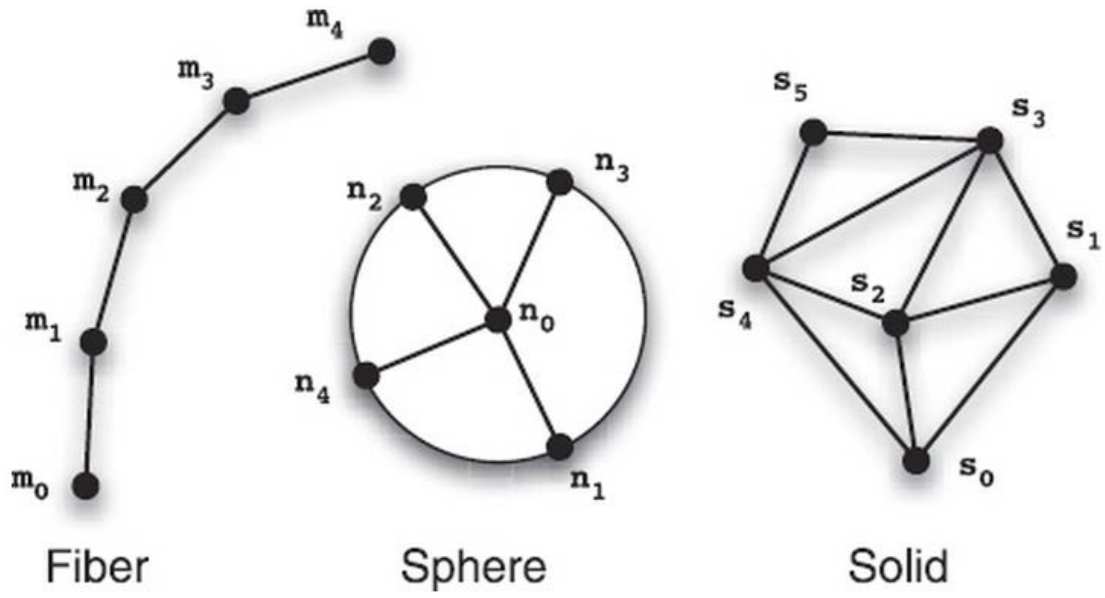

Figure 33 Elementary Objects in Cytosim. Points are describing all objects in the simulation. The points change coordinates in the viscous medium, but the relative distances between some points are conserved (lines). Fiber: A fiber is modelled as an equidistributed sequence of points. Sphere: it is composed of a central point and peripheral points (that can move), located in a distance r from the center. Right: A solid is a set of points that behaves like a solid body. Its shape and size are constants. (Nedelec et al., 2007)

A lot of studies have already used simulations with Cytosim (Foethke, Makushok, Brunner, & Nédélec, 2009; Gibeaux, Politi, Nedelec, Antony, & Knop, 2013; Pinot et al., 2009; Ward et al., 2015). Those studies show the interest to choose such software to understand the dynamics of the cytoskeleton in different conditions. Nevertheless, those study focuses on microtubule dynamics only. Cytosim has never been used to study the behaviour of the actin cytoskeleton in geometrically controlled conditions. Gaëlle Letort developed simulations with Cytosim to study such systems. I worked in close interaction with her to understand/predict, thanks to feedbacks between simulations and experiments, first, the growth of actin elements under different constraints and, second, the contraction of actin networks according to their biochemical composition and their structural organization.

1st project

I. Geometrical and mechanical properties control actin filament organization

The spatial distribution of actin nucleator directs the growth and assembly of actin filaments to form defined network geometries in 2D and 3D. Moreover the diversity of those geometries might be correlated with specific myosin driven contractile regimes.

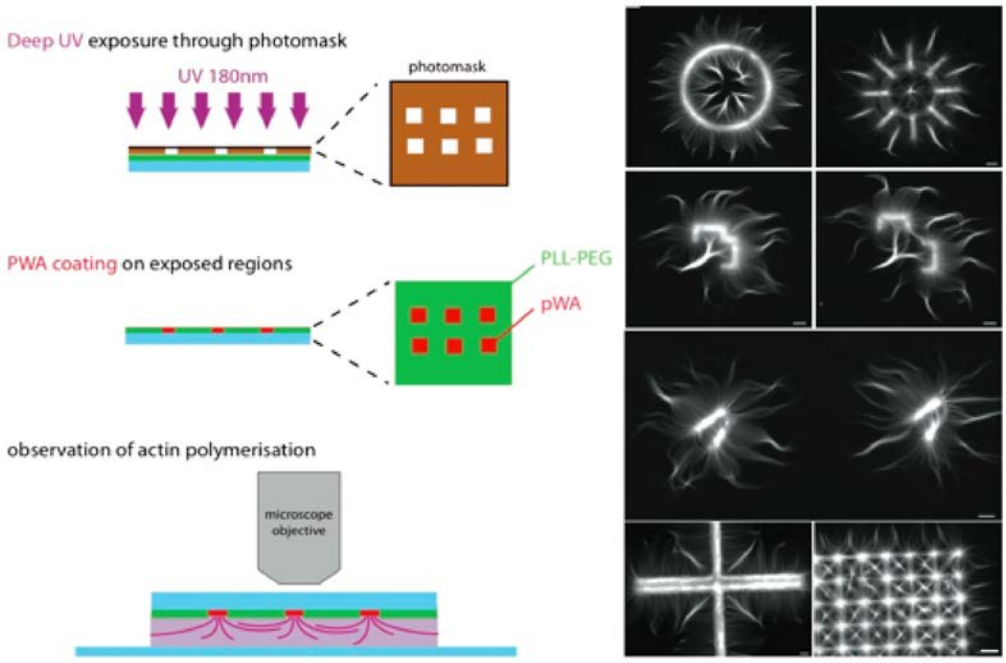

Figure 34 Reconstitution of actin assembly on micropatterned surfaces, (Reymann et al., 2010).

To get deeper insight in those processes, we studied the interplay between network geometry, dynamics and their ability to generate mechanical forces

A particular attention was devoted to the study of the role of actin network geometry and size. To achieve this goal, we developed a micropatterning method that enables the spatial control of actin nucleation sites for in vitro assays (Figure 34 and Reymann et al., 2010). Shape, orientation and distance between nucleation regions control filament orientation and length, filament–filament interactions and filopodium-like bundle formation. However, the basic mechanical and probabilistic laws that govern actin assembly in higher-order structures are still unknown.

In the study below, Gaëlle Letort in collaboration with the group of François Nedelec at the EMBL (Heidelberg, Germany) has developed in Cytosim a code that is able to simulate the growth of actin filaments from functionalized areas, which can initiate the actin filaments polymerization. Her goal was to develop a tool that can easily be used to determine the key parameters involved in directed actin assembly. I performed all the experimental work presented in this study.

Cytosim was developed specifically to model the dynamic assembly of microtubules and the role of molecular motors *in silico* (Nedelec et al. 2007). To use cytosim to study how the geometry of the nucleation area influences the overall actin organization we had to calibrate two key parameters that control interaction between neighbouring filaments, the attraction (Kpull) and the repulsion (kpush) coefficient between filaments.
To determine the adequate values for these parameters, we systematically compared experimental and in silico actin organization generated from a similar pattern.
If kpush is too low, only dense actin bundles are formed on the pattern and this is not in agreement with our experimental observation. On the opposite, if kpush is too high, actin filaments are avoiding each other without a collective organization. Similarly, if kpull is too small, the actin filaments behave like single filament and never bundle.
We determined therefore the best balance between these two parameters to obtain a good correlation between experiment and simulation. These conditions allowed us to study systematically the dynamic of actin filament organization generated by the micropatterning method.

We then studied how the variation of the angle between two opposing patterned regions influences actin filament architecture. Indeed, the proportion of parallel and antiparallel filaments along the bisector of the angle varies with the latter (Reymann et al., 2010) its mechanical property. To study the influence of the mechanical property on the overall actin organization, we tested three different conditions: a persistence length (Lp) of 15 μm corresponding to an actin filament, a lower Lp of 2 μm which could correspond to an actin filament decorated by ADF/cofilin and a Lp of 1,000 μm that could mimic actin filaments arranged in bundles. These variations in Lp revealed that the mechanical properties of the growing actin system are determinant in the collective assembly of actin.

Indeed, the more flexible filament with Lp of 2 μm rapidly deformed upon contact with a neighbouring filament limiting the collective formation of higher ordered structures such as bundles or array of parallel actin filaments (Figure 2 in Letort et al., 2015). The actin filaments with Lp of 15 μm formed depending of the contact angle an antiparallel structure or a large parallel bundle (Figure 2, Letort et al., 2015). Finally, for a high Lp of 1000 μm, actin filaments did not deform at all, and kept their initial direction of growth (Figure 2, Letort et al., 2015). Of course the distance between the two-nucleation areas also modulated the collective organization of actin filaments. This work highlighted how the length of the actin filaments and their mechanical properties depending of the geometry of the nucleation dictate the overall actin organization.

As the patterns we use encompass several nucleating areas, we tried to assess to which extent a filament growing from one area might affect the actin filaments collective assembly when it contacts the opposite nucleating region. Indeed when an actin filament encounters a nucleating area, it triggers de novo actin assembly by the so-called primer activation (Achard et al., 2010). Following this principle the number of actin filament contacting the adjacent nucleation area will influence the amount of actin filaments initiated from this pattern. Thus, we revealed how the collective growth of actin filament can trigger nucleation from adjacent nucleating zone and therefore can influence the density of the generated actin structure.

This study has revealed the fundamental parameters controlling the collective growth of actin filaments, depending on the geometry of nucleation areas. We have demonstrated that Cytosim is a very interesting tool to identify these key parameters. Moreover, we also demonstrated that Cytosim could be used as predictive tool to test the organization of the actin filaments for different complex geometries of nucleation. In fine, we highlighted several laws, which determine the collective behaviour of actin filaments in a cellular context.

PLOS | COMPUTATIONAL BIOLOGY

RESEARCH ARTICLE

Geometrical and Mechanical Properties Control Actin Filament Organization

Gaëlle Letort[1,2☯], Antonio Z. Politi[3☯], Hajer Ennomani[1], Manuel Théry[1], Francois Nedelec[3]*, Laurent Blanchoin[1]*

1 Laboratoire de Physiologie Cellulaire et Végétale, Institut de Recherches en Technologies et Sciences pour le Vivant, iRTSV, CNRS/CEA/UGA, Grenoble, France, **2** Laboratoire d'Imagerie et Systèmes d'Acquisition, CEA, LETI, MINATEC Campus, Grenoble, France, Univ. Grenoble-Alpes, Grenoble, France, **3** Cell Biology and Biophysics Unit, EMBL, Heidelberg, Germany

☯ These authors contributed equally to this work.
* nedelec@embl.de (FN); Laurent.blanchoin@cea.fr (LB)

OPEN ACCESS

Citation: Letort G, Politi AZ, Ennomani H, Théry M, Nedelec F, Blanchoin L (2015) Geometrical and Mechanical Properties Control Actin Filament Organization. PLoS Comput Biol 11(5): e1004245. doi:10.1371/journal.pcbi.1004245

Editor: Yaakov Koby Levy, Weizmann Institute of Science, ISRAEL

Received: September 25, 2014

Accepted: March 17, 2015

Published: May 27, 2015

Data Availability Statement: All relevant data are within the paper and its Supporting Information files.

Funding: This work was funded by Agence Nationale de la Recherche Grants ANR-12-BSV5-0014-02; the European Commission Seventh Framework Programme (FP7/2007–2013) under grant agreements no. 241548 and 258068; Labex Grenoble Alliance for Integrated Structural Cell Biology; and CTBU Grant from CEA to Gaëlle Letort. The funders had no role in study design, data collection and analysis, decision to publish, or preparation of the manuscript.

Abstract

The different actin structures governing eukaryotic cell shape and movement are not only determined by the properties of the actin filaments and associated proteins, but also by geometrical constraints. We recently demonstrated that limiting nucleation to specific regions was sufficient to obtain actin networks with different organization. To further investigate how spatially constrained actin nucleation determines the emergent actin organization, we performed detailed simulations of the actin filament system using Cytosim. We first calibrated the steric interaction between filaments, by matching, in simulations and experiments, the bundled actin organization observed with a rectangular bar of nucleating factor. We then studied the overall organization of actin filaments generated by more complex pattern geometries used experimentally. We found that the fraction of parallel versus antiparallel bundles is determined by the mechanical properties of actin filament or bundles and the efficiency of nucleation. Thus nucleation geometry, actin filaments local interactions, bundle rigidity, and nucleation efficiency are the key parameters controlling the emergent actin architecture. We finally simulated more complex nucleation patterns and performed the corresponding experiments to confirm the predictive capabilities of the model.

Author Summary

Many cellular processes or morphological changes, for example division and migration, strongly depend on the cytoskeleton. For successful completion of these processes in higher cells, thousands of cytoskeletal filaments need to be organized into precise higher-order structures. Identifying the most important parameters governing the emergent organization of large systems of filaments is thus a crucial step in understanding cytoskeletal systems. However, due to the complexity of these systems and the limits of imaging, this has proven to be a difficult task. To overcome this limitation we previously established an *in vitro* assay for actin filament assembly that allows controlling both the chemical components and geometrical boundaries. Here we used detailed computer simulations to

Competing Interests: The authors have declared that no competing interests exist.

rationalize the experimental observations and identify some of the physical principles governing actin organization. Such approach will ultimately allow one to predict actin network formation under various constraints.

Introduction

Actin assembles to form higher order structures [1] that are essential to cell morphogenesis, adhesion and motility [2]. A single filament can either resist or generate forces according to its local environment [3,4], but most physiological processes require the assembly of a higher ordered network [5,6]. Therefore, one needs to study the collective behavior of system composed of many thousands of actin filaments to understand their physiological functions. Indeed, whereas one actin filament could not sustain forces higher than a few pN [4], a bundle of actin filaments can resist hundreds of pN [7] and larger structures are able to bear even higher forces (nN range) [8]. In addition to the number of filaments, the architecture of the network is also adapted to achieve different cellular functions. At the edge of the cell, in the lamellipodium, actin filaments form a dense branched network [9–11], that seems optimal to push the membrane forward during actin-based motility [12,13]. Actin filaments are oriented with their elongating ends near the membrane, at an optimum angle of ± 35° with respect to the membrane [14, 15, 16], and being present in high density close to the membrane [17], they can efficiently sustain the protrusive force [13]. Actin filaments can also form bundles of parallel filaments, creating finger-like protrusions in the membrane called filopodia [18] that explore the extracellular matrix [19]. Actin bundles can be also used as tracks for protein or cargo transport [20,21]. These bundles can be formed by branched organization that merged into elongated parallel actin filaments [22,23]. Finally, actin filaments can form aligned structures of anti-parallel filaments in stress fibers or transverse arcs, that are site of active contraction driven by myosin motors [24,25] and are responsible for the cellular mechanical response [26]. Overall, the architecture of an actin network is expected to be directly related to its physiological function. The binding partners guide the organization of actin filaments, and conversely the binding of actin-associated proteins is sensitive to the architecture of the actin network [27,28]. Deciphering the principles governing the assembly of the different actin structural architectures is an important step towards a better understanding of the variety of cellular processes. Many excellent studies have focused on identifying the biochemical composition of the different actin organizations [6], but the physical and geometrical laws governing their architecture are still largely unknown.

In a previous work, we developed an *in vitro* method to control actin filaments assembly with a designed pattern composed of areas with different surface properties [1]. In these experiments, the geometry of the nucleation zone dictated the collective behavior of the actin filaments with some patterns resembling *in vivo* like structures [1]. The system was built from a minimal set of purified proteins, and avoiding the biochemical complexity of an *in vivo* system, it provided a well-controlled and reproducible assay to study the assembly of actin filaments in a variety of structures. Although, our study revealed how geometrical constraints affect actin assembly, the key components responsible for the formation of defined structural organizations remained poorly defined. The stochastic model developed in this study [1] helped to describe the observation but did not bring additional information on the properties of the system dictating the collective behavior. To better identify these parameters and ultimately understand the higher order architecture, we need to be able to predict the emergent actin organization, based on the microscopic properties such as the rates of actin assembly, the mechanical

properties of actin filaments, the geometry of the nucleation region, and the biochemical composition of the experimental system.

Different types of modeling are available for this purpose [29]. Collective cytoskeleton behavior has been studied at macroscopic scale with ordinary or partial differential equations [30–32]. Stochastic methods (Monte Carlo simulations) can take into account the variability arising from the intrinsic randomness of the microscopic processes [15,33–35]. The potential drawback of such detailed modeling is that they can be computationally expensive, but with modern methods [29], one can simulate systems containing thousands of filaments over hundreds of seconds. We used Cytosim [36], a versatile cytoskeleton simulation software, which can be used for a diverse range of cytoskeleton simulations. Actin filaments can be simulated with different growth and shrinkage rates and bending elasticities. Associated proteins can be added (e.g. molecular motors, crosslinkers, severing proteins, capping proteins, nucleators), and environmental constraints can be imposed (confinement, asters, solid objects, laser cutting, flow. . .). Cytosim polymer has been used to study microubule systems: self-organization [37,38], effect of confinement [39], spindles [40], asters positioning [41], nuclear positioning [42] but also to predict experimental design [43]. Nonetheless, Cytosim had never been used to study actin assembly under geometrical constraints.

Numerical experiments based on similar modeling have already been used to study the parameters controlling the global organization of cytoskeleton components. Recently, it was shown how different modes and efficiency of actin filament crosslinking would affect the self-organization of actin structures such as the contractile ring and actin cables [44, 45]. Similarly, simulations of taxane-stabilized microtubules [46] showed that geometrical constraints (cell confinement) combined with the bending properties of the filament was sufficient to create the bundling effect observed *in vitro*.

In this work, we first designed a simulation of actin organization from a nucleation region with a defined geometry, and reproduced the *in vitro* collective actin assembly behavior, with a minimum set of parameters. We then used this system to investigate how these parameters control the network organization in a range of experimental conditions. This study showed that we have identified the key parameters that define geometrically-controlled actin assembly and are able to reproduce a variety of actin organization *in silico*. Thus we believe that we have in hand a powerful predicting tool, and that numerical simulations in combination with *in vitro* experiments will help understand more complex actin processes.

http://www.ncbi.nlm.nih.gov/pubmed/23388829

Results

To study geometrically-controlled actin assembly, we previously developed an assay where actin nucleation is triggered from a micropatterned surface coated with an Nucleation Promoting Factor (NPF) (Fig 1A and [1]). The assay includes crowding agents constraining the filaments parallel to the glass. In this assay, actin nucleation occurs near the glass surface, and the growing actin structures never exceed 7μm in height, as revealed by confocal imaging (S1 Fig). The highest rise occurs immediately above the nucleating regions, while most of the network that extends away from them seems to be within 200 nm of the glass surface. This is confirmed by the fact that confocal and TIRF images of the system are comparable. The 2D model (S2 Fig) developed in Cytosim seems therefore appropriate to simulate the layer of actin assembly that is directly in contact with the glass, which is the part of the network that is most interesting in our experimental condition.

To simulate a geometrically constrained actin nucleation as used in experiments [1] we randomly disposed non-diffusible Arp2/3-like entities within the desired area (see S2, S3 Figs and

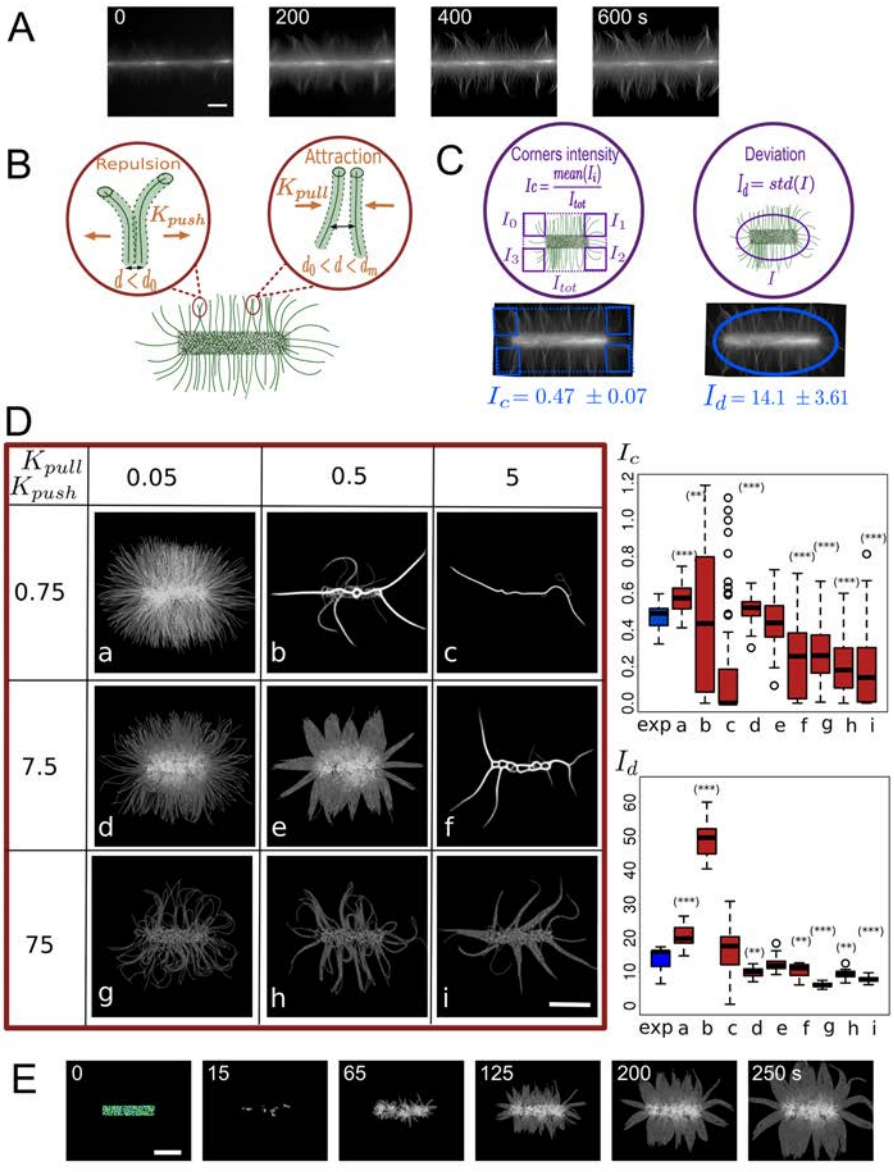
A
0
200
400
600 s
B
Repulsion
K_{push}
$d < d_0$
Attraction
K_{pull}
$d_0 < d < d_m$
C
Corners intensity
$Ic = \frac{mean(I_i)}{I_{tot}}$
I_0
I_1
I_2
I_3
I_{tot}
Deviation
$I_d = std(I)$
I
$I_c = 0.47 \pm 0.07$
$I_d = 14.1 \pm 3.61$
D
K_{pull} / K_{push}
0.05
0.5
5
0.75
7.5
75
a
b
c
d
e
f
g
h
i
I_c
I_d
exp a b c d e f g h i
E
0
15
65
125
200
250 s

Fig 1. Parameter calibration for actin growth on patterns. (A) *In vitro* actin filaments growing from an horizontal bar coated with the nucleation promoting factor pWA. Scale bar is 10 μm. (B) Schematic of steric interactions: the filaments repulse each other at short distance ($d<d_0$), and attract each other at medium range ($d_0<d<d_m$), and do not interact at longer range ($d>d_m$). Attractive and repulsive interactions are characterized by different stiffness (K_{pull}, K_{push}) that are applied to points distributed every 0.2 μm along the filaments. (C) To compare simulated and experimental data we used (left panel) the ratio I_c of average intensities in areas adjacent to pattern corner (I_i) by the total image intensity (I_{tot}). Both values are normalized by area size. To compare the bundling behavior, we measured **Id** the standard deviation of the intensity along an ellipse around the pattern (thus giving us the fluctuations of the distribution of filaments, right panel). Average corners intensity I_c and intensity deviation I_d from 10 experimental images (below images). (D) Variation of steric parameters and comparison of simulated and experimentally estimated I_c and I_d. Left: Three values were tested for K_{pull} (0.05, 0.5 and 5 pN/μm) and three values for K_{push} (0.75, 7.5 and 75 pN/μm), resulting in 9 combinations. The nucleating bar is 8 μm long and each image shows grey levels of actin density from one simulation at 250 s (scale bar is 5 μm). Right: Intensity ratio I_c and intensity deviation I_d for each set of parameters (**a-i**, red, from 20 simulations each) and experimentally estimated ratio (exp, blue). Based on their intensity ratios, the simulations shown on **d** and **e** agree well with experiment, while the ones shown on **b**, **c**, **f**, **g**, **h**, **i** are significantly different from experimental results (p-value < 0.001 (***), 0.005 (**), 0.01 (*), Kolmogorrov-Smirnov test). With the same test, conditions **a**, **b**, **d**, **f**, **g**, **h**, **i** are significantly different from experimental results based on intensity deviation analysis. (E) Simulated growth of filaments using set **e** (K_{pull} = 0.5 pN/μm, K_{push} = 7.5 pN/μm). Actin filament nucleation is triggered by contact between primers with Arp2/3-like objects placed in the central rectangle (see S1 Fig). Scale bar is 5μm. The pattern is 8 μm wide and time in seconds is indicated.

doi:10.1371/journal.pcbi.1004245.g001

Material and Methods). These Arp2/3 complexes are able to nucleate a new (daughter) filament, but only if they are already bound to an existing (mother) filament. Because they do not move by diffusion, and thus remain in the nucleating region, the Arp2/3 complexes can generate branches within the nucleation area, but not outside. This mimics the activation of the Arp2/3 complex by the pWA-peptide coated on the pattern (S2 Fig). The Arp2/3 complex acts as a mechanical link between mother and daughter filaments, constraining them relative to each other in position and in orientation, such that the pointed end of the daughter filament remains on the side of the mother filament, and the daughter barbed end grows out making a ~70° angle with the mother filament [47, 48]. In the same area, we also added fixed nucleators, which initiate the process by generating the primer filaments, and fixed binders, which may bind to any actin filament within their range, and are anchored at a fixed position with a Hookean spring. These "fixed binders" have a non-zero unbinding rate and thus they effectively create some friction acting on any filament entering the micro patterned region. This friction accounts for the constrained nucleation processes and is necessary to maintain a dense patterned area (S2 Fig).

The simulated filaments are not meant to only represent individual actin filaments, but may also represent bundles of several crosslinked filaments. We will thus refer to them as fibers. Similarly, the 'steric' interaction between fibers is meant to be effective, representing the different forces that may act between neighboring F-actins. These parameters can be varied experimentally by modifying the type and concentration of actin binding proteins, the buffer solution or fiber confinement, conditions that have been shown to induce different actin organizations [1]. Our first task was to calibrate the effective parameters of the simulation, by comparing simulations and experiments obtained with a simple pattern.

Role of actin filament steric interactions in determining the actin organization

Input of Cytosim is a configuration file specifying the values of all parameters of the model: some represent physical quantities (e.g. temperature, viscosity), some are associated with the algorithm of the simulation (e.g. time step, segmentation) and were set to get an appropriate precision. Yet, most parameters are characteristics of the real components of the system (e.g. F-actin growing speed and bending rigidity). We adopted measured values when possible, using for example the measured persistence length of 15 μm of actin filaments [6] and a rate of elongation of 0.033 μm/s (actin concentration of 1–2 μM [49]). Finally, a few parameters are associated with effective interactions for which a molecular implementation is not necessarily feasible. This is the case in particular for filament-filament interactions, which are essential to

PLOS | COMPUTATIONAL BIOLOGY

Fig 1. Parameter calibration for actin growth on patterns. (A) *In vitro* actin filaments growing from an horizontal bar coated with the nucleation promoting factor pWA. Scale bar is 10 μm. (B) Schematic of steric interactions: the filaments repulse each other at short distance ($d<d_0$), and attract each other at medium range ($d_0<d<d_m$), and do not interact at longer range ($d>d_m$). Attractive and repulsive interactions are characterized by different stiffness (K_{pull}, K_{push}) that are applied to points distributed every 0.2 μm along the filaments. (C) To compare simulated and experimental data we used (left panel) the ratio I_c of average intensities in areas adjacent to pattern corner (I_i) by the total image intensity (I_{tot}). Both values are normalized by area size. To compare the bundling behavior, we measured **Id** the standard deviation of the intensity along an ellipse around the pattern (thus giving us the fluctuations of the distribution of filaments, right panel). Average corners intensity I_c and intensity deviation I_d from 10 experimental images (below images). (D) Variation of steric parameters and comparison of simulated and experimentally estimated I_c and I_d. Left: Three values were tested for K_{pull} (0.05, 0.5 and 5 pN/μm) and three values for K_{push} (0.75, 7.5 and 75 pN/μm), resulting in 9 combinations. The nucleating bar is 8 μm long and each image shows grey levels of actin density from one simulation at 250 s (scale bar is 5 μm). Right: Intensity ratio I_c and intensity deviation I_d for each set of parameters (**a-i**, red, from 20 simulations each) and experimentally estimated ratio (exp, blue). Based on their intensity ratios, the simulations shown on **d** and **e** agree well with experiment, while the ones shown on **b**, **c**, **f**, **g**, **h**, **i** are significantly different from experimental results (p-value < 0.001 (***), 0.005 (**), 0.01 (*), Kolmogorrov-Smirnov test). With the same test, conditions **a**, **b**, **d**, **f**, **g**, **h**, **i** are significantly different from experimental results based on intensity deviation analysis. (E) Simulated growth of filaments using set **e** (K_{pull} = 0.5 pN/μm, K_{push} = 7.5 pN/μm). Actin filament nucleation is triggered by contact between primers with Arp2/3-like objects placed in the central rectangle (see S1 Fig). Scale bar is 5μm. The pattern is 8 μm wide and time in seconds is indicated.

doi:10.1371/journal.pcbi.1004245.g001

Material and Methods). These Arp2/3 complexes are able to nucleate a new (daughter) filament, but only if they are already bound to an existing (mother) filament. Because they do not move by diffusion, and thus remain in the nucleating region, the Arp2/3 complexes can generate branches within the nucleation area, but not outside. This mimics the activation of the Arp2/3 complex by the pWA-peptide coated on the pattern (S2 Fig). The Arp2/3 complex acts as a mechanical link between mother and daughter filaments, constraining them relative to each other in position and in orientation, such that the pointed end of the daughter filament remains on the side of the mother filament, and the daughter barbed end grows out making a ~70° angle with the mother filament [47, 48]. In the same area, we also added fixed nucleators, which initiate the process by generating the primer filaments, and fixed binders, which may bind to any actin filament within their range, and are anchored at a fixed position with a Hookean spring. These "fixed binders" have a non-zero unbinding rate and thus they effectively create some friction acting on any filament entering the micro patterned region. This friction accounts for the constrained nucleation processes and is necessary to maintain a dense patterned area (S2 Fig).

The simulated filaments are not meant to only represent individual actin filaments, but may also represent bundles of several crosslinked filaments. We will thus refer to them as fibers. Similarly, the 'steric' interaction between fibers is meant to be effective, representing the different forces that may act between neighboring F-actins. These parameters can be varied experimentally by modifying the type and concentration of actin binding proteins, the buffer solution or fiber confinement, conditions that have been shown to induce different actin organizations [1]. Our first task was to calibrate the effective parameters of the simulation, by comparing simulations and experiments obtained with a simple pattern.

Role of actin filament steric interactions in determining the actin organization

Input of Cytosim is a configuration file specifying the values of all parameters of the model: some represent physical quantities (e.g. temperature, viscosity), some are associated with the algorithm of the simulation (e.g. time step, segmentation) and were set to get an appropriate precision. Yet, most parameters are characteristics of the real components of the system (e.g. F-actin growing speed and bending rigidity). We adopted measured values when possible, using for example the measured persistence length of 15 μm of actin filaments [6] and a rate of elongation of 0.033 μm/s (actin concentration of 1–2 μM [49]). Finally, a few parameters are associated with effective interactions for which a molecular implementation is not necessarily feasible. This is the case in particular for filament-filament interactions, which are essential to

capture the collective behavior of growing filaments [50,51]. Actin filaments are physically not able to interpenetrate each other and within distances equal to their diameter must experience strong repulsive force. Moreover, although similarly charged, actin filaments attract each other at short range, due to the presence of counterions in the solution [50,51]. Moreover, the presence of chemically neutral polymers in the solution creates a depletion effect that also induces neighboring filaments to pack together [51, 52]. This explains how we could observe bundles *in vitro* without adding any actin filament crosslinkers to the solution. It also means that changing the experimental conditions (pH of buffer, ionic strength, concentration of polymers, etc.) may affect how actin filaments interact. Rather than trying to simulate these processes in details, we have used an ad-hoc steric interaction between simulated filaments, and calibrated the parameters of this interaction to best reproduce the behavior of the *in vitro* system. In Cytosim, a 'steric' filament-filament interaction can include both attractive and repulsive forces (Figs 1B and S2):

$$F_s = k\,(d - d_0), \quad with\ k = \begin{cases} K_{push}\ if\ d < d_0 \\ K_{pull}\ if\ d_0 \le d \le d_m \\ 0\ otherwise \end{cases} \tag{1}$$

where d is the distance between the two interacting elements, d_0 is the distance at which the fibers are at equilibrium (this is an effective fiber diameter, which is larger than the real diameter), d_m is the maximal interaction distance between fibers (the choice of these values is discussed in Material and Methods). To fix the two stiffness values, K_{push} and K_{pull} (Fig 1B), we tested a range of values and compared systematically the simulation outputs with experimental results at first using a simple pattern configuration: a horizontal bar (Fig 1A, 1C and 1D). On this pattern actin filaments assembled into a dense network on the patterned bar, with their barbed ends growing away from the pattern, filaments align parallel to each other and generate bundles growing out perpendicularly to the bar (Fig 1A and [1]). In the simulations we found that a balance between repulsing and attracting steric interactions strongly affects the organization of actin (Fig 1D). When the attractiveness was similar or higher than repulsion (Fig 1D panel b, c, f) actin fibers collapsed together. On the contrary, when the repulsion dominates (K_{push} = 75 pN/μm, Fig 1D, panel g, h, i), actin fibers are disorganized and do not generate bundle-like structure. For a quantitative comparison of simulations and experiments we computed the average local intensity in the corners of the patterned bar normalized by the total average intensity (I_c, Fig 1C). This quantity gives a measure of the spatial distribution of the filaments: when organized in bundle-like structures, fibers are less dense in the corners of the pattern thus I_c is lower than 1. A bar plot of I_c in experiment (N = 10) and for the 9 simulation scenarios (N = 20) is shown in Fig 1D. We found that the corner intensities corresponding to panels a, b, c, f, g, h, i (Fig 1D) were significantly different from experimental ones (p-value < 0.005, Kolomogorov-Smirnov test), whereas the ones corresponding to panels d and e were not (p-value>0.1). To further compare simulations and experiments, we also measured the variation of intensity along the perimeter of an ellipse around the pattern (I_d). This gives a measure of the bundling of the filaments: a high value indicates the presence of intense bundles, whereas a low value accounts for spread filaments all over the pattern. With this measurement, we found that the deviation of intensity corresponding to panels a, b, d, f, g, h, i were significantly different from experimental ones. Thus, panel e (K_{push} = 7.5 pN/μm, K_{pull} = 0.5 pN/μm) quantitatively reproduced the *in vitro* actin filaments behavior most accurately. Indeed, the actin network growing from the micro-pattern in simulation (Fig 1E and S1 Movie) was fully consistent with our experimental observations [1]. All following simulations thus used these calibrated parameters.

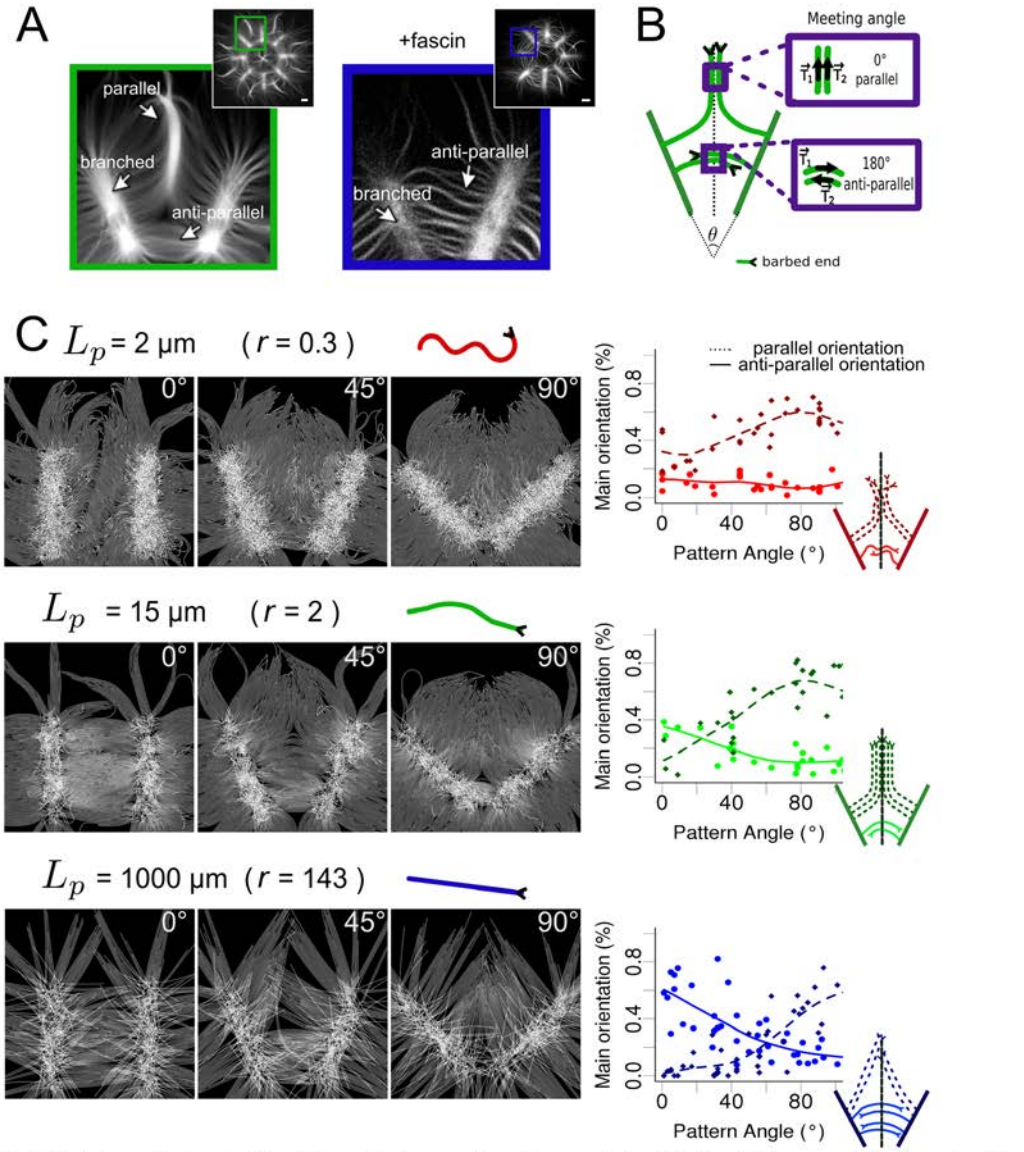

Fig 2. Effect of geometrical constraints and fiber mechanical properties on fiber organization. (A) *in vitro* actin filament organization from a star eight-fold radial array pattern coated with pWA activator, in absence (green) or presence (blue) of fascin, an actin filament cross-linker. A portion of the pattern

containing the V-shaped submotif is shown at higher magnification in both cases. (B) Schematic representation of the actin organization on two adjacent rays (V-shaped configuration): parallel (top) and anti-parallel filament structures (bottom). The presence of these two patterns is assessed from the meeting angle between filaments from opposing patterns on the middle line. (C) Left: Simulated filament growth on patterns with 3 different angles (0°, 45°, 90°) and 3 different filament persistence lengths (L_p = 2 μm, r = L_p/L = 0.3, red; L_p = 15 μm, r = 2, green; L_p = 1000 μm, r = 143, blue) (one simulation is shown in each case). Right: Proportions of the main orientation (percentage of filaments crossing the median line with a particular orientation) of filaments (dashed lines: parallel filaments, full lines anti-parallel filaments) on the median line, as a function of the angle between the two patterns.

doi:10.1371/journal.pcbi.1004245.g002

because given a certain force F applied transversally at the growing tip of the filament, its bending angle will scale as $\theta \sim FL^2/K$, where K is the filament bending stiffness ($K = k_BT\,Lp$) and L the length of the actin filament. At the bottom of the pattern, actin filaments meet while they are short, the bending required to enter a parallel structure is consequently unfavorable, and anti-parallel structures are created instead. On the top of the pattern however, actin filaments are longer as they contact opposite filaments; and consequently are easier to bend leading to parallel bundles (Fig 2B and 2C).

To further confirm this analysis, we repeated these simulations with fibers of 15 μm persistence length and varied the length of the fibers (and thus the distance between the patterns and the simulated time as well). The analysis of the presence of structures (S4 Fig) revealed that indeed the ratio between the polymer persistence length and their length will determine their collective behavior. Indeed, short actin fibers with a persistence length of 15 μm will have the same behavior than shorter fibers with 2 μm persistence length or longer fibers with 1000 μm persistence length (S4 Fig). The definition of the persistence length makes this relation between filament length and rigidity obvious for isolated filaments, but was necessary to demonstrate in the context of collective filaments behavior.

Thus, both the geometrical conditions of nucleation and the mechanical properties of the simulated filaments are key parameters controlling the formation of anti-parallel or parallel structures.

Actin filaments reaching a branched network can cross it and/or generate new filaments by nucleation

We next simulated a pattern containing two parallel pWA (Arp2/3 activator) bars of width 3 μm to study the "primer effect". This effect is based on the ability of a drifting actin filament to contact the nucleation area and trigger actin assembly (S2 and S3 Figs). The *in vitro* experiment was constructed such that a growing actin filament coming into contact with a virgin patterned region will nucleate new actin filament on its side [55]. However, when two or more patterned regions are in close proximity, a region of pWA may already be covered by an actin network (Fig 3A). We therefore have two possible scenarios for the fate of a filament reaching a pattern of pWA on which a branched network is already present (Fig 3A): (i) the filament gets entangled in this network and stop growing, (ii) the filament can nucleate new filaments as if the pattern was virgin (and get entangled or not). To find which scenario is correct, we compared simulations and *in vitro* experiments by systematically varying the distance between the two bars. As control condition, i.e. non-interaction between the two patterns, we selected cases where the distance d between adjacent bars is above (d_∞ = 80 μm). In this case filaments from one bar do not reach the other bar.

To assess the contribution of a neighboring pattern on the overall actin network we computed:

$$\rho_{ext}(d) = \frac{I(d,\ t_f)}{I(d,\ t_i)} - \frac{I(d_\infty,\ t_f)}{I(d_\infty,\ t_i)},$$

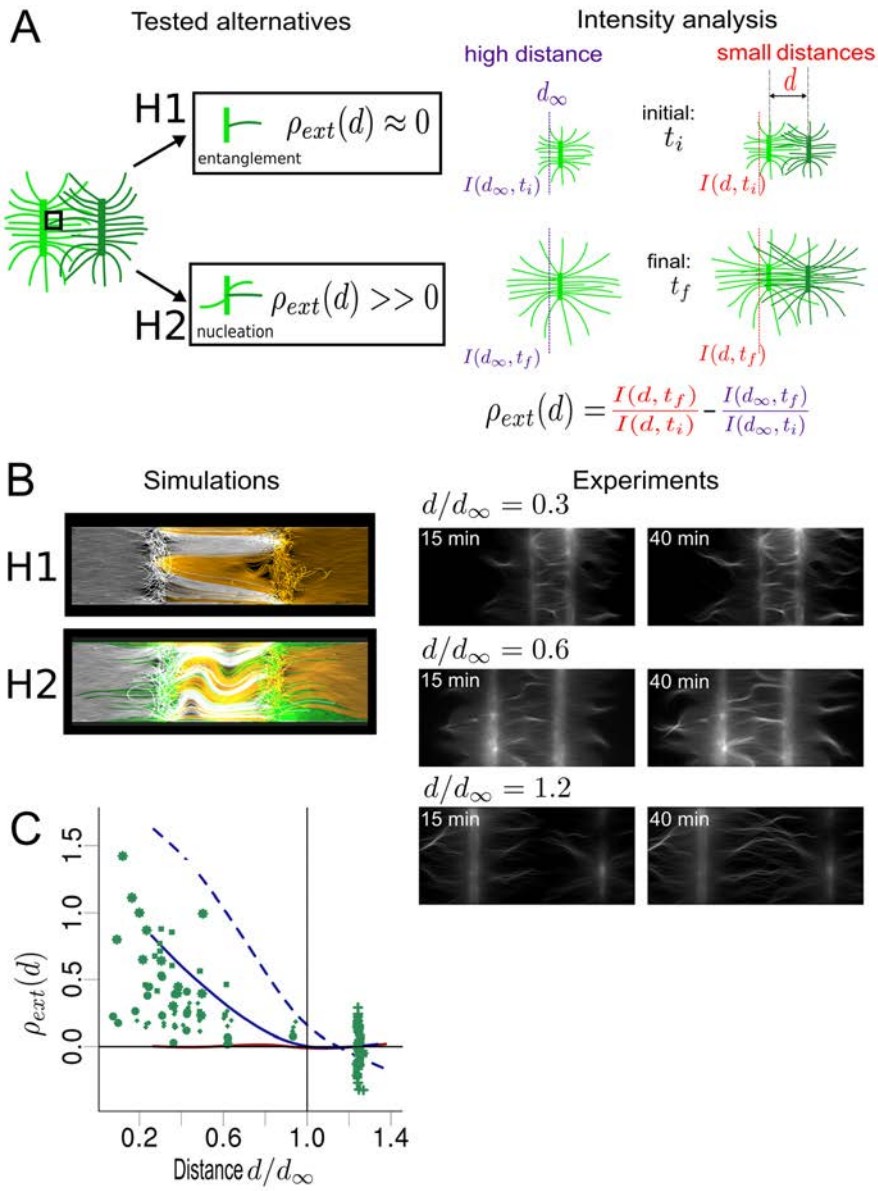
A
Tested alternatives
H1
$\rho_{ext}(d) \approx 0$
entanglement
H2
$\rho_{ext}(d) >> 0$
nucleation
Intensity analysis
high distance
small distances
d_∞
d
initial:
t_i
$I(d_\infty, t_i)$
$I(d, t_i)$
final:
t_f
$I(d_\infty, t_f)$
$I(d, t_f)$
$\rho_{ext}(d) = \frac{I(d,t_f)}{I(d,t_i)} - \frac{I(d_\infty,t_f)}{I(d_\infty,t_i)}$
B
Simulations
H1
H2
Experiments
$d/d_\infty = 0.3$
15 min
40 min
$d/d_\infty = 0.6$
15 min
40 min
$d/d_\infty = 1.2$
15 min
40 min
C
$\rho_{ext}(d)$
0.0
0.5
1.0
1.5
0.2
0.6
1.0
1.4
Distance d/d_∞

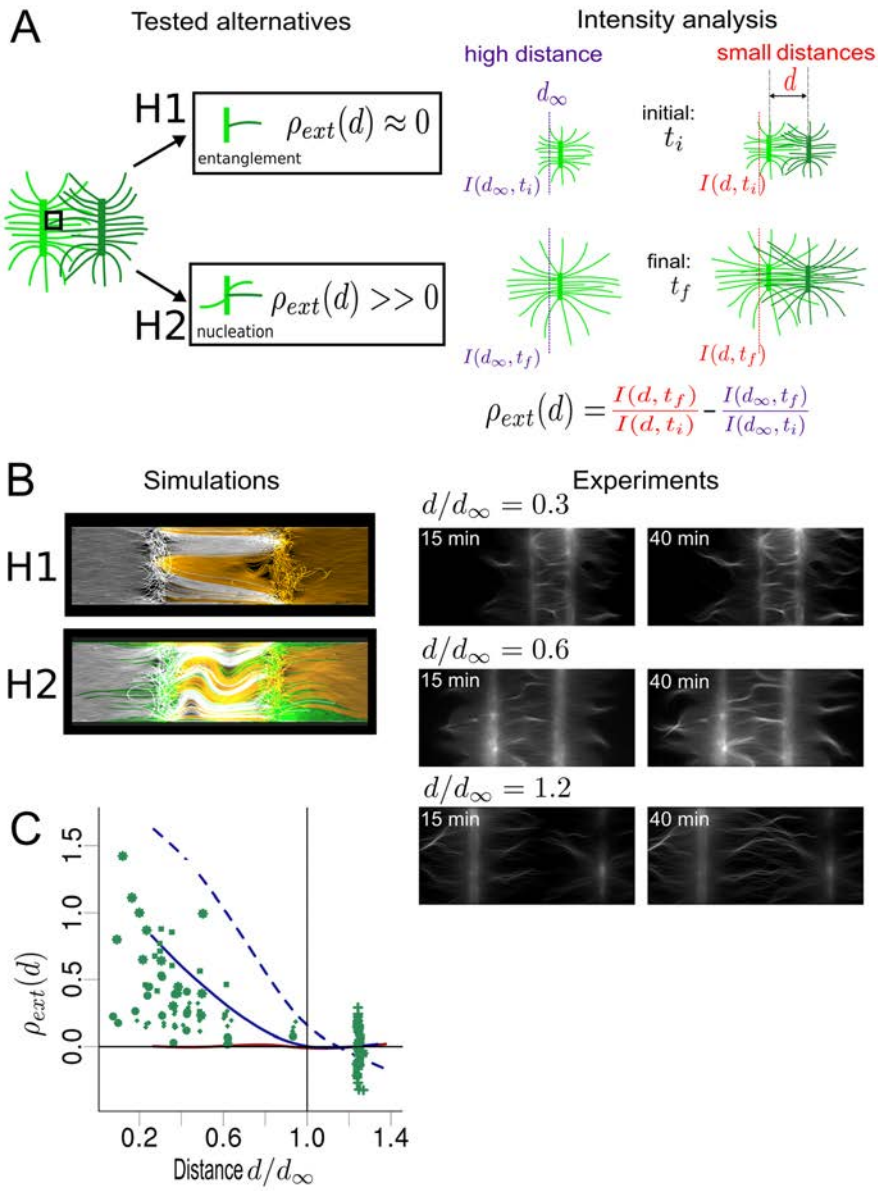
A
Tested alternatives
H1
$\rho_{ext}(d) \approx 0$
entanglement
H2
$\rho_{ext}(d) >> 0$
nucleation
Intensity analysis
high distance
small distances
d_∞
d
initial:
t_i
$I(d_\infty, t_i)$
$I(d, t_i)$
final:
t_f
$I(d_\infty, t_f)$
$I(d, t_f)$
$\rho_{ext}(d) = \frac{I(d,t_f)}{I(d,t_i)} - \frac{I(d_\infty,t_f)}{I(d_\infty,t_i)}$
B
Simulations
H1
H2
Experiments
$d/d_\infty = 0.3$
15 min
40 min
$d/d_\infty = 0.6$
15 min
40 min
$d/d_\infty = 1.2$
15 min
40 min
C
$\rho_{ext}(d)$
0.0
0.5
1.0
1.5
0.2
0.6
1.0
1.4
Distance d/d_∞

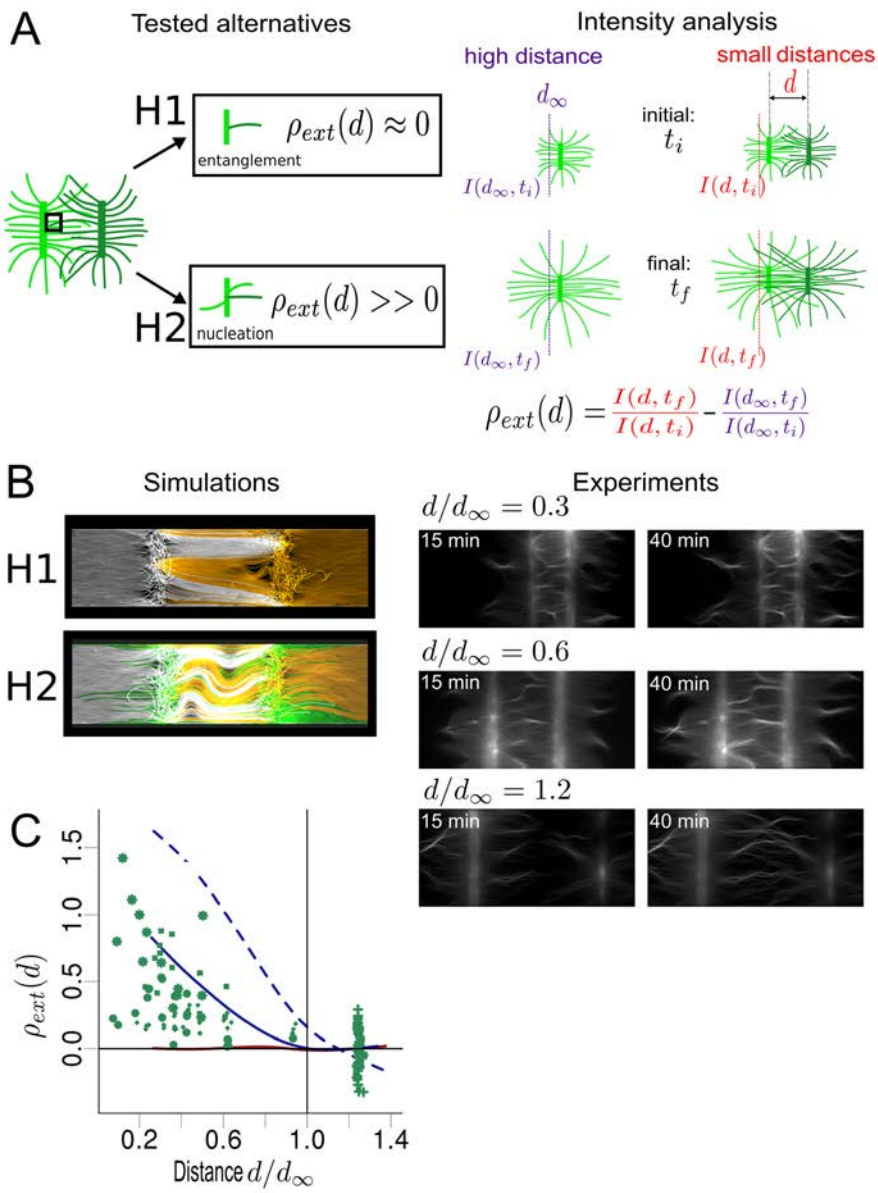
A
Tested alternatives
H1
$\rho_{ext}(d) \approx 0$
entanglement
H2
$\rho_{ext}(d) >> 0$
nucleation
Intensity analysis
high distance
small distances
d_∞
d
initial:
t_i
$I(d_\infty, t_i)$
$I(d, t_i)$
final:
t_f
$I(d_\infty, t_f)$
$I(d, t_f)$
$\rho_{ext}(d) = \frac{I(d,t_f)}{I(d,t_i)} - \frac{I(d_\infty,t_f)}{I(d_\infty,t_i)}$
B
Simulations
H1
H2
Experiments
$d/d_\infty = 0.3$
15 min
40 min
$d/d_\infty = 0.6$
15 min
40 min
$d/d_\infty = 1.2$
15 min
40 min
C
$\rho_{ext}(d)$
0.0
0.5
1.0
1.5
0.2
0.6
1.0
1.4
Distance d/d_∞

Fig 3. Actin fibers growing from adjacent patterns influence the overall actin organization. (A) Assumptions tested and analysis performed. Left: Two different hypotheses concerning the activity of a filament reaching a nucleated pattern were tested: H1 ("entanglement") and H2 ("nucleation"). Under H1, filaments stop growing and do not induce new nucleation. Under H2, filaments induce the nucleation of new filaments on the pattern that they reach. To determine which hypothesis is valid, we measured the variation of intensity in an area close to the pattern (in the outer side), and compare this variation with a control case corresponding to an isolated pattern (in the experiments, patterns separated by a distance $d >= 80$ μm are considered as isolated; in the simulation the threshold distance is $d_\infty = 10$ μm) (right). This variation (ρ_{ext}) indicates the amount of new filaments generated by the arrival of filaments coming from the other pattern (so it indicates the contribution of the second pattern). (B) Results of simulations and experiments. (Left) Simulations with a distance of $d = 7$ μm between the two patterns for hypothesis H1 and H2. Filaments coming from opposite patterns are differently colored (white and yellow); filaments generated by the primer effect are depicted in green. (Right) Results of experiment for 3 different normalized distances between patterns d/d_∞: 0.3 (top), 0.6 (middle) and 1.2 (bottom). The actin organization is shown for two different times. (C) Comparison between the simulation and experiment outputs. Quantification of the experimental results, where the distance between the two patterns was varied from 5 to 120 μm (green points). Different symbols correspond to four different experiments. Quantification derived from 100 simulations for each case, as a function of d/d_∞ where d was randomly chosen between 2 and 12 μm (lines). Under H1 (red line), ρ_{ext} does not depend on d and is near 0. On the contrary, under H2, (blue lines), ρ_{ext} is a decreasing function of d that is positive for $d < d_\infty$. Under H2, two different nucleation efficiencies were tested: a full efficiency (dashed blue line), and a 2.5% nucleation efficiency (percent of filaments reaching the opposing pattern able to trigger new nucleation; solid blue line). The vertical bar indicates the threshold where patterns were considered to be isolated.

doi:10.1371/journal.pcbi.1004245.g003

which measures to what extent the outer (away from the neighboring bar) intensity is made different by the presence of the second bar (Fig 3A). For this we calculated the intensity of the network (≈density of filaments) close to the pattern (7 μm away from the pattern center; a pattern is 3 μm wide), at two different times t_i and $t_f = t_i + 1h$ (Fig 3B). If the filaments cannot cross the pattern and get entangled, the variation of intensity at the outer sides of the pattern should be independent of the distance between the bars (Fig 3A) and thus similar to the control case ($\rho_{ext}(d) \approx 0$). On the other hand in case the filaments cross and/or nucleate on the other bar we expect the outer intensity to be higher than in the control case ($\rho_{ext}(d) > 0$) and $\rho_{ext}(d)$ would be a decreasing function of d. Because the computational costs were too high, we simulated shorter and closer pattern bars than experimental ones. To allow comparison of the results, we looked at normalized distances (d/d_∞).

We performed 100 simulations with the two different hypotheses, using a random distance d for each simulation (Fig 3B, and S5 Movie). We calculated $\rho_{ext}(d)$ for each simulation and analyzed its dependency on the normalized distance (Fig 3C) for the assumptions of entanglement (H_1 solid red line) and nucleation (H_2 dashed blue line). We then analyzed the results of four *in vitro* experiments (Fig 3B and 3C). The results are significantly positive for distances smaller than d_∞ (with 95% confidence with Wilcoxon rank test for comparison of experimental results with null distribution), and decreasing with d (p-value $< 10^{-12}$ with Spearman's rho test). We therefore found that the second hypothesis (H_2, nucleation) best matches the experimental behavior. However, a simulated nucleation efficiency of 100% was too high according to the experimental data (Fig 3C). Thus, we decreased the efficiency down to 2,5% (Fig 3C, solid blue line). This predicted low value for "primer activation" is consistent with experimental quantification of the nucleation in presence of the Arp2/3 complex [48]. We therefore can conclude that *in vitro*, actin filaments may cross over neighboring bars, nucleate new filaments, and thus influence the network on the distal side of another patterned region.

Discussion

To unveil how actin filaments can be organized into higher structures, a lot of efforts went into analyzing the role of actin-associated proteins [2,6,56]. While largely justified by the importance of protein effectors, this was also due to the lack of tools that allowed one to dissect how geometrical or physical parameters affect the overall actin architecture. However, recent technological developments such as microfluidics [57], micropatterning [1,58,59] or cytoskeleton growth into defined volumes [39] have highlighted some of the key features of biochemical-independent parameters in controlling the cytoskeleton architecture. Examples of applications

include showing how chromatin shapes the mitotic spindles organization [60] or how actin nucleators of the formin family respond to mechanical stress [61]. Using a micro-printing technique, it was also possible to demonstrate that geometry is a key parameter in controlling the macroscopic architecture of actin filaments during assembly [1]. This made it possible to document the emergent behavior by which actin assembly organizes at higher scale, depending on the initial localization of the actin nucleation-promoting factors.

Using Cytosim, we developed a model of a geometrically-constrained actin assembly, in which actin filaments/fibers are initiated from defined regions where branched nucleation occurs. This framework allowed us to study how the biophysical properties of actin filaments and their environment determine the organization of the final network. It is a tool with which one may study actin dynamics in more complicated systems. We were able to reproduce a diversity of actin organizations obtained from an initial geometry of nucleating promoting factor (Figs 1–3). We identified a combination of three essential components that determines the actin organization (Fig 4A and 4B and S6 Movie). The first one is the steric interaction between filaments, this is essential to obtain an aligned distribution of actin filaments growing away from the nucleating pattern (Figs 1 and 4B). In absence of steric interaction actin filaments have a tendency to buckle (Fig 4B1) preventing them from extending away from the nucleating region, and thus limits the contact between filaments nucleated from two different areas (Fig 4B1). These interactions are modulated *in vitro* by the chemical properties of the media. The second key component is the bending elasticity of actin bundles [62]. A persistence length of $L_p \approx 15$ μm, close to the experimentally reported persistence length for single actin filaments [62], resulted in patterns with parallel and antiparallel actin organizations similar to the patterns observed *in vitro* (Figs 2 and 4B3). The model predicted the effect of regulatory proteins, such as ADF/cofilin [54] or crosslinkers [53] that modify the persistence length, on the observed patterns. Actin filaments decorated by ADF/cofilin are softer (L_p of 2 μm [54]) and will buckle under small force and we predicted that this would preclude the efficient formation of parallel or antiparallel organizations. On the contrary, a high persistence length ($L_p = 1000$ μm) induced for example by bundling of actin filaments in the presence of crosslinkers, limited the deformation of the growing polymers. In this case we predicted that the original geometry imposed by the micropattern is maintained, indicating that this is the main parameter that defines the final macroscopic organization during actin assembly. The effect of adding fascin in our system could be simulated by adapting only the fiber persistence length, without having to change the fiber steric interactions. This suggests that the electrostatic properties of the interaction could be negligible compared to the change in elastic property of the fibers, which arise from the capacity of fascin to generate stiff bundles [63]. For the native $L_p \approx 15$ μm, the situation is more complex and the resulting actin macroscopic organization resulted from a combination of the boundary imposed by the geometry of the micropattern and the deformation induced on growing actin filament when contacting each other (Figs 2C, S4 and 4B3). Finally, a third component that is important in defining the overall actin macroscopic organization is the ability of growing actin fibers to contact the nucleating pattern and therefore trigger additional actin assembly following the 'primer' activation [55]. By doing so, the density of the actin organization will be modulated according to the efficiency of the 'primer' activation (Figs 3 and 4B4). The accessibility of the nucleating region is therefore a key parameter in controlling the overall actin organization. As demonstrated in Fig 4, the combination of these three components is sufficient to capture most of the actin organization observed *in vitro*, with the geometrically constrained actin nucleation assay.

To further test the power of our simulation tool, we predicted the overall collective behavior of actin initiated from more complex pattern geometry (Fig 4C). We simulated the actin filaments organization obtained from square and diamond dotted patterns (Fig 4C). We then

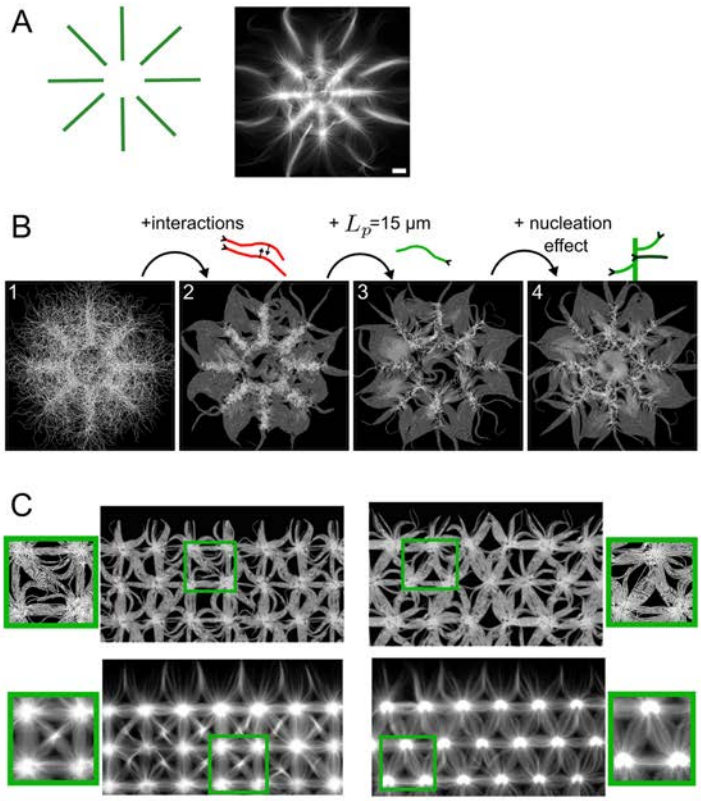

Fig 4. Contribution of studied parameters on actin organization. (A) Schematic of a micropattern, and the corresponding *in vitro* actin organization observed with TIRF microscopy. Scale bar is 10 µm. (B) The contribution of the key elements of the model on the final organization of fibers in the simulation. (B1) Fibers that are nucleated locally but do not interact with each other fail to extend away from the micropattern, (B2) Adding the steric interaction with the parameters as calibrated in Fig 1 allows filaments to co-align and extend away from the nucleation zone. (B3) Setting the persistence length to 15 µm (cf. Fig 2) makes them extend further. (B4) Adding the nucleation effect (cf. Fig 3, H2) finally leads to realistic overall densities (final time is 250 s). (C) Predictions of the actin filament organization for novel nucleation patterns. Simulations (Top) were done on a set of 8 points, distant by 6 µm, and positioned on a square (left) or triangular (right) lattice. The 8-point units were repeated 9 times using periodic boundaries. (Bottom) Experimental verification of actin organization for the geometries used.

doi:10.1371/journal.pcbi.1004245.g004

constructed the same geometries experimentally (Fig 4C). In both simulations and experiments the network were organized similarly (See Fig 4C zoomed panel). This shows that our simulation framework is predictive. In its present form our simulations with Cytosim have a number of limitations. Firstly, the high computational demands (S2 Fig), lead us to simulate the model in 2D using a reduced number of effective filaments. This likely explains why the model could not fully reproduce the formation of very thick parallel actin bundles at the bisecting line

between each ray of the 8 branched radial arrays (Fig 4). A 3D model, possibly reduced in size, but one in which single F-actin are simulated, could be used in the future to explore this further. However, even with these limitations, our current model is already useful to test a variety of geometrical configurations and predict the macroscopic organization of actin filaments. Cytosim was used here to mimic branched actin nucleation via Arp2/3, with minor modifications we could study other modalities such as formin dependent nucleation [64], the role of processive elongation induced by Vasp [65], or predict actin organization obtained by mixing several nucleation mechanisms. In the future we could investigate how myosin motors deform specific actin architectures [27] or study the movement of single myosin or myosin-driven cargo on established networks. Thus the present study sets the foundation of future research, where one will attempt to realistically reproduce *in silico* the emergent actin organization observed *in vitro*.

Materials and Methods

Simulation of filament growth from pattern

Actin filaments are simulated with Cytosim, following a Brownian dynamics approach [36]. Filaments may bend following linear elasticity, and are surrounded by an immobile viscous fluid; they grow and interact with each other (see Figs 1 and S2). Considering the low Reynolds number of a filament at this scale, inertia can be neglected and the mass of the objects is not a parameter that appears in the equations [37]. The parameters of the model were chosen to reflect the characteristics of *in vitro* actin filaments (see S1 Table). Notably, actin growth is force dependent, and the assembly speed is reduced exponentially by any antagonistic force [66] present at the barbed end:

$$v = v_0 \exp\left(\frac{\boldsymbol{f}\cdot\boldsymbol{t}}{f_s}\right), \text{ if } \boldsymbol{f}\cdot\boldsymbol{t} < 0 \text{ and } v = v_0 \text{ otherwise,}$$

with $f_s = 0.8$ pN ([67]). $\boldsymbol{f}$ and $\boldsymbol{t}$ are respectively the force vector and the normalized tangent vector at the barbed end. Moreover, considering the extensive supply of monomers in the system, depletions effects were neglected, and it was not necessary to simulate actin monomers to correctly model the increase of "polymer mass" in the system.

To simulate the formation of patterns, three entities were used: nucleator objects, Arp2/3-like complexes, and binder objects (see S2 and S3 Fig). First, we placed randomly few nucleators on the pattern area, which will nucleate new 'primer' filaments. These nucleators can trigger the nucleation of one filament each, and have a fixed position so that they remain on the pattern. To simulate the branched network generated by activated Arp2/3 on the pattern, we placed Arp2/3-like objects in the pattern, which bind to any filament that is sufficiently close. Bound Arp2/3 object will then nucleate a new filament with an angle of 70° with respect to the other filament on which it is bound. These complexes are placed in a fixed position on the pattern, but will move with the filaments after binding, without inducing any constraint. The link between the mother and daughter filament is modeled as a Hookean spring, with a torque to constrain the angle between the branches. To add some friction on the pattern, we also placed on the pattern fixed binders that may bind and unbind to the filaments, thus restraining their motion. These binders are also modeled as Hookean springs between the fixed anchoring point, and the attachment location on the fiber.

S1 Table shows the important parameter values used in the simulations. The complete configuration file used to simulate a horizontal pattern (see Fig 1) is given in Supplementary Data.

Simulation of steric interaction between filaments

The interaction between filaments is assumed to come from both depletion and electrostatic interactions. These are modeled in Cytosim as Hookean springs acting between the modeled segments, with an equilibrium distance d_0 corresponding to the diameter of a fiber. Because of excessive computational costs (S2 Fig), we could not simulate all the filaments present in the system, and reduced their number by lowering the density by roughly a factor 10. For this, we used an effective diameter $d_0 = 100\ nm$ (while the diameter of one actin filament is around 7 nm), and a maximum interaction range of $d_m = 200\ nm$ (while interactions between actin filaments mediated by electrostatic or depletion forces would be limited to tens of nm). Choosing d_0 and d_m, as well as the scale of the simulated system (length of the filaments, simulated time. . .) resulted from an empirical tradeoff between computational expenses and accuracy. With the chosen values, one filament usually interacts with its first and 2nd neighbors, and any modification of this aspect of the model can strongly affect the emergent organization. For example changing the value of d_r (defined from $d_m = d_0 + 2\ d_r$, see S5A and S5B Fig) indicated a strong effect on filament bundling. Thus the adjustment between the filament radius, interaction range, and steric coefficient values is delicate, and the calibration procedure is essential to find appropriate values of those parameters. Note that with our parameter set, each simulated filament may represent ~10 neighboring actin filaments, and one should be careful while interpreting the results at a molecular scale.

Simulation of different rigidities of actin filaments

We computed fibers of 3 different persistence lengths (2 μm, 15 μm, 1000 μm) to account for the effect of actin binding proteins. We calibrated the steric parameters for filaments having a native persistence length (15 μm), and kept these values fixed for the other persistence lengths. Indeed, we considered that the repulsive force, due to hard-core repulsion, should not be strongly affected by the addition of other proteins, so K_{push} could be kept constant for all rigidities. The electrostatic interaction term, K_{pull}, could be affected by the addition of actin binding proteins if they do change the electronic charge of the filaments, or the depletion force. However, we do not have any measure of this potential effect to recalibrate this value, and keeping the same value was sufficient to explain the experimental observations in the presence of fascin. Moreover, we found that the range of steric parameters giving patterns similar to the one observed *in vitro* was minimally affected by the value of the persistence length (S6A and S6B Fig).

The increased persistence length due to fascin addition could have been modeled by true addition of crosslinker in our simulation, or by increasing the value of K_{pull}. However, to be able to compare the behavior of fibers with different persistence lengths, we preferred to keep as many parameters as possible constant, and to vary instead the persistence length.

In all simulations we kept the same density of fibers. Therefore we do not explicitly model the decrease in fiber number that is expected from bundling. This choice was motivated by the computational costs of simulating large number of fibers. For native persistence lengths we simulated 300 to 1700 fibers, a 10 times decrease in case of bundling, i.e. 30 to 170 fibers, will not allow for comparison of the actin organizations. Instead we compared the behavior of single fibers against bundle of fibers for a same density of fibers/bundle of fibers.

We also tested how sensitive the simulations were to the chosen value of the filament persistence length, by varying it between 2 μm and 1000 μm (S7 Fig). We noticed that above a threshold, around 10 μm for the persistence length, the collective behavior of actin filaments was mostly similar with the same tendency of forming bundles (S7 Fig). Thus the choice of a precise value of 15 μm while actin persistence length is evaluated to be between 10 and 20 μm is acceptable.

Simulation of entanglement and primer effect

To simulate the entanglement effect on the pattern and its effect on actin elongation (Fig 3), we defined two different fiber types in Cytosim. Their parameters are identical, but this allowed us to define an entity in the pattern that could bind at the barbed end of actin filaments coming only from the other pattern. When a filament has one or more of these entities bound close to its end, it will stop growing. For the second scenario (primer effect), we added the possibility for these entities to nucleate a new filament when bound. By mixing the two types of entities (capping one and nucleating one), we could control the nucleation efficiency.

Supporting Information

S1 Fig. *In vitro* organization on 3D view. (A) 3D reconstruction of filaments organization done with the software Chimera from confocal microscopy imaging. Color code illustrates the Z dimension. (B) Imaging in TIRF mode limits fluorescence to the filaments that are within ~200 nm of the coverglass surface plane. Scale bar: 10 μm
(TIF)

S2 Fig. Description of the main processes that were simulated: patterning, nucleation, elongation, interaction. Cartoon representing the processes *in vitro* (left column), their implementation in Cytosim (middle column), and examples of simulations with a different implementation (right column). **Patterning:** The coverglass is covered by non-adhesive PLL-PEG polymer, and only the insolated area coated with pWA can activate the nucleation by Arp2/3 complex. Thus the patterned area is adhesive and creates friction on the filaments. We added binders (in blue) in the simulations to account for this friction (middle). We also added pre-activated complexes (orange) to initiate the nucleation. When the binders are removed, the region of high fiber density is not confined to the activated region (right). **Nucleation:** The contact between the inactive diffusing Arp2/3 complex, a pre-existing filament (primer) and the pWA allows the nucleation of a new filament by addition of diffusing monomer (left). Contact between pre-activated Arp2/3-like complex on the pattern and a filament generates nucleation of a new filament in Cytosim (middle). If the filaments are all nucleated without Arp2/3-like process (with fixed nucleators similar to those used as primers), we obtained a network that is very dense in the center, and all filaments are of similar lengths (right). **Elongation:** Under the *in vitro* conditions, with the concentration of 1–2 μM of actin, the elongation speed of filaments stayed approximately constant during the experiment (left). The growth is thus simulated with a constant rate (middle). If we added the constraint of limited amount of monomers, the filament growth slowed down during the simulation, and we obtained shorter filaments, but the global organization remained similar (right). **Interaction:** Filaments are attracting each other by electrostatic interactions due to the presence of counterions in solution and depletion force due to polymers (left). This is modeled by short range interactions calculated for each segment of a fiber in Cytosim (middle). If we remove this interaction, filaments remain disorganized (right). **Simulation**: Computation time needed to simulate a network of filaments for 150 s, as a function of the number of filaments in this network (middle). Final organization of filaments from a horizontal pattern bar with default parameters of our system (control, right).
(TIF)

S3 Fig. Simulation of actin nucleation from pattern. Time-course of a simulation with actin filament nucleated from a rectangular area. Arp2/3-like entities are represented as small orange dots. Binders are represented as blue dots. At early times (t = 1 s), few nucleators entities randomly distributed generate short actin filaments (primers, shown in white). Upon contact with

Arp2/3-like entities (t > = 10 s), these filaments are amplified by triggering the nucleation of new filaments; daughter filaments make a 70° angle with the mother filament. A zoom of a small part of the pattern is shown below. Scale bar is 1 μm.
(TIF)

S4 Fig. Effect of the ratio between fiber length and persistence length on the collective organization. Proportion of parallel fibers as function of pattern angle θ, with a persistence length L_p of 2 μm and 1000 μm, while the lengths of filaments is L = 7 μm. The ratio is defined as $r = L_p/L$. (B) Proportion of parallel filaments as a function of pattern angle θ for different fiber lengths and native persistence length. (C) Illustration of the collective organization for different ratios r (bottom).
(TIF)

S5 Fig. Effect of steric parameters. (A) Effect of varying the steric range d_r between 10 and 100 nm. All other parameters are identical to Fig 1E. Scale bar is 4 μm. (B) Effect of varying the steric range d_r, around its set value of 50 nm.
(TIF)

S6 Fig. Effect of steric parameters on non-native persistence length of fibers. Variation of steric parameters for filaments with a persistence length of 1000 μm (A) or 2 μm (B). Three values were tested for K_{pull} (0.05, 0.5 and 5 pN/μm) and three values for K_{push} (0.75, 7.5 and 75 pN/μm), resulting in 9 combinations. The nucleating bar is 8 μm long and the image shows in grey levels the simulated actin density at 250 s (scale bar is 6 μm).
(TIF)

S7 Fig. Sensitivity of actin organization on the fiber persistence length. Organization of actin fibers with 5 different persistence lengths: 2 μm, 5 μm, 10 μm, 15 μm and 1000 μm (from left to right). Pattern bar length is 8 μm and the image shows in grey levels the simulated actin density at 250 s.
(TIF)

S1 Movie. Growth of actin filaments from pattern after calibration. Growth of filaments nucleated from a rectangle, with parameters chosen as discussed in Fig 1. Pattern bar length is 8 μm, 510 actin filaments are nucleated on the pattern. Simulation runs for 250 s.
(MP4)

S2 Movie. Growth of actin filaments from a V-shape with persistence length of 15 μm. Filament persistence length is 15 μm; each rectangle is 8 μm long, nucleating 360 actin filaments. Simulations run for 250 s. Angle between pattern is 20° (left), 45° (middle) and 90° (right).
(MP4)

S3 Movie. Growth of filaments from a V-shape with persistence length of 2 μm. Actin filament persistence length is 2 μm; each rectangle is 8 μm long, nucleating 360 actin filaments. Simulations run for 250 s. Angle between pattern is 20° (left), 45° (middle) and 90° (right).
(MP4)

S4 Movie. Growth of actin filaments from a V-shape with persistence length of 1000 μm. Actin filament persistence length is 1000 μm; each rectangle is 8 μm long, nucleating 360 actin filaments. Simulations run for 250 s. Angle between pattern is 20° (left), 45° (middle) and 90° (right).
(MP4)

S5 Movie. Growth of actin filaments from pattern under entanglement and nucleation assumptions. Growth of actin filaments from two parallel rectangles; each rectangle is 5 μm wide, nucleating 135 actin filaments. Simulations run for 500 s. The top panel was simulated under the entanglement assumption. The bottom panel was simulated under the nucleation assumption. Additional actin filaments whose nucleation is triggered when actin filaments reach the neighboring rectangles are shown in green.
(MP4)

S6 Movie. Growth of actin filaments from a star-like shaped pattern. Growth of actin filaments from a star-like pattern based on the calibrated parameters of this study. The pattern is composed of 8 rectangles 8 μm in length, nucleating 230 or more actin filaments each. Simulation time is 250 s.
(MP4)

S1 Table. Main parameters used in the simulation.
(DOCX)

Acknowledgments

We wish to acknowledge A. Kawska, B. White, F. Vaggi and CH. Tan who first simulated this system during the EMBO practical course Microscopy, Modeling and Biophysical Methods in 2010. We are grateful to Fabrice Senger for his help in the elaboration of S1 Fig.

Author Contributions

Conceived and designed the experiments: GL AZP HE MT FN LB. Performed the experiments: GL AZP HE. Analyzed the data: GL. Contributed reagents/materials/analysis tools: GL AZP HE FN. Wrote the paper: GL AZP FN LB.

References

1. Reymann A-C, Martiel J-L, Cambier T, Blanchoin L, Boujemaa-Paterski R, Théry M. Nucleation geometry governs ordered actin networks structures. Nat Mater. 2010; 9: 827–832. doi: 10.1038/nmat2855 PMID: 20852617
2. Pollard TD, Cooper JA. Actin, a central player in cell shape and movement. Science. 2009; 326: 1208–1212. doi: 10.1126/science.1175862 PMID: 19965462
3. Mogilner A, Oster G. Cell motility driven by actin polymerization. Biophys J. 1996; 71: 3030–3045. PMID: 8968574
4. Mogilner A, Oster G. Force generation by actin polymerization II: the elastic ratchet and tethered filaments. Biophys J. 2003; 84: 1591–1605. PMID: 12609863
5. Fletcher DA, Mullins RD. Cell mechanics and the cytoskeleton. Nature. 2010; 463: 485–492. doi: 10.1038/nature08908 PMID: 20110992
6. Blanchoin L, Boujemaa-Paterski R, Sykes C, Plastino J. Actin dynamics, architecture, and mechanics in cell motility. Physiol Rev. 2014; 94: 235–263. doi: 10.1152/physrev.00018.2013 PMID: 24382887
7. Bathe M, Heussinger C, Claessens MM, Bausch AR, Frey E. Cytoskeletal bundle mechanics. Biophys J. 2008; 94: 2955–2964. PMID: 18055529
8. Deguchi S, Ohashi T, Sato M. Tensile properties of single stress fibers isolated from cultured vascular smooth muscle cells. J Biomech. 2006; 39: 2603–2610. PMID: 16216252
9. Svitkina TM, Borisy GG. Arp2/3 complex and actin depolymerizing factor/cofilin in dendritic organization and treadmilling of actin filament array in lamellipodia. J Cell Biol. 1999; 145: 1009–1026. PMID: 10352018
10. Small JV. Actin filament organization in the fish keratocyte lamellipodium. J Cell Biol. 1995; 129: 1275–1286. PMID: 7775574
11. Iwasa JH, Mullins RD. Spatial and Temporal Relationships between Actin-Filament Nucleation, Capping, and Disassembly. Curr Biol. 2014; 17: 395–406.

12. Keren K, Pincus Z, Allen GM, Barnhart EL, Marriott G, Mogilner A,et al. Mechanism of shape determination in motile cells. Nature. 2008; 453: 475–480. doi: 10.1038/nature06952 PMID: 18497816

13. Mogilner A. Mathematics of cell motility: have we got its number? J Math Biol. 2009; 58: 105–134. doi: 10.1007/s00285-008-0182-2 PMID: 18461331

14. Quint DA, Schwarz JM. Optimal orientation in branched cytoskeletal networks. J Math Biol. 2011; 63: 735–755. doi: 10.1007/s00285-010-0389-x PMID: 21140151

15. Schaus TE, Taylor EW, Borisy GG. Self-organization of actin filament orientation in the dendritic-nucleation/array-treadmilling model. Proc Natl Acad Sci USA. 2007; 104: 7086–7091. PMID: 17440042

16. Weichsel J, Urban E, Small JV, Schwarz US. Reconstructing the orientation distribution of actin filaments in the lamellipodium of migrating keratocytes from electron microscopy tomography data. Cytometry A. 2012; 81: 496–507. doi: 10.1002/cyto.a.22050 PMID: 22499256

17. Zimmermann J, Brunner C, Enculescu M, Goegler M, Ehrlicher A, Käs J, et al. Actin filament elasticity and retrograde flow shape the force-velocity relation of motile cells. Biophys J. 2012; 102: 287–295. doi: 10.1016/j.bpj.2011.12.023 PMID: 22339865

18. Small J V, Isenberg G, Celis JE. Polarity of actin at the leading edge of cultured cells. Nature. 1978; 272: 638–639. PMID: 565473

19. Mattila PK, Lappalainen P. Filopodia: molecular architecture and cellular functions. Nat Rev Mol Cell Biol. 2008; 9: 446–454. doi: 10.1038/nrm2406 PMID: 18464790

20. Zhuravlev PI, Minakova MS, Papoian GA. Theory of active transport in filopodia and stereocilia. Proc Natl Acad Sci U S A. 2012; 109:10849–54. doi: 10.1073/pnas.1200160109 PMID: 22711803

21. Howard J. Molecular motors: structural adaptations to cellular functions. Nature. 2012; 389: 561–567.

22. Svitkina TM, Bulanova EA, Chaga OY, Vignjevic DM, Kojima S, Vasiliev JM, et al. Mechanism of filopodia initiation by reorganization of a dendritic network. J Cell Biol. 2003; 160: 409–421. PMID: 12566431

23. Vignjevic D, Yarar D, Welch MD, Peloquin J, Svitkina T, Borisy GG, et al. Formation of filopodia-like bundles in vitro from a dendritic network. J Cell Biol. 2003; 160: 951–962. PMID: 12642617

24. Hotulainen P, Lappalainen P. Stress fibers are generated by two distinct actin assembly mechanisms in motile cells. J Cell Biol. 2006; 173: 383–394. PMID: 16651381

25. Burnette DT, Manley S, Sengupta P, Sougrat R, Davidson MW, Kachar B, et al. A role for actin arcs in the leading-edge advance of migrating cells. Nat Cell Biol. 2011; 13: 371–381. doi: 10.1038/ncb2205 PMID: 21423177

26. Tojkander S, Gateva G, Lappalainen P. Actin stress fibers—assembly, dynamics and biological roles. J Cell Sci. 2012; 125: 1855–1864. doi: 10.1242/jcs.098087 PMID: 22544950

27. Reymann A-C, Boujemaa-Paterski R, Martiel J-L, Guérin C, Cao W, Théry M, Blanchoin L. Actin network architecture can determine myosin motor activity. Science. 2012; 336: 1310–1314. doi: 10.1126/science.1221708 PMID: 22679097

28. Hayakawa K, Tatsumi H, Sokabe M. Actin filaments function as a tension sensor by tension-dependent binding of cofilin to the filament. J Cell Biol. 2011; 195: 721–727. doi: 10.1083/jcb.201102039 PMID: 22123860

29. Pollard TD, Berro J. Mathematical models and simulations of cellular processes based on actin filaments. J Biol Chem. 2009; 284: 5433–5437. doi: 10.1074/jbc.R800043200 PMID: 18940808

30. Mogilner A, Edelstein-keshet L. Regulation of actin dynamics in rapidly moving cells: a quantitative analysis. Biophys J. 2002; 83: 1237–1258. PMID: 12202352

31. Carlsson AE. Stimulation of actin polymerization by filament severing. Biophys J. 2006; 90: 413–422. PMID: 16258044

32. Fallqvist B, Kulachenko A, Kroon M. Modelling of cross-linked actin networks—Influence of geometrical parameters and cross-link compliance. J Theor Biol. 2014; 350: 57–69. doi: 10.1016/j.jtbi.2014.01.032 PMID: 24491254

33. Lan Y, Papoian GA. The stochastic dynamics of filopodial growth. Biophys J. 2008; 94: 3839–3852. doi: 10.1529/biophysj.107.123778 PMID: 18234810

34. Kawska A, Carvalho K, Manzi J, Boujemaa-Paterski R, Blanchoin L, Martiel JL, et al. How actin network dynamics control the onset of actin-based motility. Proc Natl Acad Sci USA. 2012; 109: 14440–14445. doi: 10.1073/pnas.1117096109 PMID: 22908255

35. Friedrich BM, Fischer-Friedrich E, Gov NS, Safran SA. Sarcomeric pattern formation by actin cluster coalescence. Plos Comput Biol. 2012; 8: e1002544. doi: 10.1371/journal.pcbi.1002544 PMID: 22685394

36. Nedelec F, Foethke D. Collective Langevin dynamics of flexible cytoskeletal fibers. New J Phys. 2007; 9: 427–427.

37. Kozlowski C, Srayko M, Nedelec F. Cortical microtubule contacts position the spindle in C. elegans embryos. Cell. 2007; 129: 499–510. PMID: 17482544

38. Foethke D, Makushok T, Brunner D, Nedelec F. Force and length dependent catastrophe activities explain interphase microtubule organization in fission yeast. Mol Syst Biol. 2009; 5: 241. doi: 10.1038/msb.2008.76 PMID: 19293826

39. Pinot M, Chesnel F, Kubiak JZ, Arnal I, Nedelec FJ,Gueroui Z. Effects of confinement on the self-organization of microtubules and motors. Curr Biol. 2009; 19: 954–960. doi: 10.1016/j.cub.2009.04.027 PMID: 19427215

40. Loughlin R, Heald R, Nedelec F. A computational model predicts Xenopus meiotic spindle organization. J Cell Biol. 2010; 191: 1239–1249. doi: 10.1083/jcb.201006076 PMID: 21173114

41. Athale CA, Dinarina A, Nedelec F, Karsenti E. Collective behavior of minus-ended motors in mitotic microtubule asters gliding toward DNA. Phys Biol. 2014; 11: 16008.

42. Gibeaux R, Politi AZ, Nedelec F, Antony C, Knop M. Spindle pole body-anchored Kar3 drives the nucleus along microtubules from another nucleus in preparation for nuclear fusion during yeast karyogamy. Genes Dev. 2013; 27: 335–349. doi: 10.1101/gad.206318.112 PMID: 23388829

43. Rupp B, Nedelec F. Patterns of molecular motors that guide and sort filaments. Lab Chip. 2012; 12: 4903–4910. doi: 10.1039/c2lc40250e PMID: 23038219

44. Laporte D, Ojkic N, Vavylonis D, Wu JQ. α-Actinin and fimbrin cooperate with myosin II to organize actomyosin bundles during contractile-ring assembly. Mol Biol Cell. 2012; 23: 3094–3110. doi: 10.1091/mbc.E12-02-0123 PMID: 22740629

45. Tang H, Laporte D, Vavylonis D. Actin cable distribution and dynamics arising from cross-linking, motor pulling, and filament turnover. Mol Biol Cell. 2014; 25: 3006–3016. doi: 10.1091/mbc.E14-05-0965 PMID: 25103242

46. Kim M, Rejniak KA. Mechanical aspects of microtubule bundling in taxane-treated circulating tumor cells. Biophys J. 2014; 107: 1236–1246. doi: 10.1016/j.bpj.2014.07.009 PMID: 25185559

47. Mullins RD, Heuser JA, Pollard TD. The interaction of Arp2/3 complex with actin: Nucleation, high affinity pointed end capping, and formation of branching networks of filaments. Proc Natl Acad Sci USA. 1998; 95: 6181–6186. PMID: 9600938

48. Blanchoin L, Amann KJ, Higgs HN, Marchand J- B, Kaiser DA, Pollard TD. Direct observation of dendritic actin filament networks nucleated by Arp2/3 complex and WASP/Scar proteins. Nature. 2000; 404: 1007–1011. PMID: 10801131

49. Pollard TD. Rate constants for the reactions of ATP- and ADP-actin with the ends of actin filaments. J Cell Biol. 1986; 103: 2747–2754. PMID: 3793756

50. Yu X, Carlsson AE. Multiscale Study of Counterion-Induced Attraction and Bundle Formation of F-Actin Using an Ising-like Mean-Field Model. Biophys J. 2003; 85: 3532–3543. PMID: 14645048

51. Biron D, Moses E, Borukhov I, Safran SA. Inter-filament Attractions Narrow the Length Distribution of Actin Filaments. Europhys Lett. 2004; 73: 5.

52. Hosek M, Tang J. Polymer-induced bundling of F actin and the depletion force. Phys Rev E. 2004; 69: 51907.

53. Mogilner A, Rubinstein B. The physics of filopodial protrusion. Biophys J. 2005; 89: 782–795 PMID: 15879474

54. McCullough BR, Blanchoin L, Martiel JL, De la Cruz EM. Cofilin increases the bending flexibility of actin filaments: implications for severing and cell mechanics. J Mol Biol. 2008; 381: 550–558. doi: 10.1016/j.jmb.2008.05.055 PMID: 18617188

55. Achard V, Martiel J-L, Michelot A, Guérin C, Reymann A-C, Blanchoin L, et al. A "primer"-based mechanism underlies branched actin filament network formation and motility. Curr Biol. 2010; 20: 423–428. doi: 10.1016/j.cub.2009.12.056 PMID: 20188562

56. Mullins RD, Hansen SD. In vitro studies of actin filament and network dynamics. Curr Opin Cell Biol. 2013; 25: 6–13. doi: 10.1016/j.ceb.2012.11.007 PMID: 23267766

57. Jégou A, Carlier M-F, Romet-Lemonne G. Microfluidics pushes forward microscopy analysis of actin dynamics. Bioarchitecture. 2011; 6: 271–276. PMID: 22545179

58. Portran D, Gaillard J, Vantard M, Thery M. Quantification of MAP and molecular motor activities on geometrically controlled microtubule networks. Cytoskeleton. 2013; 70: 12–23. doi: 10.1002/cm.21081 PMID: 23027541

59. Pugieux C, Dmitrieff S, Tarnawska K, Nedelec F. Spindle assembly on immobilized chromatin micropatterns. Methods Enzymol. 2014; 540: 435–448. doi: 10.1016/B978-0-12-397924-7.00024-8 PMID: 24630121

60. Dinarina A, Pugieux C, Corral MM, Loose M, Spatz J, Karsenti E, et al. Chromatin shapes the mitotic spindle. Cell. 2009; 138: 502–513 doi: 10.1016/j.cell.2009.05.027 PMID: 19665972

61. Jégou A, Carlier M-F, Romet-Lemonne G. Formin mDia1 senses and generates mechanical forces on actin filaments. Nat Commun. 2013; 4: 1883. doi: 10.1038/ncomms2888 PMID: 23695677

62. Isambert H, Venier P, Maggs AC, Fattoum A, Kassab R, Pantaloni D, et al. Flexibility of actin filaments derived from thermal fluctuations. Effect of bound nucleotide, phalloidin, and muscle regulatory proteins. J Biol Chem. 1995; 270: 11437–11444. PMID: 7744781

63. Claessens M, Bathe M, Frey E, Bausch A. Actin-binding proteins sensitively mediate F-actin bundle stiffness. Nat Mat. 2006; 5: 748–753.

64. Pruyne D, Evangelista M, Yang C, Bi E, Zigmond S, Bretscher A, et al. Role of formins in actin assembly: nucleation and barbed-end association. Science. 2002; 297: 612–615. PMID: 12052901

65. Krause M, Bear JE, Loureiro JJ, Gertler FB. The Ena/VASP enigma. J Cell Sci. 2002; 10: 4721–4726.

66. Peskin C, Odell G, Oster G. Cellular motions and thermal fluctuations: the Brownian ratchet. Biophys J. 2002; 65: 316–324.

67. Footer MJ, Kerssemakers JWJ, Theriot JA, Dogterom M. Direct measurement of force generation by actin filament polymerization using an optical trap. Proc Natl Acad Sci USA. 2007; 104: 2181–2186. PMID: 17277076

Supporting Information

S1 Fig.

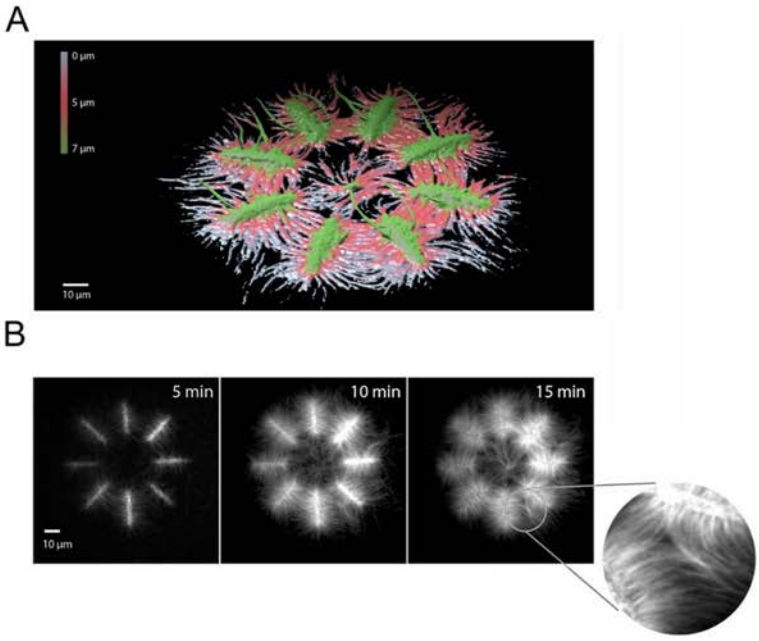

S2 Fig.

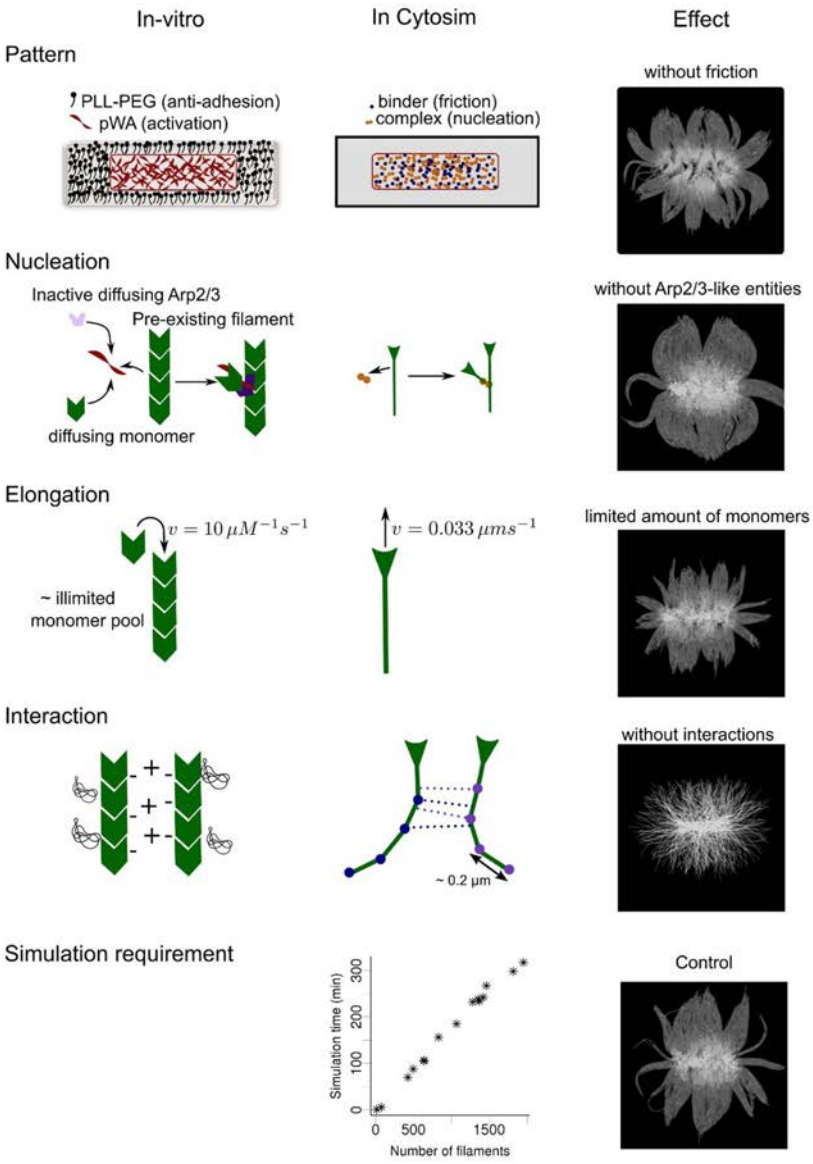
In-vitro
In Cytosim
Effect
Pattern
PLL-PEG (anti-adhesion)
pWA (activation)
binder (friction)
complex (nucleation)
without friction
Nucleation
Inactive diffusing Arp2/3
Pre-existing filament
diffusing monomer
without Arp2/3-like entities
Elongation
$v = 10\,\mu M^{-1}s^{-1}$
~ illimited
monomer pool
$v = 0.033\,\mu ms^{-1}$
limited amount of monomers
Interaction
~ 0.2 µm
without interactions
Simulation requirement
Simulation time (min)
0
100
200
300
0
500
1500
Number of filaments
Control

2

S3 Fig.

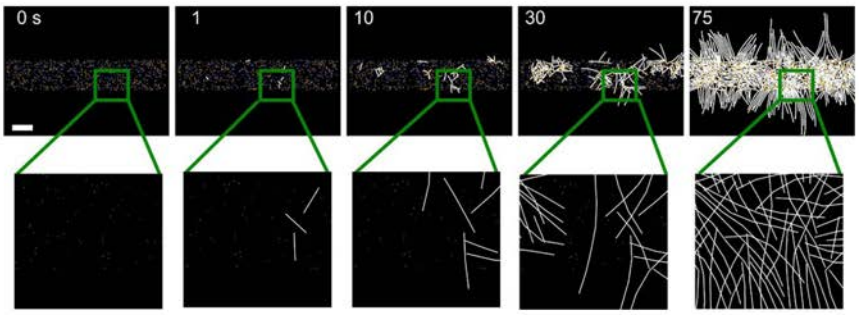

S4 Fig.

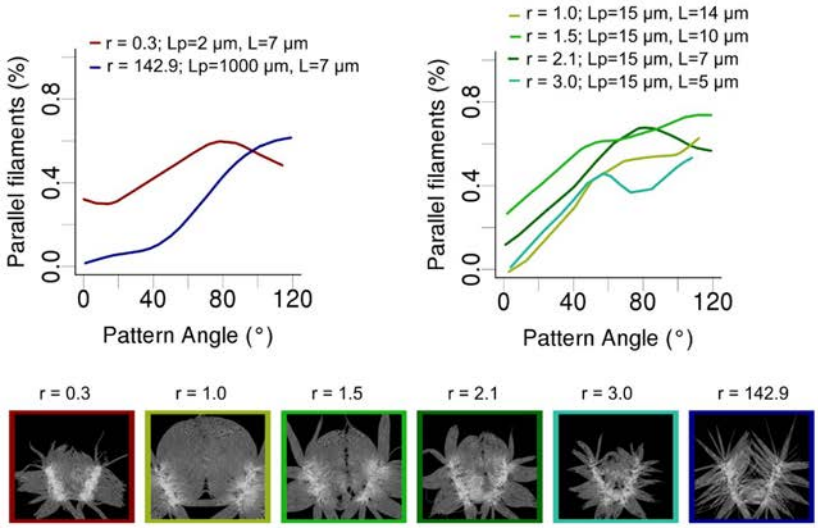

S5 Fig.

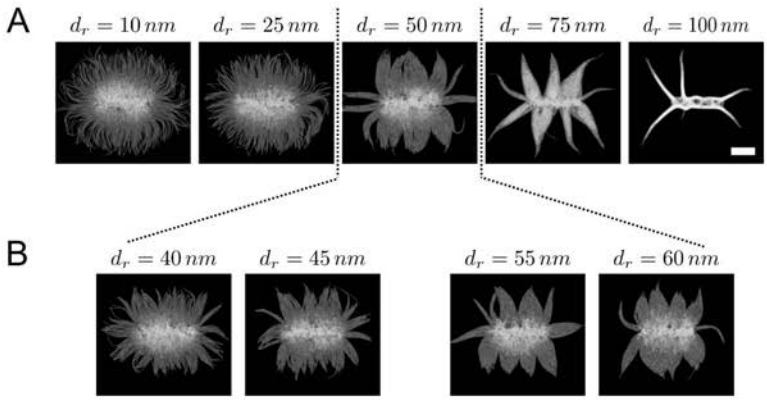
A
$d_r = 10\,nm$
$d_r = 25\,nm$
$d_r = 50\,nm$
$d_r = 75\,nm$
$d_r = 100\,nm$
B
$d_r = 40\,nm$
$d_r = 45\,nm$
$d_r = 55\,nm$
$d_r = 60\,nm$

S6 Fig.

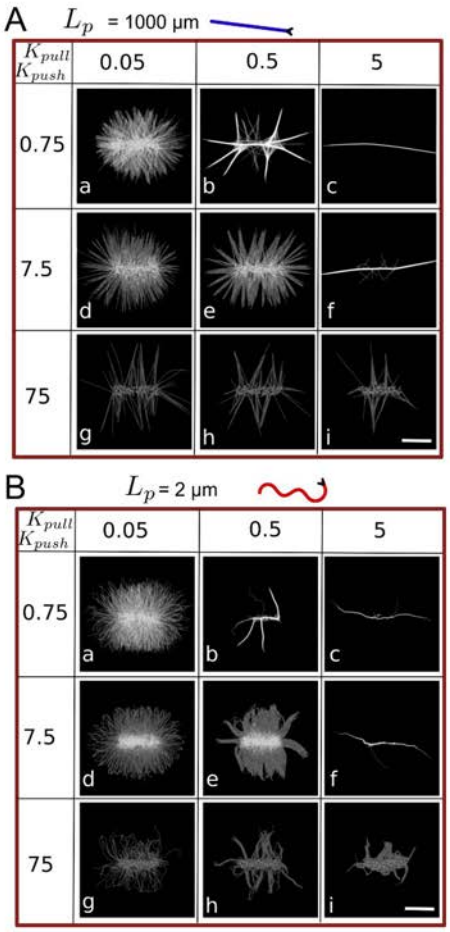

S7 Fig.

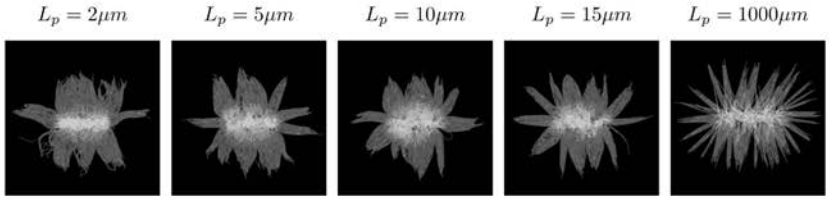

5

S1 Table. Main parameters used in the simulation.

Name	Value	Description
Global		
Time step	0.01 s	Computational parameter
Viscosity	0.18 pN s/µm²	Viscosity of the solution containing methylcellulose
kT	0.0042 pN µm	Thermal energy at 25°C
Actin filaments		
Rigidity	0.06 pN µm²	Flexural rigidity: Lp * kT, whith Lp, actin persistence length, chosen as 15 µm [62]. Varied in Figure 2 and Figure S6.
Segmentation	0.2 µm	Computational parameter
Growing speed	0.033 µm/s	Elongation speed under no force (), for 1 µM of actin monomers [49].
Growing force	0.8 pN	Stall force () [67]. Growing velocity is slowed down by loading force on barbed end:
Steric diameter	100 nm	Simulated fiber diameter , discussed in Material and Methods
Steric maximal range	200 nm	Maximal interacting distance, , discussed in Material and Methods
Steric parameters		See Figure 1, S2 and Material and Methods
Fixed nucleator		
Nucleation rate	1 s^{-1}	Rate of nucleation, fast to simulate primers. Empirical
Unbinding rate	0	No detachment
Stiffness	30 pN/µm	Stiffness of the Hookean spring to attach the nucleator to its position. Empirical, low so that the initial position will not be a strong constraint
Number	10	Few primers
Arp2/3 complex		
Nucleation rate	0.5	Nucleation rate when bound to an existing filament
Binding rate	1	Fast binding rate for an efficient covering of the pattern area
Binding range	0.02 µm	Can bind only to a close filament
Unbinding rate	0	No Arp2/3 debranching
Equilibrium angle	1.24 rad	Equilibrium angle between the two branches (70°, [48])
Angular stiffness	0.13 pN.µm/rad	Stiffness of the torque connecting the two branches [48]
Density (or number)	Between 300 and 1700	

Binders		
Binding range	0.02 µm	Maximal distance to which a binder can bind a filament. Empirical
Binding rate	7 s^{-1}	Rate of binding of a binder to any filament that is within the binding range distance. Empirical
Stiffness	100 pN/µm	Stiffness of the Hookean spring between the binder and the filament. Empirical
Unbinding rate	0.01 s^{-1}	Rate of unbinding of the binders. Empirical
Stiffness	100 pN/µm	Stiffness of the Hookean spring between the binder and the filament. Empirical
Number	400	Enough to create friction
Simulation		
Number of filaments	Between 300 and 1700	Range of number of filaments simulated (nucleated from Arp2/3 complex entities)
Total time simulated	Between 250 s and 500 s	

2nd project

II. Architecture and connectivity govern actin network contractility

Contractility mainly depends on the interaction of myosin with actin. However, if the general principles of contraction described in the introduction are conserved for different actin structures, we have shown that different actin organizations have different contractile response. We hypothesized that this variability may come from the actin organization. To replace those findings in a cellular context, we designed an in vitro system to reproduce and mimic the in vivo contractile structures. We were interested mainly in three types of cellular organization that span the diversity of contractile actin architecture: the lamella, the stress fibers and the cytokinesis ring.

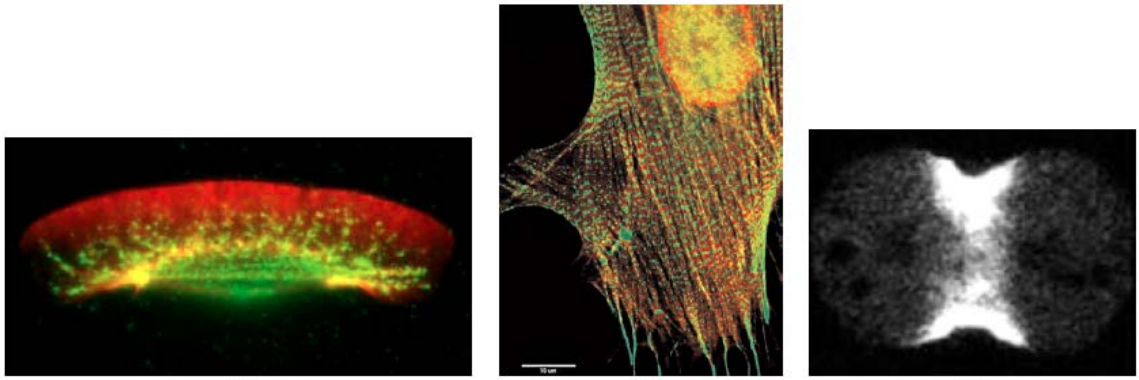

Figure 35 Contractile structures examples. (a) Myosin localization (green) and actin (red) in Keratocytes cells. Myosin is mainly present in the lamella. (b) Stress fibers in a Fibroma cell; we can observe the bonding of myosin (red) and α-actinin (green). (c) Cytokinesis ring in Dictyostelium cell. Myosin II is presented in white. Adapted from Barnhart et al. 2011; Peterson et al. 2004; Yumura 2001).

The lamella is a disordered branched network of actin filaments. The sarcomere is an array of ordered actin bundles and finally the contractile ring is made of actin bundles in a random polarity (Figure 1, Ennomani, Letort et al. in revision). To mimic such diversity in actin organization, we used the micropattern method that allowed us to generate actin filaments with an orientation encountered in a lamella, a sarcomere or a cytokinesis ring. We used ring shape patterns to simplify the analysis of the rate of contraction over time. We added myosin to the three different ring structures made of actin filaments, and observed the contractile response in these different conditions. We first confirmed that the actin organization modulates the contractile response. Indeed, the branched network and the ordered bundle contracted and deformed under the action of molecular motor, i. e myosin, while the non-organized bundle ring did not deform at all.

To establish the mechanism responsible for this difference, we used the model we implemented in Cytosim, as presented in the previous chapter. We could reproduce *in silico* with a minimum of parameters the contractile response of the disordered branched network and the array of ordered actin bundles.

In the case of disordered bundle, the simulations revealed that actin filaments are sliding along each other, without inducing a global deformation. This is probably due to the lack of connections between filaments. To valid this hypothesis, we added to our experimental system an actin crosslinker, α-actinin, restored deformation of the ring made of disordered bundles. Moreover, α-actinin slowed down the rate of deformation of the two other structures (a disordered branched network and an array of ordered actin bundles). To decipher the role of crosslinkers during actomyosin contractile response, we used cytosim to establish the degree of connectivity between actin filaments in the different conditions tested. The rate of deformation according to the value of connectivity was evaluated using our simulation and the result showed that the contractile behaviour of these 3 structures is similar. Indeed, at low connectivity (<2), the different actin organization networks had not yet percolated; all actin filaments are not connected together to form a single group, and the force generated locally by the myosin is not transmitted to the whole network. When the connectivity was between 2 and 3, the contraction rate was optimal because of the percolation level reached by the network and local forces were transmitted to the actin network to induce a global deformation. Finally, for connectivity above 3, the additional connections between the actin filaments stiffen the system and slowed down or even totally inhibited the deformation.

Interestingly, as mentioned previously in the "Actin binding protein section", both α-actinin and Arp2/3 could contribute to the network connectivity in our experimental system. Arp2/3 can connect only unconnected filaments because it binds the pointed end of the new branch. Whereas, α-actinin bridges both, connected or unconnected actin filaments. These different properties could explain the difference of percolation level for the 3 types of actin organization.

While I focused on different acto-myosin contractile regimes, the major property of the cellular cytoskeleton is its dynamic behaviour. As presented in the introduction (Letort, Ennomani, 2015), transitions between the different cellular actin organizations are a common aspect of cytoskeleton dynamics. Especially in cellular contractile structures, the organization and the level of connectivity can vary spatially and temporally. The transition from lamella to transverse arc is a very good example of actin reorganization to form a contractile structure.

To add this dynamic transition in our study, and to evaluate how these changes affect the contractile behaviour, we designed an experiment where we modified in real time the actin filament organization and its connectivity. To do so, we designed a new experimental system, where actin filaments assembly was initiated from a soft substrate. Indeed, on a soft substrate the actin structure deformation induced by myosin was reversible. With this system, we were able to control biochemically the contractile response of the actomyosin network by adding ADF/cofilin, which will act as a modulator of connectivity. When the actin structure was not deformed by the action of the myosins because the degree of connectivity was too high, addition of ADF/cofilin restored the contractile response by decreasing the level of connection between the filaments. In contrary, when the actin structure had an optimal contractile response with on optimal connectivity, addition of ADF/cofilin decreased the contractile response.

We found that the variation of actomyosin contractile response result from a combination of two inter-dependent parameters: the spatial organization of actin filaments and their degree of connectivity. The degree of connectivity determines the type of the contractile response (local sliding, global deformation or massive freezing), whereas the actin filament organization, i.e. filament alignment and polarity, control its magnitude. The local densities of molecular motors and the cross-linker have been described as key modulators of the transition from contractile to non-contractile network. Here, we have demonstrated that for a defined set of biochemical parameters the spatial organization of actin filaments can strongly impinge on the rate of contraction and the magnitude of force generation. Moreover, we showed how the mechanical properties of contractile networks could change drastically in real time as the network conformation is modified.

Architecture and connectivity govern actin network contractility

Hajer Ennomani[*1], Gaëlle Letort [*1], Christophe Guérin[1], Jean-Louis Martiel[1], Wenxiang Cao[2], François Nedelec[3], Enrique M. De La Cruz[2], Manuel Théry[#1,4] and Laurent Blanchoin[#1]

1 Institut de recherches en Technologies et Sciences pour le vivant, Laboratoire de Physiologie Cellulaire et Vegétale, CNRS/CEA/UJF/INRA Grenoble, France

2 Department of Molecular Biophysics and Biochemistry, Yale University, 260 Whitney Avenue, New Haven, CT 06520-8114, USA

3 Cell Biology and Biophysics Unit, EMBL, Meyerhofstrasse 1, D-69117, Heidelberg, Germany

4 Unité de thérapie Cellulaire, Hopital Saint-Louis, Avenue Claude Vellefaux 75010 Paris, France

* These authors contributed equally to this work

# These authors contributed equally to this work

Contact: manuel.thery@cea.fr or laurent.blanchoin@cea.fr

Summary

Actomyosin contractility plays a central role in a wide range of cellular processes including the establishment of cell polarity, cell migration, tissue integrity or morphogenesis during development [1, 2]. Contractile response involves a complex coupling between the actomyosin architecture and its biochemical composition [3-6]. To study how this coupling regulates myosin-driven contraction, we used the micropatterning method that enables the spatial control of actin assembly [7, 8]. We generated a variety of actin templates to evaluate how well defined actin structures respond to myosin-induced forces. We found that the same actin filament cross-linkers could either enhance or inhibit the contractility of a network, depending on the organization of actin within the network. We also show that filament crosslinking was necessary to sustain myosin-driven deformation and force production of dynamic actin organizations, in the presence of the disassembly factor, ADF/cofilin. Numerical simulations unified the roles of actin filament branching and crosslinking during actomyosin contraction. Specifically, we introduce the concept of "network connectivity", and show that the contractions of distinct actin architectures are described by the same master curve when considering their degree of connectivity. This makes it possible to predict the dynamic response of defined actin structures to transient changes in connectivity. More generally, this study reveals how, for a defined set of biochemical conditions, actin network contractility depends on the organization of the filament and, hence, how dynamic actin structure rearrangements modulate contractility.

Highlights

- We generated different actin architectures that span the diversity of cellular contractile structures.

- These different actin organizations respond differently to myosin-induced contraction.

- Actin filament cross-linkers can have opposite effects on the contractility of a network, depending on its organization.

- Numerical simulations highlight the role of the actin architecture-depend connectivity in modulating the contractile response.

- We characterized the dynamic response of defined actin structures to transient changes in connectivity.

- The variation of actomyosin contractile response results from a combination of two inter-dependent parameters: the spatial organization of actin filaments and their degree of connectivity.

eTOC Blurb

The composition, the organization and the geometry of the actomyosin network influence the production of contractile forces. Ennomani et al describe how the possibility to modulate network architecture and composition to finely tune the contractile response provides a large degree of mechanical adaptation and responsiveness to contractile networks.

Results and discussion

Contractile response of different actin organizations

Cellular actin filaments assemble into a variety of structures that are distinct with respect to the orientation of the filaments, and their connectivity [9-11]. The organization of actin filaments modulates the contractile response of a network. For example, branched networks are less contractile than bundles of anti-parallel filaments [6]. Here we investigate the factors that govern the coupling between filament spatial arrangement and the degree of crosslinking in the regulation of actomyosin contraction. We evaluated the contractile response of various *in vitro* reconstituted actin structures, that are branched or not, and in which filaments are either of mixed polarity, or prominently antiparallel (Figure 1). To obtain such diversity in actin architecture, we used surface micropatterning to initiate geometrically controlled actin assembly over 75 µm wide rings [7]. In this assay, well-defined surfaces coated with Actin Promoting Factor (NPF) trigger actin assembly in a reaction chamber containing a mixture of proteins including the Arp2/3 complex, actin and profilin. Throughout this study we varied the architecture and biochemical composition of the overall ring-like network. The perimeter was used as a simple and global readout of contractility (Figure 1).

We generated rings made of three different architectures (Figure 1A) that span the diversity of cellular contractile structures: 1) disordered branched networks (named: disordered networks), mimicking lamella-like structures, were assembled from a full ring coated with NPF (Figure 1A left panel); 2) a series of interconnected, ordered, antiparallel actin bundles (named: ordered bundles,), mimicking sarcomeric-like bundles, were generated by a dotted ring where only the dots were coated with NPF (Figure 1A middle panel); and 3) disordered, mixed polarity actin bundles (named:

disordered bundles), mimicking cytokinesis ring-like bundles, were generated by debranching the disordered branched meshwork described above by addition of ADF/cofilin (Figures 1A right panel, S1 and Movie S1 (for the illustration of ADF/cofilin debranching activity)). The deformation of these actin networks was triggered by the presence of double-headed (heavy-meromyosin (HMM)-like) myosin VI in the reaction mixture. Myosin VI-HMM [6] is pointed-end directed processive molecular motor [12]. Unlike myosin II, it can trigger continuous contraction and/or filament sliding (Movie S2) without the need to assemble into minifilaments. Thus using Myosin VI-HMM has the advantage that it yields in unprecedented reproducibility of the contractile response, unlike myosin II -based minifilaments, which often vary in length when reconstituted *in vitro* [6].

The contraction of actin rings by myosins follows three phases [6]: a initial phase corresponding to actin assembly and reorganization by myosins, a second phase characterized by a constant and often fast rate of contraction, and a final phase where actin is slowly compacted at the center of the ring. We measured the contraction rate during the second phase, to quantify the contractile behavior of all systems. This readout was highly reproducible across experiments.

Two types of rings contracted: the rings made of disordered branched networks and the rings made of ordered antiparallel bundles (Figure 1B, top and middle rows). Consistent with previous observations [6], the rings made of ordered antiparallel bundles contract faster than the ones made of branched networks (Figure 1C compare green and red curves and Movie S3 compare top row, left and middle rings). In contrast, the third type

of rings, corresponding to disordered bundles, deforms only little over time (Figure 1B bottom row, 1C blue curve and Movie S3 top row right ring).

To understand how different actin architectures respond to myosin-induced contraction, we performed detailed simulations of the different types of actin rings – disordered network, disordered and ordered bundles using Cytosim (Figures 1D and S2A, Movie S4 and [13, 14]). We implemented our simulation with entities mimicking molecular motors with properties similar to myosin VI (Figures 1D and S2B top panel). Thereby, we could reproduce *in silico* the diversity of contractile response for various actin architectures (Figure 1D, S2A and Movie S4 left panel, top row), and also track individual actin filaments during ring evolution (Movie S4 left panel, bottom row). Filaments in disordered bundles slide with respect to one another without inducing a global contraction (Figure 1D and Movie S4 left panel, bottom row right ring), suggesting that myosin-produced forces are not transduced into contractile dipoles in this structure. In contrast, inter-connected filaments in disordered network and ordered bundles directly lead to whole ring contraction (Movie S4 left panel, left and middle rings).

α-actinin modulates the contractile response of different actin organizations

Filament inter-connection in cells is achieved with the help of cross-linking proteins such as α-actinin, fascin, filamin, ... [15]. Strikingly, non-deforming rings comprised of disordered fibers become contractile when α-actinin is added (Figure 2A bottom row, 2B blue curve and Movie S3 bottom row right). In marked contrast, α-actinin impairs the contraction of the other types of rings (Figure 2A top and middle rows, 2B green and red

curves, and Movie S3 bottom row left and middle rings). Therefore, the effects of α-actinin on ring deformation depend on their architecture. Ring deformation also depends on the α-actinin concentration (Figure 2C). In our experimental condition with 2 μM actin monomers, the maximal rate of ring contraction of the disordered network (Figure 2C green curve) was first increased by low concentration (3 nM) of α-actinin, and then decreased progressively for higher α-actinin concentrations (ranging from 5 to 30 nM) displaying undetectable deformation at high α-actinin concentration (> 30 nM) over the timescale of our measurements. Increasing the concentration of α-actinin (Figure 2C red curve) progressively lowered the maximal deformation rate of ordered bundles. At high concentrations (>30 nM), α-actinin blocked the deformation of all types of actin architectures. The complex effect of α-actinin on the rate of myosin-induced contraction in different actin architectures suggests that both the filament organization and their physical interaction are key parameters governing the contractile response. Unfortunately, these parameters cannot be measured experimentally, but we could use numerical simulation to study how the amount of cross-linkers and branches affect actomyosin contraction.

Connectivity regulates network contraction in a biphasic manner

To the simulations containing myosin entities, we added structural elements connecting two actin filaments thereby representing the contribution of α-actinin to the system (Figures 3A and S2B bottom panel). From the simulations we calculated the maximal contraction velocity as a function of the crosslinker number for the three types of ring architectures (Figure 3B). The shrinking rate of the disordered networks, ordered bundles and disordered bundles (respectively, green, red and blue Figure 3B) were

qualitatively similar to those obtained experimentally (Figure 2C), validating that our simulations had correctly modeled the role of filament cross-linkers on the various actin architectures. Both cross-linkers and branches act as filaments connectors [16, 17]. We then estimated the global degree of "connectivity", defined as the average number of connectors per actin filament (Figure 3C, generated by the Arp2/3 complex at branched point and by the bridge made by α-actinin between two filaments). By plotting the contraction velocity with respect to the connectivity for the different actin organizations (Figure 3D), we found that they all form a bell-shaped curve centered on an optimal connectivity comprised between 2 and 3 (Figure 3D). This value corresponds to the percolation threshold (transition point from which all filaments are connected together in one single cluster, Figure 3E and [4]). Below 2 (under percolation), filaments move freely inside the structure. Thus, the deformation is dominated by local events but do not lead to global network contraction. Above 3, filaments get partially or totally blocked and can no longer be moved by myosins. The first important insight gained from this analysis was that Arp2/3 complex is a more efficient connector than α-actinin. By essence, for any given pair of filaments, there can be only one Arp2/3 connection, whereas multiple α-actinin connections are possible. Thus in terms of percolating the network, Arp2/3 complex entities are more potent than α-actinin crosslinks, because some of the later may be connecting filaments that are already linked otherwise (Figure 3C, branched vs. crosslinked connectivity). The second important insight is that, in parallel to curve shape regulation, the contraction rate also depends on the actin organization, and is maximal for ordered bundles (red curve), intermediate for the disordered network (green curve) and minimal for disordered bundles (blue curve) (Figure 3D). Indeed, ordered bundles have an optimal actin architecture in which

filaments are perfectly aligned, oriented and properly anchored to transmit local myosin work throughout the entire structure. On the other hand, randomly oriented filaments in disordered branched networks resist deformation and are inefficient at propagating myosin-induced translocation. In disordered bundles, a significant fraction of the myosins are not productive, or their work is dissipated in motor displacement rather than filament sliding. Accordingly, both the degree of connectivity and the spatial organization of filaments regulate overall actomyosin response.

Dynamic modulation of actin network connectivity

Interestingly, filament connectivity and conformation in cells vary as the network evolves from filament nucleation at the cell periphery to filament alignment and crosslinking in transverse arcs, up to filament disassembly in the cell interior [18]. Our work suggests that contractility could change accordingly during these dynamic architectural transitions. Investigating the contractile response of dynamic actin organization required an experimental system where the degree of connectivity or/and the actin filament organization could be modulated over time. One limitation in our initial experimental set up described above is that ring contraction is rapid and the structure collapses when the connectivity is optimal (2-3) or disassembles with minimum deformation when the connectivity is higher than 4. Our ability to modulate the network composition with this setup is therefore limited. To circumvent this limitation, we developed a new method to assemble controlled actin organizations on soft polyacrylamide gels (Figure S3A and [8]). The behavior of actin structures on soft substrate differs drastically from what was previously described with hard substrate. On soft gels, actin rings contract and deform the underlying substrate without detaching from it (Figures 4A and S3A, B). In these conditions, actin networks do not collapse and

disassemble as on hard substrate. Rather, they are maintained in a tensed steady state. By sequentially changing the biochemical conditions, the networks in such steady states are then amenable to dynamic changes. Because the polyacrylamide gels were produced with a defined rigidity, the forces exerted by the various actin structures on the substrate upon myosin-addition could be measured with traction force microscopy (Figures 4A and S3B). Consistent with the variation of the contractile response on hard substrate (Figure 2C), increasing concentrations of α-actinin first enhances (Figure 4B, 10 nM α-actinin, disordered network) then decreases (Figure 4B, 30 nM α-actinin) the magnitude of tension forces, resulting in a bell-shape curve for the variation of the mechanical energy in function of the concentration of α-actinin (Figure 4B). To modify the connectivity in real time, we designed an open reaction chamber (Figure S3C) that is placed on top of the soft patterned surface. Because of its bell-shape response curve (Figure 3D), our numerical model predicts that a given reduction of connectivity can have opposite effects on tensional forces depending of the initial level of network connectivity (Figure 4C). Indeed, if the contractile structure has a high degree of connectivity, a decrease in connectivity should enhance contraction (Figure 4C, red arrow). In contrast, if the structure has an optimal degree of connectivity, reductions in connectivity should block the network deformation and reduce contractility (Figure 4C, blue arrow). We tested these predictions experimentally using ADF/cofilin ability to debranch Arp2/3 network and slightly sever actin filaments, in order to modulate ring connectivity as it contracted (Figure 4D and E). As predicted, addition of ADF/cofilin to a highly connected structure increased the magnitude of the contractile forces (Figure 4D). In contrast, addition of ADF/cofilin to an actin organization with optimal connectivity reduced the magnitude of tensional forces (Figure 4E). These experiments

showed how the dynamic reorganization of actin network architecture could modulate the contractile mechanical response over time.

Conclusion remarks:

Contractile actomyosin structures in cells have different abilities to generate forces [19]. We found that these variations may result from a combination of two interrelated parameters: the spatial organization of actin filaments within the network, and their degree of connectivity. The degree of connectivity regulates the type of the contractile response (local sliding, global deformation or massive freezing), whereas the actin filament organization, i.e. the degree of filament parallel vs. antiparallel alignment, governs its magnitude. The local densities of molecular motors and cross-linker have been described as key modulators of the transition from contractile to non-contractile organization [5, 16, 20-22]. Here we have demonstrated that for a defined set of biochemical parameters the spatial organization of actin filaments can strongly impinge on the rate of contraction and the magnitude of force generation. Moreover, we showed how the contractile properties of an actin network could change drastically, as its conformation is modified. Such behaviors are likely to be important since modulations of the actin architecture are often present in vivo. Modulation occurs for example following the maturation of sarcomeres in cardomyocytes, [23, 24] during which misoriented actin filaments are transported and sorted by myosins, up to the generation of alternate distribution between myosins and croslinkers along aligned filaments, an organization that optimizes force production at large scales. Similarly, dynamic changes of connectivity and network architecture occur in the lamella of motile cells, where the protrusive branched network of short filaments is converted to transverse arcs which are long bundles of aligned and crosslinked fibers, and probably much better suited to

produce tension [18]. The possibility to modulate network architecture and composition to finely tune the contractile response provides a large degree of mechanical adaptation and responsiveness to contractile networks. This modularity is crucial for cell shape changes during migration or tissue development where the mechanical properties and the geometry of the local environment can vary considerably in space and time [25, 26].

Supplemental Data

Supplemental Data include supporting text, three figures, four movies and supplemental references can be found with this article on line at http://www.

Author Contributions

Conceived and designed the experiments: HE, GL, FN, EMDLC, MT and LB. Performed the experiments: HE and GL. Analyzed the data: HE, GL, JLM. Contributed reagents/materials/analysis tools: HE, GL, WC, CG, FN. Wrote the paper: HE, GL, FN, EMDLC, MT and LB.

Acknowledgments

This work was supported by grants from Human Frontier Science Program (RGP0004/2011 awarded to L.B. and E.M.D.L.C.), Agence Nationale de la Recherche (ANR-12-BSV5-0014 awarded to L.B.), National Institutes of Health (GM097348 awarded to E.M.D.L.C) and ERC starter Grant (310472) to MT. HE was awarded with a PhD fellowship from the IRTELIS program of the CEA.

References

1. Levayer, R., and Lecuit, T. (2012). Biomechanical regulation of contractility: spatial control and dynamics. Trends Cell Biol. *22*, 61-81.

2. Heisenberg, C.P., and Bellaiche, Y. (2013). Forces in tissue morphogenesis and patterning. Cell *153*, 948-962.

3. Thoresen, T., Lenz, M., and Gardel, M.L. (2011). Reconstitution of contractile actomyosin bundles. Biophys. J. *100*, 2698-2705.

4. Alvarado, J., Sheinman, M., Sharma, A., MacKintosh, F.C., and Koenderink, G.H. (2013). Molecular motors robustly drive active gels to a critically connected state. Nat. Phys. *9*, 591–597.

5. Kohler, S., and Bausch, A.R. (2012). Contraction mechanisms in composite active actin networks. PLoS One *7*, e39869.

6. Reymann, A.C., Boujemaa-Paterski, R., Martiel, J.L., Guérin, C., Cao, W., Chin, H.F., De La Cruz, E.M., Théry, M., and Blanchoin, L. (2012). Actin Network Architecture Can Determine Myosin Motor Activity. Science *336*, 1310-1314.

7. Reymann, A.C., Martiel, J. L., Cambier, T., Blanchoin, L., Boujemaa-Paterski, R., and Théry, M. (2010). Nucleation geometry governs ordered actin networks structures. Nat. Mat. *9*, 827-832.

8. Vignaud, T., Ennomani, H., and Thery, M. (2014). Polyacrylamide hydrogel micropatterning. Methods Cell Biol. *120*, 93-116.

9. Blanchoin, L., Boujemaa-Paterski, R., Sykes, C., and Plastino, J. (2014). Actin dynamics, architecture, and mechanics in cell motility. Physiol. Rev. *94*, 235-263.

10. Tojkander, S., Gateva, G., and Lappalainen, P. (2012). Actin stress fibers assembly, dynamics and biological roles. J. Cell Sci. *125*, 1855-1864.

11. Fletcher, D.A., and Mullins, R.D. (2010). Cell mechanics and the cytoskeleton. Nature *463*, 485-492.

12. Wells, A.L., Lin, A.W., Chen, L.Q., Safer, D., Cain, S.M., Hasson, T., Carragher, B.O., Milligan, R.A., and Sweeney, H.L. (1999). Myosin VI is an actin-based motor that moves backwards. Nature *401*, 505-508.

13. Nedelec, F., and Foethke D. (2007). Collective Langevin dynamics of flexible cytoskeletal fibers. New J. Phys. *9*, 427.

14. Letort, G., Politi, A.Z., Ennomani, H., Thery, M., Nedelec, F., and Blanchoin, L. (2015). Geometrical and mechanical properties control actin filament organization. PLoS Comput. Biol. *11*, e1004245.

15. Ahmed, W.W., and Betz, T. (2015). Dynamic cross-links tune the solid-fluid behavior of living cells. Proc. Natl. Acad. Sci. USA *112*, 6527-6528.

16. Bendix, P.M., Koenderink, G.H., Cuvelier, D., Dogic, Z., Koeleman, B.N., Brieher, W.M., Field, C.M., Mahadevan, L., and Weitz, D.A. (2008). A quantitative analysis of contractility in active cytoskeletal protein networks. Biophys. J. *94*, 3126-3136.

17. Wang, S., and Wolynes, P.G. (2012). Active contractility in actomyosin networks. Proc. Natl. Acad. Sci. USA *109*, 6446-6451.

18. Burnette, D.T., Manley, S., Sengupta, P., Sougrat, R., Davidson, M.W., Kachar, B., and Lippincott-Schwartz, J. (2011). A role for actin arcs in the leading-edge advance of migrating cells. Nat. Cell Biol. *13*, 371-381.

19. Murrell, M., Oakes, P.W., Lenz, M., and Gardel, M.L. (2015). Forcing cells into shape: the mechanics of actomyosin contractility. Nat. Rev. Mol. Cell Biol. doi: 10.1038/nrm4012.

20. Janson, L.W., Kolega, J., and Taylor, D.L. (1991). Modulation of contraction by gelation/solation in a reconstituted motile model. J. Cell Biol. *114*, 1005-1015.

21. Luo, T., Mohan, K., Iglesias, P.A., and Robinson, D.N. (2013). Molecular mechanisms of cellular mechanosensing. Nat. Mater. *12*, 1064-1071.

22. Abu Shah, E., and Keren, K. (2013). Mechanical forces and feedbacks in cell motility. Curr. Opin. Cell Biol. *25*, 550-557.

23. Craig, E.M., Dey, S., and Mogilner, A. (2011). The emergence of sarcomeric, graded-polarity and spindle-like patterns in bundles of short cytoskeletal polymers and two opposite molecular motors. J. Phys. Condens. Matter. *23*, 374102.

24. Kresh, J.Y., and Chopra, A. (2011). Intercellular and extracellular mechanotransduction in cardiac myocytes. Pflugers Arch. *462*, 75-87.

25. Elliott, H., Fischer, R.S., Myers, K.A., Desai, R.A., Gao, L., Chen, C.S., Adelstein, R.S., Waterman, C.M., and Danuser, G. (2015). Myosin II controls cellular branching morphogenesis and migration in three dimensions by minimizing cell-surface curvature. Nat. Cell Biol. *17*, 137-147.

26. DuFort, C.C., Paszek, M.J., and Weaver, V.M. (2011). Balancing forces: architectural control of mechanotransduction. Nat. Rev. Mol. Cell Biol. *12*, 308-319.

Figure legends

Figure 1: Architecture-dependent contractility of actin rings

(A) Schematic representation of the different types of actin architecture: disordered networks, ordered and disordered bundles respectively. (B) Contraction dynamics of the different actin rings, induced by myosin motors. Time is indicated in each picture. Scale bar = 25 μm. (C) Measured ring perimeter divided by initial ring perimeter, for each type of ring, as a function of time. The disordered network (green) and ordered bundles (red) both contract within a few minutes following assembly, whereas disordered bundle (blue) are not contractile within the same time-span. Each curve was obtained by averaging over a dozen of different patterns. Error bars represent SEM. (D) Simulated contractility of actin rings with different architectures. The essential features of the three types of actin rings were constructed within the cytosim platform (green: disordered network, red: ordered bundles, blue: disordered bundles), and simulated (see text). The diameter of the rings is 9 μm. The simulated dynamics of ring contraction in the presence of myosin cross-linkers (right panels) were generated here from 10 simulations in each case. The measured perimeter of the ring is divided by its initial value.

Figure 2. Effects of α-actinin on the contractility of actin rings

(A) Contraction of one representative example of each actin ring, in the presence of α-actinin: (top row) 15 nM α-actinin for the disordered network, (middle and bottom rows) 20 nM α-actinin for both the ordered and disordered bundles. (B) Normalized ring perimeters as a function of time are represented. Note that addition of α-actinin induces the disordered bundle ring to contract, whereas it decelerates contraction of the

other rings. (C) Maximal perimeters decrease speed for each type of network, as a function of the concentration of α-actinin. A dozen of ring perimeters were measured as a function of time for each architecture and each α-actinin concentration, and the extracted maximum speeds were averaged. Error bars represent S.E.M.

Figure 3. Network connectivity modulates the contractile response of actin rings

(A) Snapshots of simulated actin rings with different architectures: branched network (green), ordered bundles (red), disordered bundles (blue) in presence of 2500 crosslinkers representing α-actinin. (B) Maximal rate of ring perimeter decrease, as a function of the number of crosslinkers for each type of ring. (C) Schematic illustration (left) of the connectivity C of different actin filament generated by the Arp2/3 complex (red symbols) and α-actinin (black symbols). The network connectivity is the average of all filament connectivity values. It is expected to increase as a function of the number of connecting cross-linkers present in the system (right). (D) The maximal velocity of perimeter decrease for the different actin rings as a function of the network connectivity. (E) Size of the largest percolating cluster (normalized to the total number of actin filaments) as a function of the network connectivity, for branched network (green), ordered bundles (red) and disordered bundles (blue). Vertical lines indicate the threshold at which percolation is reached (i.e. 95% of filaments are connected).

Figure 4. Dynamic variations of actin network connectivity

(A) Contraction of a branched network ring on a patterned deformable substrate. Combined fluorescence images (top row) show actin and myosin signals, while second and third rows show the corresponding vector force and the force map reconstitution.

(B) Maximal mechanical energy of the actin disordered branched network, for the indicated α-actinin concentrations. The maximal mechanical energy is defined as the maximal deformation that ring contractions cause on their substrate. (C) Qualitative contractile behavior for the three different actin rings, as a function of the network connectivity, as predicted by the model (Figure 3D). The red arrow illustrates the effect of reducing connectivity in a highly connected actin network, while the blue arrow indicates a reduction of connectivity in a network with optimal connectivity. The contractility is enhanced in the shift represented by the red arrow, whereas it is reduced in the blue arrow. (D, E) Cartoon representations (top) of the actin architectures before and after addition of ADF/cofilin, and kinetic of the normalized total network mechanical energy as a function of time. In (D), a highly crosslinked branched actin network (100 nM α-actinin) was de-branched by addition of 100 nM ADF/cofilin. This configuration corresponds to the red arrow. In (E), a network with nearly optimal connectivity (10 nM α-actinin) is debranched by addition of 100nM ADF/ cofilin. This configuration corresponds to the blue arrow.

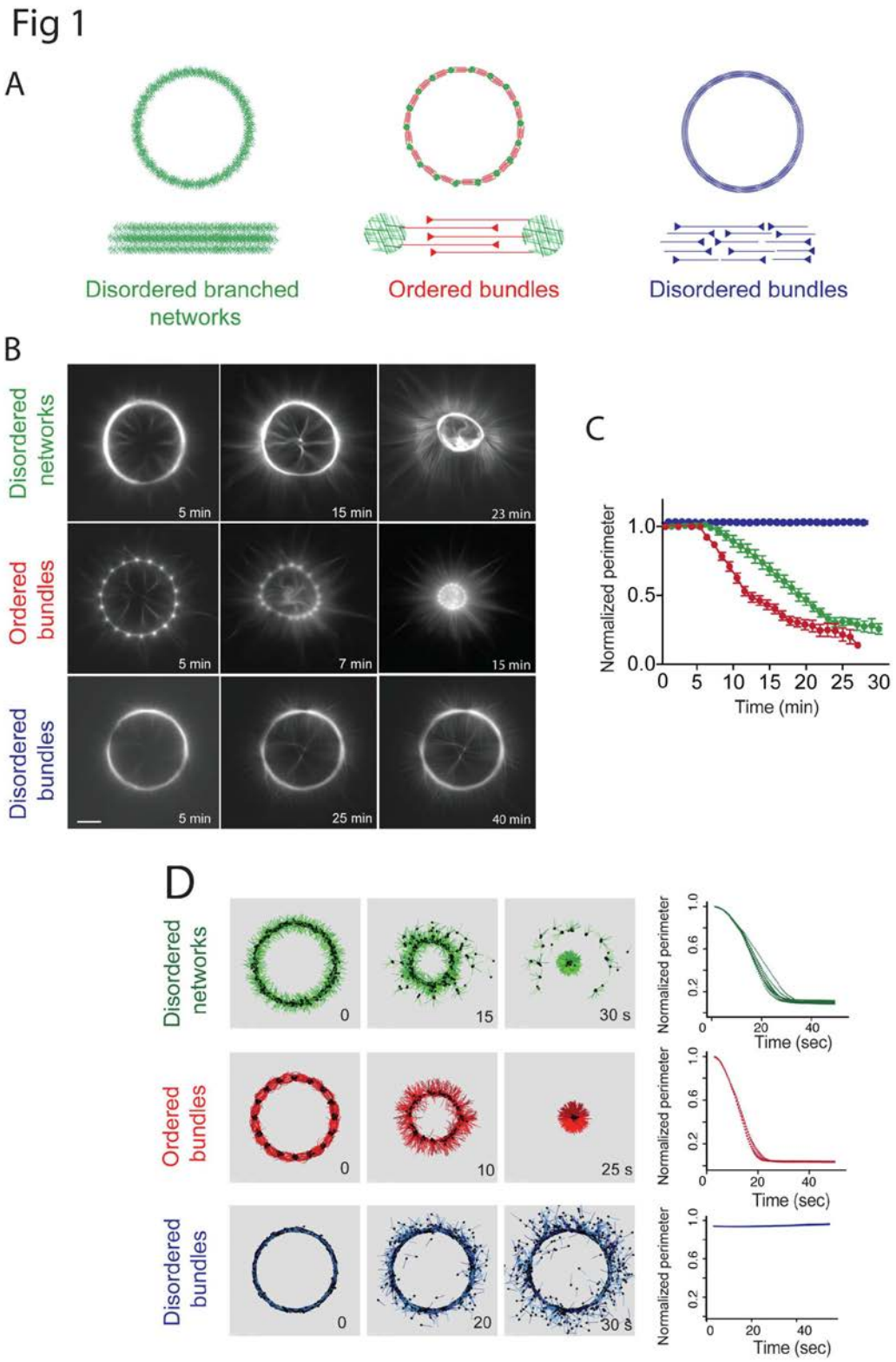
Fig 1
A
Disordered branched networks
Ordered bundles
Disordered bundles
B
Disordered networks
Ordered bundles
Disordered bundles
5 min
15 min
23 min
5 min
7 min
15 min
5 min
25 min
40 min
C
Normalized perimeter
1.0
0.5
0.0
0 5 10 15 20 25 30
Time (min)
D
Disordered networks
Ordered bundles
Disordered bundles
0
15
30 s
0
10
25 s
0
20
30 s
Normalized perimeter
Time (sec)

Fig 2

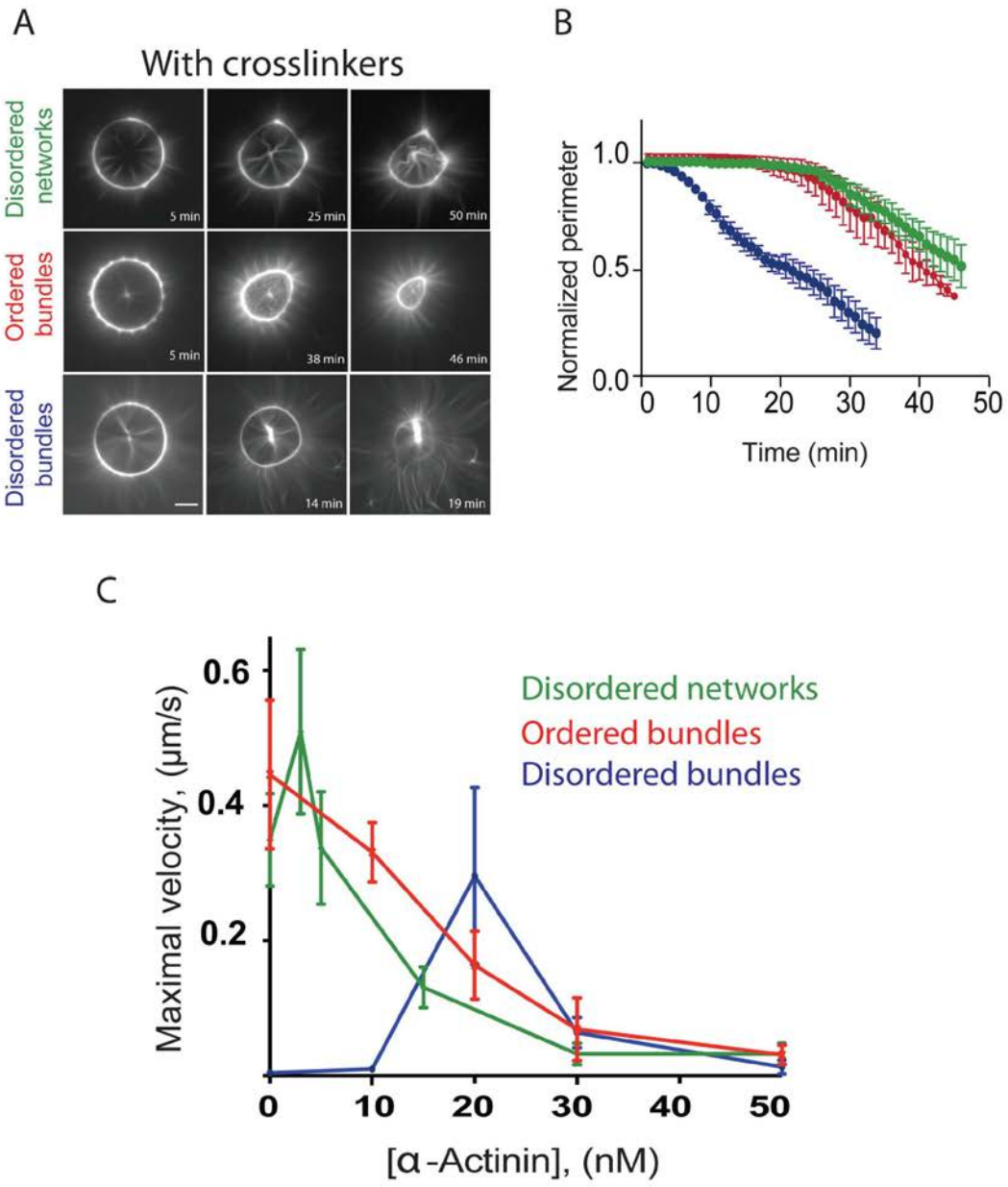
A
With crosslinkers
Disordered networks
Ordered bundles
Disordered bundles
5 min
25 min
50 min
5 min
38 min
46 min
14 min
19 min
B
Normalized perimeter
1.0
0.5
0.0
0
10
20
30
40
50
Time (min)
C
Maximal velocity, (µm/s)
0.6
0.4
0.2
0
10
20
30
40
50
[α-Actinin], (nM)
Disordered networks
Ordered bundles
Disordered bundles

Fig. 3

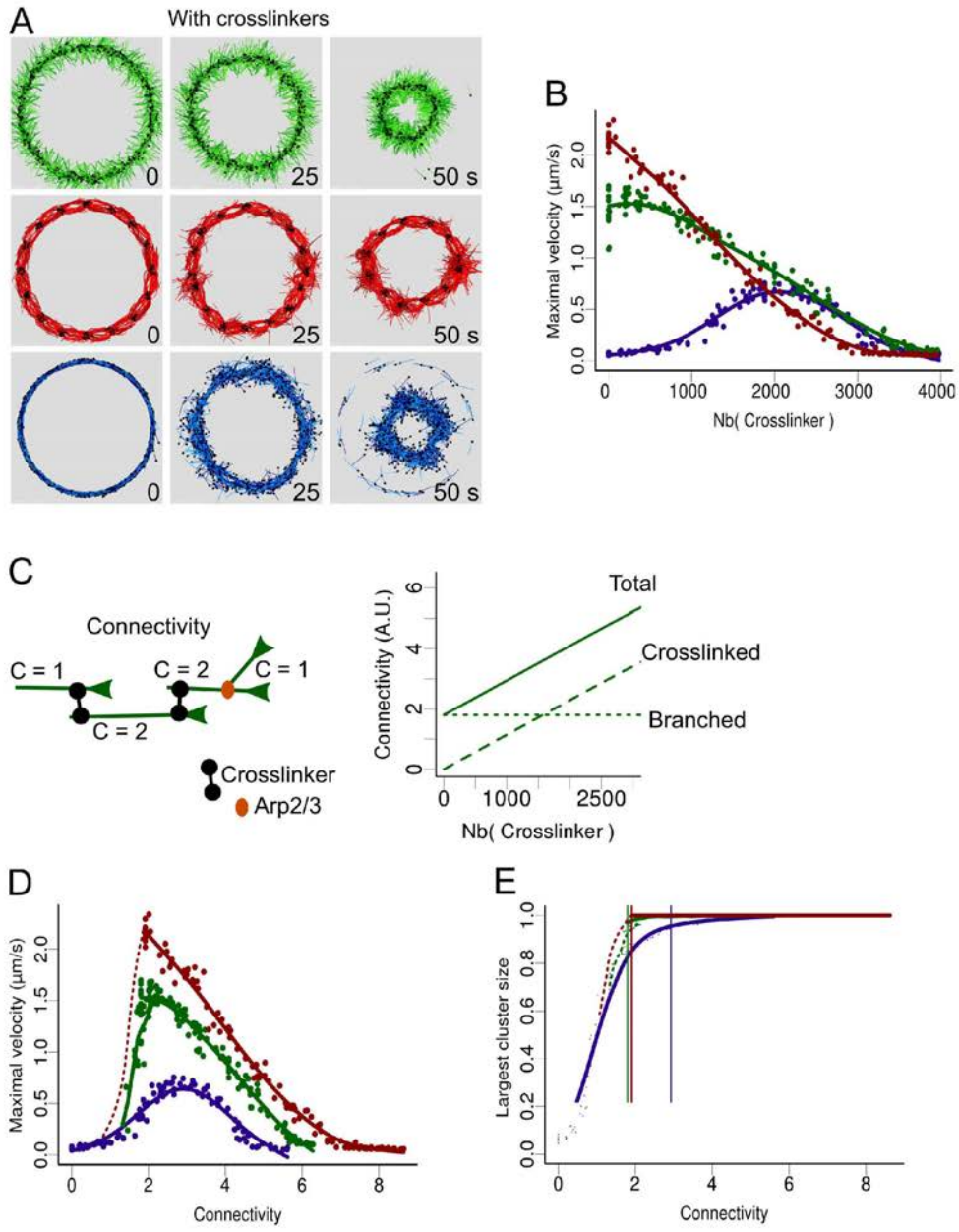
A
With crosslinkers
0
25
50 s
B
Maximal velocity (µm/s)
Nb(Crosslinker)
C
Connectivity
C = 1
C = 2
C = 1
C = 2
Crosslinker
Arp2/3
Connectivity (A.U.)
Total
Crosslinked
Branched
Nb(Crosslinker)
D
Maximal velocity (µm/s)
Connectivity
E
Largest cluster size
Connectivity

Fig 4

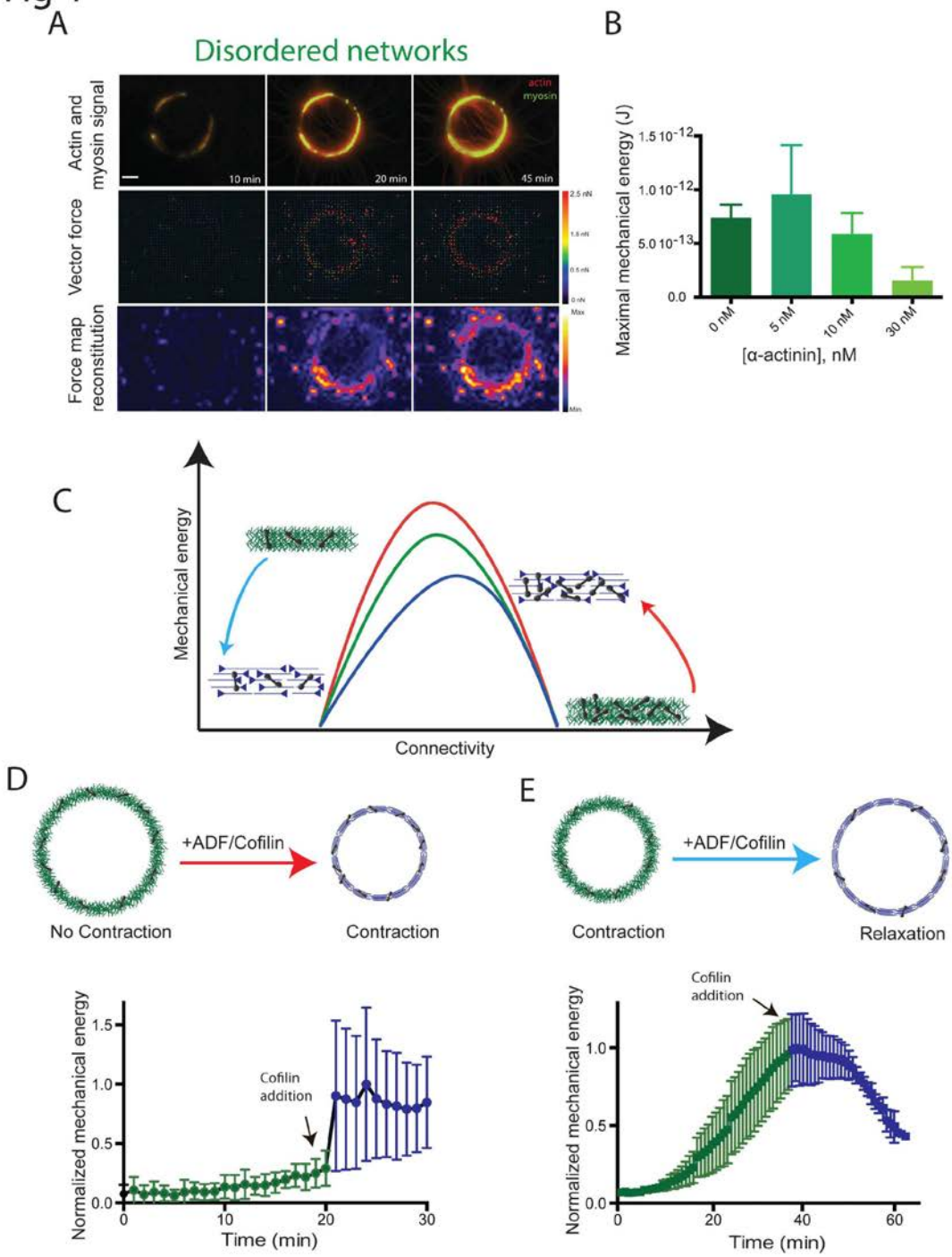
A
Disordered networks
Actin and myosin signal
actin
myosin
10 min
20 min
45 min
Vector force
Force map reconstitution
B
Maximal mechanical energy (J)
1.5 10-12
1.0 10-12
5.0 10-13
0.0
0 nM
5 nM
10 nM
30 nM
[α-actinin], nM
C
Mechanical energy
Connectivity
D
+ADF/Cofilin
No Contraction
Contraction
Normalized mechanical energy
Cofilin addition
Time (min)
E
+ADF/Cofilin
Contraction
Relaxation
Cofilin addition
Normalized mechanical energy
Time (min)

Supplemental Information

Inventory of Supplemental Information:

Supplemental data:

- Supplemental Figures: S1 related to Figure 1; S2 related to Figures 1, 2 and 3; S3 related to Figure 4.
- Supplemental Movies: S1 related to Figure S1; S2 related to Figure 1; S3 related to Figures 1 and 2, S4 related to Figure 3.
- 2 tables

Supplemental Experimental Procedures:

- Experimental methods required to perform the experiments described in this study.
- Description of the model and the numerical simulation methods used to account for the actin network contractility.

Supporting References

Fig S1

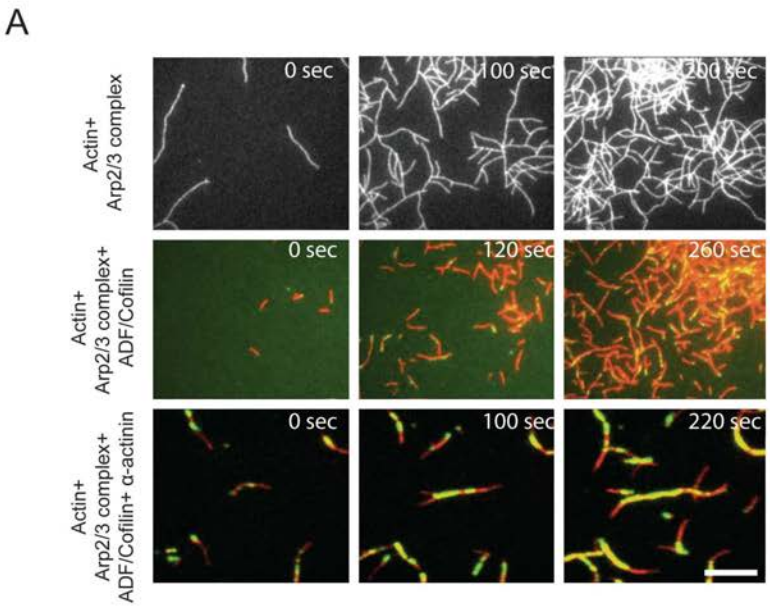
A
Actin+ Arp2/3 complex
0 sec
100 sec
200 sec
Actin+ Arp2/3 complex+ ADF/Cofilin
0 sec
120 sec
260 sec
Actin+ Arp2/3 complex+ ADF/Cofilin+ α-actinin
0 sec
100 sec
220 sec

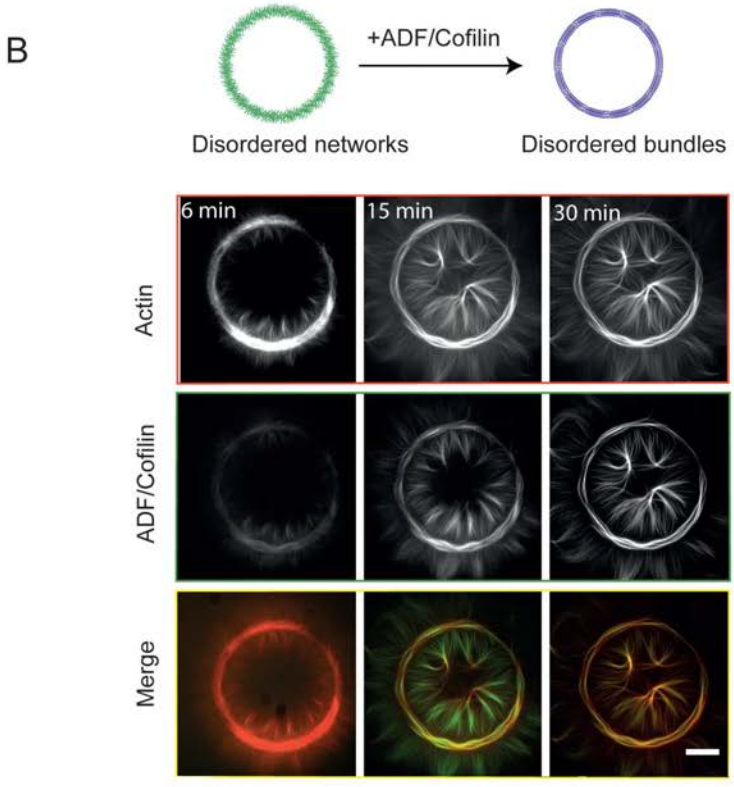
B
+ADF/Cofilin
Disordered networks
Disordered bundles
Actin
ADF/Cofilin
Merge
6 min
15 min
30 min

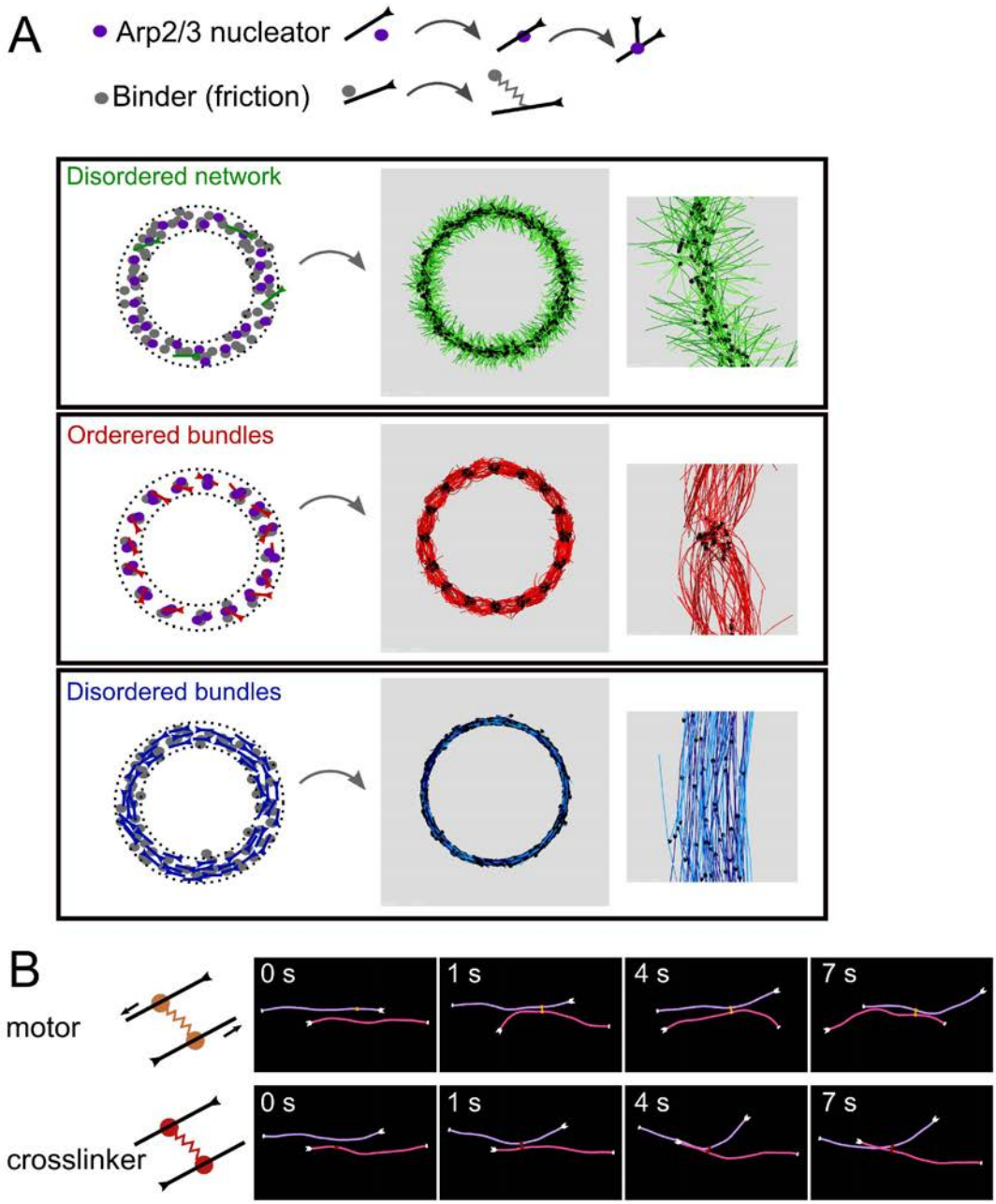
A
Arp2/3 nucleator
Binder (friction)
Disordered network
Orderered bundles
Disordered bundles
B
motor
crosslinker
0 s
1 s
4 s
7 s
0 s
1 s
4 s
7 s

Fig S3

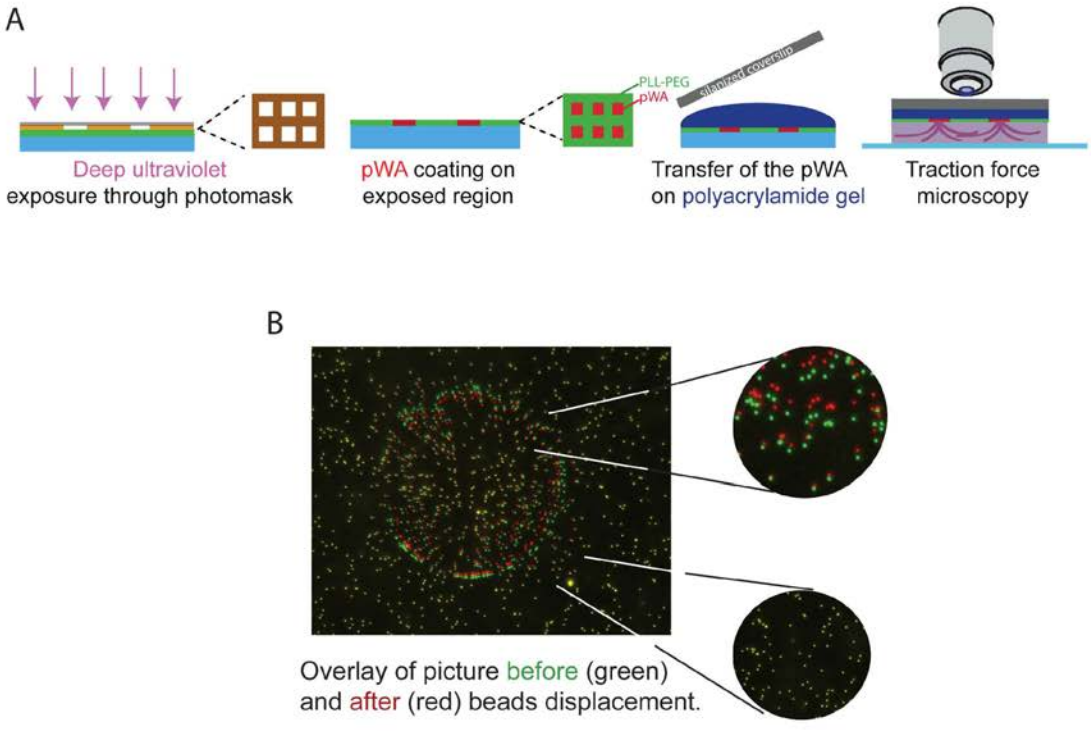
A
Deep ultraviolet
exposure through photomask
pWA coating on
exposed region
PLL-PEG
pWA
Transfer of the pWA
on polyacrylamide gel
Traction force
microscopy
B
Overlay of picture before (green)
and after (red) beads displacement.
C
PDMS well
patterns pWA
on polyacrylamid gel
PDMS on top
of the PAA gel
Addition of mix
or specific protein

Figure S1 related to Figure 1: ADF/cofilin debranching activity allows the transition between branched actin network and disordered actin fibers.

(A) Montage of time-lapse total internal reflection fluorescence microscopy (TIRFm) images showing the time course of assembly of 0.8 µM Alexa-568-labeled actin with 50 nM Arp2/3 complex (top panel), in presence of 200 nM Alexa-488-cofilin (middle panel) or 200 nM Alexa-488-cofilin and 80nM α-actinin (bottom panel). Alexa-568-actin filaments and Alexa-488-ADF/cofilin were color-coded in red and green respectively, and the decorated portions of filaments in yellow in the merged images. Scale bar= 10 µm

(B) (Top) Schematic representation of the reorganization of the actin filaments on a ring pattern upon addition of ADF/Cofilin. (Bottom) Time-lapse fluorescence microscopy of the effect of ADF/Cofilin on branched actin filaments nucleated on a micropatterned ring (actin monomers are labeled with Alexa-568 and ADF/Cofilin is labeled with Alexa-488). Top row represents the actin signal (red), middle row represents the ADF/Cofilin signal (green) and bottom row is the merge of the two signals. Scale bar= 25µm

Figure S2 related to Figures 1 and 3: Main features of the simulations

(A) (Top) Arp2/3 and binders are used to create the desired actin architecture. Arp2/3 complex-like entities induce branching from the side of an existing filament. Binder entities that can dynamically bind and unbind to filament, and are anchored to a fixed position on the substrate. They are used to simulate friction between the filaments and the pattern.

The disordered branched network (green) is created by initially distributing Arp2/3 complex-like entities, binders and a few short filament seeds on a ring (left panel). Actin filament assembly and branching is simulated with artificially high rates for ~1 second to obtain the disordered branched network.

The rings containing a series of antiparallel bundles (red) are created by initially putting 16 dots of Arp2/3 complex-like entities, binders and few primer filaments. During the fast growth phase, actin filaments are constrained between two circles to keep them circularly oriented. Actin filaments growing from the pattern dots meet in an anti-parallel fashion.

The disordered bundle rings (blue) are created by adding preformed actin filaments tangentially to the circle, randomly clockwise or anticlockwise. Binders are also distributed randomly on the ring. Light and darker shades of blue indicates opposite orientations of the actin filaments. Middle column corresponds to the simulated rings. The right column contains a detailed view of the corresponding rings.

(B, top) Schematic view of a myosin VI-like motor entity acting between two antiparallel filaments. The two identical heads move toward the minus ends of the filaments and slide the filaments apart (right).

(B, bottom) Schematic view of α-actinin like entity crosslinking two antiparallel filaments. The two static heads are linked by a spring like (Hookean) force term, constraining the filaments in their motions.

Figure S3 related to Figure 4: Soft patterning method and setup for the sequential addition of components during an experiment of ring contraction on soft pattern.

(A) Soft patterning: cartoon of the micropatterns on polyethylene glycol coated glass slide followed by their incubation with WASp-pWA to allow proteins adsorption to the micropatterned regions.

Polyacrylamide solution was added between the patterned pWA coverslip and a silanized coverslip for 20 minutes to allow the transfer of the protein from the hard to the soft substrate when the gel is fully polymerized.

(B) Overlay of beads signal before (green) and after (red) contraction illustrating beads displacement.

(C) Schematic representation of the PDMS well for the dynamic experiment.

Materials and Methods

Protein expression and purification

Actin was purified from rabbit skeletal-muscle acetone powder. Actin was labeled on lysines with Alexa-568 according to [1]. Arp2/3 complex was purified from bovine brain extracts [2]. GST-pWA, ADF/cofilin and human profilin were expressed and purified as described previously [3, 4]. Double-headed (referred to as HMM) porcine myosin VI with bound calmodulin was purified from Sf9 cells by FLAG affinity chromatography.

α-actinin: the pGex4T-1-ACTN4-6xHis construct was overexpressed in rosetta 2 DE3 pLys bacteria. The pellet was resuspended in a buffer containing 20mM Tris pH 7.5, 150mM NaCl, 1mM DTT, 1mM EDTA, 5% Glycerol and 1% Triton. After sonication, the lysate was centrifuged at 16000rpm in a JA 25.50 rotor (beckman) for 30 minutes at 4°C. The supernatant was loaded onto a glutathione sepharose 4B resin (GE Healthcare) for 2 hours at 4°C. Elution was performed by adding 100 mM glutathione buffered in 20mM Tris pH 7.5, 150 mM NaCl, 1 mM DTT, 1 mM EDTA. The eluted protein was loaded onto a Ni sepharose high performance resin (GE Healthcare) for 2 hours at 4°C. The resin was washed with a buffer containing 20mM Tris pH 7.5, 150mM NaCl, 1 mM DTT, 1 mM EDTA supplemented with 20 mM imidazole. Protein was eluted with 20 mM Tris pH 7.5, 150 mM NaCl, 1 mM DTT, 1 mM EDTA and 300 mM Imidazole and dialyzed against the storage buffer (20mM Tris pH 7.5, 150mM NaCl, 1mM DTT, 1mM EDTA) over night at 4°C. Quality and concentration were estimated with a SDS-Page gel and ACTN4 was flash frozen in liquid nitrogen and then store at -80°C.

Micropatterning

Hard patterning

Deep UV exposure through a photomask creates micropatterns on polyethylene glycol coated coverslip. pWA is adsorbed on the micropatterned regions. In the presence of the actin polymerizing mix, filaments are growing on and out of the micropattern.

Soft surface patterning

Polyacrylamide gel was prepared as described in detail previously [5] with some modifications. 20 mm^2 coverslip were silanized in order to bind the polyacrylamide gel to it. Solution of 40% polyacrylamide and 2% bisacrylamide were mixed to have a solution that contains 4% acrylamide and 0.06% bis-acrylamide corresponding to a 1.16 kPa gel rigidity. Beads were added to this mixture and then degased for 15 minutes. The polymerization solution was added between a coverslip with patterned pWA and the silanized coverslip for 20 minutes to transfer the protein from the hard to the soft substrate.

Actin polymerization

Actin polymerization was induced in a solution containing 2 µM actin monomers (7% labeled with Alexa-568), 6 µM profilin, 100 nM Arp2/3 complex 16 nM of HMM-myosin VI (GFP labeled). These proteins mixture were diluted in freshly prepared buffer containing 15 mM imidazole-HCl (pH 7.8), 0.6 mM ATP, 55 mM DTT, 1 mM EGTA, 75 mM KCl, 3.5 mM MgCl2, 1.5 mg/mL glucose, 10 µg/mL catalase, 50 µg/mL glucose oxidase, and 0.25 % w/v methylcellulose. An ATP regenerating system was also added to this medium (2 mM MgATP, 2 mM phosphoenolpyruvate, 2000 U/mL pyruvate kinase).

Semi-automated analysis of data of ring contraction rates

A specific semi-automated analysis of data was developed using ImageJ and MATLAB for the analysis of myosin induced-contraction of actin networks on patterned rings as described previously [6].

Open chamber experiment

First, PDMS mixture was prepared by adding 10 g of DMS (Sylgard 184 Silicone Elastomer; Dow Corning) for each gram of curing agent. The mixture was degased for a minimum of 45 min, spread into a thin layer of about 5 to 10 mm, and heated for 20 min at 100°C. PDMS was cooled down and attached to the soft patterning coverslip after creating a well in the middle.

Traction force microscopy

A specific semi-automated analysis of data was developed using ImageJ as explained previously [7].

Numerical simulations of architecture contractility

General features

Simulations were performed with the software Cytosim [8] as previously described [9]. Basically, actin filaments are modeled as elastic fibers surrounded by an immobile viscous fluid, and their Brownian motion is calculated following Langevin dynamics. The filaments are at steady state, as simulating their assembly dynamics is not necessary to study the contractile behavior of a network. Steric attraction and repulsion between actin filaments are included to avoid unrealistic filaments overlap, with a realistic range (20 nm, see [9] for more details). The crosslinkers are attached at fixed positions for

simplicity (Figure S2A), during the first stage of the simulation during which the system is setup. Molecular motors are made of two identical actin-binding motile "heads". Each of them can bind and unbind stochastically to filaments and move along the filaments toward the pointed end. Motors diffuse when the two heads are unattached. A motor with two heads bound to different filaments creates a Hookean spring between these filaments. The motion of the attached heads toward the pointed end of the filament generates a contractile stress (Figure S2B). The Arp2/3 complexes also act as Hookean spring between the pointed end of one filament (daughter filament) and a random position along the mother filament, with an additional torque constraint to reproduce the characteristic angular branching (Figure S2A). Finally, Binders link the filament to random positions on the patterned area, such as to reproduce the immobilization of actin on the patterned area (binders, Figure S2A). Attached binders are also represented as Hookean springs.

The main parameters used for simulating the objects are given in Table 1.

Parameter	Value	Description
General		
Temperature	25 °C	In-vitro conditions
Viscosity	0.18 pN s / μm²	In-vitro conditions (in the presence of methylcellulose)
Simulated time	80 s	With a time step of 10 ms
Ring diameter	9 μm	
Actin filaments		
Persistence length	10 to 15 μm	From [1, 10].
Steric radius	5 nm	~actin filament radius
Length	see table 2	Filaments are of constant length
Molecular motor		
Binding rate	5 s^{-1}	Rate at which free myosin binds to actin filaments. This value was calculated from k_+ and the concentration of actin and myosin in the sample. (4.5-9 s^{-1}, from [11])
Binding range	36 nm	Average myosin step size. The results were relatively insensitive within the range 20 to 80 nm.
Unbinding force	3.65 pN	Typical "rupture" force required to detach actomyosin VI [12].
Maximal speed	v_m = 0.3 μm s^{-1}	Velocity of motor toward the pointed end, from [13].

Stall force	f_s = 2 pN	Parameter of the linear force velocity relationship $v = v_m(1 + \vec{f} \cdot \vec{d} / f_s)$, that determines how motors are stopped by antagonistic force. From [12, 14].
Stiffness	100 pN/µm	Elastic constant of the link between the 2 heads, empirical.
Length	0.03 µm	Link resting length, ~ myosin lever arm, [11].
Crosslinker		
		Crosslinkers are created during an initial stage, and are static during the contraction phase.
Stiffness	100 pN/µm	Elasticity constant of the link between the two extremities, same as molecular motor stiffness
Length	40 nm	Link resting length, ~ α-actinin length, [15].
Binders		
Binding rate	5 s^{-1}	Rate of attachement of a free binder to a filament. Empirical value
Binding range	30 nm	Distance of attachement. Empirical value
Unbinding rate	0.05 s^{-1}	Low detachment rate in the absence of force
Unbinding force	0.05 pN	Characteristic detachment force. A binder can easily be detached with a small force, which matches the experiments where rings detach from the substrate.
Stiffness	2 pN/µm	Elasticity constant of the Hookean spring

Table 1: The main parameters used during simulation.

Architecture simulations

The simulations are composed of two phases: during the first "growth" phase, the system is setup into the desired configuration to represent disordered networks, ordered and disordered bundles. Then crosslinkers and molecular motors are added to the actin organizations, and the system is simulated for 60 s. In this second phase, the behavior of the system is recorded and analyzed. The first phase is different for each network, but the second phase is identical in all cases.

To form a disordered branched network (Figure S2A, green), Arp2/3-like entities are distributed along the circular pattern, and primer filaments are randomly added. Nucleation and elongation occur during the first phase so that all the patterned area is covered with short, branched actin filaments.

To create a ring made of ordered bundles (Figure S2A, red), the Arp2/3-like entities and primer filaments are distributed over 16 discs of diameter 0.5 µm, regularly distributed on the ring pattern. They are also confined between two circles of radius R_1 =4.25 µm radius and R_2 =4.75 µm radius, to force them to cover a circular area corresponding to the experimental pattern. The confinement circles are removed for the second phase.

Disordered bundles (Figure S2A, blue) are generated by randomly distributing short actin filaments of desired length on the pattern area. Table 2 gives the parameters for each architecture. These parameters are chosen to obtain the same total amount of linear polymerized actin on the ring (but the number of filaments and thus their average length vary for each architecture), and the same density of "binders" by patterned area.

Disordered network		
	Number of filaments	1744
	Filament length (µm)	Between 0.95 and 1.25 uniformly distributed.
	Number of Arp2/3 entities	1569
	Number of binders	2000
Ordered fiber		
	Number of filaments	1173
	Mean filament length (µm)	Between 1.33 and 1.67 uniformly distributed
	Number of Arp2/3 entities	1122
	Number of binders	1360
Disordered fiber		
	Number of filaments	1416
	Mean filament length (µm)	Between 1.03 and 1 .37 uniformly distributed
	Number of Arp2/3 entities	0
	Number of binders	2000

Table 2: The parameters used to obtain each architecture .

Simulations analysis

The rate of contraction is determined according to the maximal velocity of ring perimeter decrease over time. Network connectivity is defined as the mean number of

static links per actin filament: e.g. if one filament has one crosslinker bound and one Arp2/3 complex entity bound, its connectivity will be 2. The connectivity indicates how one filament is locally connected to its neighbors. Filaments are connected together by crosslinkers or the Arp2/3 complex in clusters (groups of filaments all connected together). The size of the largest cluster (or the fraction of filaments that are in the largest cluster) thus gives a measure of the overall connectivity of the actin organization (when the fraction is close to 1, all filaments are connected together, and when the fraction is close to zero, the network is disconnected).

Movies legends:

Movie S1: ADF/Cofilin debranches actin filament networks created by the Arp2/3 complex. Left panel: Actin+Arp2/3 complex, middle panel: Actin+Arp2/3 complex+ ADF/cofilin, left panel: Actin+Arp2/3 complex+ ADF/cofilin+ α-actinin. Total elapsed time is 595 seconds and compressed to a 4-seconds QuickTime movie.

Movie S2: Surface-attached myosin VI slides antiparallel (red and green arrows) actin filaments. Total elapsed time is 60 seconds and compressed to a 4-seconds QuickTime movie.

Movie S3: Contraction of different ring architectures: branched network on the left, disordered bundles on the middle and ordered bundles on the right, in absence (top row) or in presence (bottom row) of α-actinin. Total elapsed time is 45 minutes and compressed to a 6-second QuickTime movie.

Movie S4: Simulation of the branched network, disordered and ordered bundles in absence (left panel) or presence (right panel) of α-actinin. (Top row) is the simulation including all filaments. (Bottom row) is the same simulation but we show only a portion of them to be able to track individual filament. Total elapsed time is 59 seconds and compressed to a 7-second QuickTime movie.

Supporting References

S1. Isambert, H., Venier, P., Maggs, A.C., Fattoum, A., Kassab, R., Pantaloni, D., and Carlier, M.-F. (1995). Flexibility of actin filaments derived from thermal fluctuations. J. Biol. Chem. *270*, 11437-11444.

S2. Higgs, H.N., Blanchoin, L., and Pollard, T.D. (1999). Influence of the C terminus of Wiskott-Aldrich syndrome protein (WASp) and the Arp2/3 complex on actin polymerization. Biochemistry *38*, 15212-15222.

S3. Reymann, A. C., Martiel, J. L., Cambier, T., Blanchoin, L., Boujemaa-Paterski, R., and Théry, M. (2010). Nucleation geometry governs ordered actin networks structures. Nat. Mat. *9*, 827-832.

S4. Suarez, C., Roland, J., Boujemaa-Paterski, R., Kang, H., McCullough, B.R., Reymann, A.C., Guérin, C., Martiel, J.L., De la Cruz, E.M., and Blanchoin, L. (2011). Cofilin tunes the nucleotide state of actin filaments and severs at bare and decorated segment boundaries. Curr Biol. *21*, 862-868.

S5. Vignaud, T., Ennomani, H., and Thery, M. (2014). Polyacrylamide hydrogel micropatterning. Methods Cell Biol. *120*, 93-116.

S6. Reymann, A.-C., Boujemaa-Paterski, R., Martiel, J.-L., Guérin, C., Cao, W., Chin, H.F., De La Cruz, E.M., Théry, M., and Blanchoin, L. (2012). Actin Network Architecture Can Determine Myosin Motor Activity. Science *336*, 1310-1314.

S7. Martiel, J.L., Leal, A., Kurzawa, L., Balland, M., Wang, I., Vignaud, T., Tseng, Q., and Théry, M. (2015). Measurement of cell traction forces with ImageJ. Methods Cell Biol. *125*, 269-287.

S8. Nedelec F., and Foethke D. (2007). Collective Langevin dynamics of flexible cytoskeletal fibers. New J Phys. *9*, 427.

S9. Letort, G., Politi, A.Z., Ennomani, H., Thery, M., Nedelec, F., and Blanchoin, L. (2015). Geometrical and mechanical properties control actin filament organization. PLoS Comput Biol. *11*, e1004245.

S10. McCullough, B.R., Blanchoin, L., Martiel, J.L., and De la Cruz, E.M. (2008). Cofilin increases the bending flexibility of actin filaments: implications for severing and cell mechanics. J. Mol. Biol. *381*, 550-558.

S11. Robblee, J.P., Olivares, A.O., and de la Cruz, E.M. (2004). Mechanism of nucleotide binding to actomyosin VI: evidence for allosteric head-head communication. J. Biol. Chem. *279*, 38608-38617.

S12. Oguchi, Y., Mikhailenko, S.V., Ohki, T., Olivares, A.O., De La Cruz, E.M., and Ishiwata, S. (2008). Load-dependent ADP binding to myosins V and VI: implications for subunit coordination and function. Proc. Natl. Acad. Sci. USA *105*, 7714-7719.

S13. Rock, R.S., Rice, S.E., Wells, A.L., Purcell, T.J., Spudich, J.A., and Sweeney, H.L. (2001). Myosin VI is a processive motor with a large step size. Proc. Natl. Acad. Sci. USA *98*, 13655-13659.

S14. Altman, D., Sweeney, H.L., and Spudich, J.A. (2004). The mechanism of myosin VI translocation and its load-induced anchoring. Cell *116*, 737-749.

S15. Wachsstock, D.H., Schwarz, W.H., and Pollard, T.D. (1993). Affinity of alpha-actinin for actin filaments determines the structure and mechanical properties of actin filament gels. Biophys. J. *65*, 205-214.

3rd project

III. Actin-crosslinkers regulate the spatial integration of mechanical constraints in contractile actin networks

III.1 Research Schema

Uri Alon is a Professor and Systems Biologist at the Weizmann Institute of Science who studies how cells work and what are the biological circuits that contribute to life function. Uri Alon publishes papers, gives talks and sings songs related to laboratory life in general. He is quite successful. One of his theoretical papers (Alon, 2009) caught my attention: he suggested scientists to stop seeing research as a straight line from question to answer, but to consider it as something more creative and *getting out of the "Cloud"* in other words "thinking out of the box".

A common schema for a scientific question is expressed in the starting point A (the question) and follows the direct and shortest way to the final point B (the answer).

However, this is not how it works. Most frequently, things change as you move from point A to point B. The actual path can take sideways and loop back. This led to the definition of a new target, point C. After few more detours, C is reached, or not, and this is how science goes (Fig. 36).

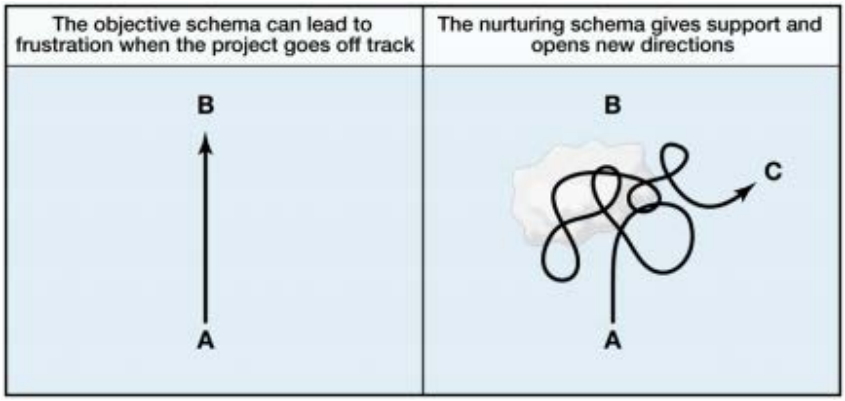

Figure 36 Schema about objectives in research. The nurturing schema in the left includes the period of time in which we have to think out of the box. (Alon et al. 2009)

Our progress in this project followed Alon's theory. We started with the idea that α-actinin increases actomyosin network disassembly, then we moved to point C which was the slowing done of actin contraction by α-actinin and finally we landed in a new point D

which corresponded to the contribution of α-Actinin to the symmetry and integrity of actomyosin networks.
I will present below the context of this project, and the way I used in vitro approaches to understand cellular observations.

III.2. Context of the study

As presented in our review (Letort, Ennomani et al., 2015), actin filaments form different types of cellular structures, and in particular they form contractile bundles called stress fibers. The stress fibers are involved in multitude of cellular processes: adhesion, migration, wound healing… (Bershadsky et al., 2006; Pellegrin & Mellor, 2007; Sandbo et al., 2011; Sanger et al., 2009; Tojkander, Gateva, & Lappalainen, 2012; Yi et al., 2012). And as we saw previously in the manuscript (II.2.2 section), there are different types of stress fibers that can be classified into three categories: dorsal stress fibers, transverse arcs and ventral stress fibers (Khatau et al. 2009; Tojkander et al., 2012). It is important for this study to remind that those structures are very dynamics and highly interdependent (Hotulainen and Lappalainen, 2006; Burnette et al. 2011; Fan et al. 2010; Shemesh et al. 2009; Tojkander et al., 2012).

There are more than twenty distinct proteins that interact with the stress fibers, but the majority of their specific functions have remained obscure (Tojkander et al., 2012). Among these proteins, a major one is α-actinin. α-actinin is a ubiquitous cytoskeletal protein, which is part of the actin filaments crosslinking proteins superfamily. There are 4 isoforms of human α-actinin that have already been identified: muscles α-actinin-2 and α-actinin-3, and non-muscles α-actinin-1 and α-actinin-4 (Blanchard et al. 1989). This protein can be in particular found in cell-to-cell, cell to extra-cellular matrix contact areas and cellular protrusions. By creating links between the cytoskeleton and different proteins involved in cellular junctions, α-actinin might be a crucial actor in multiple cellular processes. Some of the α-actinin roles were uncovered; in particular this protein is supposed to be one of the major links between actin filaments and focal adhesions and to contribute in the de adhesion phenomenon. Indeed it interacts with proteins that regulate the detachment process of migratory cell (Otey & Carpen, 2004). A variety of studies stated the evidence of the significance of α-actinin in the contractile response of the cell.

However, nowadays, listing the whole functions of α-actinin as well as the precise roles of their crosslinking to actin filaments *in vivo*, has been elusive. Here we focused on the role of α-actinin as a component to tune the cellular actin filament structures cohesion, which is required for cell shape integrity maintenance and motility assurance.

This study below was performed by Fabrice Senger and Amandine Pitaval for the in vivo experiments. However, their observations raised some questions on the action of α-actinin on the networks that cannot be easily answered in their system due to the cellular level of complexity. By using the *in vitro* system, we were able to get more insights into the molecular mechanisms controlling cytoskeleton symmetry. The combination of *in vivo* and *in vitro* experiments allowed us to explore the role of α-actinin inside the cell.

III.3. In vivo observations

To elucidate the role of α-actinin in the maintenance of stress fiber network, Fabrice Senger and Amandine Pitaval, depleted this protein from Human Retinal Pigment Epithelial (RPE1) cells.

To do so, they designed short interfering RNA (siRNA) that downregulated the expression of α-actinin 1 and 4. As these two isoforms were interdependent. (Downregulations of one isoform increased the expression of the other), it was necessary to perform a co-transfection of siRNAs against both α-actinin 1 and 4. The Western blot analysis validated that expression levels of both proteins were efficiently decreased.

In order to better visualize the effect of α-actinin1 and 4 knockdowns, they combined the immunofluorescence staining with the cellular micro-patterning technique, which is a good tool to improve inter-cellular reproducibility of actin networks.

Two main effects were observed in the depleted cells: one on the contractile actin network architecture, and the other one on nucleus position.

On the crossbow used as pattern shape (Figure 37, left schema), cells form two big peripheral actin bundles in the back (the most intense bundles in the cell), radial actin bundles in the front, followed by transverse arcs and stress fibers along the longest axis of the cell. Although the same structures are present in α-actinin depleted cells, but their positioning /orientations were highly different (Figure 37).

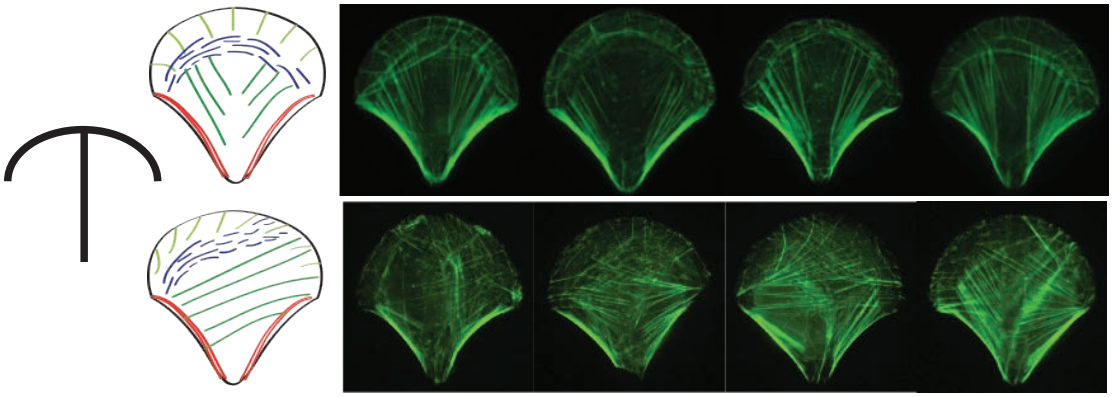

Figure 37. Actin immunofluorescent staining on RPE1 crossbow shape patterned-cells. (Top row) corresponds to the actin immunofluorescence staining for the CTRL-cells. (Bottom row) corresponds to the actin immunofluorescence staining for the siRNA1 and 4 cells. These results reveal disrupted stress fiber network in the α-actinin 1 and 4 depleted cells.

At first glance, control cell architecture on a crossbow-shaped micropatterns seems to respect a vertical symmetry axis (along the crossbow main axis). This was further quantified by splitting the two halves determined by this crossbow axis, flipping one of the two halves and finally comparing the orientation of actin fibers (Figure 38).

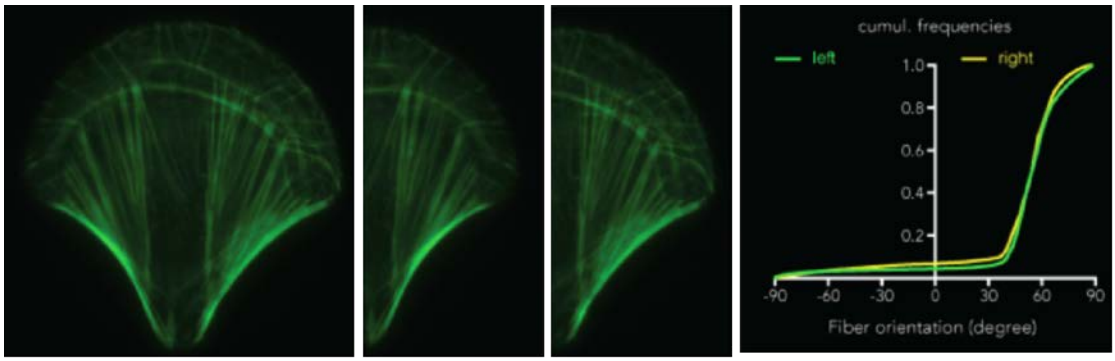

Figure 38 Fiber orientations for the control cells. Actin immunofluorescent siCTRL-cells splitting image into two halves according the long axis of the cell, and comparing the orientation of the actin stress fibers in both sides of the cell. Fibers from both sides of the cell follow the same orientation.

The plot shows the angular distributions of the fibers for the two halves. They are almost identical. This example suggests that a yet unknown mechanism ensures that the symmetry of the extra-cellular adhesion pattern is transmitted to the intra-cellular actin network.

Strikingly this symmetry of fiber orientation was lost in siACTN1ACTN4 treated cells. Indeed the maximal deviation between the two angular distributions was much higher (Figure 39).

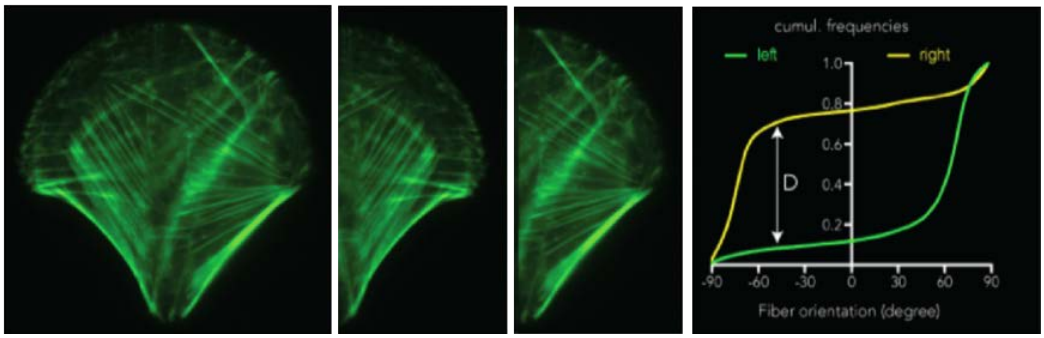

Figure 39 Fiber orientations for the siACTN1ACTN4 cells. Actin immunofluorescent of the downregulated cells with the same technic as above (splitting image into two halves according the long axis of the cell, and comparing the orientation of the actin stress fibers in both sides of the cell). This result reveals the difference in fiber orientation in both sides of the cell due to the lack of crosslinkers.

This suggested that the α-actinin affects the establishment of intra-cellular actin network symmetry, and supports cell ability to transfer spatial information from its environment to its internal organisation.

To gain further insight in the mechanism supporting these differences, we designed in vitro experiments in which we varied the concentration of α-actinin. Actin networks contraction appeared to be highly sensitive to these variations.

III.4. In vitro observation

To test how the α-actinin concentration affects the acto-myosin networks, we used a pattern made of dots forming a ring. Indeed, actin filaments growing out of adjacent dots aligned and formed anti-parallel structures, mimicking the observed organisation of the stress fibers in the cell (Figure 40). The ring shape allowed us to have an easy read-out of the contractile behaviour of the structure, and thus to quantify the impact of α-actinin on it.

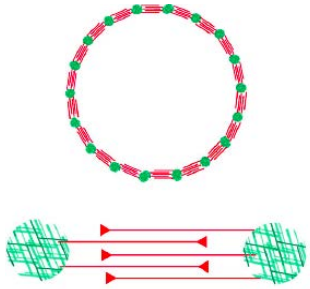

Figure 40 Schematic representation of in vitro system used to mimic the cellular stress fibers. The shape of the pattern is a ring of dots. Branched networks (green) will be formed on the dots and actin filament growing out of adjacent dots aligned and form antiparallel bundles (red)

With this system, we were thus able to identify different effects that α-actinin can have on stress-fiber like organised networks. By characterising them, we tried to determine if they could account for the in vivo observation.
The first obvious observation that can be made thanks to this system is that the dynamic of contraction of the ring is affected by the concentration of α-actinin.

III.4.1 α-Actinin slows down myosin-induced contraction.

I measured the time required for the completion of ring contraction in the presence of various concentrations of α-actinin (0, 10 and 30 nM) (Figure 41).

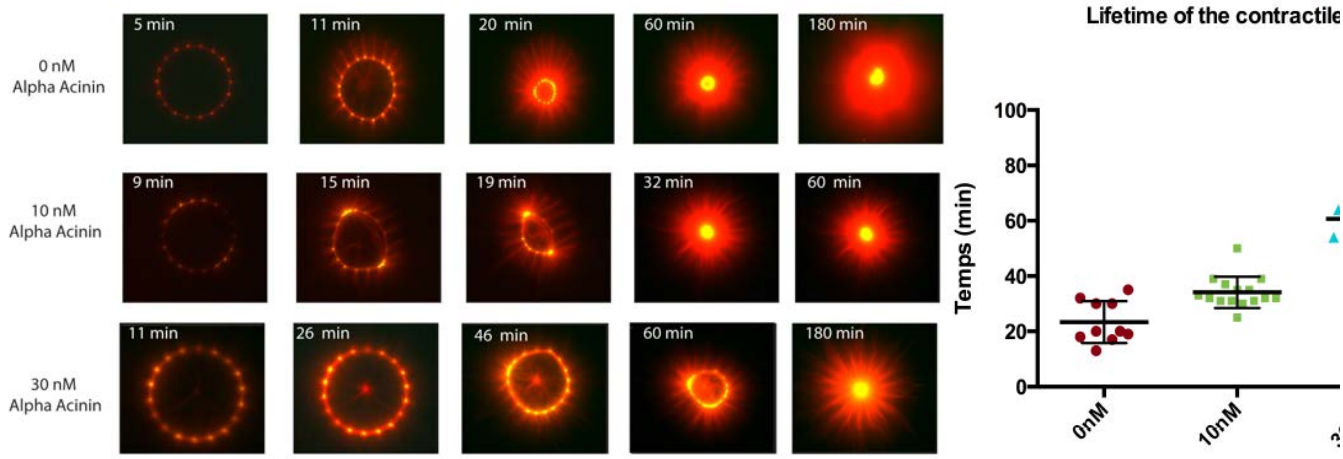

Figure 41 Crosslinked acto-myosin network are slower than non-crosslinked one. Left panel shows time lapse of the actomyosin micropatterns structures with different concentration of α-actinin (0, 10 and 30 nM respectively). Actin is presented in red and myosin is in green. Right panel reveals the analysis of the contractile ring lifetime for the 3 different concentrations. We can obviously see that the actomyosin network in absence of α-actinin, have an average of 20 minutes to fully contract the structure and in presence of 30 nM α-actinin, it takes an average of 60 minutes for the whole ring deformation.

Network contraction appeared to be slowed down as we increase the α-actinin concentration. This could be explain by the fact that crosslinked actin filaments are much more stiffs than single actin filament (Gardel et al. 2004). Consequently, crosslinked actin bundles are harder, thus slower, to contract than single actin filament. However, control and downregulated cells had similar temporal dynamics. Thus this slowing effect of α-actinin did not seem to be important in the in vivo situation.

The changes on the network rather than the timing seemed then to be more indicated to be relevant in our study. The disassembly effect of α-actinin on acto-myosin network is then being an important point to focus on.

III.4.2 α-Actinin favours actin filaments disassembly

Previously we saw that the addition of α-actinin on homogeneous rings of branched actin filaments modified myosin-induced network deformation (Figure 42). In the absence of actinin, actin rings contracted regularly up to the formation of a dense star-shaped network. In the presence of actinin, we observed a massive network disassembly during the first stages of ring contraction.

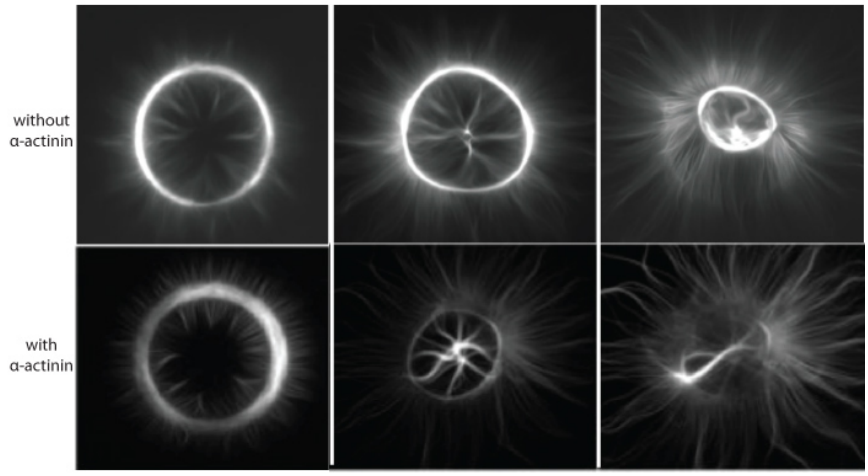

Figure 42 α-actinin favours the disassembly of the acto-myosin structures. Previous experiments for the 2nd project of the manuscript, on different pattern: full ring pattern instead of dotted ring. First row corresponds to the time lapse of the actin structure contraction in absence of α-actinin. Bottom row represents the time lapse of the actin structure contraction in presence of α-actinin. This reveals that the presence of α -actinin enables the disassembly of the acto-myosin structures.

This effect of α-actinin on acto-myosin network could be a factor to explain the *in vivo* observed differences.

To quantify network disassembly, I measured the variations of actin network fluorescence in absence or presence (50 nM) of α-actinin as the ring reached half of its initial perimeter (Figure 43). Network disassembly before full contraction was observed only in the presence of α-actinin. Our interpretation was that cross-linked filaments were less able to deform, slide or change shape and were broken into pieces by myosin mechanical work. This observation does not fit as well our in vivo observation, since we

noticed that the spatial organisation and not the presence, of contractile stress fibers was affected between the two (control and downregulated) conditions.

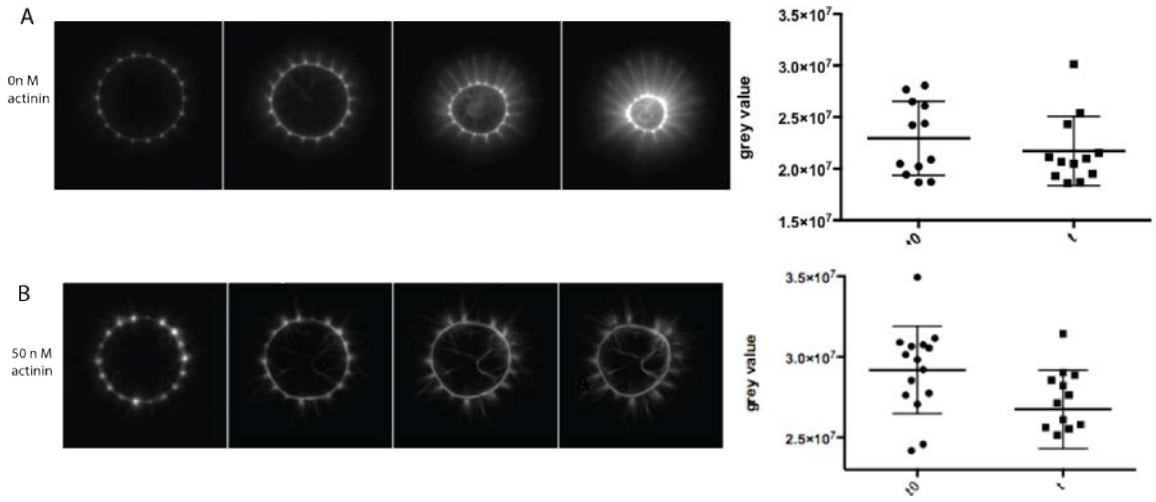

Figure 43 Effect of α-actinin on the disassembly of the contractile acto-myosin structure with the designed *in vitro* system. (A) Time lapse of acto-myosin structure contraction in absence of α-actinin and the corresponding analysis about grey value of actin fluorescence in the beginning (t0) and the end (t) of the movie. This shows that there is no big difference between the integrated fluorescent intensity between the two time points (B) Time lapse of acto-myosin structure contraction in presence of 50 nM α-actinin and the corresponding analysis about grey value of the actin fluorescence in the beginning (t0) and the end (t) of the movie. That reveals a decrease in the integrated fluorescence before and after contraction, which means a loss of actin fluorescence so disassembly of the actin filaments due to the crosslinker.

Interestingly, while analysing data, we found striking differences in network shapes during contraction with or without crosslinker. As the *in vivo* changes seemed to be mainly morphological, we decided to deepen our analysis in this direction.

III.4.3. α-Actinin ensures the symmetry of contractile actin network

Deforming ring rarely maintained their shape during the entire contraction process. The initial distribution of myosins seems to modulate those changes. But this was not observed in presence of α-actinin. Crosslinked rings maintain their initial shape and position during the whole contraction (Figure 44). We monitored ring contraction and measured ring perimeter and position over time.

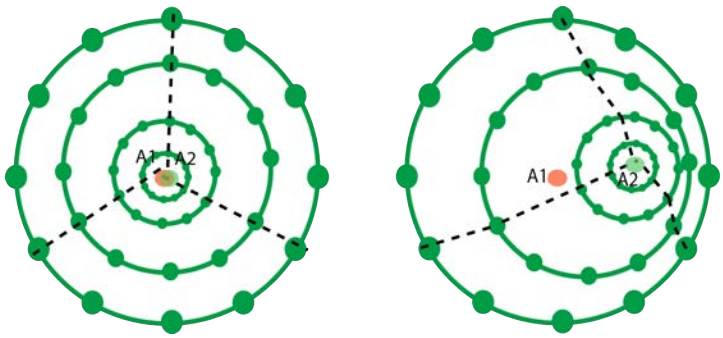

Figure 44 Integrity while ring deformation hypothesis. On the left, a projection of the deformed ring during contraction when the structure keeps the same initial shape. On the right, we have a projection of the deformed ring during contraction when the structure does not keep the same initial shape and loose its centre of mass. A1 and A2 represent the mass centre before and after contraction respectively

The figure below shows on the left projections of time-lapse images in the absence (top) or presence (bottom) of α-actinin as well as the centre of mass centre of the ring at the end of the contraction (Figure 45).

Crosslinked rings end up their contraction closer to their initial centre of mass than non-crosslinked networks.

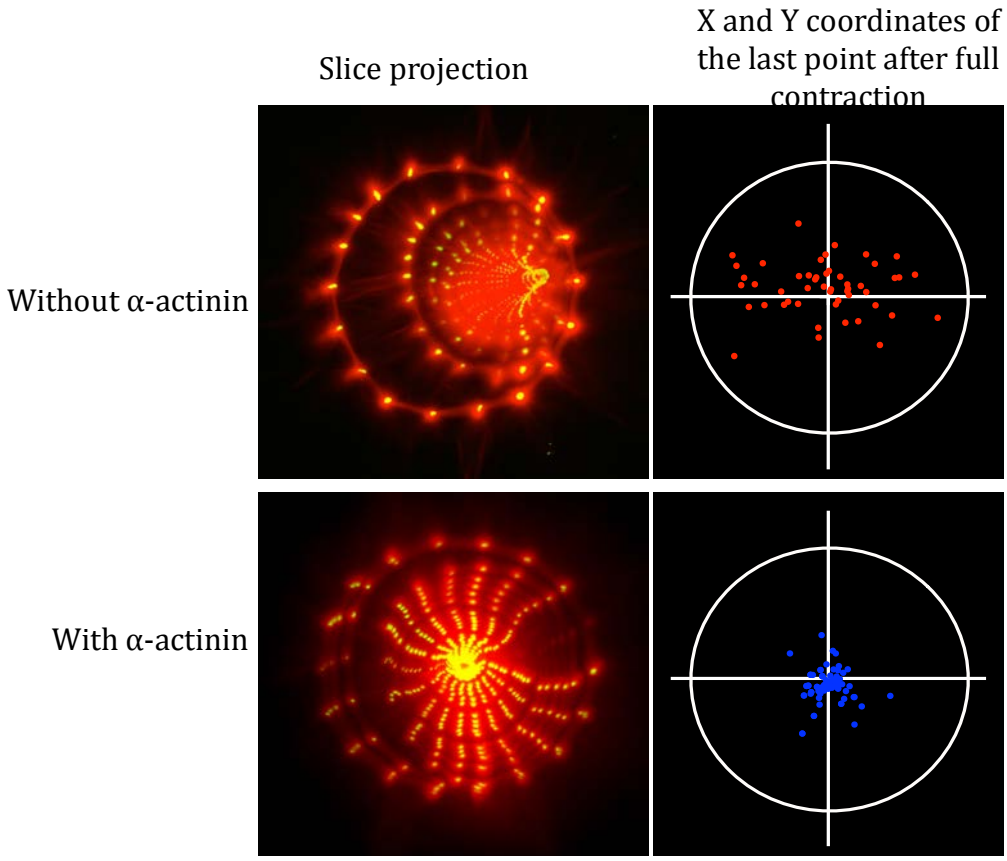

Figure 45 α-Actinin ensures the symmetry of contractile actin network. Top row; represents the slice projection of a pattern without α-actinin presence and its analysis about x and y coordinates of the centre of mass in the end of the contraction. Bottom row; correspond to an example of pattern slice projection in presence of α-actinin and its mass centre coordinates after full contraction. Theses results reveal the symmetry and integrity of the acto-myosin structure in presence of crosslinker.

We also investigated the deformation homogeneity of actin structures by analysing the circularity of the rings shape as they contracted (Figure 46). The circularity measures how close is a shape to a disc having the same area: Circularity $= 4\pi \times (Area/(\text{Perimeter}^2))$. Circularity is 1 if the shape is a perfect circle and close to 0 if the shape is highly elongated.

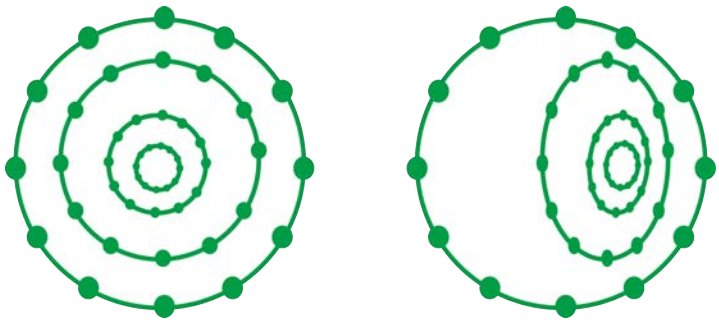

Figure 46 Hypothesis about α-actinin effect on the pattern circularity. On the left, the pattern keeps it initial shape after deformation and on the right the pattern is not a perfect circle anymore.

According to this measure, rings that were crosslinked with α-actinin maintain a more circular shape as they contracted (Figure 47).

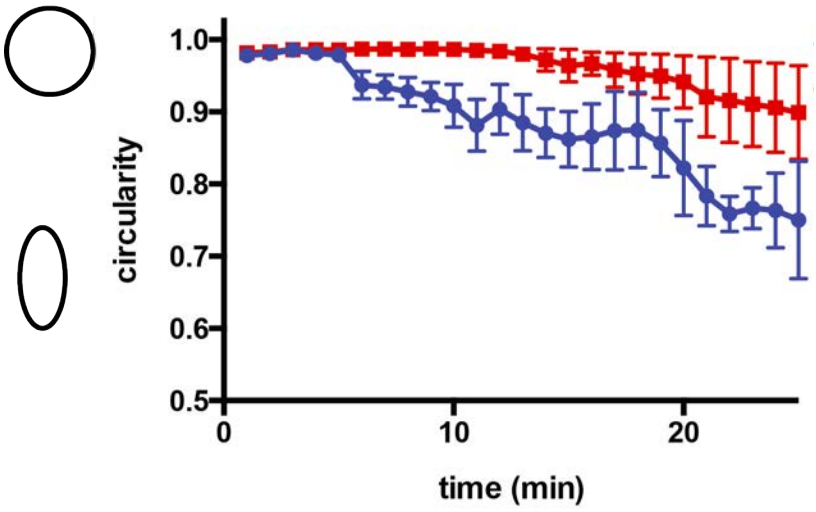

Figure 47 Pattern circularity during time in presence or in absence of α-actinin. Red curve: 20 nM α-actinin and blue curve 0 nM α-actinin. These results reveal that in absence of crosslinker the ring does not keep its circular shape during the contraction and the deformation. A representation of the level of circularity is present on the left of the plot.

From this we concluded that α-actinin was involved in the regulation of network homogeneity and symmetry during contraction. We think that α-actinin supports filaments connections to external attachment sites and to other filaments of the network. Mechanical constraints are better balanced in a well cross-linked structure and therefore contraction can respect the geometry (i.e. symmetry axis and centre of mass) of external and initial boundary conditions.

III.5. In vivo nucleus positioning

To further investigate the consequences of cell architecture asymmetry, Amandine looked at the position of nuclei in control or α-actinin 1 and 4 depleted cells. She stained nuclei and measured their xy coordinates (Figure 48).

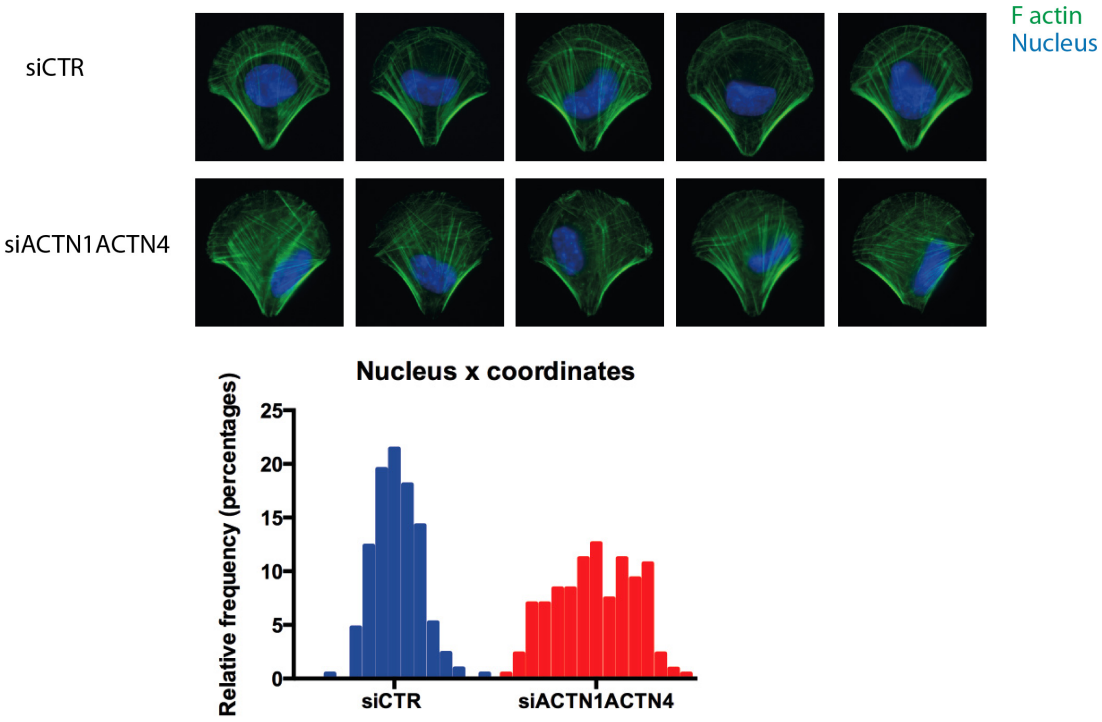

Figure 48 Effect of α-actinin on the nucleus positioning. F actin (green) and nucleus (blue) staining for different control and α-actinin 1 and 4 depleted cells. The bottom of the figure corresponds to the coordinate of the nucleus according the x-axis and their relative frequency. This figure indicates that the presence of crosslinkers is essential to keep the position of nucleus stable.

Nuclei were close to cell centre in control cells and more distant from it in α-actinin depleted cells. The relative frequency of the nucleus coordinate unambiguously

showed the increased dispersion of nuclei position in the siACTN1ACTN4 cells (Figure 48).

We can conclude from those considerations that the α-actinin is essential for the cell symmetry. Indeed, in the absence of crosslinker, the network looses its symmetry with respect to extra-cellular adhesion cues. This asymmetric network may be responsible for nucleus displacement away from the cell centre.

III.6. Conclusion

In this study, we could find a way to impose controlled adhesion patterns with a single symmetry axis to cells.

Transverse arcs result from the stacking, crosslinking and contraction of actin filaments assembled along cell adhesive edges. On crossbow shaped micropatterns, these arcs ensure the physical connection of all portions forming the cell front. Thereby the left and right side of the cell front were physically linked and mechanically connected. The acto-myosin based inward displacement of those arcs enforces nucleus positioning at the cell centre.

Upon α-actinin knockdown the actin bundles assembled at the cell front were less inter-connected. Any subtle left-right asymmetry could bias their inward motion since local contraction were not transmitted to the opposite cell side. This biased motion results in the formation of misoriented actin bundles with respect to the symmetry of cell adhesion pattern. As a consequence, nuclei were moved away from the symmetry axis and from the cell centre. So cell internal architecture, no longer fits with the external cues imposed by the microenvironment (Figure 49).

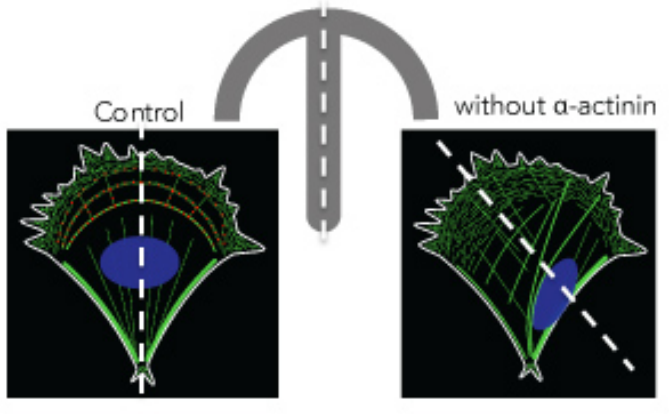

Figure 49 α-actinin regulates the spatial integration of mechanical constraints in contractile actin networks. Actin fibers (green) assembled in the front of the depleted cell were not crosslinked. This loss of connections could contribute to a biased motion and a misoriented actin bundles formation. As a consequence, the nucleus (blue) is moved away from the symmetry axis of the pattern (white dashed line) and from the cell centre.

Conclusion and Perspectives

I. Conclusion

During my PhD, I was interested in studying the properties of reconstituted actomyosin contractile systems. The goal was to understand how/if the actin architecture can mediate the contractile response. For this purpose, I was interested first in building a variety of actin organization that will serve next as substrate for myosin during contraction. To understand the general principles that dictate geometrically-controlled actin assembly, we developed a model using Cytosim that allowed us to identify key parameters including filaments/filaments interaction, filament mechanical property and contact activation between actin filaments growing from the adjacent pattern and the nucleation area (Letort et al. 2015). These actin templates were used then to evaluate the response of oriented actin structures to myosin-induced contractility. Contractility – the internal generation of force or tension by the actomyosin machinery – has emerged as a critical regulator of a wide range of processes during development. Tremendous efforts have deepened our understanding of the biochemical and mechanical properties of the actomyosin contractile units encountered in the complex cell environment. Yet, how the structural organization of actin filaments regulates myosin-driven contraction remained to be established when I started my PhD. I demonstrated that crosslinking level modulates the myosin-induced deformation of actin networks according to their architecture. I showed also that crosslinkers are necessary to sustain myosin-driven deformation and force production of dynamic actin networks in the presence of disassembly factors (ADF/cofilin). In addition, we developed numerical simulation in order to relate the observed myosin-driven actin deformation with the underlying microscopic mechanism. The fact that we were able to tune myosin-driven deformation of minimal reconstituted actin networks, for which we control the actin organization and dynamics, demonstrates that our study captures fundamental rules coordinating myosin-mediated contractility and force production.

We concluded from our experimental and theoretical analysis that the contraction of actin structures due to molecular motors is not following the same response according to their architecture. Indeed, the degree of connectivity between the actin filaments, which form a define architecture, determines the shape of the contractile response. The amplitude of the

contraction is in addition controlled by the organization of actin filaments and the nature of the entities connecting the filaments within the structure. All these results are illustrated in the figure below

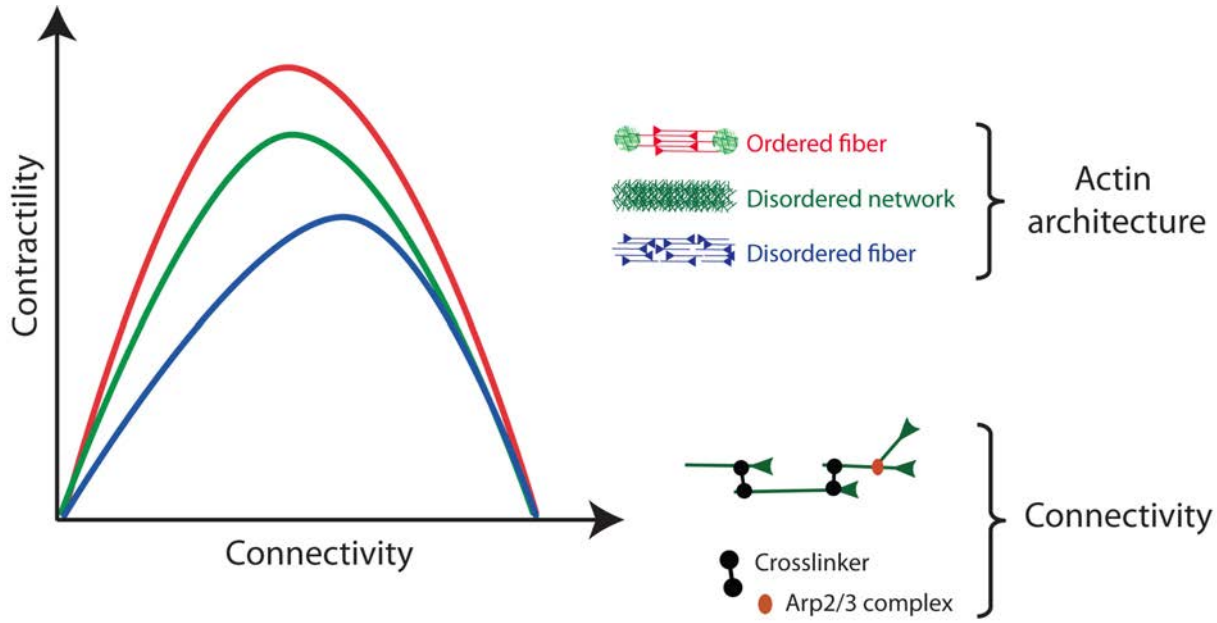

Figure 50 Architecture and connectivity rules in actin network contractility. Mechanical response of three different actin architectures in function of connectivity: ordered fiber, disordered network, and disordered fiber. The degree of connectivity between the actin filaments, which form a define architecture, determines the shape of the contractile response. (Ennomani &Letort; 2015 in revision)

II. Perspectives

In this work below, I was able to dissect the mechanism involved in the contractile response of different actin architectures and propose an explanation on the variability of this response. Using the same experimental design, it is now possible to address a variety of important questions related to the property of actomyosin organizations. One interesting aspect that we could study with our experimental system is the length dependence of contractile elements. I did some preliminary experiments in this direction that I will present in the following paragraph.

II.1. Reconstituted contractile actin fibers and force measurement

This project started with the idea of mimicking a stress fiber, and studied how the biochemical composition and physical parameters of these fibers could affect the contractile response. For this purpose, I designed a chrome mask with dots that are separate from each other by a distance varying from 10 to 200 μm. Actin filaments nucleated from the dots are growing away from the nucleating area and generate bundles of actin filaments oriented in parallel or antiparallel way. According to the distance between the dots the middle antiparallel fibers will have different lengths (Figure 51).

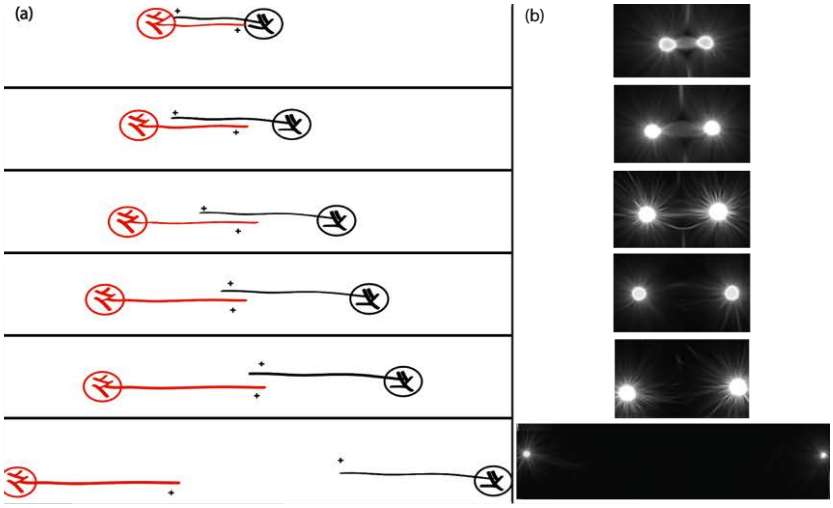

Figure 51 *In vitro* reconstituted minimal system. (a) Schematic drawing of the designed patterns to study the length effect of the stress fiber as well as the biochemical concentration on the contractile response. (b) Actin filaments assembly on the designed patterns showing the behaviour of the minimal structure.

We first tried different concentrations of Myosin VI (8/16/24 nM) to test how the concentration of myosin affects the contractile response. I focused on the contractile behaviour of the antiparallel bundle created in the middle of the dotted patterns (Figure 52 A). While keeping the same actin concentration and increasing the myosin concentration, we could observe that the fiber made of antiparallel filament is getting thinner. Indeed, the experiments at 24 nM myosin had the thinnest fibers because the high density of myosin generates high contractile force on the actin bundles (Figure 52).

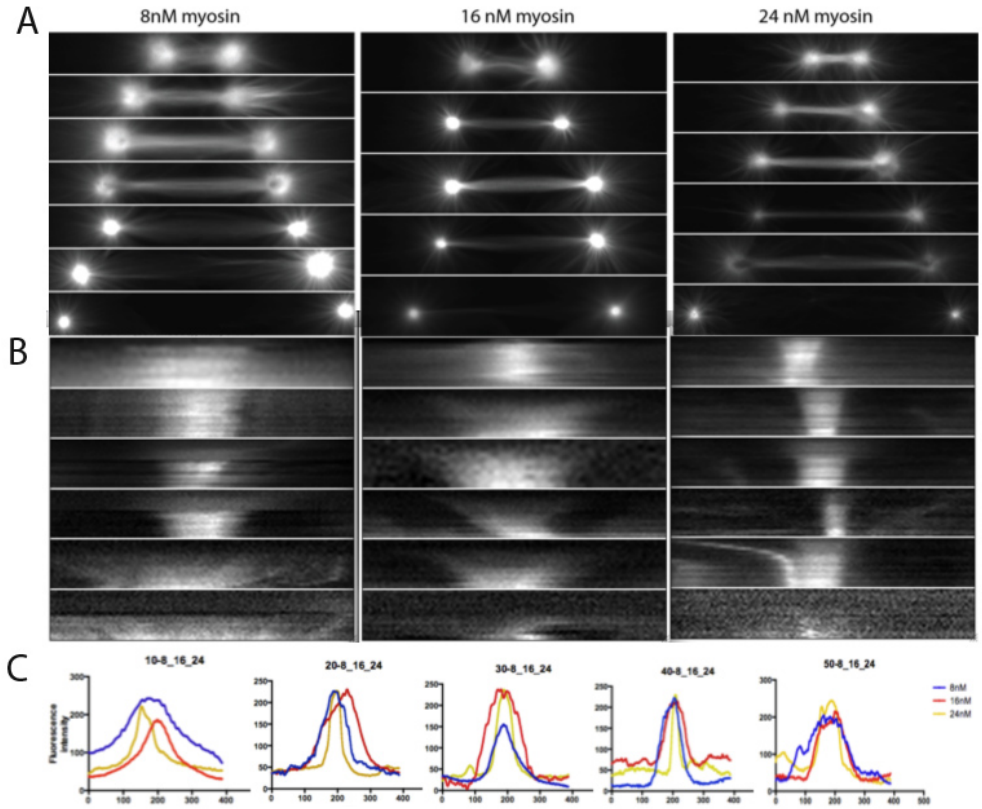

Figure 52 Effect of the biochemistry and antiparallel filament overlapping length on the fiber behaviour. (A) Different myosin concentration (8, 16 and 24 nM) on the same patterns showing difference in the fiber thickness; fibers with 8nM myosin concentration are larger than 16 nM, which are also larger than 24 nM. (B) Linescans of the fiber cross-section showing the compaction of the antiparallel actin filaments during time after myosin activity. (C) Plots of the fluorescence intensity along the fiber cross-section confirming the thickness difference noticed with the overlapping distance and myosin density.

We could also notice that the length of the antiparallel bundles (overlap distance between antiparallel actin filaments) plays a key role during contraction. When we compare the thickness of the fiber for identical biochemical conditions, we could observe the bundle thickness decreases with the decrease of the overlap section (same myosin concentration are concentrating and contracting less anti parallel area) (Figure 53 B)

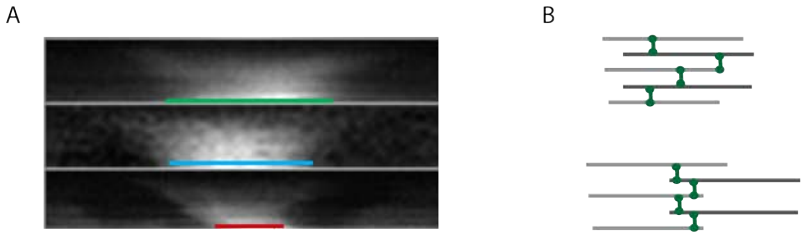

Figure 53 Effect of myosin on the antiparallel bundle length. A: From top to bottom, Kymographs of patterns with 30, 40 and 50 μm distance between dots. We can clearly see that while decreasing the overlapping distance the bundle get thinner. 30 μm bundle (green line) is thicker than the 40 μm bundle (blue line), which is also thicker than 50 μm bundle (red line). B: the hypothesis that could explain this finding. Grey lines represent actin filament with different polarity and the green is the myosin. For the first case, when the overlap is high, myosin could be generates force from everywhere on the bundle, but when the overlap is not large, myosin will be concentrated on the antiparallel filaments, and the force generated will be higher.

To access to the estimation of the force generated by the molecular motor in this reconstituted system, we planned to use the laser ablation method coupled to soft patterning, which is a passive method of force measuring used before by Tanner et al., 2010 to estimate forces generated by intracellular components. This technique is based on a well-focused pulse laser that cuts intracellular structures (Figure 54).

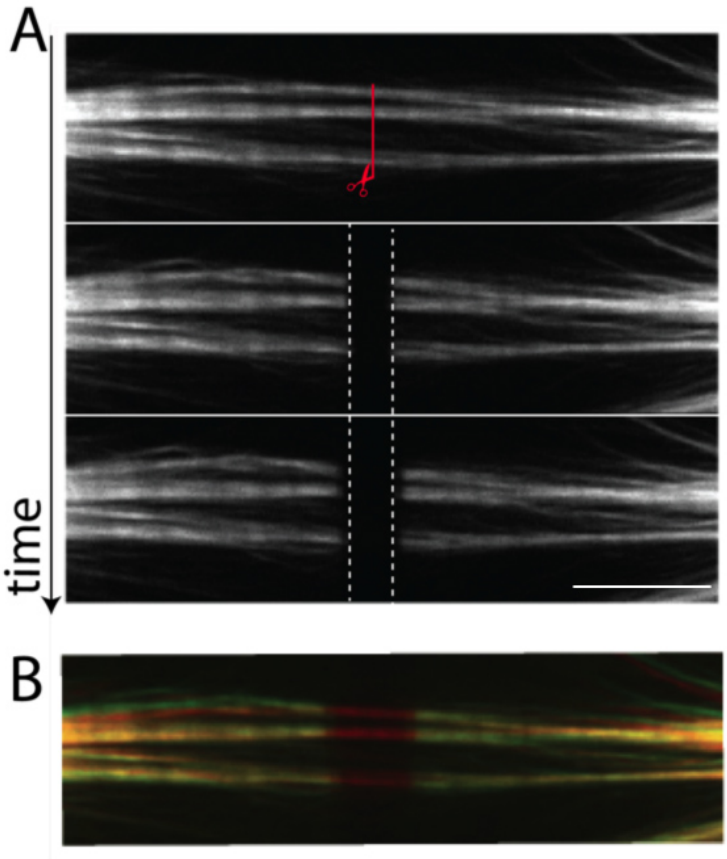

Figure 54 Force measurement indications with laser ablation technic. (A) Fiber under tension before and after ablation. Scissors showing the place of the cut. Dashed line corresponds to the gap created after relaxation. Time interval was 5 seconds. Scale bar = 20 μm. (B) Overlay images with colour code: red represents the fiber before ablation and green represents the same fiber 10 seconds after ablation.

What we can notice from these preliminary experiments, is that right after laser ablation, the bundle relaxes and a gap is created near the ablation site 10 seconds after the performed cut, the bundle continues relaxation. Now, we are in very good position to correlate the length of a define actomyosin structure its biochemical composition and the force generated during contraction. We can also visualize the dynamic of the different protein interacting with the actin bundles during contraction and relaxation after laser ablation. With this experiment set up we can really understand some basic rules behind stress fibers contractile properties.

II.2. Physiological biochemistry for reconstituted actin bundles

We can propose in the future to use more physiological biochemistry in our reconstituted systems. Indeed, the myosin that we were using in our *in vitro* experiments is the myosin VI-HMM (Ennomani & Letrot et al. 2015). This myosin is pointed-end directed processive molecular motor. Unlike myosin II, it could trigger continuous contraction and/or filament sliding without the need to assemble into minifilaments. Thus using Myosin VI-HMM had the advantage that it yields in unprecedented reproducibility in the contractile response. Since myosin VI is involved in the cellular cargo transport (Sweeney et al., 2007) and myosin II is involved in the contractility, we could challenge ourselves and use a more physiological myosin in our in vitro reconstituted systems, in order to best mimic the cellular contractile system at all levels (architectural and biochemical levels). We could also combine these myosins with different ways to initiate actin assembly using different actin nucleators. We can test in parallel both actin filaments initiated by the Arp2/3 complex or by formins. The polarity of the actin organization and its architecture will vary according to the nucleator. By doing this we hope to have a large understanding of key parameters controlling actomyosin systems.

Bibliography

Achard, V., Martiel, J. L., Michelot, A., Guérin, C., Reymann, A. C., Blanchoin, L., & Boujemaa-Paterski, R. (2010). A "primer"-based mechanism underlies branched actin filament network formation and motility. *Current Biology 20*, 423–8.

Albert, B., Johnson, A., Lewis, J., Raff, M., Roberts, K., & Walter, P. (2002). *Molecular Biology of the Cell. Garland Science New York*.

Alon, U. (2009). How To Choose a Good Scientific Problem. *Molecular Cell*, *35*, 726–728.

Altman, D., Sweeney, H. L., & Spudich, J. a. (2004). The mechanism of myosin VI translocation and its load-induced anchoring. *Cell*, *116*, 737–749.

Alvarado, J., Sheinman, M., Sharma, A., MacKintosh, F. C., & Koenderink, G. H. (2013). Molecular motors robustly drive active gels to a critically connected state. *Nature Physics*, *9*, 591–597.

Andrianantoandro, E., & Pollard, T. D. (2006). Mechanism of Actin Filament Turnover by Severing and Nucleation at Different Concentrations of ADF/Cofilin. *Molecular Cell*, *24*(1), 13–23.

Aratyn-Schaus, Y., Oakes, P. W., & Gardel, M. L. (2011). Dynamic and structural signatures of lamellar actomyosin force generation. *Molecular Biology of the Cell*, *22*, 1330–1339.

Avraham, K. B., Hasson, T., Steel, K. P., Kingsley, D. M., Russell, L. B., Mooseker, M. S., … Jenkins, N. A. (1995). The mouse Snell's waltzer deafness gene encodes an unconventional myosin required for structural integrity of inner ear hair cells. *Nature Genetics*, *11*, 369–375.

Bamburg, J. R., Harris, H. E., & Weeds, A. G. (1980). Partial purification and characterization of an actin depolymerizing factor from brain. *FEBS Letters*, *121*, 178–182.

Bar-Ziv, R., Tlusty, T., Moses, E., Safran, S. A., & Bershadsky, A. (1999). Pearling in cells: a clue to understanding cell shape. *Proceedings of the National Academy of Sciences USA*, *96*, 10140–10145.

Barnhart, E. L., Lee, K. C., Keren, K., Mogilner, A., & Theriot, J. A. (2011). An adhesion-dependent switch between mechanisms that determine motile cell shape. *PLoS Biology*, *9*, 100–105.

Batchelder, E. L., Hollopeter, G., Campillo, C., Mezanges, X., Jorgensen, E. M., Nassoy, P., … Plastino, J. (2011). Membrane tension regulates motility by controlling lamellipodium organization. *Proceedings of the National Academy of Sciences USA*, *108*, 11429–11434.

Bendix, P. M., Koenderink, G. H., Cuvelier, D., Dogic, Z., Koeleman, B. N., Brieher, W. M., … Weitz, D. A. (2008). A quantitative analysis of contractility in active cytoskeletal protein networks. *Biophysical Journal*, *94*, 3126–3136.

Bergert, M., Chandradoss, S. D., Desai, R. A., & Paluch, E. (2012). Cell mechanics control rapid transitions between blebs and lamellipodia during migration. *Proceedings of the National Academy of Sciences* , *109*, 14434–14439.

Bershadsky, A. D., Ballestrem, C., Carramusa, L., Zilberman, Y., Gilquin, B., Khochbin, S., … Kozlov, M. M. (2006). Assembly and mechanosensory function of focal adhesions: experiments and models. *European Journal of Cell Biology*, *85*, 165–73.

Blanchard, A., Ohanian, V., & Critchley, D. (1989). The structure and function of alpha-actinin. *Journal of Muscle Research and Cell Motility*, *10*, 280–289.

Blanchoin, L., Amann, K. J., Higgs, H. N., Marchand, J. B., Kaiser, D. a, & Pollard, T. D. (2000). Direct observation of dendritic actin filament networks nucleated by Arp2/3 complex and WASP/Scar proteins. *Nature*, *404*, 1007–1011.

Blanchoin, L., Boujemaa-paterski, R., Sykes, C., & Plastino, J. (2014). Actin dynamics, architecture, and mechanics in cell motility. *Physiological Reviews*, *94*, 235–263.

Blanchoin, L., & Pollard, T. D. (1999). Mechanism of interaction of Acanthamoeba actophorin (ADF/Cofilin) with actin filaments. *Journal of Biological Chemistry*, *274*, 15538–15546.

Blanchoin, L., & Pollard, T. D. (1999). Mechanism of Interaction of Acanthamoeba Mechanism of Interaction of Acanthamoeba Actophorin (ADF / Cofilin) with Actin Filaments. *The Journal of Biological Chemistry*, *274*, 15538–15546.

Blanchoin, L., Pollard, T. D., & Mullins, R. D. R. D. (2000). Interactions of ADF/cofilin, Arp2/3 complex, capping protein and profilin in remodeling of branched actin filament networks. *Current Biology*, *10*, 1273–1282.

Bovellan, M., Romeo, Y., Biro, M., Boden, A., Chugh, P., Yonis, A., … Charras, G. (2014). Cellular control of cortical actin nucleation. *Current Biology*, *24*, 1628–1635.

Brawley, C. M., & Rock, R. S. (2009). Unconventional myosin traffic in cells reveals a selective actin cytoskeleton.*PNAS*, *106*, 9685–9690.

Bray, D., & White, J. (1988). Cortical flow in animal cells. *Science*, *239*, 883–888.

Breitsprecher, D., Koestler, S. A., Chizhov, I., Nemethova, M., Mueller, J., Goode, B. L., Small, J. V., Rottner, K. & Faix, J. (2011). Cofilin cooperates with fascin to disassemble filopodial actin filaments. *Journal of Cell Science*, *124*, 3305–3318.

Bretscher, A., & Weber, K. (1980). Fimbrin, a new microfilament-associated protein present in microvilli and other cell surface structures. *Journal of Cell Biology*, *86*, 335–340.

Burnette, D. T., Manley, S., Sengupta, P., Sougrat, R., Davidson, M. W., Kachar, B., & Lippincott-Schwartz, J. (2011). A role for actin arcs in the leading-edge advance of migrating cells. *Nature Cell Biology*, *13*, 371–382.

Burridge, K., & Wittchen, E. S. (2013). The tension mounts: Stress fibers as force-generating mechanotransducers. *The Journal of Cell Biology*, *200*, 9–19.

Burtnick, L. D., Koepf, E. K., Grimes, J., Jones, E. Y., Stuart, D. I., McLaughlin, P. J., & Robinson, R. C. (1997). The crystal structure of plasma gelsolin: Implications for actin severing, capping, and nucleation. *Cell*, *90*, 661–670.

Campillo, C., Sens, P., Köster, D., Pontani, L. L., Lévy, D., Bassereau, P., Nassoy, P., Sykes, C. (2013). Unexpected Membrane Dynamics Unveiled by Membrane Nanotube Extrusion. *Biophysical Journal*, *104*, 1248–1256.

Carlsson, A. E. (2001). Growth of Branched Actin Networks against Obstacles. *Biophysical Journal*, *81*, 1907–1923.

Chan, C., Beltzner, C. C., & Pollard, T. D. (2009). Cofilin Dissociates Arp2/3 Complex and Branches from Actin Filaments. *Current Biology*, *19*, 537–545.

Charras, G. T., Hu, C., Coughlin, M., & Mitchison, T. J. (2006). Reassembly of contractile actin cortex in cell blebs. *Journal of Cell Biology*, *175*, 477–490.

Chen, L., Nakamura, M., Schindler, T., Parker, D., & Bryant, Z. (2012). Engineering controllable bidirectional molecular motors based on myosin. *Nature Nanotechnology*, *7*, 252–256.

Chereau, D., Kerff, F., Graceffa, P., Grabarek, Z., Langsetmo, K., & Dominguez, R. (2005). Actin-bound structures of Wiskott-Aldrich syndrome protein (WASP)-homology domain 2 and the implications for filament assembly. *Proceedings of the National Academy of Sciences USA*, *102*, 16644–16649.

Chuan, P., Spudich, J. a., & Dunn, A. R. (2011). Robust mechanosensing and tension generation by myosin VI. *Journal of Molecular Biology*, *405*, 105–112. h

Clark, A. G., Dierkes, K., & Paluch, E. K. (2013). Monitoring actin cortex thickness in live cells. *Biophysical Journal*, *105*, 570–80.

Cooper, M. G. (2000). *The cell: a molecular approach* (2nd Edition).

De La Cruz, E. M. (2009). How cofilin servers an actin filament. *Biophysical Revue*, *29*, 997–1003.

De La Cruz, E. M., Ostap, E. M., & Sweeney, H. L. (2001). Kinetic mechanism and regulation of myosin VI. *The Journal of Biological Chemistry*, *276*, 32373–32381.

Dobrzyński, M., Rodríguez, J., Kaandorp, J., & Blom, J. G. (2007). Computational methods for diffusion-influenced biochemical reactions. *Bioinformatics*, *23*, 1969–1977.

Dunn, A. R., Chuan, P., Bryant, Z., & Spudich, J. A. (2010). Contribution of the myosin VI tail domain to processive stepping and intramolecular tension sensing. *Proceedings of the National Academy of Sciences USA, 107*, 7746–7750.

Elam, W. A., Kang, H., & De La Cruz, E. M. (2013). Biophysics of actin filament severing by cofilin. *FEBS Letters*, *587*, 1215–1219.

Elting, M. W., Bryant, Z., Liao, J. C., & Spudich, J. A. (2011). Detailed tuning of structure and intramolecular communication are dispensable for processive motion of myosin VI. *Biophysical Journal*, *100*, 430–439.

Ennomani, H., Letort, G., Guérin, C., Martiel, J. L., Cao, W., Nedelec, F., De La Cruz, E. M, Théry, M., & Blanchoin, L. (*in revision*). Architecture and connectivity govern actin network contractility.

Fan, L., Pellegrin, S., Scott, A., & Mellor, H. (2010). The small GTPase Rif is an alternative trigger for the formation of actin stress fibers in epithelial cells. *Journal of Cell Science*, *123*, 1247–1252.

Feierbach, B., & Chang, F. (2001). Roles of the fission yeast formin for3p in cell polarity, actin cable formation and symmetric cell division. *Current Biology*, *11*, 1656–1665.

Fishkind, D. J., & Wang, Y. L. (1993). Orientation and three-dimensional organization of actin filaments in dividing cultured cells. *Journal of Cell Biology*, *123*, 837–848.

Foethke, D., Makushok, T., Brunner, D., & Nédélec, F. (2009). Force- and length-dependent catastrophe activities explain interphase microtubule organization in fission yeast. *Molecular Systems Biology*, *5*, 1–6.

Fujiwara, K., & Pollard, T. D. (1976). Fluorescent antibody localization of myosin in the cytoplasm, cleavage furrow and mitotic spindle of human cells. *Journal of Cell Biology*, *71*, 848–875.

Gardel, M. L., Schneider, I. C., Aratyn-schaus, Y., Waterman, C. M. (2010). Mechanical integration of actin and adhesion dynamics in cell migration. *Annual Review of Cell and Developmental Biology*, *26*, 315–333.

Gardel, M. L., Shin, J. H., MacKintosh, F. C., Mahadevan, L., Matsudaira, P., & Weitz, D. A. (2004). Elastic behavior of cross-linked and bundled actin networks. *Science*, *304*, 1301–1305.

Gibeaux, R., Politi, A. Z., Nedelec, F., Antony, C., & Knop, M. (2013). Spindle pole body-anchored Kar3 drives the nucleus along microtubules from another nucleus in preparation for nuclear fusion during yeast karyogamy. *Genes & Development*, *27*, 335–349.

Glotzer, M. (2005). The molecular requirements for cytokinesis. *Science*, *307*, 1735–1739.

Gordon, A. M., Homsher, E., & Regnier, M. (2000). Regulation of Contraction in Striated Muscle. *Physiological Reviews*, *80*, 853–924.

Green, R. A., Paluch, E., & Oegema, K. (2012). Cytokinesis in Animal Cells. *Annual Review of Cell and Developmental Biology*, *28*, 29–58.

Gressin, L., Guillotin, A., Guérin, C., Blanchoin, L., & Michelot, A. (2015). Architecture Dependence of Actin Filament Network Disassembly. *Current Biology*, *25*, 1437–1447.

Gunst, S. J., & Zhang, W. (2008). Actin cytoskeletal dynamics in smooth muscle: a new paradigm for the regulation of smooth muscle contraction. *American Journal of Physiology - Cell Physiology*, *295*, 576–587.

Gutsche-Perelroizen, I., Lepault, J., Ott, A., & Carlier, M. F. (1999). Filament assembly from profilin-actin. *Journal of Biological Chemistry*, *274*, 6234–6243.

He, X., & Dembo, M. (1997). A Dynamical Model of Cell Division. *Dynamics of Cell and Tissue Motion*, 55–65.

Hertzano, R., Shalit, E., Rzadzinska, A. K., Dror, A. A., Song, L., Ron, U.,Avraham, K. B. (2008). A Myo6 mutation destroys coordination between the myosin heads, revealing new functions of myosin VI in the stereocilia of mammalian inner ear hair cells. *PLoS Genetics*, *4*:e1000207

Hochmuth, R. M. (2000). Micropipette aspiration of living cells. *Journal of Biomechanics*, *33*, 15–22.

Hodge, T., & Cope, M. J. (2000). A myosin family tree. *Journal of Cell Science*, *113*, 3353–3354.

Hotulainen, P., & Lappalainen, P. (2006). Stress fibers are generated by two distinct actin assembly mechanisms in motile cells. *Journal of Cell Biology*, *173*, 383–394.

HUXLEY, A. (1957). Muscle structure and theories of contraction. *Progress in Biophysics and Biophysical Chemistry*, *7*, 255–318.

Ichetovkin, I., Grant, W., & Condeelis, J. (2002). Cofilin produces newly polymerized actin filaments that are preferred for dendritic nucleation by the Arp2/3 complex. *Current Biology*, *12*, 79–84.

Ishikawa, H., Bischoff, R., & Holtzer, H. (1969). Formation of arrowhead complexes with heavy meromyosin in a variety of cell types. *Journal of Cell Biology, 43, 312-328*

Iwasa, J. H., & Mullins, R. D. (2007). Spatial and Temporal Relationships between Actin-Filament Nucleation, Capping, and Disassembly. *Current Biology*, *17*, 395–406.

Kamasaki, T., Osumi, M., & Mabuchi, I. (2007). Three-dimensional arrangement of F-actin in the contractile ring of fission yeast. *Journal of Cell Biology*, *178*, 765–771.

Khatau, S. B., Hale, C. M., Stewart-Hutchinson, P. J., Patel, M. S., Stewart, C. L., Searson, P. C., … Wirtz, D. (2009). A perinuclear actin cap regulates nuclear shape. *Proceedings of the National Academy of Sciences USA*, *106*, 19017–19022.

Kinosian, H. J., Newman, J., Lincoln, B., Selden, L. a, Gershman, L. C., & Estes, J. E. (1998). Ca2+ regulation of gelsolin activity: binding and severing of F-actin. *Biophysical Journal*, *75*, 3101–3109.

Kodera, N., Yamamoto, D., Ishikawa, R., & Ando, T. (2010). Video imaging of walking myosin V by high-speed atomic force microscopy. *Nature*, *468*, 72–76.

Koenderink, G. H., Dogic, Z., Nakamura, F., Bendix, P. M., MacKintosh, F. C., Hartwig, J., Weitz, D. A. (2009). An active biopolymer network controlled by molecular motors. *Proceedings of the National Academy of Sciences USA*, *106*, 15192–15197.

Köhler, S., Schaller, V., & Bausch, A. R. (2011). Collective Dynamics of Active Cytoskeletal Networks. *PloS One*, *6: e23798*

Köhler, S., Schmoller, K. M., Crevenna, A. H., & Bausch, A. R. (2012). Regulating contractility of the actomyosin cytoskeleton by pH. *Cell Reports*, *2*, 433–9.

Kolomeisky, A. B. (2007). Channel-facilitated molecular transport across membranes: Attraction, repulsion, and asymmetry. *Physical Review Letters*, *98*, 1–4.

Kovar, D. R., & Pollard, T. D. (2004). Insertional assembly of actin filament barbed ends in association with formins produces piconewton forces. *Proceedings of the National Academy of Sciences USA*, *101*, 14725–14730.

Kron, S. J., & Spudich, J. A. (1986). Fluorescent actin filaments move on myosin fixed to a glass surface. *Proceedings of the National Academy of Sciences USA*, *83*, 6272–6276.

Kumar, N., Tomar, A., Parrill, A. L., & Khurana, S. (2004). Functional dissection and molecular characterization of calcium-sensitive actin-capping and actin-depolymerizing sites in villin. *The Journal of Biological Chemistry*, *279*, 45036–45046.

Landau, L. D., & Lifshitz, E. M. (1986). Theory of Elasticity, vol. 7. *Course of Theoretical Physics*, *3*, 109.

Langanger, G., Moeremans, M., Daneels, G., Sobieszek, A., De Brabander, M., & De Mey, J. (1986). The molecular organization of myosin in stress fibers of cultured cells. *The Journal of Cell Biology*, *102*, 200–9.

Lavoie, T. L., Dowell, M. L., Lakser, O. J., Gerthoffer, W. T., Fredberg, J. J., Seow, C. Y., … Solway, J. (2009). Disrupting Actin-Myosin-Actin Connectivity in Airway Smooth Muscle as a Treatment for Asthma? *Proceedings of the American Thoracic Society*, *6*, 295–300.

Lecuit, T., Lenne, P. F., & Munro, E. (2011). Force Generation, Transmission, and Integration during Cell and Tissue Morphogenesis. *Annual Review of Cell and Developmental Biology*, *27*, 157–184.

Lemerle, C., Di Ventura, B., & Serrano, L. (2005). Space as the final frontier in stochastic simulations of biological systems. *FEBS Letters*, *579*, 1789–1794.

Lenz, M., Gardel, M. L., & Dinner, A. R. (2012). Requirements for contractility in disordered cytoskeletal bundles. *New Journal of Physics*, *14*, 0–17.

Letort, G., Politi, A., Ennomani, H., Thery, M., Nedelec, F., & Blanchoin, L. (2015). Geometrical and mechanical properties control actin filament organization. *PLOS Computational Biology*. 11: e1004245.

Letort, G., Ennomani, H., Gressin L., Thery, M., & Blanchoin, L. (2015). Dynamic reorganization of actin cytoskeleton. *F1000 review*, *in press*.

Levayer, R., & Lecuit, T. (2012). Biomechanical regulation of contractility : spatial control and dynamics. *Trends in Cell Biology*, *22*, 61–81.

Lieleg, O., Claessens, M. M. A. E., & Bausch, A. R. (2010). Structure and dynamics of cross-linked actin networks. *Soft Matter*, *6*, 218.

Littlefield, R., Almenar-Queralt, A., & Fowler, V. M. (2001). Actin dynamics at pointed ends regulates thin filament length in striated muscle. *Nature Cell Biology*, *3*, 544–551.

Lodish, H., Berk, A., Lawrence, S., Zipursky, P., Matsudaira, D., & Darnell, J. (2000). *Molecular Cell Biology, 4th edition*.

Luo, W., Yu, C. H., Lieu, Z. Z., Allard, J., Mogilner, A., Sheetz, M. P., & Bershadsky, A. D. (2013). Analysis of the local organization and dynamics of cellular actin networks. *The Journal of Cell Biology*, *202*, 1057–73.

Mabuchi, I. (1983). An actin-depolymerizing protein (depactin) from starfish oocytes: Properties and interaction with actin. *Journal of Cell Biology*, *97*, 1612–1621.

Machesky, L. M., & Gould, K. L. (1999). The Arp2/3 complex: A multifunctional actin organizer. *Current Opinion in Cell Biology*, *11*, 117–121.

Maddugoda, M. P., Crampton, M. S., Shewan, A. M., & Yap, A. S. (2007). Myosin VI and vinculin cooperate during the morphogenesis of cadherin cell-cell contacts in mammalian epithelial cells. *Journal of Cell Biology*, *178*(3), 529–540.

Mahaffy, R. E., & Pollard, T. D. (2006). Kinetics of the formation and dissociation of actin filament branches mediated by Arp2/3 complex. *Biophysical Journal*, *91*, 3519–3528.

Marchand, J. B., Kaiser, D. a, Pollard, T. D., & Higgs, H. N. (2001). Interaction of WASP/Scar proteins with actin and vertebrate Arp2/3 complex. *Nature Cell Biology*, *3*, 76–82.

Marsland, D., & Landau, J. V. (1954). The mechanisms of cytokinesis: temperature-pressure studies on the cortical gel system in various marine eggs. *Journal of Experimental Zoology*, *125*, 507–539.

Maupin, P., & Pollard, T. D. (1986). Arrangement of actin filaments and myosin-like filaments in the contractile ring and of actin-like filaments in the mitotic spindle of dividing HeLa cells. *Journal of Ultrastructure and Molecular Structure Research*, *94*, 92–103.

McCullough, B. R., Blanchoin, L., Martiel, J. L., & De La Cruz, E. M. (2008). Cofilin Increases the Bending Flexibility of Actin Filaments: Implications for Severing and Cell Mechanics. *Journal of Molecular Biology*, *381*, 550–558.

McCullough, B. R., Grintsevich, E. E., Chen, C. K., Kang, H., Hutchison, A. L., Henn, A., … De La Cruz, E. (2011). Cofilin-linked changes in actin filament flexibility promote severing. *Biophysical Journal*, *101*, 151–159. Retrieved from

Milligan, R. A., Whittaker, M., & Safer, D. (1990). Molecular structure of F-actin and location of surface binding sites. *Nature*, 348, 217–221

Mishra, M., Kashiwazaki, J., Takagi, T., Srinivasan, R., Huang, Y., Balasubramanian, M. K., & Mabuchi, I. (2013). In vitro contraction of cytokinetic ring depends on myosin II but not on actin dynamics. *Nature Cell Biology*, *15*, 853–9.

Mogilner, A., Wollman, R., & Marshall, W. F. (2006). Quantitative Modeling in Cell Biology: What Is It Good for? *Developmental Cell*, *11*, 279–287.

Morone, N., Fujiwara, T., Murase, K., Kasai, R. S., Ike, H., Yuasa, S., Kusumi, A. (2006). Three-dimensional reconstruction of the membrane skeleton at the plasma membrane interface by electron tomography. *Journal of Cell Biology*, *174*, 851–862.

Munjal, A., & Lecuit, T. (2014). Actomyosin networks and tissue morphogenesis. *Development*, *141*, 1789–93.

Murakami, K., Yasunaga, T., Noguchi, T. Q. P., Gomibuchi, Y., Ngo, K. X., Uyeda, T. Q. P., & Wakabayashi, T. (2010). Structural Basis for Actin Assembly, Activation of ATP Hydrolysis, and Delayed Phosphate Release. *Cell*, *143*, 275–287.

Murrell, M., Oakes, P. W., Lenz, M., & Gardel, M. L. (2015). Forcing cells into shape: the mechanics of actomyosin contractility. *Nature Reviews Molecular Cell Biology*, *16*, 486–498.

Murrell, M. P., & Gardel, M. L. (2012). F-actin buckling coordinates contractility and severing in a biomimetic actomyosin cortex. *Proceedings of the National Academy of Sciences USA*, *109*, 20820–20825.

Nagy, S., Ricca, B., Norstrom, M. F., Courson, D. S., Brawley, C. M., Smithback, P. A., & Rock, R. S. (2008). A myosin motor that selects bundled actin for motility. *Proceedings of the National Academy of Sciences USA*, *105*, 9616–9620.

Nakamura, F., Osborn, E., Janmey, P. a., & Stossel, T. P. (2002). Comparison of filamin A-induced cross-linking and Arp2/3 complex-mediated branching on the mechanics of actin filaments. *Journal of Biological Chemistry*, *277*, 9148–9154.

Nakamura, M., Chen, L., Howes, S. C., Schindler, T. D., Nogales, E., & Bryant, Z. (2014). Remote control of myosin and kinesin motors using light-activated gearshifting. *Nature Nanotechnology*, *9*,693–697.

Naumanen, P., Lappalainen, P., & Hotulainen, P. (2008). Mechanisms of actin stress fibre assembly. *Journal of Microscopy*, *231*, 446–454.

Nedelec, F., & Foethke, D. (2007). Collective Langevin dynamics of flexible cytoskeletal fibers. *New Journal of Physics*, *9*, 427–438.

Nelson, S. R., Ali, M. Y., Trybus, K. M., & Warshaw, D. M. (2009). Random walk of processive, quantum dot-labeled myosin Va molecules within the actin cortex of COS-7 cells. *Biophysical Journal*, *97*, 509–518.

Nesmelov, Y. E., Agafonov, R. V, Negrashov, I. V, Blakely, S. E., Titus, M. A., & Thomas, D. D. (2011). Structural kinetics of myosin by transient time-resolved FRET. *Proceedings of the National Academy of Sciences USA, 108*, 1891–1896.

Oguchi, Y., Mikhailenko, S. V, Ohki, T., Olivares, A. O., De La Cruz, E. M., & Ishiwata, S. (2010). Robust processivity of myosin V under off-axis loads. *Nature Chemical Biology*, *6*, 300–305.

Otey, C. A., & Carpen, O. (2004). α-actinin revisited: A fresh look at an old player. *Cell Motility and the Cytoskeleton*, *58*, 104–111.

Otto, J. J., & Schroeder, T. E. (1990). Association of actin and myosin in the contractile ring. *Annals of the New York Academy of Sciences*, *582*, 179–184.

Pellegrin, S., & Mellor, H. (2007). Actin stress fibres. *Journal of Cell Science*, *120* , 3491–3499.

Perelroizen, I., Didry, D., Chem, J. B., Christensen, H., Chua, N., & Carlier, M. F. (1996). Role of Nucleotide Exchange and Hydrolysis in the Function of Profilin in Actin Assembly. *The Journal of Biological Chemistry*, *271*, 12302–12309.

Perelroizen, I., Marchand, J. B., Blanchoin, L., Didry, D., & Carlier, M. F. (1994). Interaction of profilin with G-actin and poly(L-proline). *Biochemistry*, *33*, 8472–8478.

Peterson, L. J., Rajfur, Z., Maddox, A. S., Freel, C. D., Chen, Y., Edlund, M. Burridge, K. (2004). Simultaneous Stretching and Contraction of Stress Fibers In Vivo. *Molecular Biology of the Cell*, *15*, 3497–3508.

Petrella, E. C., Machesky, L. M., Kaiser, D. A., & Pollard, T. D. (1996). Structural requirements and thermodynamics of the interaction of proline peptides with profilin. *Biochemistry*, *35*, 16535–16543.

Pinot, M., Chesnel, F., Kubiak, J. Z., Arnal, I., Nedelec, F. J., & Gueroui, Z. (2009). Effects of Confinement on the Self-Organization of Microtubules and Motors. *Current Biology*, *19*, 954–960.

Pollard, T. D. (1986). Rate constants for the reactions of ATP- and ADP-actin with the ends of actin filaments. *The Journal of Cell Biology*, *103*, 2747–54.

Pollard, T. D., Blanchoin, L., & Mullins, R. D. (2000). Molecular mechanisms controlling actin filament dynamics in nonmuscle cells. *Annual Review of Biophysics and Biomolecular Structure*, *29*, 545–576.

Pollard, T. D., & Borisy, G. G. (2003). Cellular motility driven by assembly and disassembly of actin filaments. *Cell*, *112*, 453–465.

Pollard, T. D., & Cooper, J. A. (1984). Quantitative Analysis of the Effect of Acanthamoeba Profilin on Actin Filament Nucleation and Elongation. *Biochemistry*, 23 , 6631–6641

Pollard, T. D., Earnshaw, W. C., Earnshaw, J., & Lippincott-Schwartz, J. (2002). *Cell biology*. Lebenslauf.

Purcell, T. J., Sweeney, H. L., & Spudich, J. A. (2005). A force-dependent state controls the coordination of processive myosin V. *Proceedings of the National Academy of Sciences USA*, *102*, 13873–13878.

Revenu, C., Athman, R., Robine, S., & Louvard, D. (2004). The co-workers of actin filaments: from cell structures to signals. *Nature Reviews. Molecular Cell Biology*, *5*, 635–646.

Reymann, A. C., Boujemaa-Paterski, R., Martiel, J. L., Guerin, C., Cao, W., Chin, H. F., De La Cruz, E. M., Théry, M. & Blanchoin, L. (2012). Actin Network Architecture Can Determine Myosin Motor Activity. *Science*, *336*, 1310–1314.

Reymann, A. C., Martiel, J. L., Cambier, T., Blanchoin, L., Boujemaa-Paterski, R., & Théry, M. (2010). Nucleation geometry governs ordered actin networks structures. *Nature Materials*, *9*, 827–832.

Robblee, J. P., Olivares, A. O., & De La Cruz, E. M. (2004). Mechanism of nucleotide binding to actomyosin VI: Evidence for allosteric head-head communication. *Journal of Biological Chemistry*, *279*, 38608–38617.

Robinson, D. N., & Spudich, J. A. (2000). Towards a molecular understanding of cytokinesis. *Trends in Cell Biology*, *10*, 228–237.

Robinson, R. C., Turbedsky, K., Kaiser, D. A., Marchand, J. B., Higgs, H. N., Choe, S., & Pollard, T. D. (2001). Crystal structure of Arp2/3 complex. *Science*, *294*,1679-1684.

Rock, R. S., Rice, S. E., Wells, a L., Purcell, T. J., Spudich, J. A., & Sweeney, H. L. (2001). Myosin VI is a processive motor with a large step size. *Proceedings of the National Academy of Sciences USA*, *98*, 13655–13659.

Rogers, S. L., Wiedemann, U., Stuurman, N., & Vale, R. D. (2003). Molecular requirements for actin-based lamella formation in Drosophila S2 cells. *Journal of Cell Biology*, *162*, 1079–1088.

Rohatgi, R., Ma, L., Miki, H., Lopez, M., Kirchhausen, T., Takenawa, T., & Kirschner, M. W. (1999). The interaction between N-WASP and the Arp2/3 complex links Cdc42-dependent signals to actin assembly. *Cell*, *97*, 221–231.

Rouiller, I., Xu, X. P., Amann, K. J., Egile, C., Nickell, S., Nicastro, D., Hanein, D. (2008). The structural basis of actin filament branching by the Arp2/3 complex. *Journal of Cell Biology*, *180*, 887–895.

Sahlender, D. A., Roberts, R. C., Arden, S. D., Spudich, G., Taylor, M. J., Luzio, J. P., Buss, F. (2005). Optineurin links myosin VI to the Golgi complex and is involved in Golgi organization and exocytosis. *Journal of Cell Biology*, *169*, 285–295.

Salbreux, G., Charras, G., & Paluch, E. (2012). Actin cortex mechanics and cellular morphogenesis. *Trends in Cell Biology*, *22*, 536–45.

Sandbo, N., Lau, A., Kach, J., Ngam, C., Yau, D., & Dulin, N. O. (2011). Delayed stress fiber formation mediates pulmonary myofibroblast differentiation in response to TGF-β. *American Journal of Physiology - Lung Cellular and Molecular Physiology*, *301*, 656–666.

Sanger, J. W., Wang, J., Holloway, B., Du, A., & Sanger, J. M. (2009). Myofibrillogenesis in skeletal muscle cells in zebrafish. *Cell Motility and the Cytoskeleton*, *66*, 556–566.

Schafer, D. A., & Cooper, J. A. (1995). *Control of actin assembly at filament ends*. *Annual review of cell and developmental biology*, 14, 305-338.

Schafer, D. A., Jennings, P. B., & Cooper, J. A. (1996). Dynamics of capping protein and actin assembly in vitro: Uncapping barbed ends by polyphosphoinositides. *Journal of Cell Biology*, *135*, 169–179.

Schaus, T. E., Taylor, E. W., & Borisy, G. G. (2007). Self-organization of actin filament orientation in the dendritic-nucleation/array-treadmilling model. *Proceedings of the National Academy of Sciences USA*,, *104*, 7086–7091.

Schindler, T. D., Chen, L., Lebel, P., Nakamura, M., & Bryant, Z. (2014). Engineering myosins for long-range transport on actin filaments. *Nature Nanotechnology*, *9*, 33–8.

Schroeder, T. E. (1970). The contractile ring. *Journal of Cell Biology*, *53*, 419–434.

Schroeder, T. E. (1990). The contractile ring and furrowing in dividing cells. *Annals of the New York Academy of Sciences*, *582*, 78–87.

Schutt, C. E., Myslik, J. C., Rozycki, M. D., Goonesekere, N. C., & Lindberg, U. (1993). The structure of crystalline profilin-beta-actin. *Nature*, *365*, 810–816.

Shemesh, T., Verkhovsky, A. B., Svitkina, T. M., Bershadsky, A. D., & Kozlov, M. M. (2009). Role of focal adhesions and mechanical stresses in the formation and progression of the lamellipodium-lamellum interface. *Biophysical Journal*, *97*, 1254–64.

Shin, J. H., Gardel, M. L., Mahadevan, L., Matsudaira, P., & Weitz, D. A. (2004). Relating microstructure to rheology of a bundled and cross-linked F-actin network in vitro. *Proceedings of the National Academy of Sciences USA*, *101*, 9636–9641.

Spudich, J. A. (2012). One path to understanding energy transduction in biological systems. *Nature Medicine*, *18*, 1478–1482.

Staiger, C. J., & Blanchoin, L. (2006). Actin dynamics: old friends with new stories. *Current Opinion in Plant Biology*, *9*, 554–562.

Stauffer, D., & Aharony, A. (1994). *Introduction to percolation theory*. CRC press.

Suarez, C., Roland, J., Boujemaa-Paterski, R., Kang, H., McCullough, B. R., Reymann, A. C., Blanchoin, L. (2015). Cofilin Tunes the Nucleotide State of Actin Filaments and Severs at Bare and Decorated Segment Boundaries. *Current Biology*, *21*, 862–868.

Svitkina, T. M., & Borisy, G. G. (1999). Arp2/3 complex and actin depolymerizing factor/cofilin in dendritic organization and treadmilling of actin filament array in lamellipodia. *Journal of Cell Biology*, *145*, 1009–1026.

Symons, M., Li, R., & Mitchison, T. (1991). Control of actin polymerization in fibroblasts. *The Journal of Cell Biology*, *114*, 503–313.

Theriot, J. A., & Mitchison, T. J. (1991). Actin microfilament dynamics in locomoting cells. *Nature*. 352, 126–131.

Thoresen, T., Lenz, M., & Gardel, M. L. (2013). Thick filament length and isoform composition determine self-organized contractile units in actomyosin bundles. *Biophysical Journal*, *104*, 655–65.

Tojkander, S., Gateva, G., & Lappalainen, P. (2012). Actin stress fibers--assembly, dynamics and biological roles. *Journal of Cell Science*, *125*, 1855–64.

Toyoshima, Y. Y., Kron, S. J., McNally, E. M., Niebling, K. R., Toyoshima, C., & Spudich, J. A. (1987). Myosin subfragment-1 is sufficient to move actin filaments in vitro. *Nature*, *328*, 536–539.

Tseng, Y., Fedorov, E., McCaffery, J. M., Almo, S. C., & Wirtz, D. (2001). Micromechanics and ultrastructure of actin filament networks crosslinked by human fascin: a comparison with alpha-actinin. *Journal of Molecular Biology*, *310*, 351–366.

Vavylonis, D., Kovar, D. R., O'Shaughnessy, B., & Pollard, T. D. (2006). Model of formin-associated actin filament elongation. *Molecular Cell*, *21*, 455–466.

Vavylonis, D., Yang, Q., & O'Shaughnessy, B. (2005). Actin polymerization kinetics, cap structure, and fluctuations. *Proceedings of the National Academy of Sciences USA*, *102*, 8543–8548.

Veigel, C., Wang, F., Bartoo, M. L., Sellers, J. R., & Molloy, J. E. (2002). The gated gait of the processive molecular motor, myosin V. *Nature Cell Biology*, *4*, 59–65.

Vicente-Manzanares, M., Ma, X., Adelstein, R. S., & Horwitz, A. R. (2009). Non-muscle myosin II takes centre stage in cell adhesion and migration. *Nature Reviews. Molecular Cell Biology*, *10*,778-790.

Vignaud, T., Ennomani, H., & Théry, M. (2014). Polyacrylamide Hydrogel Micropatterning. *Methods in Cell Biology*, *120*, 93–116.

Vinson, V. K., De La Cruz, E. M., Higgs, H. N., & Pollard, T. D. (1998). Interactions of Acanthamoeba profilin with actin and nucleotides bound to actin. *Biochemistry*, *37*, 10871–10880.

Wachsstock, D. H., Schwartz, W. H., & Pollard, T. D. (1993). Affinity of alpha-actinin for actin determines the structure and mechanical properties of actin filament gels. *Biophysical Journal*, *65*, 205–214.

Wang, S., & Wolynes, P. G. (2012). Active contractility in actomyosin networks. *Proceedings of the National Academy of Sciences USA*, *109*, 6446–6451.

Wang, Y. L. (1985). Exchange of actin subunits at the leading edge of living fibroblasts: Possible role of treadmilling. *The Journal of Cell Biology*, *101*, 597–602.

Wanger, M., Keiser, T., Neuhaus, J. M., & Wegner, A. (1985). The actin treadmill. *Canadian Journal of Biochemistry and Cell Biology*, *63*, 414–421.

Ward, A., Hilitski, F., Schwenger, W., Welch, D., Lau, a. W. C., Vitelli, V., Dogic, Z. (2015). Solid friction between soft filaments. *Nature Materials*, 14, 583–588.

Warner, C. L., Stewart, A., Luzio, J. P., Steel, K. P., Libby, R. T., Kendrick-Jones, J., & Buss, F. (2003). Loss of myosin VI reduces secretion and the size of the Golgi in fibroblasts from Snell's waltzer mice. *EMBO Journal*, *22*, 569–579.

Watanabe, T. M., Tokuo, H., Gonda, K., Higuchi, H., & Ikebe, M. (2010). Myosin-X induces filopodia by multiple elongation mechanism. *Journal of Biological Chemistry*, *285*, 19605–19614.

Way, M., Gooch, J., Pope, B., & Weeds, a. G. (1989). Expression of human plasma gelsolin in Escherichia coli and dissection of actin binding sites by segmental deletion mutagenesis. *Journal of Cell Biology*, *109*, 593–605.

Wegner, a. (1976). Head to tail polymerization of actin. *Journal of Molecular Biology*, *108*, 139–150.

Welch, M. D., Rosenblatt, J., Skoble, J., Portnoy, D. a, & Mitchison, T. J. (1998). Interaction of human Arp2/3 complex and the Listeria monocytogenes ActA protein in actin filament nucleation. *Science*, *281*, 105–108.

Wu, J. Q., Kuhn, J. R., Kovar, D. R., & Pollard, T. D. (2003). Spatial and temporal pathway for assembly and constriction of the contractile ring in fission yeast cytokinesis. *Developmental Cell*, *5*, 723–734.

Xu, J., Schwarz, W. H., Käs, J. a, Stossel, T. P., Janmey, P. a, & Pollard, T. D. (1998). Mechanical properties of actin filament networks depend on preparation, polymerization conditions, and storage of actin monomers. *Biophysical Journal*, *74*, 2731–2740.

Yamashiro-Matsumura, S., & Matsumura, F. (1986). Intracellular localization of the 55-kD actin-bundling protein in cultured cells: Spatial relationships with actin, alpha-actinin, tropomyosin, and fimbrin. *Journal of Cell Biology*, *103*, 631–640.

Yi, J., Wu, X. S., Crites, T., & Hammer, J. A. (2012). Actin retrograde flow and actomyosin II arc contraction drive receptor cluster dynamics at the immunological synapse in Jurkat T cells. *Molecular Biology of the Cell*, *23*, 834–852.

Yumura, S. (2001). Myosin II dynamics and cortical flow during contractile ring formation in Dictyostelium cells. *The Journal of Cell Biology*, *154*, 137–146.

Zhang, W., & Robinson, D. N. (2005). Balance of actively generated contractile and resistive forces controls cytokinesis dynamics. *Proceedings of the National Academy of Sciences USA*, *102*, 7186–7191.

Zheng, X., Diraviyam, K., & Sept, D. (2007). Nucleotide effects on the structure and dynamics of actin. *Biophysical Journal*, *93*, 1277–1283.

Summary

Cellular contractility – the internal generation of force by a cell orchestrated by the actomyosin machinery – is a critical regulator of a wide range of cellular processes including the establishment of cell polarity, cell migration, tissue integrity or morphogenesis during development. Disruptions of the force generation and of mechanical properties of living cells affect their physiological functions and consequently can lead to pathological defects including cancer. However, the parameters or mechanisms that drive force production by the actin-myosin system and their mode of regulation in cells are not fully understood. During my PhD, I used biomimetic system made of a minimum set of proteins to study the properties of actomyosin contractile systems. The goal was to understand how/if the actin architecture can mediate the contractile response. For this purpose, I was first interested in building a variety of actin organization that will serve next as substrate for myosin during contraction. To understand the general principles that dictate geometrically-controlled actin assembly, we developed a model that allowed us to identify key parameters including filaments/filaments interaction, filament mechanical property and contact activation between actin filaments growing from the adjacent pattern and the nucleation area. These actin templates were used then to evaluate the response of oriented actin structures to myosin-induced contractility. I demonstrated that crosslinking level modulates the myosin-induced deformation of actin networks according to their architecture. I showed also that crosslinkers are necessary to sustain myosin-driven deformation and force production of dynamic actin networks. In addition, we developed numerical simulation in order to relate the observed myosin-driven actin deformation with the underlying microscopic mechanism. This work revealed how diverse cellular actin networks contract differently to a define set of biochemical conditions and hence how dynamic rearrangements can modulate network contractility.